Parameterschätzung und Modellevaluation für komplexe Systeme

Dissertation

zur Erlangung des mathematisch-naturwissenschaftlichen Doktorgrades

"Doctor rerum naturalium"

der Georg-August-Universität Göttingen

im Promotionsprogramm PROPHYS

der Georg-August University School of Science (GAUSS)

vorgelegt von

Jan Schumann-Bischoff

aus Gehrden

Göttingen, 2016

Betreuungsausschuss

Prof. Dr. Florentin Wörgötter, Computational Neuroscience Group,
Third Institute of Physics, Georg-August University, Göttingen

Prof. Dr. Ulrich Parlitz, Biomedical Physics Group,
Max Planck Institute for Dynamics and Self-Organization, Göttingen

Prof. Dr. Stefan Luther, Biomedical Physics Group,
Max Planck Institute for Dynamics and Self-Organization, Göttingen

Mitglieder der Prüfungskommission

Referent: Prof. Dr. Ulrich Parlitz, Biomedical Physics Group,
Max Planck Institute for Dynamics and Self-Organization, Göttingen

Korreferent: Prof. Dr. Florentin Wörgötter, Computational Neuroscience Group,
Third Institute of Physics, Georg-August University, Göttingen

Weitere Mitglieder der Prüfungskommission:

Prof. Dr. Stefan Luther, Biomedical Physics Group,
Max Planck Institute for Dynamics and Self-Organization, Göttingen

Prof. Dr. Wolfram Kollatschny, Extragalaktische Astrophysik,
Institut für Astrophysik, Georg-August-Universität Göttingen

Prof. Dr. Dr. Andreas Dillmann, Institut für Aerodynamik und Strömungstechnik,
Deutsches Zentrum für Luft- und Raumfahrt (DLR), Göttingen

Prof. Dr. Marc Timme, Network Dynamics,
Max Planck Institute for Dynamics and Self-Organization, Göttingen

Tag der mündlichen Prüfung: 6. April 2016

Contents

1 Introduction

Nowadays computer simulations are important tools to investigate, analyze, and predict the behavior of real world processes and constructions. In engineering the complex dynamics of electronic circuits, the aerodynamic behavior of planes, or the stability of buildings are simulated, to just give a few practically relevant examples. Scientists use simulations in various disciplines such as systems biology, solid state physics, or geosciences to analyze or predict the outcomes of experiments.

For that, mathematical models are used where it is known or assumed that they describe the process of interest sufficiently well. Nevertheless, a mathematical model usually describes the reality only approximately. Predictions or simulations based on these models contain errors. It is highly desirable to reduce them and, thereby, to increase the accuracy of the simulations. A promising approach to achieve this is to make use of observed data of the same or a comparable process one aims to simulate. One can take advantage of them by using appropriate *state and parameter estimation* methods [1–13] which adjust or control the mathematical model and its parameterization by means of the data. An improved model may then lead to more realistic results of the simulation.

Another field of application of state and parameter estimation methods is to reconstruct full states of an only partially observed process. In many situations it is only possible to measure some but not all quantities of a dynamical process. A complete observation might be too expensive or technically simply not feasible. This is, for example, a common situation in climatology. It exist a huge amount of meteorological stations including stations on the ground, satellites, and radar systems distributed allover the planet. They provide an enormous amount of data within a period of time which are then used to reconstruct the complete state of the atmosphere at the end of the time interval. This state is then used to initialize a weather forecast [14–16].

To give another example, let us consider a neuron or a cardiomyocyte. Assume that data of the membrane voltage are available. The different ion currents are not measured, although one is interested in them. Nevertheless, they can be estimated using a mathematical model of the cell which forms a link between the voltage and the currents [17]. This includes the estimation of the model parameters.

In general, a state and parameter estimation algorithm can be used to fit a mathematical model to data and estimate the model parameters as well as the full states (including not measured quantities). Due to its practical importance the development and investigation of estimation algorithms is an active research area. They were substantially promoted during the last decades, among others, by the geoscientific (climatology, oceanography, ...), the nonlinear dynamics, and in engineering communities.

In this context the question arises how accurate and unique the estimated solutions

for the states and parameters would be. It is important to know whether the measured signals contain enough information for a precise estimation. Hence, it is essential to know about the *observability* [18–26]. This includes the identification of redundant model parameters [27–29]. The knowledge about the observability can help to reduce the complexity of the mathematical model without decreasing its accuracy in describing the measured signal. Methods used to address this question are developed and investigated, for example, in the control theory [21, 23].

This work covers both topics, state and parameter estimation and observability with a focus on nonlinear dynamical systems. An optimization based estimation algorithm is used where different strategies for its initialization are investigated and compared. It is crucial for a reliable performance of the optimization algorithm to provide a correct implementation of derivatives of the cost function (also called objective or error function). Hence, special attention is paid to a numerically exact computation of derivatives. Furthermore, the observability of nonlinear systems discrete and continuous in time is investigated to identify parameters and state variables which are difficult to reconstruct or even redundant. This includes the question of how many quantities should be measured for a precise estimation of states and parameters. Finally, the suggested methods are applied to experimentally measured data from the Shinriki oscillator [30] (a nonlinear electronic circuit).

2 State and parameter estimation

In many scientific processes (time dependent) signals of certain quantities can be measured and other signals can not, or the effort is relatively high. Nevertheless, one is often interested in these quantities that are difficult to access. For example, it is relatively easy to measure the temperature, pressure, humidity, etc. on the ground, but measuring these quantities directly in the higher atmosphere (e.g. by plane or weather balloons) is much more sophisticated or expensive. Or, measuring the membrane voltage of a neuron or a cardiomyocyte is more common than measuring currents through the ion channels directly. If a mathematical model describing the process is available, then a *state and parameter estimation algorithm* can be used to estimate the states, including the not measured quantities, and the parameters based on the measured signals.

In geosciences, where state and parameter estimation is known as *data assimilation* [3], estimation methods are operationally used to estimate states of the atmosphere by means of large scale weather models from data measured on the ground, by radar, by satellite, etc. [16]. The state of the atmosphere at the end of an estimation interval may then be used as initial state for numerical weather forecast [14].

Dependent on the process, the mathematical models include (nonlinear) partial differential equations, iterated maps, or ordinary differential equations (ODEs). Many estimation methods have been developed in the past, as methods based on synchronization [10, 11], particle filters [1–3], Kalman filters [4, 6–8], or optimization based methods [9, 12, 13], to name but a few.

Different methods have various fields of application. A *filter*, e.g. a Kalman filter, which estimates the state at the time t only uses data from past times $t' \leq t$ [31]. Filters can be applied if future data $t' > t$ are not available. For example, Kalman filters can be used in navigation devices to estimate the position on earth based on a mathematical model and (noisy) signals sent, for example, from satellites [32]. If future data at $t' > t$ would be available, then they would not influence and, therefore, can not improve the accuracy of the estimates at the time t.

Conceptually different are *smoothers*. They use data of the whole interval $[t_0, t_1]$ to estimate at time t, where $t_0 \leq t, \leq t_1$[31]. Hence, future data at $t' > t$ can influence (and hopefully improve) the accuracy of estimates at the time t. This situation usually occurs in (physical) experiments and is, therefore, in the focus of this chapter. A typical procedure is that, first, data (e.g. in form of time series) are measured in a time interval $[t_0, t_1]$, and, afterwards, within this interval, states and parameters of the system are estimated. Therefore, future data at $t' > t$ exist and can be used to increase the accuracy of estimates at the time t.

In the following chapters the optimization based state and parameter estimation method from Ref. [33] is used which is similar to *weak constraint 4D-Var* [34–37]. As

with smoothers, estimates at the time $t \in [t_0, t_1]$ depend on data within the entire interval $[t_0, t_1]$. One substantial advantage of this estimation method is that errors in the model equations are allowed (no perfect model assumption), i.e. the estimated trajectories do not have to fulfill the model equations exactly. This is especially important when dealing with nonlinear and chaotic models. In Ref. [38] it was demonstrated for a Lorenz 63 model [39] that the longer the estimation window is, the more local minima the cost function exhibits (in their case, errors in the model equations are prohibited).

This estimation method is used in Chap. 4, Chap. 7, Chap. 8, and Chap. 9. The goal of Sec. 2.2 is to provide its statistical (bayesian) background leading to a cost function Eq. (2.24) or Eq. (2.27), where the minimizing trajectory and parameters are considered as the solution of the estimation problem. In Sec. 2.1 some used probabilistic definitions are provided. Properties of the cost function, including the role of its single terms, are discussed in Sec. 2.3. The link to Chap. 4, Chap. 7, Chap. 8, and Chap. 9 is discussed in Sec. 2.4.

2.1 Statistical definitions

The purpose of this section is to provide a few basic statistical definitions required for the bayesian statistics presented in Sec. 2.2. This overview is based on the definitions provided by the textbooks [8, 31].

We consider a real valued continuous random variable x. When performing a random experiment the random variable x will take a specific value x. The probability of the realization can be computed by means of the *probability density function* (PDF)

$$P(x) \ . \tag{2.1}$$

Since x is continuous, the probability that x lies in a certain interval $[x_l, x_u]$ can be computed and is given by

$$\int_{x_l}^{x_u} P(x)\mathrm{d}x \ . \tag{2.2}$$

Furthermore, the pdf is normalized,

$$\int_{-\infty}^{\infty} P(x)\mathrm{d}x = 1 \ . \tag{2.3}$$

For a set of N continuous random variables $\mathrm{x}_1, \ldots, \mathrm{x}_N$ the *joint PDF* is defined by

$$P(x_1, \ldots, x_N) = P(\mathbf{x}) \tag{2.4}$$

with $\mathbf{x} = (x_1, \ldots, x_N)$ and defines the probability that all N random variables take specific values.

If $\mathrm{x}_1, \ldots, \mathrm{x}_N$ are *independent*, then

$$P(x_1, \ldots, x_N) = \prod_{n=1}^{N} P(x_n) \ . \tag{2.5}$$

Equivalently, if two vectors $\mathbf{x}$ and $\mathbf{y}$ of random variables are independent, then

$$P(\mathbf{x}, \mathbf{y}) = P(\mathbf{x})P(\mathbf{y}) \ . \tag{2.6}$$

The *conditional PDF* $P(x|y)$ of random variables x and y describes the probability that event x occurs if event y already occurred and is defined by

$$P(x|y) = \frac{P(x, y)}{P(y)} \ . \tag{2.7}$$

For two random vectors $\mathbf{x}$ and $\mathbf{y}$ the conditional PDF is defined by

$$P(\mathbf{x}|\mathbf{y}) = \frac{P(\mathbf{x}, \mathbf{y})}{P(\mathbf{y})} \ . \tag{2.8}$$

Since for the joint PDF it is $P(\mathbf{x}, \mathbf{y}) = P(\mathbf{y}, \mathbf{x})$, we can directly derive the *Bayes' theorem*

$$P(\mathbf{x}|\mathbf{y}) = \frac{P(\mathbf{y}|\mathbf{x})P(\mathbf{x})}{P(\mathbf{y})} \ . \tag{2.9}$$

This theorem is the basis of the probabilistic approach of state and parameter estimation presented in Sec. 2.2. In the context of Bayesian statistics $P(\mathbf{x})$ is also called the *prior* probability distribution, $P(\mathbf{x}|\mathbf{y})$ is called the *posterior* probability distribution, and $P(\mathbf{y}|\mathbf{x})$ is the *likelihood* , see Ref. [8].

2.2 Probabilistic approach

In this section we want to consider a probabilistic background of state and parameter estimation. To simplify the discussion we first focus on state estimation only. A detailed discussion about this probabilistic approach based on Bayesian statistics can be found in Refs. [8, 31, 40], for example. The goal of state estimation is to find a trajectory $\{\mathbf{x}(n)\}$, $n = 0, \ldots, N$ for the estimation window, consisting of $N + 1$ model states $\mathbf{x}(n) = [x_1(n), \ldots, x_D(n)]^{\mathrm{tr}} \in \mathbb{R}^D$ at the times n based on some data. Before introducing data into the formalism, as in Ref. [40], first the time evolution of the model state is considered without data. If the model evolving the state $\mathbf{x}(n)$ in time is deterministic, then $\mathbf{x}(n)$ is fully determined given some other state $\mathbf{x}(m)$. In general, the model is not deterministic. Hence, one can only use the joint PDF $P(\mathbf{x}(N), \mathbf{x}(N-1), \ldots, \mathbf{x}(n), \ldots, \mathbf{x}(1), \mathbf{x}(0))$ of the trajectory $\{\mathbf{x}(n)\}$ to compute statistical properties like, for example, expectation values for single states or complete trajectories, or variances. Together with the definition of

the conditional PDF Eq. (2.8) we compute [40]

$$\begin{aligned} P(\mathbf{x}(N), \mathbf{x}(N-1), \ldots, \mathbf{x}(n), \ldots, \mathbf{x}(1), \mathbf{x}(0)) \\ = P(\mathbf{x}(N)|\mathbf{x}(N-1), \ldots, \mathbf{x}(n), \ldots, \mathbf{x}(1), \mathbf{x}(0)) \\ \cdot P(\mathbf{x}(N-1), \ldots, \mathbf{x}(n), \ldots, \mathbf{x}(1), \mathbf{x}(0)) \end{aligned} \tag{2.10}$$

Now, we assume a *Markov process* of order one [8, 31, 40]. That is, the state $\mathbf{x}(n+1)$ only depends on the state $\mathbf{x}(n)$ and not on earlier states $\mathbf{x}(n-1), \mathbf{x}(n-2), \ldots, \mathbf{x}(0)$. Then, we obtain for the PDF, see Ref. [40],

$$P(\mathbf{x}(N)|\mathbf{x}(N-1), \ldots, \mathbf{x}(n), \ldots, \mathbf{x}(1), \mathbf{x}(0)) = P(\mathbf{x}(N)|\mathbf{x}(N-1)) \ . \tag{2.11}$$

Inserted into Eq. (2.10) and recursively applied the definition of the conditional probability Eq. (2.8), we obtain [8, 31, 40]

$$\begin{aligned} P(\{\mathbf{x}(n)\}) &= P(\mathbf{x}(N), \mathbf{x}(N-1), \ldots, \mathbf{x}(n), \ldots, \mathbf{x}(1), \mathbf{x}(0)) \\ &= P(\mathbf{x}(0)) \prod_{n=0}^{N-1} P(\mathbf{x}(n+1)|\mathbf{x}(n)) \ . \end{aligned} \tag{2.12}$$

Now we consider data in form of a measured (noisy) time series $\{\boldsymbol{\eta}(n)\}$, $n = 0, \ldots, N$. At the time n the data consist of the data vector $\boldsymbol{\eta}(n) = [\eta_1(n), \ldots, \eta_L(n)]^{\mathrm{tr}} \in \mathbb{R}^L$ and is given via the output of the measurement function $\mathbf{h}$,

$$\boldsymbol{\eta}(n) = \mathbf{h}(\mathbf{x}(n)) + \boldsymbol{\epsilon}(n) \ , \tag{2.13}$$

where measurement noise $\boldsymbol{\epsilon}(n)$ is assumed to be white [31]. That is, $\{\boldsymbol{\epsilon}(n)\}$, $n = 0, \ldots, N$, is independent in time, which means that $\boldsymbol{\epsilon}(n)$ and $\boldsymbol{\epsilon}(m)$ are independent if $n \neq m$. Therefore, if $n \neq m$, $\boldsymbol{\eta}(n)$ and $\boldsymbol{\eta}(m)$ are conditionally independent given $\{\mathbf{x}(n)\}$. For the function $P(\{\boldsymbol{\eta}(n)\}|\{\mathbf{x}(n)\})$ we get then

$$P(\{\boldsymbol{\eta}(n)\}|\{\mathbf{x}(n)\}) = \prod_{n=0}^{N} P(\boldsymbol{\eta}(n)|\{\mathbf{x}(n)\}) \ . \tag{2.14}$$

Since $\boldsymbol{\eta}(n)$ depends on $\mathbf{x}(n)$, and not on $\mathbf{x}(m)$, $m \neq n$, we get for the function [8]

$$P(\{\boldsymbol{\eta}(n)\}|\{\mathbf{x}(n)\}) = \prod_{n=0}^{N} P(\boldsymbol{\eta}(n)|\mathbf{x}(n)) \ . \tag{2.15}$$

We are now interested in finding the PDF of $\{\mathbf{x}(n)\}$ *given the data* $\{\boldsymbol{\eta}(n)\}$,

$$P(\{\mathbf{x}(n)\}|\{\boldsymbol{\eta}(n)\}) \ . \tag{2.16}$$

Using Bayes' theorem Eq. (2.9) we have

$$P(\{\mathbf{x}(n)\}|\{\boldsymbol{\eta}(n)\}) = \frac{P(\{\boldsymbol{\eta}(n)\}|\{\mathbf{x}(n)\})P(\{\mathbf{x}(n)\})}{P(\{\boldsymbol{\eta}(n)\})} \ . \tag{2.17}$$

Since the denominator does not depend on $\{\mathbf{x}(n)\}$ and hence is constant, together with Eq. (2.12) and Eq. (2.15) it is [8, 31]

$$P(\{\mathbf{x}(n)\}|\{\boldsymbol{\eta}(n)\}) \propto P(\mathbf{x}(0)) \prod_{n=0}^{N} P(\boldsymbol{\eta}(n)|\mathbf{x}(n)) \prod_{n=0}^{N-1} P(\mathbf{x}(n+1)|\mathbf{x}(n)) \ . \tag{2.18}$$

The solution $\{\hat{\mathbf{x}}(n)\}$ which maximizes $P(\{\mathbf{x}(n)\}|\{\boldsymbol{\eta}(n)\})$ is the most probable trajectory.

In the following it is assumed that the model describing the time evolution of the trajectory is given by a nonlinear iterated map

$$\mathbf{x}(n+1) = \mathbf{F}(\mathbf{x}(n)) + \mathbf{u}(n) \ . \tag{2.19}$$

By assumption the model error $\mathbf{u}(n)$ is independent in time. Furthermore, $\mathbf{u}(n)$ and $\boldsymbol{\epsilon}(n)$ (see Eq. (2.13)) are normally distributed with a mean of zero and the covariance matrices Σ_u and Σ_ϵ. Then, we get for the PDFs

$$\begin{aligned} &P(\mathbf{x}(n+1)|\mathbf{x}(n)) \\ &\quad = \frac{1}{\sqrt{(2\pi)^D \det(\Sigma_\mathrm{u})}} \exp\left(-\frac{1}{2}[\mathbf{x}(n+1) - \mathbf{F}(\mathbf{x}(n))]^\mathrm{tr} \Sigma_\mathrm{u}^{-1} [\mathbf{x}(n+1) - \mathbf{F}(\mathbf{x}(n))]\right) \end{aligned} \tag{2.20}$$

and [8]

$$\begin{aligned} &P(\boldsymbol{\eta}(n)|\mathbf{x}(n)) \\ &\quad = \frac{1}{\sqrt{(2\pi)^L \det(\Sigma_\epsilon)}} \exp\left(-\frac{1}{2}[\boldsymbol{\eta}(n) - \mathbf{h}(\mathbf{x}(n))]^\mathrm{tr} \Sigma_\epsilon^{-1} [\boldsymbol{\eta}(n) - \mathbf{h}(\mathbf{x}(n))]\right) \ . \end{aligned} \tag{2.21}$$

For simplicity, Σ_u and Σ_ϵ are are assumed to be constant over time n. Furthermore we have to choose a PDF $P(\mathbf{x}(0))$ for the initial values $\mathbf{x}(0)$. We assume that $\mathbf{x}(0)$ is normally distributed around the background state $\mathbf{x}_b$ with a covariance matrix Σ_b [34],

$$P(\mathbf{x}(0)) = \frac{1}{\sqrt{(2\pi)^D \det(\Sigma_\mathrm{b})}} \exp\left(-\frac{1}{2}[\mathbf{x}_b - \mathbf{x}(0)]^\mathrm{tr} \Sigma_\mathrm{b}^{-1} [\mathbf{x}_b - \mathbf{x}(0)]\right) \ . \tag{2.22}$$

The background state is then for example the final estimated state (or a short term prediction) of a previous estimation window ending at $n \leq 0$.

Due to the monotony of the logarithm the trajectory $\{\hat{\mathbf{x}}(n)\}$ which maximizes Eq. (2.18) is equal to the trajectory which minimizes the *cost function* [31]

$$C(\{\mathbf{x}(n)\}) \propto -\ln[P(\{\mathbf{x}(n)\}|\{\boldsymbol{\eta}(n)\})] \tag{2.23}$$

with

$$C(\{\mathbf{x}(n)\}) = \frac{1}{2}[\mathbf{x}_b - \mathbf{x}(0)]^{\mathrm{tr}}\Sigma_{\mathrm{b}}^{-1}[\mathbf{x}_b - \mathbf{x}(0)] + \frac{1}{2}\sum_{n=0}^{N}[\boldsymbol{\eta}(n) - \mathbf{h}(\mathbf{x}(n))]^{\mathrm{tr}}\Sigma_{\epsilon}^{-1}[\boldsymbol{\eta}(n) - \mathbf{h}(\mathbf{x}(n))] + \frac{1}{2}\sum_{n=0}^{N-1}[\mathbf{x}(n+1) - \mathbf{F}(\mathbf{x}(n))]^{\mathrm{tr}}\Sigma_{\mathrm{u}}^{-1}[\mathbf{x}(n+1) - \mathbf{F}(\mathbf{x}(n))] \ . \tag{2.24}$$

Minimizing Eq. (2.24) for state estimation is also known in the geosciences as *weak-constraint 4D-Var* [34–37] and will be discussed more detailed in Sec. 2.3. The factors in front of the exponential functions in Eq. (2.20), Eq. (2.21), and Eq. (2.22) are constant and hence do not affect the minimizing trajectory $\{\hat{\mathbf{x}}(n)\}$. Since $C(\{\mathbf{x}(n)\})$ depends on the whole trajectory $\{\mathbf{x}(n)\}$ and not only on the initial values $\mathbf{x}(0)$, minimizing $C(\{\mathbf{x}(n)\})$ is a very high dimensional optimization problem.

Another approach to obtain statistical moments (expectation values, variances, ...) of the PDF Eq. (2.18) is by means of path integrals and Monte Carlo simulations [1, 14, 41, 42].

2.3 4D-Var

In Sec. 2.2 a statistical background for state estimation, based on Bayesian statistics, was presented. Finally, the cost function Eq. (2.24) was derived where the minimizing trajectory $\{\hat{\mathbf{x}}(n)\}$ maximizes the probability Eq. (2.18) and is hence considered as the solution of the state estimation problem.

Now we also want to estimate the model parameters in addition to the model states. Therefore, the model Eq. (2.19) and hence the cost function Eq. (2.24) additionally depend on the parameter vector $\mathbf{p} \in \mathbb{R}^{N_{\mathrm{p}}}$. Then, the (error free) model is given by

$$\mathbf{x}(n+1) = \mathbf{F}(\mathbf{x}(n), \mathbf{p}) \tag{2.25}$$

and the model including errors $\mathbf{u}(n)$ is given by

$$\mathbf{x}(n+1) = \mathbf{F}(\mathbf{x}(n), \mathbf{p}) + \mathbf{u}(n) \ , \tag{2.26}$$

so that the cost function is then given by

$$
\begin{aligned}
C(\{\mathbf{x}(n)\},\mathbf{p}) = \quad & \underbrace{\frac{1}{2}\sum_{n=0}^{N}[\boldsymbol{\eta}(n)-\mathbf{h}(\mathbf{x}(n))]^{\mathrm{tr}}\Sigma_{\epsilon}^{-1}[\boldsymbol{\eta}(n)-\mathbf{h}(\mathbf{x}(n))]}_{C_1} \\
& + \underbrace{\frac{1}{2}\sum_{n=0}^{N-1}[\mathbf{x}(n+1)-\mathbf{F}(\mathbf{x}(n),\mathbf{p})]^{\mathrm{tr}}\Sigma_{\mathrm{u}}^{-1}[\mathbf{x}(n+1)-\mathbf{F}(\mathbf{x}(n),\mathbf{p})]}_{C_2} \\
& + \underbrace{\frac{1}{2}[\mathbf{x}_b-\mathbf{x}(0)]^{\mathrm{tr}}\Sigma_{\mathrm{b}}^{-1}[\mathbf{x}_b-\mathbf{x}(0)]}_{C_3} \; . \qquad (2.27)
\end{aligned}
$$

The trajectory $\{\hat{\mathbf{x}}(n)\}$ and the parameters $\hat{\mathbf{p}}$ which minimize $C(\{\mathbf{x}(n)\},\mathbf{p})$ are considered as the solution of the state and parameter estimation problem. In the geosciences this state and parameter estimation algorithm is known as *weak-constraint 4D-Var* [34–37]. 'Weak-constraint' means here that the model equations at the solution $\{\hat{\mathbf{x}}(n)\}$ do not have to be fulfilled exactly. Errors in the model equations are allowed by $\mathbf{u}(n) \neq 0$ in Eq. (2.26). '4D' comes from the four dimensional atmospheric or oceanographic space (three space and one time dimension) and hence shows the origin of the name in the geosciences.

Its properties will be discussed in the following. Summand C_1 penalizes the difference between the output $\{\mathbf{h}(\mathbf{x}(n))\}$ and the (noisy) data $\{\boldsymbol{\eta}(n)\}$. The smaller the difference is, the closer the trajectory is to the data. Σ_ϵ is the covariance matrix of the measurement noise (see Eq. (2.13)). Often one has knowledge about the noise in the data and can hence define Σ_ϵ. It was already stated that model errors $\mathbf{u}(n)$ are allowed having the covariance matrix Σ_{u}. Model errors are penalized by the term C_2. The smaller C_2 is, the better the model equations are fulfilled. C_3 penalizes the difference between the initial values $\mathbf{x}(0)$ of the trajectory and the background $\mathbf{x}_b$. As mentioned in Sec. 2.2 $\mathbf{x}_b$ might be the final state or a short term prediction of a previous estimation window. Σ_{b} is the covariance matrix of its distribution. If one has no knowledge about $\mathbf{x}_b$, then one might drop this term by setting $C_3 = 0$. Minimizing $C(\{\mathbf{x}(n)\},\mathbf{p})$ is a very high dimensional optimization problem where a full trajectory and the model parameters (together $D\cdot(N+1)+N_{\mathrm{p}}$ quantities) have to be estimated.

Often models are given by ODEs instead of iterated maps. Then one can discretize the ODE (e.g. by Euler steps, or more accurate Runge-Kutta fourth order steps) and replace $\mathbf{F}(\mathbf{x}(n),\mathbf{p})$ in Eq. (2.26) by the discretization scheme.

It is also possible to formulate the cost function Eq. (2.27) in continuous time by using models given by ODEs and replacing the sums by integrals and minimize the cost function by solving the Euler-Lagrange equations [8, 13, 31]. This, however, has the disadvantage that parameter estimation would not be easily possible. An approach to estimate model parameters in the time continuous case is to interpret them as additional

model variables with the trivial dynamics

$$\dot{\mathbf{p}} = 0 \ . \tag{2.28}$$

One might also assume a perfect model, i.e. prohibit errors in the model equations by setting $\mathbf{u}(n) = 0$ in Eq. (2.26). Then, the state and parameter estimation problem is reduced to minimizing the cost function

$$\begin{aligned} C(\mathbf{x}(0), \mathbf{p}) = \quad & \underbrace{\frac{1}{2} \sum_{n=0}^{N} [\boldsymbol{\eta}(n) - \mathbf{h}(\mathbf{x}(n))]^{\mathrm{tr}} \Sigma_{\epsilon}^{-1} [\boldsymbol{\eta}(n) - \mathbf{h}(\mathbf{x}(n))]}_{C_1} \\ & + \underbrace{\frac{1}{2} [\mathbf{x}_b - \mathbf{x}(0)]^{\mathrm{tr}} \Sigma_{\mathrm{b}}^{-1} [\mathbf{x}_b - \mathbf{x}(0)]}_{C_3} \\ \text{subject to} \quad & \mathbf{x}(n+1) = \mathbf{F}(\mathbf{x}(n), \mathbf{p}) \ , \ n = 0, \ldots, N-1 \ . \end{aligned} \tag{2.29}$$

State and parameter estimation by minimizing Eq. (2.29) is also known as *strong constraint 4D-Var*[43, 44], where the addition 'strong constraint' comes from the fact that the model equations at the solution $\{\hat{\mathbf{x}}(n)\}$ have to be fulfilled exactly. As formulated here, minimizing Eq. (2.29) is a much lower dimensional optimization problem because only the initial values $\mathbf{x}(0)$ and the parameters $\mathbf{p}$, i.e. in total $D + N_{\mathrm{p}}$ quantities, have to be estimated. In the nonlinear dynamics community state and parameter estimation by minimizing a cost function like Eq. (2.29) is also known as a *single shooting* method [9]. Strong constraint 4D-Var has the disadvantage that the cost function can exhibit local minima when the length of the estimation window is getting larger. This is demonstrated in Ref. [38] using the Lorenz 63 model.

2.4 Relation to other chapters

Weak constraint 4D-Var, the state and parameter estimation algorithm discussed in Sec. 2.3, is based on minimizing the cost function Eq. (2.27). The fact that the entire model trajectory is estimated (and not only its initial values) in addition to the model parameters makes the optimization problem to solve very high dimensional ($\sim 10^5$ and more numerical values to estimate). Based on Bayesian statistics in Sec. 2.2 a probabilistic background is provided for weak constraint 4D-Var assuming Gaussian measurement noise in the data and Gaussian errors in the Markovian model.

To estimate variables and parameters of models given by ODEs an optimization based estimation method [33] similar to weak-constraint 4D-Var is used in the following chapters. The cost function suggested in Ref. [33] is revisited in Chap. 4, Eq. (5), Chap.7, Eq. (10), and Chap. 8, Eq. (33). In these chapters, the probabilistic background of the cost functions is not discussed. Instead, in each chapter the cost function is directly defined with the aim, on the one hand, to penalize the difference between the data and the model output (via measurement function) and, on the other hand, to penalize the

error in the model equations. In both cases the cost function is quadratic. Hence, the structure of the weak constraint 4D-Var cost function can be considered as a motivation of the cost functions used in Chap. 4, Chap.7, and Chap. 8.

In Chap. 4, Chap.7, and Chap. 8 the ODEs are discretized by a central difference approximation which requires an additional term in the cost function to enforce a smooth estimated trajectory by penalizing non-smooth trajectories via Hermite-interpolation [33]. Furthermore, another term is added to the cost function which enforces model parameters and the trajectory to stay in predefined bounds.

The focus of Chap. 4 is on the implementation of the optimization problem. Since minimizing the cost function is a very high dimensional optimization problem it is crucial to choose a suitable optimization algorithm. As in Ref. [33], the Levenberg-Marquardt (LM) optimization algorithm [45, 46] is used for minimizing the cost function. The LM algorithm requires a high dimensional Jacobian which, in our case, has a sparse structure (i.e. most elements of the Jacobian are always zero). A correct implementation of the Jacobian is important to obtain accurate estimates and a proper convergence of the LM algorithm. In Chap. 4 *automatic differentiation* (AD) [47, 48] is discussed and used to compute derivatives and sparsity patterns.

In Chap. 7 also the LM algorithm is used to minimize the cost function, where derivatives are computed by means of AD. The LM algorithm has to be initialized with an initial guess consisting of entire trajectories for all model variables and values for the model parameters. Therefore, among other things, different strategies of creating an initial guess are compared in Chap. 7 using a 9-dimensional chaotic Lorenz-96 model [49]. Furthermore, it is also investigated how the success of state and parameter estimation depends on the choice and the number of observed variables.

The focus of Chap. 8 is on a method for identifying redundant model parameters and variables, where the results are then verified by using the estimation method from Ref. [33].

In Chap. 9.4 the estimation method from Ref. [33] is used to estimate states and parameters of an experimentally observed time series from the electronic Shinriki oscillator. Before applying the estimation method, redundant model variables and parameters are identified and removed from the estimation problem.

3 Observability

State and parameter estimation methods, as the optimization based algorithm described in Sec. 2.3, are used to recover states and parameters of mathematical models based on experimentally measured data. Therefore, it is important to know if the observed signal contains enough information for a unique solution of the estimated quantities. If the same signal can be described sufficiently well (via a measurement function) using different state vectors or parameter values, then a unique reconstruction of these quantities is (almost) not possible. Ways to improve the accuracy of the estimates include to provide more data (e.g. measure more variables) or to reduce the number of parameters for estimation. Hence, knowing about the *observability* of a system can help to improve the experimental setup or the accuracy of state and parameter estimation.

The observability of linear systems was considered, for example, in Ref. [18–21]. It is a global (state independent) property and can be investigated by means of the *observability matrix*. Based on delay and derivative coordinates [50–53], the observability for linear maps and ODEs is revisited in Sec. 3.1 with a brief introduction to this topic.

In contrast, the observability of nonlinear systems, considered for example in [21–26], is often a local (state and parameter dependent) property only. As revisited in Sec. 3.2 for nonlinear ODEs, it can be computed based on derivative coordinates [25, 26, 54].

3.1 Observability in linear systems

Before considering the observability of nonlinear systems, it is useful to first consider the observability of linear systems [18–21, 23]. We start with a system of linear ODEs

$$\dot{\mathbf{x}}(t) = \mathbf{F}\mathbf{x}(t) \tag{3.1}$$

$$\mathbf{y}(t) = \mathbf{H}\mathbf{x}(t) \ , \tag{3.2}$$

where $\mathbf{x} = (x_1, \ldots, x_D)^{\mathrm{tr}} \in \mathbb{R}^D$ are the model variables and $\mathbf{F}$ is a known real $D \times D$ matrix. The measurement function Eq. (3.2) gives the linear relation between the model variables and the output column vector $\mathbf{y} \in \mathbb{R}^L$ of the system by the $L \times D$ matrix $\mathbf{H}$. The output $\mathbf{y}(t)$ of the system corresponds to a signal an experimentalist might measure when performing an experiment. If, for example, an experiment can be described by a $D = 4$ dimensional linear model and measured data from the experiment can be described by the second model variable, then one would choose $\mathbf{H} = \big(0, 1, 0, 0\big)$.

Next, we consider $D - 1$ time derivatives of the output $\mathbf{y}(t)$ ($\mathbf{y}^{(m)}(t)$ denotes the mth

time derivative),

$$\begin{aligned}
\mathbf{y}(t) &= \mathbf{H}\mathbf{x}(t) \\
\dot{\mathbf{y}}(t) &= \mathbf{H}\dot{\mathbf{x}}(t) = \mathbf{H}\mathbf{F}\mathbf{x}(t) \\
\ddot{\mathbf{y}}(t) &= \mathbf{H}\ddot{\mathbf{x}}(t) = \mathbf{H}\mathbf{F}\dot{\mathbf{x}}(t) = \mathbf{H}\mathbf{F}^2\mathbf{x}(t) \\
&\vdots \\
\mathbf{y}^{(D-1)}(t) &= \mathbf{H}\mathbf{F}^{D-1}\mathbf{x}(t) \ .
\end{aligned} \tag{3.3}$$

With $D_M = DL$ and the $D_M \times D$ *observability matrix*

$$\mathcal{O} = \begin{pmatrix} \mathbf{H} \\ \mathbf{H}\mathbf{F}^1 \\ \mathbf{H}\mathbf{F}^2 \\ \vdots \\ \mathbf{H}\mathbf{F}^{D-1} \end{pmatrix} \tag{3.4}$$

the set of linear equations Eq. (3.3) can be summarized to

$$\begin{pmatrix} \mathbf{y}(t) \\ \dot{\mathbf{y}}(t) \\ \vdots \\ \mathbf{y}^{(D-1)}(t) \end{pmatrix} = \mathcal{O} \cdot \mathbf{x}(t) \ . \tag{3.5}$$

If $\mathbf{x}(t)$ is a unique solution of Eq. (3.5), then the system is observable. Suppose one would experimentally measure $\{\mathbf{y}(t), \dot{\mathbf{y}}(t), \ldots, \mathbf{y}^{(D-1)}(t)\}$ and the system is observable. Then the state $\mathbf{x}(t)$ could be uniquely estimated from the measurement.

To find a condition for the uniqueness, suppose that two solutions $\mathbf{x}_1(t)$ and $\mathbf{x}_2(t)$ fulfill Eq. (3.5). Then we have (see Ref. [20, Chap. 6.2.1])

$$\mathcal{O}[\mathbf{x}_1(n) - \mathbf{x}_2(n)] = 0 \ . \tag{3.6}$$

If $\mathcal{O}$ has full rank D, then, according to the rank-nullity theorem [55, Chap. 2.6.1], the null space of $\mathcal{O}$ only contains the null vector. This implies $\mathbf{x}_1(t) = \mathbf{x}_2(t)$ and, therefore, $\mathbf{x}(t)$ in Eq. (3.5) is a unique solution. The states of the linear system Eq. (3.1) and Eq. (3.2) are observable if the observability matrix $\mathcal{O}$ has full rank [20, 23].

Next, we consider a linear discrete map,

$$\mathbf{x}(n+1) = \mathbf{F}\mathbf{x}(n) \tag{3.7}$$

$$\mathbf{y}(n) = \mathbf{H}\mathbf{x}(n) \ , \tag{3.8}$$

with the model variable $\mathbf{x} = (x_1, \ldots, x_D)^{\mathrm{tr}} \in \mathbb{R}^D$, the known $D \times D$ matrix $\mathbf{F}$, and the $L \times D$ measurement matrix $\mathbf{H}$.

To specify a criterion for observability in linear maps, we first consider m iterations

of the model Eq. (3.7)

$$\mathbf{x}(n+m) = \mathbf{F}^m \mathbf{x}(n) \ , \tag{3.9}$$

where $\mathbf{F}^m = \mathbf{F} \cdot \mathbf{F} \cdot \ldots$ are m matrix multiplications of $\mathbf{F}$. Next, we consider $D-1$ iterations of the model and its output,

$$\begin{aligned} \mathbf{y}(n) &= \mathbf{H}\mathbf{x}(n) \\ \mathbf{y}(n+1) &= \mathbf{H}\mathbf{F}^1\mathbf{x}(n) \\ \mathbf{y}(n+2) &= \mathbf{H}\mathbf{F}^2\mathbf{x}(n) \\ &\vdots \\ \mathbf{y}(n+D-1) &= \mathbf{H}\mathbf{F}^{D-1}\mathbf{x}(n) \ . \end{aligned} \tag{3.10}$$

With $D_M = DL$ and the $D_M \times D$ observability matrix

$$\mathcal{O} = \begin{pmatrix} \mathbf{H} \\ \mathbf{H}\mathbf{F}^1 \\ \mathbf{H}\mathbf{F}^2 \\ \vdots \\ \mathbf{H}\mathbf{F}^{D-1} \end{pmatrix} \tag{3.11}$$

the set of linear equations Eq. (3.10) can be summarized to

$$\begin{pmatrix} \mathbf{y}(n) \\ \mathbf{y}(n+1) \\ \vdots \\ \mathbf{y}(n+D-1) \end{pmatrix} = \mathcal{O} \cdot \mathbf{x}(n) \ . \tag{3.12}$$

As in the case of linear ODEs the state vector $\mathbf{x}(n)$ can be uniquely determined from $\mathbf{y}(n)$ and its time delays if $\mathcal{O}$ has full rank. Note, that $\mathcal{O}$ in Eq. (3.11) has a similar structure as $\mathcal{O}$ in Eq. (3.4). If $\mathcal{O}$ has full rank, then the system is globally observable (globally because $\mathcal{O}$ is independent of a specific $\mathbf{y}(t)$ and $\mathbf{x}(t)$).

3.2 Observability in nonlinear ODEs

In the following the observability analysis for nonlinear systems will be considered [21–26, 54]. The nonlinear system is given by ODEs,

$$\dot{\mathbf{x}}(t) = \mathbf{F}(\mathbf{x}(t)) \tag{3.13}$$

$$\mathbf{y}(t) = \mathbf{h}(\mathbf{x}(t)) \ , \tag{3.14}$$

with the model variables $\mathbf{x} \in \mathbb{R}^D$, and the output of the system $\mathbf{y} \in \mathbb{R}^L$. To analyze the observability of this nonlinear system, as in [25, 26], time derivatives of $\mathbf{y}(t)$ are derived,

$$\begin{aligned}
\mathbf{y}(t) &= \mathbf{h}(\mathbf{x}(t)) \\
\dot{\mathbf{y}}(t) &= \frac{\mathrm{d}\mathbf{h}(\mathbf{x}(t))}{\mathrm{d}t} = \frac{\partial \mathbf{h}(\mathbf{x}(t))}{\partial \mathbf{x}} \frac{\mathrm{d}\mathbf{x}(t)}{\mathrm{d}t} = \frac{\partial \mathbf{h}(\mathbf{x}(t))}{\partial \mathbf{x}} \mathbf{F}(\mathbf{x}(t)) \\
\ddot{\mathbf{y}}(t) &= \frac{\mathrm{d}}{\mathrm{d}t}\left[\frac{\partial \mathbf{h}(\mathbf{x}(t))}{\partial \mathbf{x}} \mathbf{F}(\mathbf{x}(t))\right] = \frac{\partial}{\partial \mathbf{x}}\left[\frac{\partial \mathbf{h}(\mathbf{x}(t))}{\partial \mathbf{x}} \mathbf{F}(\mathbf{x}(t))\right] \frac{\mathrm{d}\mathbf{x}(t)}{\mathrm{d}t} \\
&= \frac{\partial}{\partial \mathbf{x}}\left[\frac{\partial \mathbf{h}(\mathbf{x}(t))}{\partial \mathbf{x}} \mathbf{F}(\mathbf{x}(t))\right] \mathbf{F}(\mathbf{x}(t)) \\
\dddot{\mathbf{y}}(t) &= \frac{\partial}{\partial \mathbf{x}}\left[\frac{\partial}{\partial \mathbf{x}}\left[\frac{\partial \mathbf{h}(\mathbf{x}(t))}{\partial \mathbf{x}} \mathbf{F}(\mathbf{x}(t))\right] \mathbf{F}(\mathbf{x}(t))\right] \mathbf{F}(\mathbf{x}(t)) \\
&\vdots \quad ,
\end{aligned} \tag{3.15}$$

where $\partial/\partial \mathbf{x}$ applied to a vector valued function denotes the Jacobian of the function with respect to $\mathbf{x}$. The recursion in Eq. (3.15) motivates to define the *Lie derivatives* [25, 26]

$$\mathcal{L}_{\mathrm{F}}^{k} \mathbf{h}(\mathbf{x}(t)) = \frac{\partial}{\partial \mathbf{x}}\left[\mathcal{L}_{\mathrm{F}}^{k-1} \mathbf{h}(\mathbf{x}(t))\right] \mathbf{F}(\mathbf{x}(t)) \quad \text{with} \quad \mathcal{L}_{\mathrm{F}}^{0} \mathbf{h}(\mathbf{x}(t)) = \mathbf{h}(\mathbf{x}(t)) \ . \tag{3.16}$$

Based on the definition of the Lie derivatives, with $D_M = L \cdot K$ and by summarizing the $K-1$ time derivatives of $\mathbf{y}(t)$, see Eq. (3.15), we define the *derivative coordinate map* [25, 26, 51]

$$G : \mathbb{R}^D \to \mathbb{R}^{D_M} \ , \quad \mathbf{x} \mapsto \mathbf{G}(\mathbf{x}) \tag{3.17}$$

with

$$\mathbf{G}(\mathbf{x}(t)) = \begin{pmatrix} \mathbf{y}(t) \\ \dot{\mathbf{y}}(t) \\ \ddot{\mathbf{y}}(t) \\ \vdots \\ \mathbf{y}^{(K-1)} \end{pmatrix} = \begin{pmatrix} \mathcal{L}_{\mathrm{F}}^{0} \mathbf{h}(\mathbf{x}(t)) \\ \mathcal{L}_{\mathrm{F}}^{1} \mathbf{h}(\mathbf{x}(t)) \\ \mathcal{L}_{\mathrm{F}}^{2} \mathbf{h}(\mathbf{x}(t)) \\ \vdots \\ \mathcal{L}_{\mathrm{F}}^{(K-1)} \mathbf{h}(\mathbf{x}(t)) \end{pmatrix} \ . \tag{3.18}$$

The function $\mathbf{G}(\mathbf{x}(t))$ tells us how the output $\mathbf{y}(t)$ of the system and its time derivatives depend on $\mathbf{x}(t)$. If $\mathbf{x}(t)$ can be uniquely reconstructed from $\mathbf{G}(\mathbf{x}(t))$, that is, from $\mathbf{y}(t)$ and its (higher) time derivatives (which are assumed to be experimentally accessible), then the system is observable at $\mathbf{x}(t)$ [56]. In other words, if G is uniquely invertible at $\mathbf{x}(t)$, then the system is *locally observable* at $\mathbf{x}(t)$. The invertibility can be investigated by means of the rank of the Jacobian matrix $\mathrm{D}\mathbf{G}(\mathbf{x})$ (see also Sec. 6.I). If the Jacobian has full rank, then G is locally invertible, and therefore the system is locally observable at $\mathbf{x}(t)$.

Model parameters $\mathbf{p}$ could be included in the observability analysis, if one interprets

them as additional model variables with the model equations

$$\dot{\mathbf{p}} = 0 \ . \tag{3.19}$$

3.3 Relation to other chapters

In Sec. 3.1 and Sec. 3.2 the concept of observability was introduced for linear and nonlinear systems. It was stated that for nonlinear ODEs the local invertibility of the derivative coordinate map Eq. (3.17) is a criterion for observability. An advantage of using derivative coordinates is that the map and its Jacobian matrix often can be derived analytically. Nevertheless, due to the recursively defined Lie derivatives in Eq. (3.17) the size of terms involved, when deriving higher order time derivatives, is often growing rapidly. This might make it difficult to compute them in practice. Furthermore, in the observability analysis presented in Sec. 3.1 and Sec. 3.2, statements are only made for whole systems. The question how accurate individual model variables (or parameters) can be reconstructed is not addressed.

This point is the main issue of Chap. 5 and Chap. 6. Based on the concept of observability, a local measure is suggested which quantifies how accurate model variables and parameters can be reconstructed from the measured signal. Instead of using a derivative coordinate map Eq. (3.17), the analysis is based on delay coordinates. An increase of the dimension of the delay reconstruction map is, in principle, possible without running into the previously mentioned problems regarding large terms when using time derivative coordinates.

Additionally, the analysis suggested in Chap. 5 and Chap. 6 is applied in Chap. 7 to Chap. 9 where the obtained results are, partially, compared to results from state and parameter estimation.

Furthermore, the delay reconstruction map provides the basis for the analysis in Chap. 8. The aim is to provide a method which can be used to identify locally redundant model variables and parameters.

4 Nonlinear system identification employing automatic differentiation

The following pages contain the article

> J. Schumann-Bischoff, S. Luther, and U. Parlitz. "Nonlinear system identification employing automatic differentiation". In: *Commun. Nonlinear. Sci. Numer. Simul.* 18.10 (Oct. 2013), pp. 2733–2742. DOI: 10.1016/j.cnsns.2013.02.017.

The content of this paper was of my own conceptual design. This includes the selection and combination of the used methods. I planned, developed, performed, and analyzed all simulations for this article. I designed and created all figures, tables, and the listings in this article. Furthermore, I wrote the text of Sec. 2 to Sec. 6 which was then revised by the other authors. The abstract, Sec. 1 ('Introduction'), and Sec. 7 ('Conclusion') were written collaboratively with the other authors.

Commun Nonlinear Sci Numer Simulat 18 (2013) 2733–2742

Contents lists available at SciVerse ScienceDirect

Commun Nonlinear Sci Numer Simulat

journal homepage: www.elsevier.com/locate/cnsns

Nonlinear system identification employing automatic differentiation

Jan Schumann-Bischoff, Stefan Luther, Ulrich Parlitz *

Max Planck Institute for Dynamics and Self-Organization, Am Faßberg 17, 37077 Göttingen, Germany
Institute for Nonlinear Dynamics, Georg-August-Universität Göttingen, Am Faßberg 17, 37077 Göttingen, Germany
DZHK (German Center for Cardiovascular Research), Partner Site Göttingen, and Heart Research Center Göttingen, D-37077 Göttingen, Germany

ARTICLE INFO

Article history:
Received 1 November 2012
Received in revised form 26 February 2013
Accepted 28 February 2013
Available online 15 March 2013

Keywords:
Nonlinear modelling
Parameter estimation
Delay differential equations
Data assimilation

ABSTRACT

An optimization based state and parameter estimation method is presented where the required Jacobian matrix of the cost function is computed via automatic differentiation. Automatic differentiation evaluates the programming code of the cost function and provides exact values of the derivatives. In contrast to numerical differentiation it is not suffering from approximation errors and compared to symbolic differentiation it is more convenient to use, because no closed analytic expressions are required. Furthermore, we demonstrate how to generalize the parameter estimation scheme to delay differential equations, where estimating the delay time requires attention.

1. Introduction

For many processes in physics or other fields of science mathematical models exist (in terms of differential equations, for example), but not all state variables are easily accessible (measurable) and proper values of model parameters may be (partly) unknown. In particular, detailed biological cell models (e.g., cardiac myocytes [1]) may include many variables which are difficult to access experimentally and, in addition, depend on up to hundreds of physical parameters whose values have to be determined. To estimate unobserved variables (as a function of time) and model parameters different identification methods have been devised [2–14,16–18,20,19]. These methods have in common that an attempt is made to adjust the model output (in general a function of the state variables) to some (experimentally) observed time series. To achieve agreement, unobserved variables and unknown model parameters are suitably adjusted such that the model reproduces and follows the observed time series. In geosciences and meteorology (e.g., whether forecasting) this procedure is often called *data assimilation* and describes the process of incorporating new (incoming) data into a computer model of the real system.

A general framework for state estimation provides, for example, the path integral formalism including a saddle point approximation [15,16]. This formalism can be used to state the estimation problem as an optimization problem [19,12–14,18]. If an optimization method is employed that is based on gradient descent (such as the well-known Levenberg–Marquard method [21,22]), in general the Jacobian matrix of the cost function has to be provided, whose derivation may be quite cumbersome (and error-prone), depending on the structure of the cost function and the underlying mathematical model of the dynamical system. To estimate the Jacobian matrix one may approximate it by numerical derivatives (often spoiled by unacceptably large truncation errors) or use symbolic mathematics, which requires, however, that the function to be derived has to be given in closed form.

* Corresponding author at: Max Planck Institute for Dynamics and Self-Organization, Am Faßberg 17, 37077 Göttingen, Germany. Tel.: +49 551 5176 369.
E-mail addresses: jan.schumann-bischoff@ds.mpg.de (J. Schumann-Bischoff), stefan.luther@ds.mpg.de (S. Luther), ulrich.parlitz@ds.mpg.de (U. Parlitz).

1007-5704/$ - see front matter © 2013 Elsevier B.V. All rights reserved.
http://dx.doi.org/10.1016/j.cnsns.2013.02.017

A convenient alternative to both of these methods is *automatic differentiation* [24] where exact numerical values of the required derivatives are computed by analyzing a given source code implementation of the cost function. As will be shown here automatic differentiation leads in this context not only to a very flexible and efficient algorithm for computing the required Jacobian but also provides the sparsity pattern of the Jacobian which is exploited by suitable optimization methods. In Section 2 we will give a formal description of the optimization problem to be solved for state and parameter estimation. Then we briefly present in Section 3 the concept of automatic differentiation in the form used here. As an illustrative example we show in Section 4 how to estimate the model parameters of the Lorenz-96 model. In Section 5 we discuss how to estimate the delay time in delay differential equations and provide in Section 6 an example (Mackey–Glass model).

2. State and parameter estimation method

The method used here to adapt a model to a time series is based on minimizing a cost function and was introduced in Ref. [19]. For completeness we present in the following an extended version covering also delay differential equations (DDEs).

We assume that a multivariate R-dimensional time series $\{\boldsymbol{\eta}(n)\}$ is given consisting of $N+1$ samples $\boldsymbol{\eta}(n)\hat{=}\boldsymbol{\eta}(t_n)\in\mathbb{R}^R$ measured at times $\mathcal{T}=\{t_n=n\cdot\Delta t|n=0,1,\ldots,N\}$. For simplicity the observation times t_n are equally spaced (with a fixed time step Δt) and start at $t_0=0$. The estimation method can easily be extended to nonuniformly sampled observations (see Ref. [19]). Here we consider the general case of a model given by a set of coupled delay differential equations (DDEs)

$$\frac{\mathrm{d}\boldsymbol{y}(t)}{\mathrm{d}t}=\boldsymbol{F}(\boldsymbol{y}(t),\boldsymbol{y}_\tau(t),\boldsymbol{p},t), \tag{1}$$

with $\boldsymbol{y}_\tau(t)=\boldsymbol{y}(t-\tau)$. The state vector (s) $\boldsymbol{y}(t)=(y_1(t),\ldots,y_D(t))^{\mathrm{T}}$, the delay parameter $\tau\in\mathbb{R}$ and the U model parameters $\boldsymbol{p}=(p_1,\ldots,p_U)^{\mathrm{T}}$ are unknown and have to be estimated from the time series $\{\boldsymbol{\eta}(n)\}$. Estimating τ can not be conducted as estimating $\boldsymbol{p}$, because $\boldsymbol{F}(\boldsymbol{y}(t),\boldsymbol{y}_\tau(t),\boldsymbol{p},t)$ does *not* explicitly depend on τ. In fact $\boldsymbol{F}(\boldsymbol{y}(t),\boldsymbol{y}_\tau(t),\boldsymbol{p},t)$ depends on $\boldsymbol{y}_\tau(t)$ which is a function of τ. We shall later come back to this topic.

Note that (1) also describes (as a special case) models given by coupled ordinary differential equations (ODEs). In this case the right-hand side of (1) is independent of $\boldsymbol{y}_\tau(t)$ and thus can be replaced by $\boldsymbol{F}(\boldsymbol{y}(t),\boldsymbol{p},t)$ (see Ref. [19] for details).

To estimate the unknown quantities a measurement function

$$\boldsymbol{z}(t)=\boldsymbol{h}(\boldsymbol{y}(t),\boldsymbol{q},t), \tag{2}$$

is required to represent the relation between model states $\boldsymbol{y}(t)$ and the $\boldsymbol{z}(t)$ corresponding to the observations $\{\boldsymbol{\eta}(n)\}$. This measurement function may contain V additional unknown parameters $\boldsymbol{q}=(q_1,\ldots,q_V)^{\mathrm{T}}$ that also have to be estimated using information from the given time series $\{\boldsymbol{\eta}(n)\}$.

2.1. Cost function

The goal of the estimation process is to find a set of values for all unknown quantities such that the model equations provide via measurement function (2) a model times series $\{\boldsymbol{z}(t_n)\}$ that matches the experimental time series $\{\boldsymbol{\eta}(t_n)\}$. In other words, the average difference between $\boldsymbol{\eta}(t_n)$ and $\boldsymbol{z}(t_n)$ should be small. Furthermore, the model equations should be fulfilled as well as possible. This means that modeling errors $\boldsymbol{u}(t)$ are allowed, but should be small. Therefore, model (1) is extended to

$$\frac{\mathrm{d}\boldsymbol{y}(t)}{\mathrm{d}t}=\boldsymbol{F}(\boldsymbol{y}(t),\boldsymbol{y}_\tau(t),\boldsymbol{p},t)+\boldsymbol{u}(t). \tag{3}$$

The smaller $\boldsymbol{u}(t)$ is the better the model Eq. (1) are fulfilled. Next, for simplicity, $\boldsymbol{u}(t)$ and $\boldsymbol{y}(t)$ will be discretized at the times in $\mathcal{T}$. This means that $\boldsymbol{y}(t)$ will be sampled at the same time when data are observed. With $\boldsymbol{y}(n)\hat{=}\boldsymbol{y}(n\cdot\Delta t)\hat{=}\boldsymbol{y}(t_n)$ and $\mathcal{Y}(a,b)=\{\boldsymbol{y}(n)|n=a,a+1,\ldots,b\}$ the set of values of the discretized model variables can be written as $\mathcal{Y}(0,N)$. The quantities in $\mathcal{Y}(0,N)$ have to be estimated in addition to $\boldsymbol{p}$ and $\boldsymbol{q}$. With the same discretization we have $\{\boldsymbol{u}(n)\}=\{\boldsymbol{u}(t_n)\}$. At this point we assume a fixed (not to be estimated) delay $\tau=k\cdot\Delta t$ with $k\in\mathbb{N}$ which is not necessarily equal to the delay parameter of the physical process underlying the data. This simplifies the discretization of the delayed variable to $\boldsymbol{y}_\tau(t)=\boldsymbol{y}(n\cdot\Delta t-k\cdot\Delta t)=\boldsymbol{y}((n-k)\cdot\Delta t)=\boldsymbol{y}(n-k)=\boldsymbol{y}_k(n)$. The set of the discretized delayed variable is then $\mathcal{Y}_k(0,N)=\mathcal{Y}(-k,N-k)$. Note that $\mathcal{Y}(-k,N-k)=\mathcal{Y}(-k,-1)\cup\mathcal{Y}(0,N-k)$. Since $\mathcal{Y}(0,N-k)\subset\mathcal{Y}(0,N)$, $\mathcal{Y}(0,N-k)$ contains no additional quantities to be determined. Only the variables in $\mathcal{Y}(-k,-1)$ are additional quantities which have to be estimated. Typically the delay time is much shorter than the length of the time series $N\cdot\Delta t$ and hence the number of elements in $\mathcal{Y}(-k,-1)$ is much smaller than in $\mathcal{Y}(0,N)$. Therefore the number of quantities to be estimated does not increase much compared to a model given by ODEs (with similar D and N) where $\mathcal{Y}(-k,-1)$ has not to be estimated.

The discretization of (3) is then given by

$$\boldsymbol{u}(n)\approx\left.\frac{\Delta\boldsymbol{y}}{\Delta t}\right|_{t_n}-\boldsymbol{F}(\boldsymbol{y}(n),\boldsymbol{y}_k(n),\boldsymbol{p},t_n), \tag{4}$$

whereas the symbol $\frac{\Delta \boldsymbol{y}}{\Delta t}\big|_{t_n}$ stands for the finite difference approximation of $\frac{\mathrm{d}\boldsymbol{y}(t)}{\mathrm{d}t}$ at time t_n. The goal of the adaption process is to minimize (on average) the norm of $\boldsymbol{u}(n)$ *and* the norm of the difference $\boldsymbol{\eta}(t_n) - \boldsymbol{z}(t_n)$.

This leads to a cost function

$$C(\mathcal{Y}(-k,N),\boldsymbol{p},\boldsymbol{q}) = C_1 + C_2 + C_3 + C_4, \tag{5}$$

with

$$C_1 = \frac{\alpha}{N}\cdot\sum_{n=0}^{N}(\boldsymbol{\eta}(n)-\boldsymbol{z}(n))^{\mathrm{T}}\boldsymbol{A}(\boldsymbol{\eta}(n)-\boldsymbol{z}(n)), \tag{6}$$

$$C_2 = \frac{1-\alpha}{N}\cdot\sum_{n=0}^{N}\boldsymbol{u}(n)^{\mathrm{T}}\boldsymbol{B}\boldsymbol{u}(n), \tag{7}$$

$$C_3 = \frac{1-\alpha}{N}\cdot\sum_{n=3}^{N-2}(\boldsymbol{y}_{\mathrm{apr}}(n)-\boldsymbol{y}(n))^{\mathrm{T}}\boldsymbol{E}(\boldsymbol{y}_{\mathrm{apr}}(n)-\boldsymbol{y}(n)), \tag{8}$$

$$C_4 = \frac{\beta}{L}\cdot\boldsymbol{q}(\boldsymbol{w},\boldsymbol{w}_{\mathrm{l}},\boldsymbol{w}_{\mathrm{u}})^{\mathrm{T}}\cdot\boldsymbol{q}(\boldsymbol{w},\boldsymbol{w}_{\mathrm{l}},\boldsymbol{w}_{\mathrm{u}}). \tag{9}$$

C_1 penalizes the difference between $\boldsymbol{\eta}(n)$ and $\boldsymbol{z}(n)$ whereas C_2 penalizes large magnitudes of $\boldsymbol{u}(n)$. A, B, and E are weight matrices that will be specified later. At the minimum of (5) the solution $(\hat{\mathcal{Y}}(-k,N),\hat{\boldsymbol{p}},\hat{\boldsymbol{q}})$ is obtained which is considered as the solution of the estimation problem. In the term C_3 a Hermite interpolation is performed to determine $\boldsymbol{y}_{\mathrm{apr}}(n)$ from neighboring points and the time derivatives which are, according to (3), given by

$$\boldsymbol{G}(\boldsymbol{y}(t),\boldsymbol{y}_\tau(t),\boldsymbol{p},t) = \boldsymbol{F}(\boldsymbol{y}(t),\boldsymbol{y}_\tau(t),\boldsymbol{p},t) + \boldsymbol{u}(t). \tag{10}$$

With Eq. (10) the Hermite interpolation reads

$$\begin{aligned}\boldsymbol{y}_{\mathrm{apr}}(n) = {}& \frac{11}{54}[\boldsymbol{y}(n-2)+\boldsymbol{y}(n+2)] + \frac{8}{27}[\boldsymbol{y}(n-1)+\boldsymbol{y}(n+1)] + \frac{\Delta t}{18}[\boldsymbol{G}(\boldsymbol{y}(n-2),\boldsymbol{y}_k(n-2),\boldsymbol{p},t_{n-2})\\ & - \boldsymbol{G}(\boldsymbol{y}(n+2),\boldsymbol{y}_k(n+2),\boldsymbol{p},t_{n+2})] + \frac{4\Delta t}{9}[\boldsymbol{G}(\boldsymbol{y}(n-1),\boldsymbol{y}_k(n-1),\boldsymbol{p},t_{n-1}) - \boldsymbol{G}(\boldsymbol{y}(n+1),\boldsymbol{y}_k(n+1),\boldsymbol{p},t_{n+1})].\end{aligned} \tag{11}$$

Smoothness of $\mathcal{Y}(0,N)$ is enforced by small differences $\boldsymbol{y}_{\mathrm{apr}}(n) - \boldsymbol{y}(n)$. The term C_3 suppresses non-smooth (oscillating) solutions which may occur without this term in the cost function. Let

$$\boldsymbol{w} = (\mathcal{Y}(0,N),\mathcal{Y}(-k,-1),\boldsymbol{p},\boldsymbol{q}) = (\mathcal{Y}(-k,N),\boldsymbol{p},\boldsymbol{q}) = (w_1,\ldots,w_L), \tag{12}$$

be a vector containing all quantities to be estimated.[1] Again, if the model is given by ODEs, $\mathcal{Y}(-k,-1)$ does not occur in $\boldsymbol{w}$. Hence for ODEs we obtain

$$\boldsymbol{w} = (\mathcal{Y}(0,N),\boldsymbol{p},\boldsymbol{q}). \tag{13}$$

To force $\boldsymbol{w}$ to stay between the lower and upper bounds $\boldsymbol{w}_{\mathrm{l}}$ and $\boldsymbol{w}_{\mathrm{u}}$, respectively, $\boldsymbol{q}(\boldsymbol{w},\boldsymbol{w}_{\mathrm{l}},\boldsymbol{w}_{\mathrm{u}}) = (q_1,\ldots,q_L)^{\mathrm{T}}$ is defined as

$$q_i(w_i,w_{\mathrm{l},i},w_{\mathrm{u},i}) = \begin{cases} w_{\mathrm{u},i} - w_{\mathrm{i}} & \text{for} \quad w_i \geqslant w_{\mathrm{u},i} \\ 0 & \text{for} \quad w_{\mathrm{l},i} < w_{\mathrm{i}} < w_{\mathrm{u},i} \\ w_{\mathrm{l},i} - w_{\mathrm{i}} & \text{for} \quad w_i \leqslant w_{\mathrm{l},i}, \end{cases} \tag{14}$$

q_i is zero if the value of w_i lies within its bounds. To enforce this, the positive parameter β is set to a large number, e.g., 10^5. In this paper the matrices $\boldsymbol{A}$, $\boldsymbol{B}$ and $\boldsymbol{E}$ are diagonal matrices. The diagonal elements can be used for an individual weighting.

The homotopy parameter α can be used to adjust whether the solution should be close to data ($\alpha \approx 1$) or have a smaller error in fulfilling the model equations (see Ref. [18]). In [20] a possible technique is described to find an optimal α. Furthermore one might use continuation (see Ref. [18]) where α is stepwise decreased. Starting with $\alpha \approx 1$ results in a solution close to the data. Then, α is slightly decreased and the previously obtained solution is used as an initial guess and the cost function is be optimized again. This procedure is repeated until the value $\alpha = 0.5$ is reached.

Note that the cost function can be written in the form

$$C(\boldsymbol{w}) = \sum_{j=1}^{J} H_j(\boldsymbol{w})^2 = \|\boldsymbol{H}(\boldsymbol{w})\|_2^2, \tag{15}$$

where $\boldsymbol{H}(\boldsymbol{w})$ is a high dimensional vector valued function of the high dimensional vector $\boldsymbol{w}$. To optimize (15) we use an implementation of the Levenberg–Marquardt algorithm [21,22] called `sparseLM` [23]. Although $C(\boldsymbol{w})$ will be optimized, `sparseLM` requires $\boldsymbol{H}(\boldsymbol{w})$ and the sparse Jacobian of $\boldsymbol{H}(\boldsymbol{w})$ as input. In the next section we discuss how to derive the Jacobian and its sparsity structure.

[1] Here we assume that a fixed but arbitrary rule is used to order the elements of the sets $\mathcal{Y}(0,N)$ and $\mathcal{Y}(-k,-1)$ to define the elements of the vector $\boldsymbol{w}$.

3. Automatic differentiation

The technique used here to estimate the variables and the parameters of a model from time series is based on minimizing the cost function (5) which can be written in the form of Eq. (15). The Levenberg–Marquardt algorithm used to minimize this cost function needs the vector valued function $\boldsymbol{H}(\boldsymbol{w})$ and its Jacobian $\partial\boldsymbol{H}/\partial\boldsymbol{w}$ with the elements $\partial H_j/\partial w_l$ as input. Remember that the Jacobian has a sparse structure, i.e. it has many elements which are always zero. To compute this sparse Jacobian there exist three different techniques: *numerical differentiation*, *symbolic differentiation* and *automatic differentiation* (symbolic differentiation includes differentiation by hand). These techniques have particular advantages and disadvantages. *Numerical differentiation* is easy to implement, but numerically not exact. Furthermore, the sparsity pattern can not be detected reliably. *Symbolic differentiation* is numerically exact, but the function to be differentiated has to be available as a single expression. Deriving the Jacobian by hand usually is very error prone. Symbolic differentiation tools may help at this point, however, a change in the cost function requires deriving a new Jacobian. As an alternative the concept of *automatic differentiation* can be used. It is easy to implement, numerically exact and the sparsity pattern of the Jacobian can be detected automatically. Only the source code of the cost function is required by the automatic differentiation tool. Using automatic differentiation requires additional computational resources.

After weighing up the pros and cons of the discussed methods for computing the Jacobian we came to the conclusion that the concept of automatic differentiation is the most suitable one. Automatic differentiation is used here in terms of the tool (library) ADOL-C [25,26]. ADOL-C provides functions to derive the numerical values of the Jacobian $\partial\boldsymbol{H}/\partial\boldsymbol{w}$ of the function $\boldsymbol{H}(\boldsymbol{w})$. Furthermore the sparsity pattern of $\partial\boldsymbol{H}/\partial\boldsymbol{w}$ can be detected and the numerical values of the non-vanishing elements can be derived (this functionality requires the graph coloring package ColPack [27]).

We used the Python interface [31] to ADOL-C wrapping functions of the ADOL-C library to Python. The advantage of using the Python interface instead of the C interface is that the cost function can be coded directly in Python using [30] arrays. ADOL-C is based on operator overloading. This means, that for computing the Jacobian the function to be differentiated has to be available as source code, only, with an input $\boldsymbol{w}$ and return $\boldsymbol{H}(\boldsymbol{w})$. For evaluating the cost function usually the elements of $\boldsymbol{w}$ have a numerical data type (e.g., integer, float, ...).

Typically deriving the sparsity pattern takes much more time than computing the non-zero values. However, this is more or less negligible because the detection of the sparsity pattern only has to be performed once, whereas the computation of the values of the non-zero elements occurs several times (always when the Jacobian has to be computed for a certain input $\boldsymbol{w}$, usually in each iteration of a numerical minimization routine).

For the examples in Sections 4 and 6 the time needed by ADOL-C used for computing the Jacobian of Eq. (15) was compared with the time needed by the used minimization routine (sparseLM) and the results are shown in Table 1. It turned out that the time needed by ADOL-C is much shorter than the time needed by sparseLM, i.e. the time needed to evaluate the cost function is negligible. Hence using ADOL-C does not lead to a significant increase of CPU time needed to solve the estimation problem.

4. Lorenz-96 model

As described in Section 2 the estimation method can be used to adapt a system of ODEs to a time series (without time delay). As our first example we use the Lorenz-96 model that was introduced by E. Lorenz in 1996 [28]. Here the $D = 80$ dimensional system is used given by the set of ODEs

$$\frac{\mathrm{d}y_i(t)}{\mathrm{d}t} = y_{i-1}(t)\cdot(y_{i+1}(t) - y_{i-2}(t)) - y_i(t) + p, \tag{16}$$

whereas $i = 1,\ldots,D$ is a cyclic index. This means that for $i = D$ it is $\boldsymbol{y}_{i+1} = \boldsymbol{y}_1$. For $i = 1$ it is $i - 1 = D$ and $i - 2 = D - 1$. To compare the results from the estimation process a twin experiment is performed. The time series $\{\boldsymbol{\eta}(t_n)\}$ with $t_n \in \{0, 0.01, 0.02, \ldots, 10\}$ is generated by integrating a similar model

$$\frac{\mathrm{d}x_i(t)}{\mathrm{d}t} = x_{i-1}(t)\cdot(x_{i+1}(t) - x_{i-2}(t)) - x_i(t) + 8.17, \tag{17}$$

Table 1
CPU times needed for evaluation of the values of the sparse Jacobian compared to the CPU time needed by the optimization routine. For the Mackey–Glass model only the CPU time for $\tau \in [2.3, 2.4]$ from the **second step** of estimating the delay time is shown. The time values were measured on a 1.3 GHz Dual core computer with 3 GB memory.

Example:	Mackey–Glass model	80-dim Lorenz96 system
Section	6	4
CPU time for:		
cost function calls	1.07 s	31.8 s
Jacobian calls (ADOL-C)	2.34 s	155 s
optimizer (sparseLM)	3.14 s	21845 s

with the same dimension and cyclic index and taking the solution to build a noisy $R = D/2 = 40$ dimensional multivariate time series by "observing" every second model variable,

$$\boldsymbol{\eta}_{\mathrm{ts}}(t_n) = (x_1(t_n), x_3(t_n), x_5(t_n), \ldots x_{D-1}(t_n)). \tag{18}$$

A common type of noise in experimentally observed time series is white noise which is given by normally distributed random numbers with a variance σ^2 and a mean which is zero. Adding the noise to the clean time series we obtain a noisy multivariate time series

$$\boldsymbol{\eta}(t_n) = \boldsymbol{\eta}_{\mathrm{ts}}(t_n) + \boldsymbol{r}(t_n), \quad \boldsymbol{r}(t_n) = (r_1(t_n), r_2(t_n), \ldots, r_R(t_n)) \quad \text{with} \quad r_i(t_n) \sim \mathcal{N}(0, \sigma^2), \tag{19}$$

which is typical for experiments with measurement noise. To quantify the power of the clean signal and the noise one can define the signal-to-noise-ratio (SNR in dB) for each time series as

$$\mathrm{SNR}(\{\eta_i(t_n)\}) = 10 \cdot \log_{10}\left(\frac{\sum_{n=0}^{N+1}(\eta_{\mathrm{ts},i}(t_n) - \overline{\eta}_{\mathrm{ts},i})^2}{\sum_{n=0}^{N+1} r_i(t_n)^2}\right), \tag{20}$$

(the overbar denotes the mean). The smaller the SNR the more measurement noise is present.

In this example the observed time series is given by

$$\boldsymbol{\eta}(t_n) = (x_1(t_n), x_3(t_n), x_5(t_n), \ldots x_{D-1}(t_n)) + \boldsymbol{r}(0, 1.0), \tag{21}$$

with a mean of the SNR of $\overline{\mathrm{SNR}}(\{\boldsymbol{\eta}(t_n)\}) = 1/R \cdot \sum_{i=1}^{R} \mathrm{SNR}(\{\eta_i(t_n)\}) \approx 10.7\mathrm{dB}$. The measurement function is given by

$$\boldsymbol{h}(\boldsymbol{y}(t), t) = (y_1(t), y_3(t), y_5(t), \ldots y_{D-1}(t)). \tag{22}$$

Next, the model (16) is adapted to $\{\boldsymbol{\eta}(t_n)\}$ and the model variables and the parameter are estimated from the time series. The weighting matrices of the cost function (5) were fixed to: $\boldsymbol{A} = \mathbb{1}_{D/2}$ ($D/2 \times D/2$ unity matrix), $\boldsymbol{B} = \mathbb{1}_D, \boldsymbol{E} = 10^5 \cdot \mathbb{1}_D$ and $\beta = 10^5$. As mentioned in Section 2.1, continuation with α is used here. This means that α was set to the following values: $0.9999, 0.999, 0.99, 0.9, 0.5$. First, the cost function was optimized with $\alpha = 0.9999$, then the resulting solution was used as the initial guess for the next optimization of the cost function with $\alpha = 0.999$. This procedure was repeated until $\alpha = 0.5$ is reached. The solution of the optimization problem with $\alpha = 0.5$ was then considered as the solution of the estimation problem. The results of the estimated solution for the model variables are shown in Fig. 1. One can see a good coincidence of the model variables $\boldsymbol{y}(t)$ on the one hand and the "true" solution $\boldsymbol{x}(t)$ on the other hand. This is also the case for the observations $\{\boldsymbol{\eta}(t_n)\}$ and $\boldsymbol{h}(\boldsymbol{y}(t))$. Furthermore the modeling error $\boldsymbol{u}(t)$ is small.

5. Delay differential equations and the estimation of delay parameters

An application where the cost function becomes rather complex and automatic differentiation turns out to be beneficial is the estimation of parameters and states of DDEs. How to derive the delayed variable $\boldsymbol{y}_k(n) = \boldsymbol{y}(n-k)$ from $\boldsymbol{y}(n)$ for $\tau = k \cdot \Delta t$ with $k \in \mathbb{N}$ was already discussed in Section 2.1. In this case $\mathcal{Y}_k(0, N)$ can be computed from $\mathcal{Y}(0, N)$ without interpolation. However, if $k \in \mathbb{R}_+$ this approach does not work anymore. One has to interpolate $\mathcal{Y}(0, N)$ to approximate $\mathcal{Y}_k(0, N)$. Because Δt will be small a linear interpolation should be sufficient and hence is used here.

In the general case we have $\tau = (k' + l) \cdot \Delta t$ with $\tau \in \mathbb{R}_+, k' \in \mathbb{N}$ and $l \in [0, 1[$. Note that, due to these restrictions on k' and l, k' and l are uniquely defined for a given τ. Using this substitution for τ the delayed variable can be written as

$$\boldsymbol{y}_k(n) = \boldsymbol{y}_\tau(t_n) = \boldsymbol{y}(t_n - \tau) = \boldsymbol{y}(t_n - (k' + l) \cdot \Delta t) = \boldsymbol{y}(n \cdot \Delta t - (k' + l) \cdot \Delta t) = \boldsymbol{y}((n - k' + l) \cdot \Delta t) = \boldsymbol{y}(n - k' + l), \tag{23}$$

and with linear interpolation between $\boldsymbol{y}(n - k')$ and $\boldsymbol{y}(n - k' + 1)$ we obtain

$$\boldsymbol{y}_k(n) = \boldsymbol{y}(n - k' + l) = \boldsymbol{y}(n - k') + \frac{\boldsymbol{y}(n - k' + 1) - \boldsymbol{y}(n - k')}{\Delta t} \cdot l \cdot \Delta t = \boldsymbol{y}(n - k') + \left[\boldsymbol{y}(n - k' + 1) - \boldsymbol{y}(n - k')\right] \cdot l, \tag{24}$$

with $\boldsymbol{y}_k(n) \in [\boldsymbol{y}(n - k'), \boldsymbol{y}(n - k\prime + 1)]$ for $n = 0, 1, \ldots, N$. Note, that for $l = 0$ we have $\tau = k' \cdot \Delta t$ and hence the same situation as in Section 2.1, were $\boldsymbol{y}_k(n) = \boldsymbol{y}(n - k')$ can be computed without an interpolation of the model variables.

One possibility to estimate τ is discussed now. First, τ must be added in Eq. (12) to the quantities to be estimated. Next, bounds for τ must be set in Eq. (9). This means that there are bounds to k' so that (if the smallest bound of τ is zero) we have $k' \in [1, K]$. If τ and therefore k' and l would be fixed and not estimated, $\boldsymbol{w}$ (Eq. (12)) would be $\boldsymbol{w} = (\mathcal{Y}(-k', N), \boldsymbol{p}, \boldsymbol{q})$. When τ will be estimated, the number of elements in the history $\mathcal{Y}(-k', -1)$ can vary during the optimization process due to variations in τ (performed by the optimizer) and in k'. Because the number of elements of $\boldsymbol{w}$ has to stay constant during one optimization process, the history with the largest possible number of elements, given by $\mathcal{Y}(-K, -1)$, must be added to $\boldsymbol{w}$, which then becomes $\boldsymbol{w} = (\mathcal{Y}(-K, N), \boldsymbol{p}, \boldsymbol{q}, \tau)$. Estimating τ with this approach has one major disadvantage. When the optimizer evaluates the cost function with a certain τ, first k' and l have to be derived from τ. Next k' is used as an index to define the intervals $[\boldsymbol{y}(n - k'), \boldsymbol{y}(n - k' + 1)]$ with $n = 0, 1, \ldots, N$ where to interpolate the model variables for deriving the delayed variables $\boldsymbol{y}_k(n)$ with $n = 0, 1, \ldots, N$. The cost function depends on the model equations, the model equations depend on the delayed variable and the delayed variable is, as shown in Eq. (24), a function of the model variables. Only the latter ones are quantities to be estimated. Hence the (sparse) Jacobian $\partial H_i(\boldsymbol{w})/\partial w_j$ of $\boldsymbol{H}(\boldsymbol{w})$ (see Eq. (15)) depends on the (sparse) Jacobian

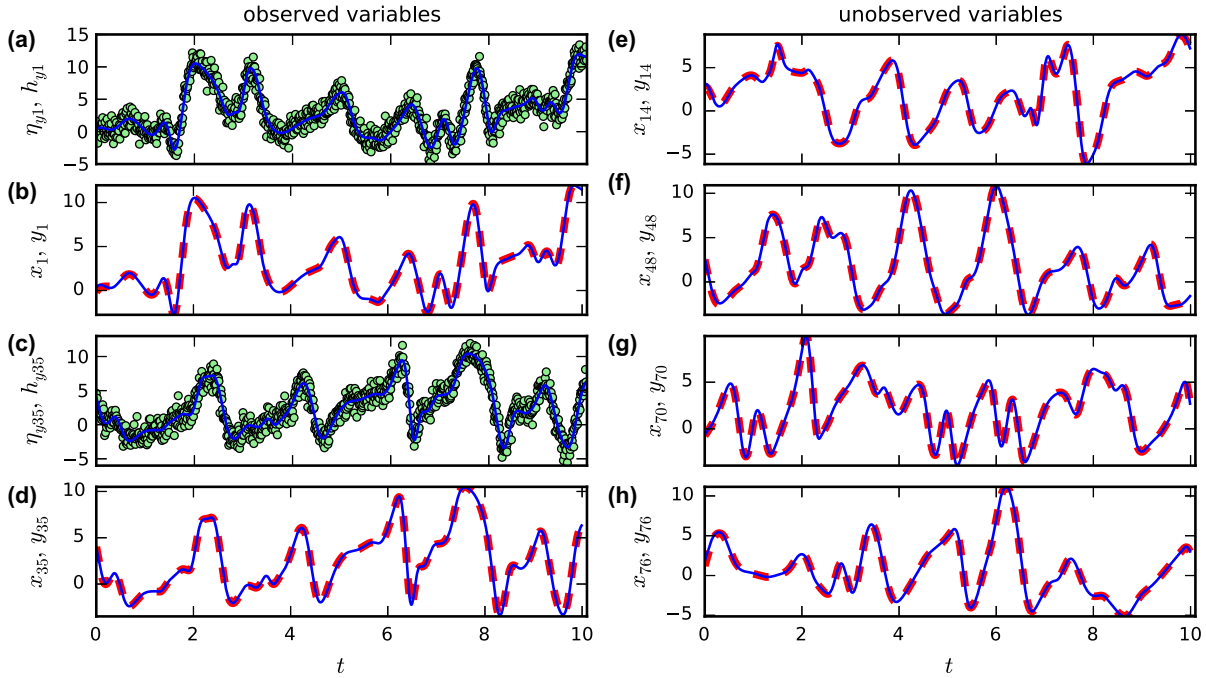

Fig. 1. Adaption of the 80 dimensional Lorenz96 model (Eq. (16)) to the time series $\{\boldsymbol{\eta}(t_n)\}$ (Eq. (17), green circles). Every second model variable was observed. Left-hand side: The model output given by the measurement function $\boldsymbol{h}(t)$ (Eq. (22), blue lines) was adapted to $\{\boldsymbol{\eta}(t_n)\}$ ((a), (c)). (b) and (d) show the "true" solution x_i (red dashed lines) with the corresponding estimates y_i (blue lines),whereas for these quantities there exist measurements η_{yi}. Right-hand side: (e), (f), (g) and (h) show estimates for the model variables y_i (blue lines) and the "true" solutions x_i (red dashed lines). Note that for all cases shown on the right-hand side there exist no measurements. The model parameter is estimated to $p = 8.165$, whereas 8.17 is used for generating the data by (17). Note that only a few of the 80 estimated model variables (with and without data) are shown. (For interpretation of the references to color in this figure legend, the reader is referred to the web version of this article.)

$\partial \boldsymbol{y}_k(n)/\partial \boldsymbol{y}(n)$ of the delayed variables to the model variables. For any specific n there exist K possible intervals $[\boldsymbol{y}(n-\tilde{k}), \boldsymbol{y}(n-\tilde{k}+1)]$ with $\tilde{k} \in [1, K]$ where the linear interpolation might be performed although there is only the *one* interval with $\tilde{k} = k'$ where it finally will be performed. The derivative of the linear interpolation to the model variable can be written as $\partial \boldsymbol{y}_k(n)/\partial \boldsymbol{y}(n) = \partial \boldsymbol{y}_{(\tilde{k}+l)\Delta t}(n)/\partial \boldsymbol{y}(n)$ with $\tilde{k} = 0, 1, \ldots, N$. Since only for $\tilde{k} = k'$ a linear interpolation is performed, the relevant elements of the Jacobian matrix corresponding to $\tilde{k} \neq k$ are zero. Nevertheless, these elements which are zero at this step are not necessarily zero during the entire optimization process. Therefore these elements must be included in the sparsity pattern of nonzero elements, although, most of the time, they are zero. The sparsity pattern must not change during an optimization process. This fact would lead to a significant increase of (possible) nonzero elements in the Jacobian and hence would remove the advantage of dealing with a sparse Jacobian.

To avoid these problems the estimation of the delay parameter is divided into two steps:

First step: The cost function is minimized for several fixed delays, $\tau = k \cdot \Delta t$ with $k \in \mathbb{N}$. In this case, as described in Section 2.1, no interpolation is necessary for computing the delayed variable. The solution of this step is $\hat{C}(\tau)$. This means that the assigned value is the value of the cost function in its minimum for a given τ. $\hat{C}(\tau)$ has a global minimum close to $\tau_{\min} = k_{\min} \cdot \Delta t$.

Second step: From the first step we have values for the cost function *only* around the minimum at $\tau_{\min} - \Delta t, \tau_{\min}$ and $\tau_{\min} + \Delta t$, as illustrated in Fig. 2. The global minimum at $\hat{\tau}$ is either in the interval $\hat{\tau} \in [\tau_{\min} - \Delta t, \tau_{\min}]$ or in the interval $\hat{\tau} \in [\tau_{\min}, \tau_{\min} + \Delta t]$. Now, τ is estimated as well. As described at the beginning of this section, the delayed variable is computed by linear interpolation of the model variable. The cost function is minimized two times: once with $\tau \in [\tau_{\min} - \Delta t, \tau_{\min}]$ and then with $\tau \in [\tau_{\min}, \tau_{\min} + \Delta t]$. The solution (model variables, parameters, delay time) obtained for the interval with the smallest value of the cost function after the optimization procedure is then taken as the final solution.

6. Example: Mackey–Glass model

As an example of a DDE we consider the Mackey–Glass model [29]. This time delay model is given by

$$\frac{\mathrm{d}y(t)}{\mathrm{d}t} = p_1 \cdot \frac{y(t-\tau)}{1 + y(t-\tau)^{10}} - p_2 y(t), \tag{25}$$

and has the two model parameters p_1, p_2 beside the delay parameter τ. To generate a data time series a twin experiment is performed. This means that the model (similar to Eq. (15))

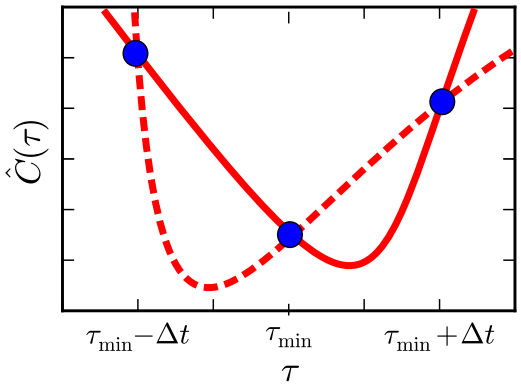

Fig. 2. Estimation of the delay parameter: An illustration of the cost function $\hat{C}(\tau)$ around the minimum at $\tau_{\min}$ is shown. The values of $\hat{C}(\tau)$ shown by the (blue) dots where obtained by the **first step** of estimating the delay parameter. The global minimum of $\hat{C}(\tau)$ at $\hat{\tau}$ is either in the interval $\hat{\tau} \in [\tau_{\min} - \Delta t, \tau_{\min}]$ or in the interval $\hat{\tau} \in [\tau_{\min}, \tau_{\min} + \Delta t]$, as illustrated by the (red) dashed and continuous lines. Both lines describe possible behaviors of $\hat{C}(\tau)$ between the (blue) dots. To determine whether the global minimum is in $[\tau_{\min} - \Delta t, \tau_{\min}]$ or $[\tau_{\min}, \tau_{\min} + \Delta t]$ both intervals are investigated separately in the **second step** using linear interpolation of the state variable. (For interpretation of the references to color in this figure legend, the reader is referred to the web version of this article.)

$$\frac{\mathrm{d}x(t)}{\mathrm{d}t} = 2 \cdot \frac{x(t-2.38)}{1+x(t-2.38)^{10}} - 1 \cdot x(t), \tag{26}$$

was integrated first. The solution is then used to generate the (noisy) time series

$$\eta(t_n) = x(t_n) + \mathcal{N}(0, 0.1), \tag{27}$$

with $t_n \in \{0, 0.1, \ldots, 60\}$ and $N = 601$ with timesteps $\Delta t = 0.1$ (SNR = 8.0 dB according to Eq. (20)).

Next the model (25) was adapted to $\{\eta(t_n)\}$ using the measurement function

$$h(y(t), \bullet, \bullet) = y(t). \tag{28}$$

The parameters p_1, p_2 and τ were estimated in addition to the model variable. As described in Section 5 the estimation of τ is divided into two steps:

- First τ is fixed to several different values $\tau = k \cdot \Delta t$ with $k = 3, 4, \ldots, 100$ and $\Delta t = 0.1$. For each fixed τ the cost function is minimized. The value of the cost function at its minimum is denoted by $\hat{C}(\hat{\mathcal{Y}}(-k, N), \hat{\boldsymbol{p}}, \bullet, \tau)$. Its dependence on τ is shown in Fig. 3. One can see a clear minimum at $\tau = 2.3$. Due to the step size of $\Delta t = 0.1$ and the smoothness around this minimum one can expect that the global minimum is either at $\tau \in [2.2, 2.3]$ or at $\tau \in [2.3, 2.4]$.
- Second the cost function is minimized two times (first with the bounds $\tau \in [2.2, 2.3]$ and second with $\tau \in [2.3, 2.4]$). In each case the delayed variable is approximated by linear interpolation according to Eq. (24). Remember that due to the bounds the index k' does *not* change during each optimization process and hence does not have to be recomputed from τ in each iteration. Only l changes.

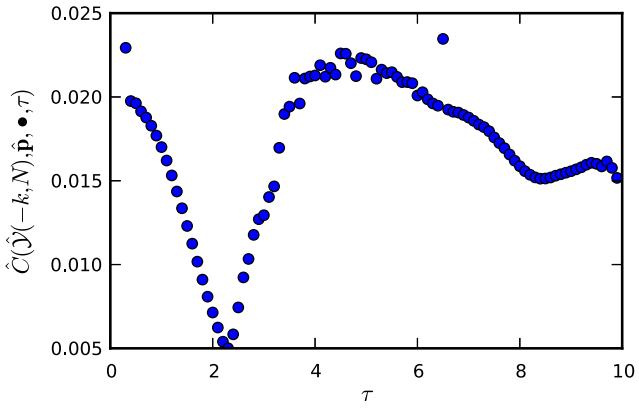

Fig. 3. Cost function for adaption of the Mackey–Glass (25) model to a time series generated in a twin experiment with Eq. (27).

Table 2
Model parameters p_1, p_2 and delay parameter τ of the Mackey–Glass model (25) estimated by adapting the model (25) to the time series given by Eq. (27). According to Fig. 3 the cost function $\hat{C}(\hat{\mathcal{Y}}(-k,N),\hat{\boldsymbol{p}},\bullet,\tau)$ has its global minimum either in $\tau \in [2.2, 2.3]$ or in $\tau \in [2.3, 2.4]$. Minimizing the cost function and estimating τ in addition to the model parameters and variables for both intervals results in a smaller $\hat{C}(\hat{\mathcal{Y}}(-k,N),\hat{\boldsymbol{p}},\bullet,\tau)$ for $\tau \in [2.3, 2.4]$.

	(p_1, p_2)	τ	$\hat{C}(\ldots,\tau)$
data	(2,1)	2.38	
estim. $\tau \in [2.2, 2.3]$	(1.73,0.86)	2.300	$5.41 \cdot 10^{-3}$
estim. $\tau \in [2.3, 2.4]$	(1.98,0.99)	2.387	$4.99 \cdot 10^{-3}$

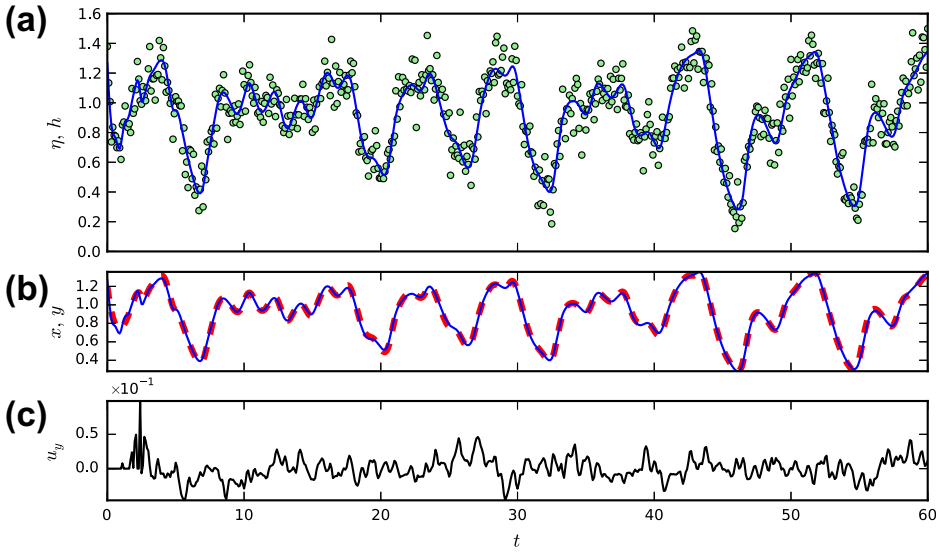

Fig. 4. Adaption of the Mackey–Glass (25) model to the time series η (see (27), green circles) which was generated by the original "true" solution x (red dashed line,) unknown to the estimation algorithm) using the measurement function $h(y(t),\bullet,\bullet)$ (blue line, see (28)). The estimated solution for the model variable is y (blue line in (b)) and u (black line in (c)) is the error in the approximation of the model equation (see (4)). The delay time $\tau \in [2.3, 2.4]$ was also estimated beside the model parameters and all estimated values are shown in tab. 2. (For interpretation of the references to color in this figure legend, the reader is referred to the web version of this article.)

For all performed estimation processes the weighting matrices of the cost function (5) (in this cases they are scalar) and α were fixed to: $A = B = 1, E = 10^3, \beta = 10^5$ and $\alpha = 0.5$. The results for the estimated parameters and the delay parameter are shown in Table 2. For $\tau \in [2.3, 2.4]$ the cost function $\hat{C}(\ldots,\tau)$ at its minimum has a smaller value than for $\tau \in [2.2, 2.3]$. Hence the solution for $\tau \in [2.3, 2.4]$ was chosen as the final result. Furthermore the estimated values for p_1, p_2 and τ coincide much better with the "true" values used to generate $\{\eta(t_n)\}$ (compared to the estimated values with $\tau \in [2.2, 2.3]$). The estimated model variable for $\tau \in [2.3, 2.4]$ is shown in Fig. 4. One can see a good coincidence of the model variable $y(t)$ on the one hand and the "true" solution $x(t)$ (Fig. 4b) and the data $\{\eta(t_n)\}$ (Fig. 4a) on the other hand with a small modeling error $u(t)$ (Fig. 4c).

7. Conclusions

Many optimization based system identification methods require information about derivatives of the underlying cost function in order to converge to the desired optimum. In general this information has to be provided by the user (or programmer) in terms of a Jacobian matrix, for example. Our examples show that this (typically cumbersome) task can be conveniently handled by means of automatic differentiation. This versatile tool from applied mathematics and computer science not only gives exact numerical values of the required derivatives, but also provides (and respects) the sparsity structure of the Jacobian matrix which may be exploited by any calling algorithm. These features have been demonstrated with a particular optimization algorithm (SparseLM) that enabled parameter and state estimation of the high dimensional Lorenz-96 system and the Mackey–Glass delay differential equation. A challenge for future research will be, for example, a successful application of the proposed parameter estimation to electrophysiological models of cardiac myocytes.

Our implementation (Python, C) of the estimation algorithm and a Python wrapper for sparseLM are available for download [32]. Other possible fields of application in nonlinear dynamics are bifurcation analysis and the computation of Lyapunov exponents and (covariant) Lyapunov vectors [33].

Acknowledgements

The research leading to the results has received funding from the European Community's Seventh Framework Program FP7/2007-2013 under grant agreement No. HEALTH-F2-2009-241526, EUTrigTreat. This work received support through Deutsche Forschungsgemeinschaft (SFB 1002 Modulatorische Einheiten bei Herzinsuffizienz). This work was supported by the DZHK (Deutsches Zentrum für Herz-Kreislauf-Forschung – German Centre for Cardiovascular Research). We thank H.D.I. Abarbanel and J. Bröcker for interesting and inspiring discussions on state and parameter estimation.

Appendix A. Python example for automatic differentiation using ADOL-C

For illustration we present and discuss a Python example showing how to derive the sparse Jacobian of a function $\boldsymbol{H}(\boldsymbol{w})$ in Listing 1.

```
1  import numpy as np
2  import adolc
3
4  def H(w):
5      h = np.zeros(3,dtype=w.dtype)
6      h[0] = 3*w[0]**2 + w[1]*w[3]
7      h[1] = 4*w[2]**3
8      h[2] = 5*w[0] + 2*np.exp(np.sin(w[1]*w[2]))
9      return h
10
11 w0 = np.array([4.,2.,3.,1.])
12
13 # Trace H(w)
14 # ----------
15 adolc.trace_on(0)
16 aw = adolc.adouble(w0)
17 adolc.independent(aw)
18
19 Hfunc = H(aw)
20
21 adolc.dependent(Hfunc)
22 adolc.trace_off()
23
24 # Evaluate function jacobian at this point
25 w = np.array([-2.,3.,1.,-4.])
26
27 # Evaluate function
28 valH = adolc.function(0,w)
29
30 # Evaluate dense jacobian
31 jacH = adolc.jacobian(0,w)
32 # Out jacH:
33 #    [[-12.  -4.    0.    3.]
34 #    [  0.   0.   12.    0.]
35 #    [  5.  -2.280 -6.840 0.]]
36
37 # Derive sparsity pattern and evaluate values of nonzeros at w0
38 # -------------------------------------------------------------
39 options = [0, 0, 0, 0]
40 [nnz, rind, cind, val] = adolc.colpack.sparse_jac_no_repeat(0,w0,options)
41 # Out nnz (number non-zeros): 7
42 # Out rind (row indices):
43 #    [0 0 0 1 2 2 2]
44 # Out cind (column indices):
45 #    [0 1 3 2 0 1 2]
46 # Out val (values):
47 #    [  24.  1.  2. 108.  5. 4.356 2.904]
48
49 # Evaluate values of nonzeros at w using nnz,
50 # rind, cind and valH from the  previous step
51 # -------------------------------------------
52 [nnz, rind, cind, val] = adolc.colpack.sparse_jac_repeat(0,w,nnz, rind,cind,val)
53 # Out nnz (number non-zeros): 7
54 # Out rind (row indices):
55 #    [0 0 0 1 2 2 2]
56 # Out cind (column indices):
57 #    [0 1 3 2 0 1 2]
58 # Out val (values):
59 #    [-12. -4. 3. 12. 5. -2.280 -6.840]
```

Fig. Listing. Simple Python example demonstrating the derivation of the (sparse) Jacobian of the function $\boldsymbol{H}(\boldsymbol{w})$ usind the automatic differentiation tool ADOL-C.

Before ADOLC can compute the numerical values of the Jacobian data type an internal function representation of H (w), called trace, is created in lines 15–22. To do this the data type of the elements of the input vector is changed to the ADOL-C

data type 'adouble' (line 16). Many (mathematical) functions are overloaded for this data type and can hence be used in the function to be differentiated. FOR-loops, WHILE-loops, IF . . .THEN statements, etc. are also allowed under certain conditions. In lines 28 and 31 the function H (w) and its dense Jacobian are computed using the previously created trace for a new $\boldsymbol{w}$. In line 40 the sparsity pattern of the Jacobian is detected and used in line 52 to compute the numerical values of its non-zero elements. The output in lines 33–35 and lines 55–59 show that the computed dense and sparse Jacobians are equal for the same $\boldsymbol{w}$.

References

[1] Clayton RH, Bernus O, Cherry EM, Dierckx H, Fenton FH, Mirabella L, et al. Challenges and open questions. Prog Biophys Mol Biol 2011;104:22–48.
[2] Parlitz U, Junge L, Kocarev L. Synchronization based parameter estimation from time series. Phys Rev E 1996;54:6253–529.
[3] Voss HU, Timmer J, Kurths J. Nonlinear dynamical system identification from uncertain and indirect measurements. Int J Bifurcation Chaos 2004;14:1905–33.
[4] Ghosh D, Banerjee S. Adaptive scheme for synchronization-based multiparameter estimation from a single chaotic time series and its applications. Phys Rev E 2008;78:056211.
[5] Abarbanel HDI, Creveling DR, Jeanne JM. Estimation of parameters in nonlinear systems using balanced synchronization. Phys Rev E 2008;77:016208.
[6] Sorrentino F, Ott E. Using synchronization of chaos to identify the dynamics of unknown systems. Chaos 2009;19:033108.
[7] Szendro IG, Rodríguez MA, López JM. On the problem of data assimilation by means of synchronization. J Geophys Res 2009;114:D20109.
[8] Yu W, Chen G, Cao J, Lü J, Parlitz U. Parameter identification of dynamical systems from time series. Phys Rev E 2007;75:067201.
[9] Yu D, Parlitz U. Estimating parameters by autosynchronization with dynamic restrictions. Phys Rev E 2008;77:066221.
[10] Ghosh D. Nonlinear-observer based synchronization scheme for multiparameter estimation. EPL 2008;84:40012.
[11] Fairhurst D, Tyukin I, Nijmeijer H, van Leeuwen C. Observers for canonic models of neural oscillators. Math Model Nat Phenom 2010;5(3):146–85.
[12] Creveling DR, Gill PE, Abarbanel HDI. State and parameter estimation in nonlinear systems as an optimal tracking problem. Phys Lett A 2008;372:2640–4.
[13] Quinn JC, Bryant PH, Creveling DR, Klein SR, Abarbanel HDI. Parameter and state estimation of experimental chaotic systems using synchronization. Phys Rev E 2009;80:016201.
[14] Abarbanel HDI, Creveling DR, Farsian R, Kostuk M. Dynamical state and parameter estimation. SIAM J Appl Dyn Syst 2009;8:1341–81.
[15] Abarbanel HDI. Effective actions for statistical data assimilation. Phys Lett A 2009;373:4044404.
[16] Quinn JC, Abarbanel HDI. State and parameter estimation using Monte Carlo evaluation of path integrals. QJR Meteorol Soc 2010;136(652):1855–67.
[17] Abarbanel HDI, Kostuk M, Whartenby W. Data assimilation with regularized nonlinear instabilities. QJR Meteorol Soc 2010;136(648):769–83.
[18] Bröcker J. On variational data assimilation in continuous time. QJR Meteorol Soc 2010;136:1906–19.
[19] Schumann-Bischoff J, Parlitz U. State and parameter estimation using unconstrained optimization. Phys Rev E 2011;84:056214.
[20] Bröcker J, Szendro I. Sensitivity and out–of–sample error of continuous time data assimilation. QJR Meteorol Soc 2012;138:785–801.
[21] Levenberg K. A method for the solution of certain problems in least squares. Quart Appl Math 1944;2:164–8.
[22] Marquardt D. An algorithm for least-squares estimation of nonlinear parameters. SIAM J Appl Math 1963;11:431–41.
[23] Lourakis MIA. Sparse non-linear least squares optimization for geometric vision. In: European conference on computer vision, vol. 2; 2010. p. 43–56. http://dx.doi.org/10.1007/978-3-642-15552-9_4, <http://www.ics.forth.gr/lourakis/sparseLM/>.
[24] Rall LB. Automatic differentiation: techniques and applications. Lect Notes Comput Sci 1981;120.
[25] Walther A, Griewank A. Getting started with ADOL-C, In: Naumann U, Schenk O, editor. Combinatorial Scientific Computing. Chapman-Hall CRC Computational Science; 2012. p. 181–202.
[26] Griewank A, Juedes D, Utke J. Algorithm 755: ADOL-C: a package for the automatic differentiation of algorithms written in C/C++. ACM Trans Math Softw 1996;22:131–67.
[27] ColPack: <http://www.cscapes.org/coloringpage/software.htm>, October 16, 2012.
[28] Lorenz EN. Predictability – a problem partly solved, ECMWF. Proceedings of the seminar on predictability, vol. 1. Reading, UK: Berkshire; 1996. p. 1–18.
[29] Mackey MC, Glass L. Oscillation and chaos in physiological control systems. Science 1977;197:287–9.
[30] Numpy: <http://numpy.scipy.org/>, October 16, 2012.
[31] Pyadolc: <https://github.com/b45ch1/pyadolc>, October 16, 2012.
[32] A Python wrapper for sparseLM and a Python-C implementation of the estimation method for ODEs can be downloaded from <http://www.bmp.ds.mpg.de/pysparselm.html> and <http://www.bmp.ds.mpg.de/pyodefit.html>, Gnu General Public License Version 3, 29 June 2007.
[33] Kuptsov PV, Parlitz U. Theory and computation of covariant Lyapunov vectors. J Nonlinear Sci 2012;22:727–62.

5 Quantifying uncertainty in state and parameter estimation

The following pages contain the article

> U. Parlitz, J. Schumann-Bischoff, and S. Luther. "Quantifying uncertainty in state and parameter estimation". In: *Phys. Rev. E* 89.5 (May 2014), p. 050902. DOI: 10.1103/PhysRevE.89.050902.

The idea for the approach of how to quantify the uncertainties was devised by the author U. Parlitz. I designed, implemented, and performed all required simulations in this article, except the simulation underlying Fig. 1. Furthermore, I designed and created all figures, with the exception of Fig. 1. The text was mainly written by U. Parlitz and revised by the other authors.

PHYSICAL REVIEW E **89**, 050902(R) (2014)

Quantifying uncertainty in state and parameter estimation

Ulrich Parlitz, Jan Schumann-Bischoff, and Stefan Luther
Max Planck Institute for Dynamics and Self-Organization Am Faßberg 17, 37077 Göttingen, Germany
and Institute for Nonlinear Dynamics, Georg-August-Universität Göttingen, Am Faßberg 17, 37077 Göttingen, Germany
(Received 20 November 2013; published 15 May 2014)

Observability of state variables and parameters of a dynamical system from an observed time series is analyzed and quantified by means of the Jacobian matrix of the delay coordinates map. For each state variable and each parameter to be estimated, a measure of uncertainty is introduced depending on the current state and parameter values, which allows us to identify regions in state and parameter space where the specific unknown quantity can(not) be estimated from a given time series. The method is demonstrated using the Ikeda map and the Hindmarsh-Rose model.

DOI: 10.1103/PhysRevE.89.050902 PACS number(s): 05.45.Tp, 05.45.Xt

In physics and other fields of science including quantitative biology, life sciences, and climatology, mathematical models play a crucial role for understanding and predicting dynamical processes. In the following we assume that such a model exists and is known. But even in the ideal case of a model obtained from fundamental physical laws this model typically contains some parameters whose values have to be determined depending on the physical context. Furthermore, not all state variables of the model may be easily experimentally accessible. To estimate the unknown parameters and state variables you may either devise specific experiments focusing on the quantity of interest or you can try to extract the required information from a measured time series of the process to be modeled. Technically, several estimation methods exist, including observer or synchronization schemes [1–6], particle filters [7], a path integral formalism [8,9], or optimization based algorithms [10–12]. However, these methods may fail and at this point the question arises whether the failure is due to the specific algorithm used or due to a lack of information in the available time series. In this article we address the second option and present a general approach for answering the question whether a given time series enables the estimation of parameters or variables of interest in a given model. The mathematical tool that is used to answer this question is delay reconstruction [13–17] and the basic criterion for local observability is the rank of the Jacobian matrix of the delay coordinates map. This approach was motivated by work of Letellier, Aguirre, and Maquet [18–20] who studied the question which state variables can be estimated or observed from a given time series using derivative coordinates. Observability of (continuous) dynamical systems is also a major issue in control theory [21–23] and nonlinear time series analysis [24]. Here we consider discrete time and delay coordinates, and we introduce a quantitative measure of uncertainty, which in general varies on the attractor and thus indicates where in state space estimation is more efficient and less error prone. Furthermore, we focus not only on state variables but also on observability of model parameters.

Let's assume, first, that our model of interest is a M-dimensional discrete dynamical system,

$$\mathbf{x}(n+1) = \mathbf{g}[\mathbf{x}(n), \mathbf{p}], \tag{1}$$

given by an iterated function $\mathbf{g}$ depending on the state vector $\mathbf{x}(n) = [x_1(n), \ldots, x_M(n)] \in \mathbb{R}^M$ at time n and K parameters $\mathbf{p} = (p_1, \ldots, p_K) \in \mathbb{R}^K$. This system generates the times series $\{s(n)\}$ with $s(n) = h[\mathbf{x}(n)]$ (for $n = 1, \ldots, N$), where h denotes a measurement or observation function. The time series $\{s(n)\}$ can be used to construct a D-dimensional *delay reconstruction* [13–17],

$$\begin{aligned}\mathbf{y}(n) &= [s(n), s(n+1), \ldots, s(n+D-1)] \\ &= G(\mathbf{x}(n), \mathbf{p}) \in \mathbb{R}^D,\end{aligned} \tag{2}$$

providing the *delay coordinates map* $G : \mathbb{R}^{M+K} \to \mathbb{R}^D$.

To uniquely recover the full state $\mathbf{x}$ and the parameters $\mathbf{p}$ from the observations represented by the reconstructed state $\mathbf{y}$, we require the map G to be smooth and locally invertible. More precisely, let $M + K \leqslant D$ and let $(\mathbf{x}, \mathbf{p}) \in \mathcal{U}$ where $\mathcal{U} \subset \mathbb{R}^{M+K}$ is a smooth manifold. Then G is locally invertible on the image $G(\mathcal{U}) \subset \mathbb{R}^D$ if the $D \times (M+K)$ Jacobian matrix $DG(\mathbf{x}, \mathbf{p})$ has full rank $M + K$ (i.e., G is an immersion [15]).

The map from delay reconstruction space $\mathbb{R}^D$ to the state and parameter space $\mathbb{R}^{M+K}$ is locally given by the (pseudo) inverse of the Jacobian matrix DG of the delay coordinates map G, which can be computed using a singular value decomposition

$$DG = USV^{\mathrm{tr}} \tag{3}$$

where $S = \mathrm{diag}(\sigma_1, \ldots, \sigma_{M+K})$ is a $(M+K) \times (M+K)$ diagonal matrix containing the singular values $\sigma_1 \geqslant \sigma_2 \geqslant \cdots \geqslant \sigma_{M+K} \geqslant 0$ and $U = [\mathbf{u}^{(1)}, \ldots, \mathbf{u}^{(M+K)}]$ and $V = [\mathbf{v}^{(1)}, \ldots, \mathbf{v}^{(M+K)}]$ are orthogonal matrices, represented by the column vectors $\mathbf{u}^{(i)} \in \mathbb{R}^D$ and $\mathbf{v}^{(i)} \in \mathbb{R}^{M+K}$, respectively. V^{tr} is the transposed of V coinciding with the inverse $V^{-1} = V^{\mathrm{tr}}$. Analogously, $U^{\mathrm{tr}} = U^{-1}$ and the (pseudo) inverse Jacobian matrix reads $DG^{-1} = VS^{-1}U^{\mathrm{tr}}$ where $S^{-1} = \mathrm{diag}(1/\sigma_1, \ldots, 1/\sigma_{M+K})$. Multiplying by U from the right we obtain $DG^{-1}U = VS^{-1}$ or

$$DG^{-1}\mathbf{u}^{(j)} = \frac{1}{\sigma_j}\mathbf{v}^{(j)} \quad (j = 1, \ldots, M+K). \tag{4}$$

In Fig. 1 the transformation of singular vectors Eq. (4) is illustrated for the case $M = 2$ and $K = 0$ (no unknown parameters). The diagram shows how small perturbations of $\mathbf{y}$ in delay reconstruction space result in deviations from $\mathbf{x}$ in the original state space. Most relevant for the local observability of

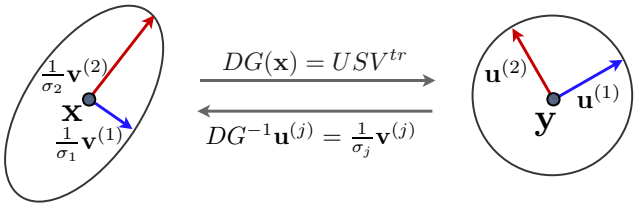

FIG. 1. (Color online) The (pseudo) inverse Jacobian matrix $DG^{-1}(\mathbf{y})$ maps perturbations of $\mathbf{y}$ in delay reconstruction space to deviations from the state $\mathbf{x}$ whose magnitudes depend on the direction of the perturbation as described by Eq. (4).

the (original) state $\mathbf{x}$ is the length of the longest principal axis of the ellipsoid given by the inverse of the smallest singular value σ_2 (see Fig. 1). Small singular values correspond to directions in state space, where it is difficult (or even impossible) to locate the true state $\mathbf{x}$ given a finite precision of the reconstructed state $\mathbf{y}$. The ratio $\sigma_{\min}/\sigma_{\max}$ of the smallest and the largest singular value is a measure of observability at the reference state $\mathbf{x}$. By averaging on the attractor we define (analogously to a similar definition for derivative coordinates [18,19]) the *observability index*

$$\bar{\gamma} = \frac{1}{N}\sum_{n=1}^{N}\frac{\sigma^2_{\min}(\mathbf{x}(n))}{\sigma^2_{\max}(\mathbf{x}(n))}. \tag{5}$$

If the perturbations of $\mathbf{y}$ are due to normally distributed measurement noise then they can be described by a symmetric Gaussian distribution centered at $\mathbf{y}$,

$$Q(\tilde{\mathbf{y}}) = \frac{\exp\left[-\frac{1}{2}(\tilde{\mathbf{y}}-\mathbf{y})^{\mathrm{tr}}\Sigma_y^{-1}(\tilde{\mathbf{y}}-\mathbf{y})\right]}{\sqrt{(2\pi)^D \det(\Sigma_y)}}, \tag{6}$$

where $\tilde{\mathbf{y}}$ is the perturbed state, $\Sigma_y = \mathrm{diag}(\rho^2,\ldots,\rho^2) = \rho^2 I_D$ denotes the $D\times D$ covariance matrix (I_D stands for the D-dimensional unit matrix), and the standard deviation ρ quantifies the noise amplitude. For (infinitesimally) small perturbations $\Delta\mathbf{y} = \tilde{\mathbf{y}} - \mathbf{y}$, this distribution is mapped by the pseudo inverse of the linearized delay coordinates map to the (nonsymmetrical) distribution

$$P(\tilde{\mathbf{x}}) = \frac{\exp\left[-\frac{1}{2}(\tilde{\mathbf{x}}-\mathbf{x})^{\mathrm{tr}}\Sigma_x^{-1}(\tilde{\mathbf{x}}-\mathbf{x})\right]}{\sqrt{(2\pi)^{M+K}\det(\Sigma_x)}}, \tag{7}$$

centered at $\mathbf{x}$ with the inverse covariance matrix

$$\begin{aligned}\Sigma_x^{-1} &= DG^{\mathrm{tr}}\Sigma_y^{-1}DG \\ &= \frac{1}{\rho^2}DG^{\mathrm{tr}}DG = \frac{1}{\rho^2}VS^2V^{\mathrm{tr}}.\end{aligned} \tag{8}$$

The marginal distribution P_j of the jth state variable centered a x_j is given by

$$P_j(\tilde{x}_j) = \frac{1}{\rho_j\sqrt{2\pi}}\exp\left[-\frac{(\tilde{x}_j - x_j)^2}{2\rho_j^2}\right], \tag{9}$$

where the standard deviation ρ_j is given by the square root of the diagonal elements of the covariance matrix $\rho_j = \sqrt{\Sigma_{x,jj}}$ that can be obtained by inverting Σ_x^{-1} [given in Eq. (8)]. Since the noise level ρ of the observations appears in Eq. (8) as a factor only we can, without loss of generality, choose $\rho = 1$ and use

$$\nu_j = \sqrt{[DG^{\mathrm{tr}}DG]^{-1}_{jj}} = \sqrt{[VS^{-2}V^{\mathrm{tr}}]_{jj}} \tag{10}$$

as a measure of *uncertainty* when estimating x_j, which can be interpreted as a noise amplification factor. The same reasoning holds for the unknown parameters $\mathbf{p}$.

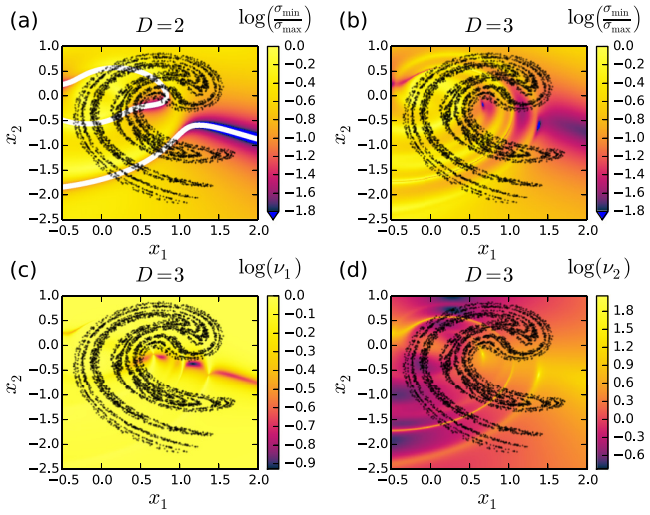

FIG. 2. (Color online) Observability of the state variables x_1 and x_2 of the Ikeda map Eq. (11) from a x_1 time series (with known parameters, $K = 0$, $M = 2$). (a), (b) Color-coded ratio of singular values $\sigma_{\min}/\sigma_{\max}$ vs. x_1 and x_2 for reconstruction dimension $D = 2$ (a) and $D = 3$ (b). The white curves in (a) indicate the location of zeros of $\det(DG)$. (c), (d) Color-coded uncertainties ν_1 (c) and ν_2 (d) of x_1 and x_2 estimates, respectively. Note the logarithmic color axes. Black dots represent the Ikeda attractor.

To illustrate this quantification of observability, we first consider the Ikeda map [25] $z(n+1) = p_1 + p_2 z(n)\exp[ip_3 - ip_4/(1+|z(n)|^2)]$ with $z(n) = x_1(n) + ix_2(n) \in \mathbb{C}$ that can also be written as

$$\begin{aligned}x_1(n+1) &= p_1 + p_2[x_1(n)\cos\theta_n - x_2(n)\sin\theta_n] \\ x_2(n+1) &= p_2[x_1(n)\sin\theta_n + x_2(n)\cos\theta_n],\end{aligned} \tag{11}$$

where $\theta_n = p_3 - p_4/[1 + x_1^2(n) + x_2^2(n)]$. For the standard parameters $p_1 = 1$, $p_2 = 0.9$, $p_3 = 0.4$, and $p_4 = 6$, this map generates the chaotic attractor shown in Fig. 2.

First, we consider a case where all parameters are known and only the variables x_1 and x_2 have to be estimated from the observable $s(n) = x_1(n)$ (i.e., $M = 2$ and $K = 0$). Figures 2(a) and 2(b) show (color-coded) the ratio of the smallest singular value $\sigma_{\min} = \sigma_M$ and the largest singular value $\sigma_{\max} = \sigma_1$ of the Jacobian matrix $DG(\mathbf{x})$ of the delay coordinates map versus x_1 and x_2. Reconstruction dimensions are $D = 2$ in Fig. 2(a) and $D = 3$ in Fig. 2(b), respectively. For $D = 2$, the white curves indicate the zeros of the determinant of $DG(\mathbf{x},\mathbf{p})$ that are computed as contour lines. As can be seen, parts of the Ikeda attractor cross these singularity manifolds or are close to regions in state space where the ratio $\sigma_{\min}/\sigma_{\max}$ is very close to zero, indicating an almost singular Jacobian matrix DG. There, state estimation is not possible, a fact that reconfirms previous results indicating that reconstruction dimensions $D > 2$ are

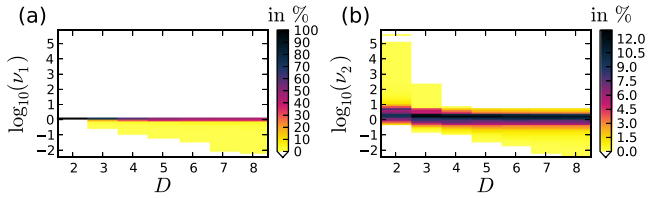

FIG. 3. (Color online) Histograms (color-coded) of uncertainties ν_1 (a) and ν_2 (b) computed from a x_1 time series of length $N = 1\,000\,000$ generated on the attractor of the Ikeda map Eq. (11) with reconstruction dimensions ranging from $D = 2$ to $D = 7$. The state variables x_1 and x_2 are estimated ($M = 2$), while all parameters are assumed to be known ($K = 0$).

required for the Ikeda map [26]. For $D = 3$, the singularities disappear and only some regions with relatively low ratios $\sigma_{\min}/\sigma_{\max}$ remain.

Figures 2(c) and 2(d) show ν_1 and ν_2 versus x_1 and x_2, respectively. For both variables their uncertainties ν_k vary and there are regions of low ν_1 but relatively large ν_2.

Figures 3(a) and 3(b) show histograms of ν_1 and ν_2 for different reconstruction dimensions D, which were obtained from an orbit of length $N = 1\,000\,000$ on the Ikeda attractor. Due to the choice $s(n) = x_1(n)$ the uncertainty ν_1 of x_1 is for all dimensions equal or less than one. For $D = 2$ the uncertainty ν_2 of x_2 reaches very high values $>10^6$ when the orbit passes those regions in state space where the Jacobian matrix DG is (almost) singular [see Fig. 2(a)]. For reconstruction dimensions $D = 3$ the ν_2 histogram is bounded by $\nu_2 < 10^3$ indicating a significant improvement and for $D = 4$ the bound reduces to $\nu_2 < 10$, a value that doesn't change anymore if the reconstruction dimension is increased furthermore. This feature is in very good agreement with previous results obtained when estimating Lyapunov exponents from Ikeda time series [26].

To obtain the histograms shown in Fig. 3 and in the following figures the model equations are used to generate a trajectory which provides a representative sample and subset of the attractor (similar to numerical computations of Lyapunov exponents).

For the results shown in Figs. 3(a) and 3(b) only the state variables are estimated and all parameters are assumed to be known ($M = 2$, $K = 0$). Figure 4 shows also the uncertainties ν_3, ν_4, ν_5, and ν_6 of the parameters p_1, p_2, p_3, and p_4 for an estimation task where all variables ($M = 2$) and all parameters ($K = 4$) are unknown. For increasing reconstruction dimension D, the distributions of all uncertainties converge with monotonically decreasing upper bounds (largest ν values quantifying large uncertainty of estimates at specific locations on the attractor).

Delay reconstruction can also be applied to observables $s(t) = h[\mathbf{x}(t)]$ from continuous dynamical systems,

$$\dot{\mathbf{x}} = \mathbf{f}(\mathbf{x},\mathbf{p}), \tag{12}$$

using a suitable *delay time* τ:

$$\mathbf{y} = \{s(t), s(t+\tau), \ldots, s[t+(D-1)\tau]\} = G(\mathbf{x},\mathbf{p}) \in \mathbb{R}^D.$$

The Jacobian matrix $DG(\mathbf{x},\mathbf{p})$ of the delay coordinates map G can be computed by solving linearized equations providing

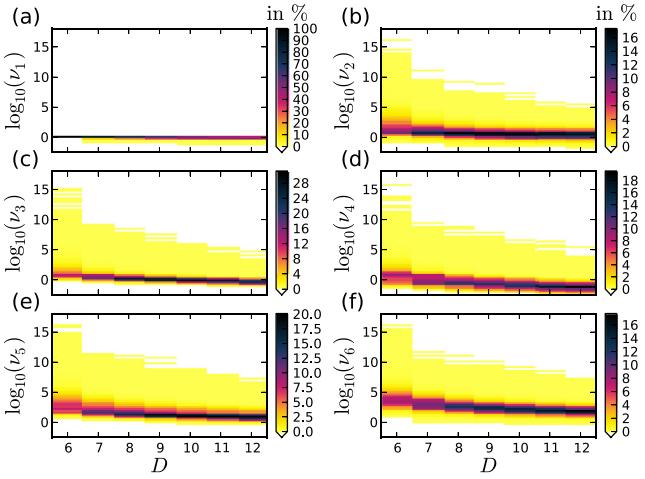

FIG. 4. (Color online) Histograms (color-coded) of uncertainties of state and parameter estimates of the Ikeda map Eq. (11) for reconstruction dimensions ranging from $D = 6$ to $D = 12$. Distributions are computed from a x_1 time series of length $N = 1\,000\,000$ generated on the Ikeda attractor. All variables ($M = 2$) and all parameters ($K = 4$) are assumed to be unknown.

the Jacobian matrices $D_x\phi^t(\mathbf{x},\mathbf{p})$ and $D_p\phi^t(\mathbf{x},\mathbf{p})$ of the flow ϕ^t generated by the system Eq. (12) [27]. To demonstrate the application of the proposed uncertainty analysis to continuous time system we use the Hindmarsh-Rose (HR) neuron model [28]

$$\begin{aligned} \dot{x}_1 &= -x_1^3 + p_1 x_1^2 + x_2 - x_3 \\ \dot{x}_2 &= 1 - p_2 x_1^2 - x_2 \\ \dot{x}_3 &= p_3\,[x_1 + p_4(p_5 - x_3)]\,. \end{aligned} \tag{13}$$

For parameter values $p_1 = 3$, $p_2 = 5$, $p_3 = 0.004$, $p_4 = 3.19$, $p_5 = 0.25$ the HR model exhibits chaotic bursting of x_1 and x_2 and slow variations of x_3 [11].

Figures 5(a) and 5(b) show the dependence of probability distributions (color-coded) of uncertainties ν_2, and ν_3, respectively, on the delay time τ chosen for performing the delay reconstruction. The reconstruction dimension equals $D = 7$. With this example, all parameters are assumed to be known ($K = 0$) and the first state variable is chosen as measured time series $s(t_n) = x_1(t_n)$ with $t_n = n\tau$. Therefore, the estimation of x_1 is not much affected by the choice of the delay time and $\nu_1 \leqslant 1$ (with $\nu_1 \approx 1$ most of the time, not shown here). As can be seen, the centers of both distributions decrease monotonically with τ indicating an improvement of the estimation accuracy for larger delay times. Figures 5(c) and 5(d) show histograms (color-coded) of uncertainties ν_2 and ν_3 versus reconstruction dimension D for $\tau = 0.1$. Larger D provides lower uncertainties ν_j and compared to Figs. 5(a) and 5(b) very large ν_j do not occur anymore. Note that corresponding columns of Figs. 5(a) and 5(b) and Figs. 5(c) and 5(d), respectively, are computed using delay coordinates covering the same window in time ranging from $\tau(D-1) = 0.1 \times 6 = 0.6$ to $\tau(D-1) = 30.1 \times 6 = 1806 \times 0.1 = 180.6$. The more densely sampling ($\tau = 0.1$) underlying Figs. 5(c) and 5(d) provides more information about the underlying dynamics and results in lower uncertainty

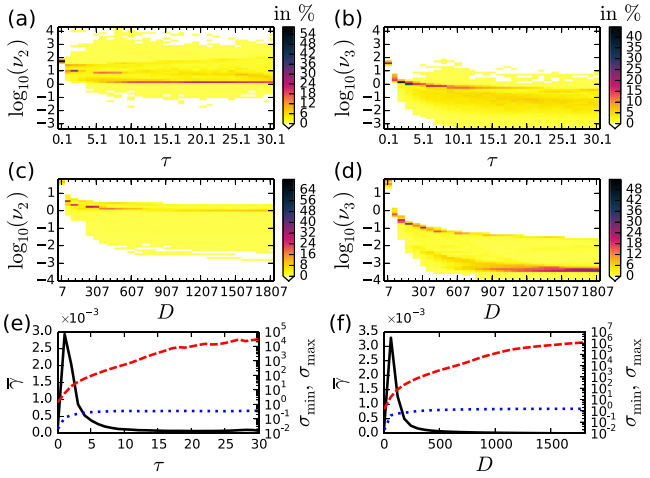

FIG. 5. (Color online) Probability distributions (color-coded) of uncertainties ν_2 and ν_3 when estimating the state variables x_1, x_2, and x_3 of the HR model Eq. (13) from a x_1 time series. In (a) and (b) the delay reconstruction dimension is fixed at $D = 7$ and the delay τ is varied. (c), (d) Distributions for $\tau = 0.1$ and different reconstruction dimensions D. Corresponding columns (histograms) of all four diagrams show results for the same window in time $(D - 1)\tau$ used upon delay reconstruction. (e), (f) Observability index $\bar{\gamma}$ (5) (solid curve), $\sigma_{\min}$ (dotted curve), and $\sigma_{\max}$ (dashed curve) vs. τ and vs. D.

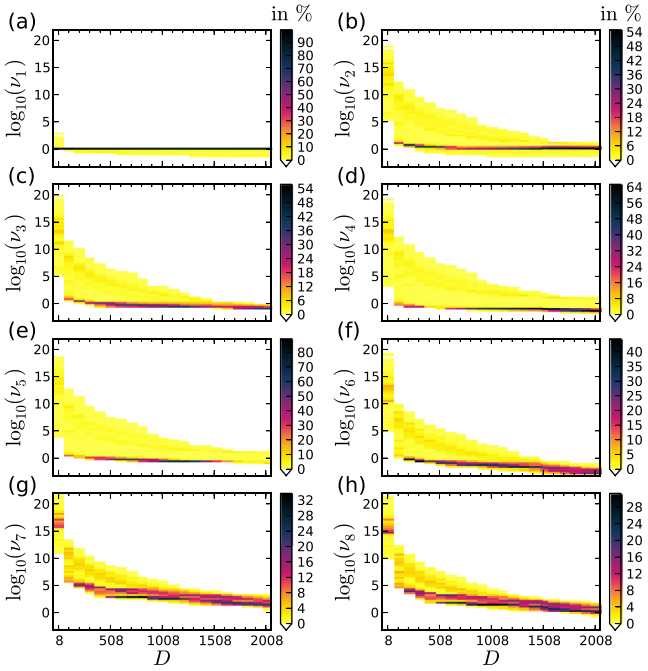

FIG. 6. (Color online) Distributions of uncertainties ν_j vs. reconstruction dimension D obtained for the HR model Eq. (13) where all three state variables and all five parameters are estimated from a x_1 time series. The delay time $\tau = 0.1$ is fixed.

values. Figures 5(e) and 5(f) show the observability index $\bar{\gamma}$ Eq. (5) and mean values of the smallest and the largest singular values $\sigma_{\min}$ and $\sigma_{\max}$ versus τ and D, respectively. While $\bar{\gamma}$ exhibits a clear peak, $\sigma_{\min}$ converges to an asymptotic value, and $\sigma_{\max}$ increases monotonically, i.e., the lengths of the ellipsoid axes in Fig. 1 decrease $(1/\sigma_{\max})$ or converge $(1/\sigma_{\min})$.

If in addition to the three state variables x_1, x_2, and x_3 also the five parameters $p_1, \ldots, p_5$ of the HR-model Eq. (13) are to be estimated from the x_1 time series then we have to cope with an estimation task with $M + K = 3 + 5 = 8$ uncertainties whose distributions for $\tau = 0.1$ are shown in Fig. 6 for delay reconstruction dimensions ranging from $D = 8$ to $D = 2008$. For increasing D the uncertainties $\nu_1, \ldots, \nu_6$ corresponding to $x_1, x_2, x_3, p_1, p_2, p_3$ decrease to values close to or below one. The uncertainties ν_7 and ν_8 of parameters p_4 and p_5, respectively, remain rather large (>1000) even for high-dimensional reconstructions. This feature indicates that it is very difficult to estimate both parameters together. In fact, if p_4 (or p_5) is known and only p_5 (or p_4) has to be estimated (together with $x_1, x_2, x_3, p_1, p_2, p_3$) then the uncertainty values of p_5 (or p_4) are much smaller and lie in the range of the uncertainties of the other parameters. Applying a state and parameter estimation algorithm [11,29] we also encountered problems (in terms of large deviations from the true values) when trying to estimate both parameters p_4 and p_5 together. These two parameters are to some degree redundant in the sense that different combinations yield (almost) the same x_1 time series and thus cannot be clearly distinguished using a x_1 time series, only.

The presented approach for quantifying uncertainties of model-based state and parameter estimation from time series provides a general criterion whether and how reliably specific model variables and parameters can be estimated from time series. This method is independent from any particular estimation method and it can be extended in several ways, including unknown parameters in the measurement function and multivariate time series. High uncertainty implies that the corresponding quantity of the model has small impact on the output and may thus be a candidate for reducing the formal model complexity by pruning. Furthermore, the information provided by the values of uncertainty can be exploited to improve state and parameter estimation methods.

ACKNOWLEDGMENTS

The research leading to these results has received funding from the European Community's Seventh Framework Program FP7/2007-2013 under grant agreement no. HEALTH-F2-2009-241526, EUTrigTreat. We acknowledge financial support by the German Federal Ministry of Education and Research (BMBF) Grant No. 031A147, the Deutsche Forschungsgemeinschaft (SFB 1002: Modulatory Units in Heart Failure), and by the German Center for Cardiovascular Research (DZHK e.V.).

[1] H. Nijmeijer and I. M. Y. Mareels, IEEE Trans. Circuits Syst. I **44**, 882 (1997).

[2] H. J. C. Huijberts, T. Lilge, and H. Nijmeijer, Int. J. Bif. Chaos **11**, 1997 (2001).

[3] U. Parlitz, L. Junge, and L. Kocarev, Phys. Rev. E **54**, 6253 (1996).
[4] D. Ghosh and S. Banerjee, Phys. Rev. E **78**, 056211 (2008).
[5] H. D. I. Abarbanel, D. R. Creveling, and J. M. Jeanne, Phys. Rev. E **77**, 016208 (2008).
[6] F. Sorrentino and E. Ott, Chaos **19**, 033108 (2009).
[7] P. J. van Leeuwen, Q. J. R. Meteorol. Soc. **136**, 1991 (2010).
[8] H. D. I. Abarbanel, Phys. Lett. A **373**, 4044 (2009).
[9] J. C. Quinn and H. D. I. Abarbanel, Q. J. R. Meteorol. Soc. **136**, 1855 (2010).
[10] D. R. Creveling, P. E. Gill, and H. D. I. Abarbanel, Phys. Lett. A **372**, 2640 (2008).
[11] J. Schumann-Bischoff and U. Parlitz, Phys. Rev. E **84**, 056214 (2011).
[12] J. Bröcker, Q. J. R. Meteorol. Soc. **136**, 1906 (2010).
[13] D. Aeyels, SIAM J. Contr. Optimiz. **19**, 595 (1981).
[14] F. Takens, Lect. Notes Math. **898**, 366 (1981).
[15] T. Sauer, J. A. Yorke, and M. Casdagli, J. Stat. Phys. **65**, 579 (1991).
[16] H. Kantz and T. Schreiber, *Nonlinear Time Series Analysis*, Cambridge Nonlinear Science Series 7 (Cambridge University Press, Cambridge, 1997).
[17] H. D. I. Abarbanel, *Analysis of Observed Chaotic Data* (Springer Verlag, Berlin, 1997), 2nd ed.
[18] C. Letellier, L. A. Aguirre, and J. Maquet, Phys. Rev. E **71**, 066213 (2005); Comm. Nonl. Sci. Num. Sim. **11**, 555 (2006).
[19] C. Letellier and L. A. Aguirre, Phys. Rev. E **79**, 066210 (2009).
[20] M. Frunzete, J.-P. Barbot, and C. Letellier, Phys. Rev. E **86**, 026205 (2012).
[21] R. Hermann and A. J. Krener, IEEE Trans. Autom. Contr. **AC-22**, 728 (1977).
[22] E. D. Sontag, *Mathematical Control Theory: Deterministic Finite Dimensional Systems* (Springer, New York, 1998), 2nd ed.
[23] H. Nijmeijer, Int. J. Control **36**, 867 (1982).
[24] H. U. Voss, J. Timmer, and J. Kurths, Int. J. Bif. Chaos **14**, 1905 (2004).
[25] K. Ikeda, Opt. Commun. **30**, 257 (1979).
[26] P. Bryant, R. Brown, and H. D. I. Abarbanel, Phys. Rev. Lett. **65**, 1523 (1990).
[27] H. Kawakami, IEEE Trans. Circ. Syst. **CAS-31**, 248 (1984).
[28] J. L. Hindmarsh and R. M. Rose, Proc. R. Soc. Lond. B **221**, 87 (1984).
[29] J. Schumann-Bischoff, S. Luther, and U. Parlitz, Commun. Nonlin. Sci. Num. Sim. **18**, 2733 (2013).

6 Local observability of state variables and parameters in nonlinear modeling quantified by delay reconstruction

The following pages contain the article

> U. Parlitz, J. Schumann-Bischoff, and S. Luther. "Local observability of state variables and parameters in nonlinear modeling quantified by delay reconstruction". In: *Chaos: An Interdisciplinary Journal of Nonlinear Science* 24.2 (June 2014), p. 024411. DOI: 10.1063/1.4884344.

The idea for the approach of how to quantify the uncertainties was devised by the author U. Parlitz. I designed, implemented, and performed all required simulations in this article, except the simulation underlying Fig. 1 and Fig. 2. Furthermore, I designed and created all figures, with the exception of Fig. 1 and Fig. 2. The text was mainly written by U. Parlitz and revised by the other authors.

Local observability of state variables and parameters in nonlinear modeling quantified by delay reconstruction

Ulrich Parlitz,[1,2,a)] Jan Schumann-Bischoff,[1,2,b)] and Stefan Luther[1,2,c)]
[1]*Max Planck Institute for Dynamics and Self-Organization, Am Faßberg 17, 37077 Göttingen, Germany*
[2]*Institute for Nonlinear Dynamics, Georg-August-Universität Göttingen, Am Faßberg 17, 37077 Göttingen, Germany*

(Received 15 December 2013; accepted 9 June 2014; published online 23 June 2014)

Features of the Jacobian matrix of the delay coordinates map are exploited for quantifying the robustness and reliability of state and parameter estimations for a given dynamical model using a measured time series. Relevant concepts of this approach are introduced and illustrated for discrete and continuous time systems employing a filtered Hénon map and a Rössler system.
 [http://dx.doi.org/10.1063/1.4884344]

For many physical processes, dynamical models (differential equations or iterated maps) are available but often not all of their variables and parameters are known or can be (easily) measured. In meteorology, for example, sophisticated large scale models exist, which have to be continuously adapted to the true temporal changes of temperatures, wind speed, humidity, and other relevant physical quantities. To obtain a model that "follows" reality, measured data have to be repeatedly incorporated into the model. In geosciences, this procedure is called *data assimilation*, but the task to track state variables and system parameters by means of estimation methods occurs also in other fields of physics and applications. However, not all observables provide the information required to estimate a particular unknown quantity. In this article, we consider this problem of *observability* in the context of chaotic dynamics, where sensitive dependence on initial conditions complicates any estimation method. A quantitative characterization of local observability employing delay coordinates is used to answer the question where in state and parameter space estimation of a particular state variable or parameter is feasible and where not.

I. INTRODUCTION

To describe and forecast dynamical processes in physics and many other fields of science mathematical models are used, like, for example, ordinary differential equations (ODEs), partial differential equations (PDEs), or iterated maps. Some of these models are derived from first principles, while others are the result of a general black-box modeling approach (e.g., based on neural networks). These models typically contain two kinds of variables and parameters: those that can be directly measured or are known beforehand (e.g., fundamental physical constants) and others whose values are unknown and very difficult to access.[1,2] To estimate the latter estimation methods have been devised that aim at extracting the required information from the dynamics, here, represented by the model equations and the experimentally observed dynamical evolution of the underlying process. Different approaches for solving this dynamical estimation problem have been devised in the past, including (nonlinear) observer or synchronization schemes,[3–13] particle filters,[14] a path integral formalism,[15,16] or optimization based algorithms.[17–19]

Before applying such an estimation method, one may ask whether the available time series (observable) actually contains the required information to estimate a particular unknown value. In control theory, this is called *observability* problem and it can for linear systems of ODEs be analyzed and answered by means of the so-called observability matrix.[20,21] Using derivative coordinates, this approach can be generalized for nonlinear continuous systems.[20,22,23] For state estimation of chaotic systems, Letellier *et al.*[24–28] considered continuous dynamical systems

$$\dot{\mathbf{x}} = \mathbf{f}(\mathbf{x}) \tag{1}$$

that generate some measured signal $s(t) = h(\mathbf{x}(t)) \in \mathbb{R}$, where $\mathbf{x} \in \mathcal{U} \subset \mathbb{R}^M$ is the state of the system, $\mathcal{U}$ is a smooth submanifold of $\mathbb{R}^M$, and $h : \mathbb{R}^M \to \mathbb{R}$ denotes a measurement or observation function. Consider now D-dimensional derivative coordinates[29–33] of the measured signal $s(t)$

$$\mathbf{y} = \left(s, \dot{s}, \ddot{s}, \ldots, s^{(D-1)}\right) = F(\mathbf{x}) \in \mathbb{R}^D, \tag{2}$$

where $s^{(k)}$ stands for the k-th temporal derivative of $s(t)$, D is the *reconstruction dimension*, and F is called *derivative coordinates map*.[31] If this map is (at least locally) invertible, then we can uniquely determine the full state vector $\mathbf{x}(t) \in \mathcal{U}$ from the signal $s(t)$ and its higher derivatives.[34] Furthermore, small perturbations in $\mathbf{y}$ should correspond to small perturbations in $\mathbf{x}$ and vice versa. Therefore, we want the map $F : \mathcal{U} \to F(\mathcal{U}) \subset \mathbb{R}^D$ to be an *immersion*, i.e., a smooth map whose derivative map is one-to-one at every point of $\mathcal{U}$, or equivalently, whose Jacobian matrix $DF(\mathbf{x})$ has full rank on the tangent space (here, $\operatorname{rank}(DF(\mathbf{x})) = M \; \forall \mathbf{x} \in \mathcal{U}$). This does *not* imply that the map F itself is one-to-one ($F(\mathbf{x}) = F(\mathbf{z}) \Rightarrow \mathbf{x} = \mathbf{z}$), since the derivative coordinates (2) may provide states $\mathbf{y} \in \mathbb{R}^D$ with two (or more) pre-images

[a)]Electronic mail: ulrich.parlitz@ds.mpg.de
[b)]Electronic mail: jan.schumann-bischoff@ds.mpg.de
[c)]Electronic mail: stefan.luther@ds.mpg.de

separated by a *finite* distance. Therefore, the observability analysis presented in the following is *local*, only, because it is based on analyzing (the rank of) the Jacobian matrix DF. The (global) one-to-one property of the map F is *not* checked (what would be necessary, and for compact U also sufficient, to show that F is an *embedding*[31]).

The $D \times M$ Jacobian matrix $DF(\mathbf{x})$ can be computed by means of the vector field given in Eq. (1). In fact, for linear ODEs, the Jacobian matrix $DF(\mathbf{x})$ conforms with the *observability matrix* known from (linear) control theory.[25] To estimate the rank of $DF(\mathbf{x})$, Letellier *et al.*[24,25] suggest to compute the eigenvalues $\mu_k \geq 0$ of the $M \times M$ matrix

$$A(\mathbf{x}) = DF^{tr}(\mathbf{x}) \cdot DF(\mathbf{x}). \tag{3}$$

Nonzero eigenvalues of $A(\mathbf{x})$ indicate full rank of $DF(\mathbf{x})$ and, thus, local invertibility of F at $\mathbf{x}$. To quantify the (local) invertibility of $F(\mathbf{x})$ and, thus, the (local) observability of the full state $\mathbf{x}$ Aguirre *et al.*[24,25] introduced the *observability index*

$$\delta(\mathbf{x}) = \frac{\mu_{min}(A)}{\mu_{max}(A)}, \tag{4}$$

where $\mu_{min}(A)$ and $\mu_{max}(A)$ denote the smallest and the largest eigenvalues of the matrix A, respectively. Time averaging (along the available trajectory for $0 \leq t \leq T$) yields

$$\bar{\delta} = \frac{1}{T}\int_0^T \delta(\mathbf{x}(t))dt. \tag{5}$$

Instead of derivative coordinates, we consider in the following delay coordinates.[29–33] Furthermore, we extend the observability analysis to parameter estimation and compute a specific measure of uncertainty[35] for each state variable or parameter to be estimated. Last not least, we are not only interested in quantifying the average observability (like $\bar{\delta}$ in Eq. (5)) but also in local variations that can be exploited during the state and parameter estimation process.

II. DELAY COORDINATES AND OBSERVABILITY

To motivate the concepts to be presented, in the following, we shall first consider a discrete time system (iterated map), where all model parameters are known and only state variables have to be estimated from the measured time series.

A. Estimating state variables of a filtered Hénon map

For an M dimensional discrete system

$$\mathbf{x}(n+1) = \mathbf{g}(\mathbf{x}(n)), \tag{6}$$

which generates the times series $\{s(n)\}$ with $s(n) = h(\mathbf{x}(n))$, where $n = 1,\ldots, N$, we can construct D dimensional *delay coordinates*[29–33] with reconstructed states

$$\begin{aligned}\mathbf{y}(n) &= (s(n), s(n+1), \ldots., s(n+D-1)),\\ &= G_+(\mathbf{x}(n)) \in \mathbb{R}^D.\end{aligned} \tag{7}$$

Again we assume that all states of interest $\mathbf{x}$ lie within a smooth manifold $\mathcal{U} \subset \mathbb{R}^M$. Here, we consider delay coordinates *forward* in time. The function G_+ is therefore called *forward delay coordinates map* $G_+ : \mathcal{U} \to G_+(\mathcal{U}) \subset \mathbb{R}^D$. It is also possible to use delay coordinates *backward* in time, or mixed forward and backward, and we shall address this issue in Sec. II B.

As already discussed with derivative coordinates in Sec. I, a state $\mathbf{x} = (x_1,\ldots,x_M)$ is locally observable from the time series $\{s(n)\}$, if G_+ is an immersion, i.e., if the Jacobian matrix $DG_+(\mathbf{x})$ has maximal (full) rank M at $\mathbf{x}$. The corresponding $D \times M$ Jacobian matrix $DG_+(\mathbf{x})$ can be computed using the iterated map Eq. (6). If the Jacobian matrix $DG_+(\mathbf{x})$ has maximal rank M (assuming $M \leq D$), then, G_+ is locally invertible (on $G_+(\mathcal{U})$). "Local" means that still a delay vector $\mathbf{y}$ could possess different pre images (separated by a finite distance).

To motivate and illustrate this analysis, we consider the Hénon map

$$x_1(n+1) = 1 - ax_1^2(n) + bx_2(n), \tag{8}$$

$$x_2(n+1) = x_1(n) \tag{9}$$

with parameters $a = 1.4$ and $b = 0.3$. In the following, we shall assume that the dynamics of this system is observed via a filtered signal $s(n)$ provided by an FIR-filter

$$\begin{aligned}s(n) &= x_1(n) + cx_1(n-1),\\ &= x_1(n) + cx_2(n) = h(\mathbf{x}(n))\end{aligned} \tag{10}$$

with filter parameter c.

For two dimensional delay coordinates, the delay coordinates map reads

$$\begin{aligned}G_+(\mathbf{x}(n)) &= (s(n), s(n+1)),\\ &= (x_1(n) + cx_2(n), 1 - ax_1^2(n) + bx_2(n) + cx_1(n))\end{aligned}$$

or

$$G_+(\mathbf{x}) = (x_1 + cx_2, 1 - ax_1^2 + bx_2 + cx_1). \tag{11}$$

The Jacobian matrix of the map G_+ is given by

$$DG_+(\mathbf{x}) = \begin{pmatrix} 1 & c \\ -2ax_1 + c & b \end{pmatrix} \tag{12}$$

and its determinant

$$\det(DG_+(\mathbf{x})) = 2acx_1 + b - c^2 \tag{13}$$

vanishes for all states $\mathbf{x} = (x_1, x_2)$ on the singular line

$$x_1^s = \frac{c^2 - b}{2ac}. \tag{14}$$

For $c \to 0$, the FIR-filter is (asymptotically) deactivated and the critical line disappears ($c \to 0 \Rightarrow x_1^s \to -\infty$). For $0.0867 < c < 3.66$, however, the critical line crosses the chaotic attractor as shown for $c = 0.5$ in Fig. 1(a).

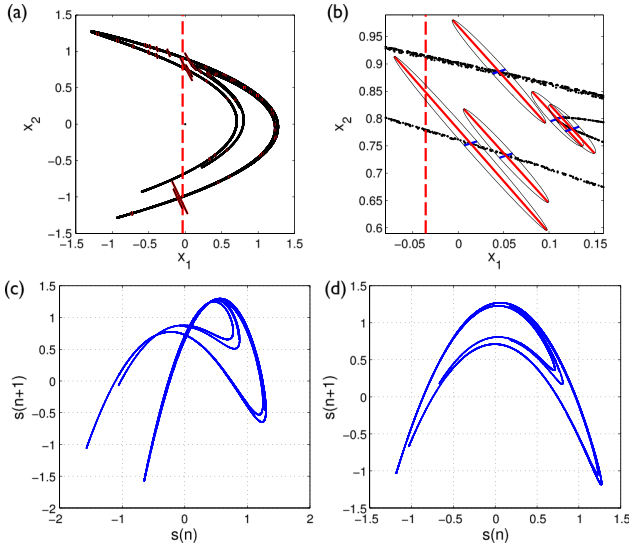

FIG. 1. (a) and (b) Hénon attractor and singular axes $\frac{1}{\sigma_1}\mathbf{v}^{(1)}$ (short, blue) and $\frac{1}{\sigma_2}\mathbf{v}^{(2)}$ (longer, red) for filter parameter $c=0.5$. (c) and (d) delay coordinates for $c=0.5$ ($x_1^s=-0.0357$) and $c=0.08$ ($x_1^s=-1.311$).

B. Forward, backward, and mixed delay coordinates

Instead of using state space reconstruction based on forward delay coordinates (7), one could also use *backward* delay coordinates

$$\begin{aligned}\mathbf{y}(n) &= (s(n),\, s(n-1),\ldots,\, s(n-D+1)),\\ &= G_-(\mathbf{x}(n)) \in \mathbb{R}^D\end{aligned} \tag{15}$$

or more general, a combination of forward and backward components

$$\begin{aligned}\mathbf{y}(n) &= (s(n-D_-),\ldots s(n-1), s(n), s(n+1),\\ &\quad \ldots, s(n+D_+)),\\ &= G_\pm(\mathbf{x}(n); D_-, D_+) \in \mathbb{R}^D\end{aligned} \tag{16}$$

called *mixed* delay coordinates in the following, with reconstruction dimension $D=1+D_-+D_+$. To obtain the backward components $s(n-k)=h((\mathbf{x}(n-k)$, the inverse map $\mathbf{x}(n-1)=\mathbf{g}^{-1}(\mathbf{x}(n))$ and its Jacobian matrix are required (here, we assume that the dynamics is time invertible). For discrete time systems (like the Hénon example), the underlying map (6) has to be inverted and, for continuous time systems, the inverse of the flow can, in principle, be computed by integrating the system ODEs (1) backward in time. In both cases, however, problems may occur in practice, because an explicit form of the inverse map may not exist and backward integration of dissipative systems results in diverging solutions and numerical instabilities (for longer integration times). Despite these difficulties inclusion of backward components turns out to be beneficial for the estimation task as will be demonstrated in the following for the Hénon examples and the Rössler system.

C. Noisy observations and uncertainty

At states $(x_1,\, x_2)$ with $x_1 \neq x_1^s$, the delay coordinates map G is, in principle, invertible, but the inverse can be very susceptible to perturbations in $\mathbf{y}$ like measurement noise. To quantify the robustness and the sensitivity of the inverse with respect to noise, we consider the singular value decomposition of the Jacobian matrix DG of the delay coordinates map

$$DG = U\cdot S\cdot V^{tr}, \tag{17}$$

where $S=\mathrm{diag}(\sigma_1,\ldots,\sigma_M)$ is an $M\times M$ diagonal matrix containing the singular values $\sigma_1\geq\sigma_2\geq\ldots\geq\sigma_M\geq 0$ and $U=(\mathbf{u}^{(1)},\ldots,\,\mathbf{u}^{(M)})$ and $V=(\mathbf{v}^{(1)},\ldots,\,\mathbf{v}^{(M)})$ are orthogonal matrices, represented by the column vectors $\mathbf{u}^{(i)}\in\mathbb{R}^D$ and $\mathbf{v}^{(i)}\in\mathbb{R}^M$, respectively. V^{tr} is the transposed of V coinciding with the inverse $V^{-1}=V^{tr}$. Analogously, $U^{tr}=U^{-1}$ and the inverse Jacobian matrix reads

$$DG^{-1} = V\cdot S^{-1}\cdot U^{tr}, \tag{18}$$

where $S^{-1}=\mathrm{diag}(1/\sigma_1,\ldots,1/\sigma_M)$. Multiplying by U from the right, we obtain $DG^{-1}U=V\cdot S^{-1}$ or

$$DG^{-1}\mathbf{u}^{(m)} = \frac{1}{\sigma_m}\mathbf{v}^{(m)}, \quad (m=1,\ldots,M). \tag{19}$$

This transformation is illustrated in Fig. 2 and it describes how small perturbations of $\mathbf{y}$ in delay reconstruction space result in deviations from $\mathbf{x}$ in the original state space. Most relevant for the observability of the (original) state $\mathbf{x}$ is the length of the longest principal axis of the ellipsoid given by the inverse of the smallest singular value σ_M (see Fig. 2). Small singular values correspond to directions in state space, where it is difficult (or even impossible) to locate the true state $\mathbf{x}$ given a finite precision of the reconstructed state $\mathbf{y}$. For the filtered Hénon map, we find that the closer the state $\mathbf{x}$ is to the critical line given by x_1^s (14), the more severe is this uncertainty. This is illustrated in Figs. 1(a) and 1(b), where at some points $\mathbf{x}$, the ellipses spanned by the column vectors of the matrix $V\cdot S^{-1}$ are plotted. Figure 3 shows (color coded) the logarithm of the ratio smallest singular value $\sigma_{min}=\sigma_M$ (here: $M=2$) divided by the largest singular value $\sigma_{max}=\sigma_1$ vs. state variables x_1 and x_2 in a range of coordinates containing the chaotic Hénon attractor. In Fig. 3(a), $D=2$ dimensional forward delay (7) is considered, where at x_1^s, the smallest singular value $\sigma_{min}=\sigma_M=\sigma_2$ vanishes indicating the singularity (14) illustrated in Figs. 1(a) and 1(b). If the reconstruction dimension D is increased from $D=2$ to $D=3$, the singularity disappears as can be seen in Fig. 3(b) showing the ratio $\sigma_{min}/\sigma_{max}$

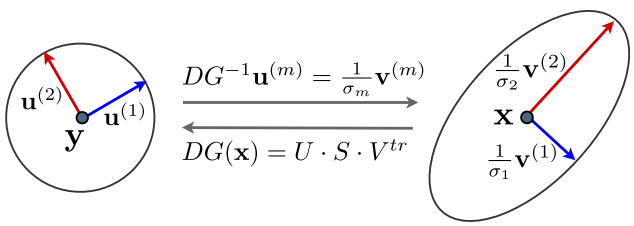

FIG. 2. The inverse Jacobian $DG^{-1}(\mathbf{y})$ maps perturbations of $\mathbf{y}$ in delay reconstruction space to deviations from the state $\mathbf{x}$ whose magnitudes depend on the direction of the perturbation as described by Eq. (19).

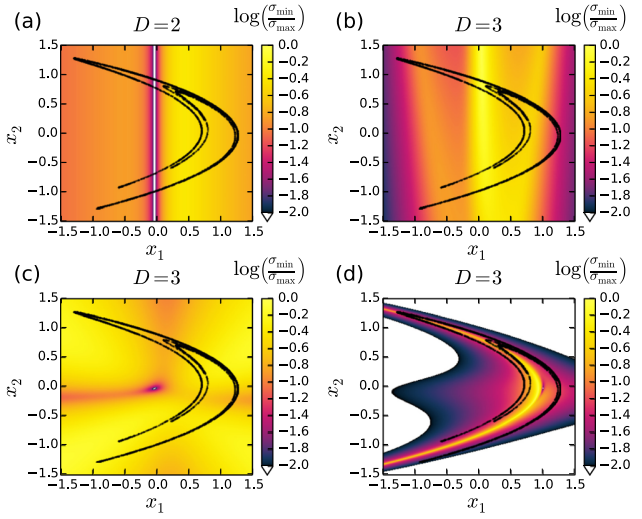

FIG. 3. Local observability of the filtered Hénon map (8)–(10). Logarithm of the (color coded) ratio of the smallest singular value $\sigma_{min} = \sigma_M$ ($M = 2$) divided by largest singular value $\sigma_{max} = \sigma_1$ vs. coordinates x_1 and x_2 for $c = 0.5$. (a) $D = 2$ dimensional forward delay coordinates (7), (b) $D = 3$ dimensional forward delay coordinates (7), (c) $D = 3$ dimensional mixed delay coordinates (16) ($D_- = 1 = D_+$), and (d) $D = 3$ dimensional backward delay coordinates (15).

(color coded) for $D = 3$ dimensional forward delay coordinates. For comparison, Figs. 3(c) and 3(d) show results obtained with mixed delay coordinates (16) and backward delay coordinates (15), respectively. The white areas in Fig. 3(d) correspond to ratios $\sigma_{min}/\sigma_{max} < 0.01$ indicating poor observability (due to fast divergence of backward iterates of the Hénon map). Further increase of the reconstruction dimension ($D = 4$ or $D = 5$) results in larger values of $\sigma_{min}/\sigma_{max}$ (not shown here).

To assess the observability on the Hénon attractor, we computed histograms of ratios $\sigma_{min}/\sigma_{max}$ at 10^6 points. Figure 4 shows these histograms for the same coordinates used to generate the corresponding diagrams in Fig. 3. The best results (large ratios) provide mixed delay coordinates (Fig. 4(c)). We speculate that this is due to the fact that forward and backward components cover different directions in state space (similar to Lyapunov vectors corresponding to positive and negative Lyapunov exponents).

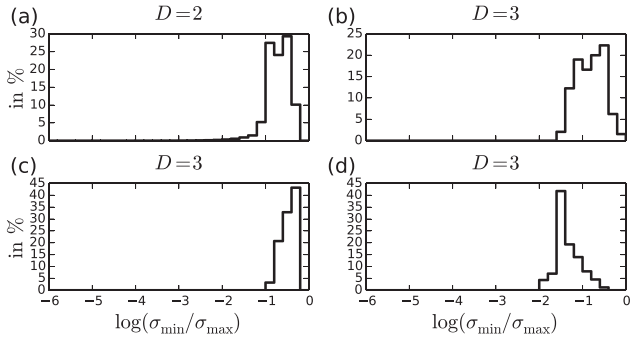

FIG. 4. Histograms of ratios $\sigma_{min}/\sigma_{max}$ computed at 10^6 points of the Hénon attractor with: (a) $D = 2$ dimensional forward delay coordinates (7), (b) $D = 3$ dimensional forward delay coordinates (7), (c) $D = 3$ dimensional mixed delay coordinates (16) ($D_- = 1 = D_+$), and (d) $D = 3$ dimensional backward delay coordinates (15). Compare corresponding diagrams in Fig. 3.

If the perturbations of the reconstructed state $\mathbf{y}$ are due to normally distributed, independent measurement noise, then they can be described by a symmetric Gaussian distribution centered at $\mathbf{y}$

$$Q(\tilde{\mathbf{y}}) = \frac{\exp\left[-\frac{1}{2}(\tilde{\mathbf{y}} - \mathbf{y})^{tr}\Sigma_y^{-1}(\tilde{\mathbf{y}} - \mathbf{y})\right]}{\sqrt{(2\pi)^D \det(\Sigma_y)}}, \tag{20}$$

where $\Sigma_y = \mathrm{diag}(\rho^2,\ldots,\rho^2) = \rho^2 I_D$ denotes the $D \times D$ covariance matrix (I_D stands for the D-dimensional unit matrix) and the standard deviation ρ quantifies the noise amplitude. For (infinitesimally) small perturbations $\Delta\mathbf{y} = \tilde{\mathbf{y}} - \mathbf{y}$, this distribution is mapped by the (pseudo) inverse of the delay coordinates map to the (non-symmetrical) distribution

$$P(\tilde{\mathbf{x}}) = \frac{\exp\left[-\frac{1}{2}(\tilde{\mathbf{x}} - \mathbf{x})^{tr}\Sigma_x^{-1}(\tilde{\mathbf{x}} - \mathbf{x})\right]}{\sqrt{(2\pi)^M \det(\Sigma_x)}} \tag{21}$$

centered at $\mathbf{x}$ with the inverse covariance matrix

$$\Sigma_x^{-1} = DG^{tr} \cdot \Sigma_y^{-1} \cdot DG = \frac{1}{\rho^2} DG^{tr} \cdot DG, \tag{22}$$

$$= \frac{1}{\rho^2} V \cdot S^2 \cdot V^{tr}. \tag{23}$$

The marginal distribution P_j of a given state variable $\tilde{x}_j$ centered at x_j is given by

$$P_j(\tilde{x}_j) = \frac{1}{\rho_j\sqrt{2\pi}} \exp\left[-\frac{(\tilde{x}_j - x_j)^2}{2\rho_j^2}\right], \tag{24}$$

where the standard deviation ρ_j is given by the square root of the diagonal elements of the covariance matrix

$$\rho_j = \sqrt{\Sigma_{x,jj}}. \tag{25}$$

Using Eq. (22), the standard deviation of the marginal distribution P_j can be written

$$\rho_j = \rho\sqrt{[DG^{tr} \cdot DG]_{jj}^{-1}} = \rho\sqrt{[V \cdot S^{-2} \cdot V^{tr}]_{jj}} \tag{26}$$

and we consider in the following the factor

$$\nu_j = \sqrt{[DG^{tr} \cdot DG]_{jj}^{-1}} = \sqrt{[V \cdot S^{-2} \cdot V^{tr}]_{jj}} \tag{27}$$

as our measure of *uncertainty* when estimating x_j, because it quantitatively describes how the initial standard deviation ρ is amplified when estimating variable x_j.[35]

Figure 5 shows the uncertainties ν_1 and ν_2 vs. (x_1, x_2) for different $D = 3$ dimensional delay coordinates. In Figs. 4(a) and 4(b), results obtained with $D = 3$ dimensional forward delay coordinates (7) are given. Large uncertainties occur mainly in a vertical stripe located near the singularity at x_1^s (Eq. (14)) occurring for $D = 2$. Figures 5(c)–5(f) show uncertainties of x_1 and x_2 obtained with mixed delay

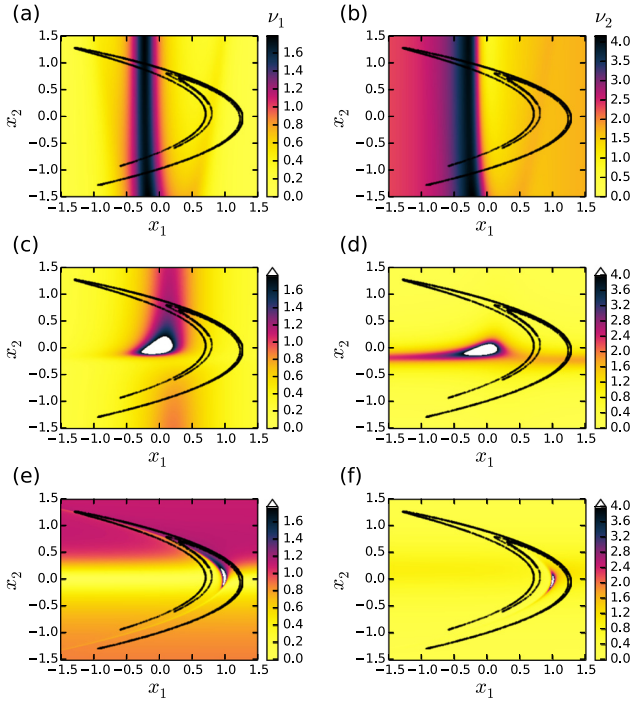

FIG. 5. Uncertainty (27) of the variables x_1 and x_2 of the Hénon map for $c=0.5$ and different $D=3$ dimensional delay coordinates. (a) and (b) forward coordinates (7), (c) and (d) mixed coordinates (16), and (e) and (f) backward coordinates (15).

coordinates ((c) and (d)) and backward delay coordinates ((e) and (f)). For mixed delay coordinates (Figs. 5(c) and 5(d)) areas with very high uncertainties occur near the origin, but along the attractor ν_1 and ν_2 take only relatively low values. This is also confirmed by the ν-histograms on the attractor given in Fig. 6 for the same delay coordinates as used in Fig. 4. Again, the mixed delay coordinates turn out to be superior to the purely forward or backward coordinates. Furthermore, the dependence of the range of uncertainty values on the type of coordinates is different for different variables. While the uncertainty ν_1 of x_1 increases when changing from forward to backward delay coordinates (Figs. 6(a) and 6(e)), the uncertainty of x_2 exhibits the opposite trend (Figs. 6(b) and 6(f)).

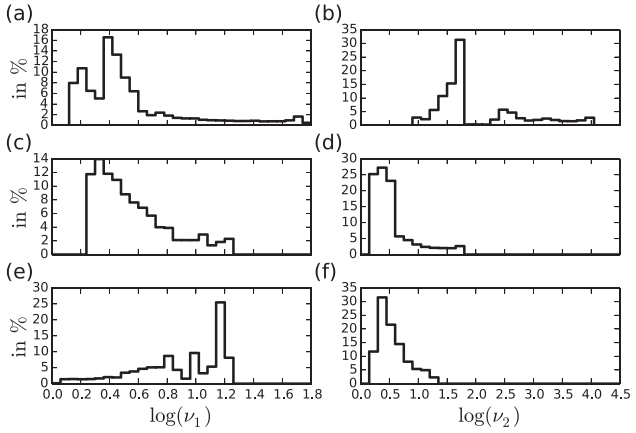

FIG. 6. Histograms of uncertainties (27) of x_1 and x_2 on the Hénon attractor (computed at 10^6 points) for $D=3$ and $c=0.5$ with (a) and (b) forward, (c) and (d) mixed, and (e) and (f) backward delay coordinates (compare Fig. 4).

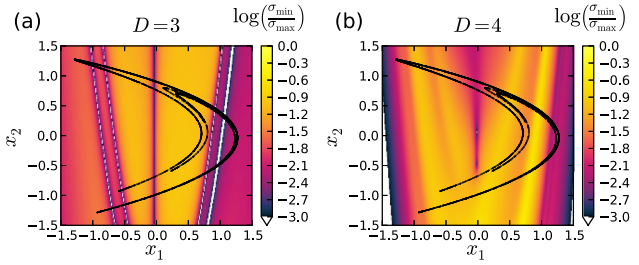

FIG. 7. Logarithm of ratio smallest singular value $\sigma_{min}=\sigma_3$ divided by largest singular value $\sigma_{max}=\sigma_1$ vs. x_1 and x_2 for the case of $M+P=3$ unknowns (x_1, x_2, $p_1=a$). The diagram shows the plane $p_1=a=1.4$ in the three dimensional estimation space. The other parameters are $b=0.3$ and $c=0.5$. Diagrams (a) and (b) show the results obtained with forward delay reconstruction dimensions $D=3$ and $D=4$, respectively.

D. State and parameter estimation

Until now, only the state variables x_1 and x_2 are considered as unknowns to be estimated and the parameters a and b of the Hénon map and c of the FIR filter are assumed to be known. We shall now consider the general case including unknown parameters $\mathbf{p}=(p_1,\ldots,p_P)\in\mathbb{R}^P$ of the dynamical system and unknown parameters $\mathbf{q}=(q_1,\ldots,q_Q)\in\mathbb{R}^Q$ of the measurement function $h(\mathbf{x},\mathbf{q})$. Let the dynamical model be a M-dimensional discrete

$$\mathbf{x}(n+1)=\mathbf{g}(\mathbf{x}(n),\mathbf{p}) \tag{28}$$

or a continuous

$$\dot{\mathbf{x}}=\mathbf{f}(\mathbf{x},\mathbf{p}) \tag{29}$$

dynamical system generating a flow

$$\phi^t:\mathbb{R}^M\to\mathbb{R}^M \tag{30}$$

with discrete $t=n\in\mathbb{Z}$ or continuous $t\in\mathbb{R}$ time. Furthermore, let's assume that a time series $\{s(n)\}$ of length N is given observed via the measurement function

$$s(t)=h(\phi^t(\mathbf{x},\mathbf{p}),\mathbf{q}) \tag{31}$$

from a trajectory starting at $\mathbf{x}$.

This provides the D-dimensional delay coordinates

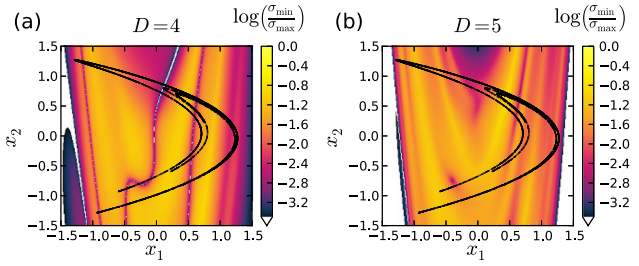

FIG. 8. Logarithm of the ratio of singular values $\sigma_{min}/\sigma_{max}=\sigma_4/\sigma_1$ vs. x_1 and x_2 for the case of $M+P=4$ unknown quantities (x_1, x_2, $p_1=a$, $p_2=b$). The diagrams show the x_1-x_2 plane at fixed $p_1=a=1.4$ and $p_2=b=0.3$ in the four dimensional estimation space for $c=0.5$. Diagrams (a) and (b) show the results obtained with forward delay reconstruction dimensions $D=4$ and $D=5$, respectively.

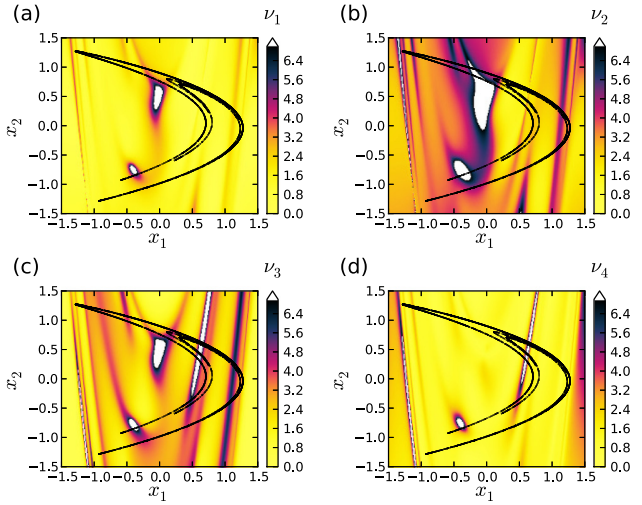

FIG. 9. Estimation of uncertainties ν_j ($j=1,\ldots,M=4$) of variables (x_1, x_2) and parameters ($p_1=a$, $p_2=b$) of the Hénon map (8) obtained with $D=5$ dimensional forward delay coordinates.

$$\begin{aligned}\mathbf{y} &= (s(-D_-\tau_-),\ldots,s(-\tau_-),s(0),s(\tau_+),\ldots,s(D_+\tau_+)),\\ &= G(\mathbf{x},\mathbf{p},\mathbf{q};D_-,D_+,\tau_-,\tau_+)\in\mathbb{R}^D \end{aligned} \tag{32}$$

with $D=1+D_-+D_+$. Here, the delay coordinates map G is considered as a function of: (i) the state $\mathbf{x}$ and the parameters $\mathbf{p}$ of the underlying system, (ii) the parameters $\mathbf{q}$ of the measurement function, (iii) the dimension parameters D_- and D_+, and (iv) the delay times τ_- and τ_+ in backward and forward directions, respectively. The option to use different delay times, τ_- and τ_+ for the backward and forward iterations is motivated by the fact that for dissipative systems backward solutions $\phi^{\tau_-}(\mathbf{x})$ quickly diverge and therefore a choice $\tau_-<\tau_+$ may be more appropriate. For the same reason, D_- has typically to be smaller than D_+. Since the reconstruction dimensions and the delay times are chosen a priori and are not part of the estimation problem they shall not be listed as arguments of G to avoid clumsy notation. The Jacobian matrix $DG(\mathbf{x},\mathbf{p},\mathbf{q})$ of G has the structure

$$DG(\mathbf{x},\mathbf{p},\mathbf{q}) = (A,B,C), \tag{33}$$

where

$$A=\begin{pmatrix} \frac{\partial h(\phi^{-D_-\tau_-}(\mathbf{x},\mathbf{p}),\mathbf{q})}{\partial x_1} & \cdots & \frac{\partial h(\phi^{-D_-\tau_-}(\mathbf{x},\mathbf{p}),\mathbf{q})}{\partial x_M}\\ \vdots & \vdots & \vdots\\ \frac{\partial h(\phi^{-\tau_-}(\mathbf{x},\mathbf{p}),\mathbf{q})}{\partial x_1} & \cdots & \frac{\partial h(\phi^{-\tau_-}(\mathbf{x},\mathbf{p}),\mathbf{q})}{\partial x_M}\\ \frac{\partial h(\mathbf{x},\mathbf{q})}{\partial x_1} & \cdots & \frac{\partial h(\mathbf{x},\mathbf{q})}{\partial x_M}\\ \frac{\partial h(\phi^{\tau_+}(\mathbf{x},\mathbf{p}),\mathbf{q})}{\partial x_1} & \cdots & \frac{\partial h(\phi^{\tau_+}(\mathbf{x},\mathbf{p}),\mathbf{q})}{\partial x_M}\\ \vdots & \vdots & \vdots\\ \frac{\partial h(\phi^{D_+\tau_+}(\mathbf{x},\mathbf{p}),\mathbf{q})}{\partial x_1} & \cdots & \frac{\partial h(\phi^{D_+\tau_+}(\mathbf{x},\mathbf{p}),\mathbf{q})}{\partial x_M} \end{pmatrix},$$

$$B=\begin{pmatrix} \frac{\partial h(\phi^{-D_-\tau_-}(\mathbf{x},\mathbf{p}),\mathbf{q})}{\partial p_1} & \cdots & \frac{\partial h(\phi^{-D_-\tau_-}(\mathbf{x},\mathbf{p}),\mathbf{q})}{\partial p_P}\\ \vdots & \vdots & \vdots\\ \frac{\partial h(\phi^{-\tau_-}(\mathbf{x},\mathbf{p}),\mathbf{q})}{\partial p_1} & \cdots & \frac{\partial h(\phi^{-\tau_-}(\mathbf{x},\mathbf{p}),\mathbf{q})}{\partial p_P}\\ 0 & \cdots & 0\\ \frac{\partial h(\phi^{\tau_+}(\mathbf{x},\mathbf{p}),\mathbf{q})}{\partial p_1} & \cdots & \frac{\partial h(\phi^{\tau_+}(\mathbf{x},\mathbf{p}),\mathbf{q})}{\partial p_P}\\ \vdots & \vdots & \vdots\\ \frac{\partial h(\phi^{D_+\tau_+}(\mathbf{x},\mathbf{p}),\mathbf{q})}{\partial p_1} & \cdots & \frac{\partial h(\phi^{D_+\tau_+}(\mathbf{x},\mathbf{p}),\mathbf{q})}{\partial p_P} \end{pmatrix},$$

$$C=\begin{pmatrix} \frac{\partial h(\phi^{-D_-\tau_-}(\mathbf{x},\mathbf{p}),\mathbf{q})}{\partial q_1} & \cdots & \frac{\partial h(\phi^{-D_-\tau_-}(\mathbf{x},\mathbf{p}),\mathbf{q})}{\partial q_L}\\ \vdots & \vdots & \vdots\\ \frac{\partial h(\phi^{-\tau_-}(\mathbf{x},\mathbf{p}),\mathbf{q})}{\partial q_1} & \cdots & \frac{\partial h(\phi^{-\tau_-}(\mathbf{x},\mathbf{p}),\mathbf{q})}{\partial q_L}\\ \frac{\partial h(\mathbf{x},\mathbf{q})}{\partial q_1} & \cdots & \frac{\partial h(\mathbf{x},\mathbf{q})}{\partial q_L}\\ \frac{\partial h(\phi^{\tau_+}(\mathbf{x},\mathbf{p}),\mathbf{q})}{\partial q_1} & \cdots & \frac{\partial h(\phi^{\tau_+}(\mathbf{x},\mathbf{p}),\mathbf{q})}{\partial q_L}\\ \vdots & \vdots & \vdots\\ \frac{\partial h(\phi^{D_+\tau_+}(\mathbf{x},\mathbf{p}),\mathbf{q})}{\partial q_1} & \cdots & \frac{\partial h(\phi^{D_+\tau_+}(\mathbf{x},\mathbf{p}),\mathbf{q})}{\partial q_L} \end{pmatrix},$$

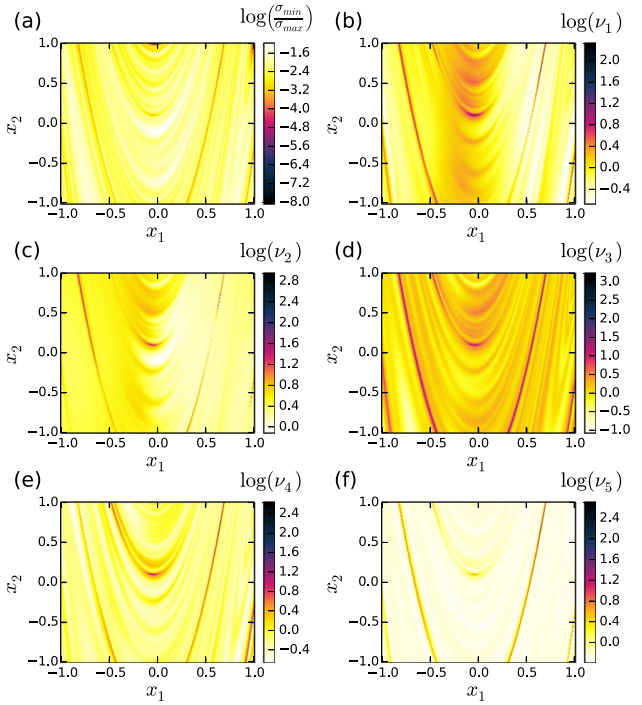

FIG. 10. Estimation of all variables $\mathbf{x}=(x_1,\ x_2)$ and model parameters $\mathbf{p}=(p_1,p_2)=(a,\ b)$ of the Hénon map (8), and the measurement function parameter $q=c$ (FIR filter (10)). The output of the FIR filter is forward embedded in $D=9$ dimensions. (a) Ratio of smallest and largest singular values. (b)–(f) Uncertainties ν_j of state variables and parameters in the plane $\{(x_1,\ x_2,\ p_1,\ p_2,\ q)$: $((x_1,\ x_2)\in[-1.,\ 1.]\times[-1.,\ 1.],\ p_1=a=1.4,\ p_2=b=0.3,\ q=c=0.5\}$.

and it can also be written as

$$DG = \begin{pmatrix} \nabla_x h(\phi^{-D_-\tau_-}(\mathbf{x},\mathbf{p}),\mathbf{q}) \cdot D_x\phi^{-D_-\tau_-}(\mathbf{x},\mathbf{p}) & \nabla_x h(\phi^{-D_-\tau_-}(\mathbf{x},\mathbf{p}),\mathbf{q}) \cdot D_p\phi^{-D_-\tau_-}(\mathbf{x},\mathbf{p}) & \nabla_q h(\phi^{-D_-\tau_-}(\mathbf{x},\mathbf{p}),\mathbf{q}) \\ \vdots & \vdots & \vdots \\ \nabla_x h(\phi^{-\tau_-}(\mathbf{x},\mathbf{p}),\mathbf{q}) \cdot D_x\phi^{-\tau_-}(\mathbf{x},\mathbf{p}) & \nabla_x h(\phi^{-\tau_-}(\mathbf{x},\mathbf{p}),\mathbf{q})) \cdot D_p\phi^{-\tau_-}(\mathbf{x},\mathbf{p}) & \nabla_q h(\phi^{-\tau_-}(\mathbf{x},\mathbf{p}),\mathbf{q}) \\ \nabla_x h(\mathbf{x},\mathbf{q}) & 0 & \nabla_q h(\mathbf{x},\mathbf{q}) \\ \nabla_x h(\phi_+^{\tau}(\mathbf{x},\mathbf{p}),\mathbf{q}) \cdot D_x\phi_+^{\tau}(\mathbf{x},\mathbf{p}) & \nabla_x h(\phi_+^{\tau}(\mathbf{x},\mathbf{p}),\mathbf{q})) \cdot D_p\phi_+^{\tau}(\mathbf{x},\mathbf{p}) & \nabla_q h(\phi_+^{\tau}(\mathbf{x},\mathbf{p}),\mathbf{q}) \\ \vdots & \vdots & \vdots \\ \nabla_x h(\phi^{D_+\tau_+}(\mathbf{x},\mathbf{p}),\mathbf{q}) \cdot D_x\phi^{D_+\tau_+}(\mathbf{x},\mathbf{p}) & \nabla_x h(\phi^{D_+\tau_+}(\mathbf{x},\mathbf{p}),\mathbf{q}) \cdot D_p\phi^{D_+\tau_+}(\mathbf{x},\mathbf{p}) & \nabla_q h(\phi^{D_+\tau_+}(\mathbf{x},\mathbf{p}),\mathbf{q}) \end{pmatrix} \tag{34}$$

with

$$\nabla_x h(\mathbf{x},\mathbf{q}) = \left(\frac{\partial h}{\partial x_1},\ldots,\frac{\partial h}{\partial x_M}\right)(\mathbf{x},\mathbf{q}), \tag{35}$$

$$\nabla_q h(\mathbf{x},\mathbf{q}) = \left(\frac{\partial h}{\partial q_1},\ldots,\frac{\partial h}{\partial q_Q}\right)(\mathbf{x},\mathbf{q}), \tag{36}$$

where $D_x\phi^t(\mathbf{x},\mathbf{p})$ and $D_p\phi^t(\mathbf{x},\mathbf{p})$ denote the Jacobian matrices of the flow ϕ^t whose elements are derivatives with respect to the state variables $\mathbf{x}$ and the parameters $\mathbf{p}$, respectively. For discrete dynamical systems (28), the Jacobians $D_x\phi^t(\mathbf{x},\mathbf{p})$ and $D_p\phi^t(\mathbf{x},\mathbf{p})$ can be computed using the chain rule and the recursion schemes

$$D_x\phi^{t+1}(\mathbf{x},\mathbf{p}) = D_x g(\phi^t(\mathbf{x},\mathbf{p}),\mathbf{p}) \cdot D_x\phi^t(\mathbf{x},\mathbf{p}), \tag{37}$$

$$D_p\phi^{t+1}(\mathbf{x},\mathbf{p}) = D_x g(\phi^t(\mathbf{x},\mathbf{p}),\mathbf{p}) \cdot D_p g(\phi^t(\mathbf{x},\mathbf{p}),\mathbf{p}) + D_p\phi^t(\mathbf{x},\mathbf{p}), \tag{38}$$

with $D_x\phi^0(\mathbf{x},\mathbf{p}) = I_D$ ($D \times D$ unit matrix) and $D_p\phi^0(\mathbf{x},\mathbf{p}) = 0$. If backward iterations are required ($D_- > 0$ and $\tau_- > 0$) similar recursion schemes exist based on the inverse map g^{-1} (providing ϕ^{-t}) and its Jacobian matrices $D_x g^{-1}$ and $D_p g^{-1}$. Instead of recursion schemes, one may also use symbolic or automatic differentiation.[36] For continuous systems (29), the required Jacobians can be obtained by simultaneously solving linearized systems equations as will be discussed in Sec. II F. Inverse maps ($D_- > 0$ and $\tau_- > 0$) may be computed via backward integration of the ODEs (at least for short periods of time before solutions diverge significantly). An extension for multivariate time series is straightforward.

E. Parameter estimation for the Hénon map

We shall now extend the discussion to include not only state estimation but also parameter estimation. For better readability, only forward delay coordinates are considered in the following, but all steps can also be done with mixed or backward delay coordinates, of course. We first consider the case, where b and c are assumed to be known and only a has to be estimated. In this case, $M = 2$ unknown variables and $P = 1$ unknown system parameter exists (while $Q = 0$). Therefore, delay coordinates with dimension $D = 3$ or higher will be used. Figure 7 shows the ratio of singular values $\sigma_{min}/\sigma_{max} = \sigma_3/\sigma_1$ vs. (x_1, x_2) in a plane in $\mathbb{R}^3$ given by $p_1 = a = 1.4$ (and fixed parameters $b = 0.3$ and $c = 0.5$). For reconstruction dimension $D = 3$, the ration $\sigma_{min}/\sigma_{max}$ is very small for extended subsets $(\mathbf{x}, \mathbf{p}) = (x_1, x_2, p_1)$ of the plane (white stripes in Fig. 7(a)). If the delay reconstruction dimension is increased to $D = 4$ (Fig. 7(b)). These regions shrink or disappear. If the dimension D is increased furthermore, the delay coordinates map has full rank in the full range of x_1 and x_2 values shown in Fig. 7 (results not shown here).

Now, we include $p_2 = b$ in the list of quantities to be estimated. Figure 8 shows the ratio of singular values $\sigma_{min}/\sigma_{max}$ for reconstruction dimensions $D = 4$ and $D = 5$. For $D = 4$ curves with very low singular value ratios $\sigma_{min}/\sigma_{max}$ exist crossing the Hénon attractor, which disappear for $D = 5$.

Figure 9 shows the uncertainties $\nu_1,\ldots,\nu_4$ (Eq. (27)) for $D = 5$. As can be seen, the values of uncertainties vary strongly in the x_1–x_2 plane and still some islands with rather large uncertainties exist.

Similar results are obtained if we include the remaining parameters c in the estimation problem. Scanning the two-dimensional x_1–x_2 subspace (plane) of the $M + P = 5$ dimensional estimation problem for $(\mathbf{x}, \mathbf{p}) = (x_1, x_2, p_1, p_2, q)$ with fixed $p_1 = a = -1.4$, $p_2 = b = 0.3$, and $q = c = 0.5$ indicates (almost) vanishing smallest singular values as long as $D \leq 8$. With $D = 9$ dimensional delay coordinates, the Jacobian matrix $DG(\mathbf{x}, \mathbf{p})$ has clearly full rank almost everywhere within the chosen range $(x_1, x_2) \in [-1., 1.] \times [-1., 1.]$ as can be seen in Fig. 10(a). Figures 10(b)–10(f) illustrate the uncertainties $\nu_1,\ldots,\nu_5$ (Eq. (27)) of x_1, x_2, p_1, p_2, q, respectively.

F. Continuous dynamical systems

To compute the Jacobian matrix $DG(\mathbf{x}, \mathbf{p})$ (34) of the delay coordinates map G, we have to compute the gradients (35) and (36) of the observation function $s = h(\mathbf{x}, \mathbf{q})$ and the Jacobian matrices $D_x\phi^t(\mathbf{x},\mathbf{p})$ and $D_p\phi^t(\mathbf{x},\mathbf{p})$ containing derivatives of the flow ϕ^t generated by the dynamical system (29) with respect to variables x_j and parameters p_j, respectively. The $M \times M$ matrix $D_x\phi^t(\mathbf{x},\mathbf{p})$ can be computed by solving the linearized dynamical equations in terms of a matrix ODE

$$\frac{d}{dt}Y = D_x f(\phi^t(\mathbf{x},\mathbf{p}),\mathbf{p}) \cdot Y, \tag{39}$$

where $\phi^t(\mathbf{x},\mathbf{p})$ is a solution of Eq. (29) with initial value $\mathbf{x}$ and Y is an $M \times M$ matrix that is initialized as $Y(0) = I_M$,

where I_M denotes the $M \times M$ identity matrix. Similarly, the $M \times P$ matrix $D_p\phi^t(\mathbf{x}, \mathbf{p})$ is obtained as a solution $Z(t)$ of the matrix ODE[37]

$$\frac{d}{dt}Z = D_x f(\mathbf{x}(t), \mathbf{p}) \cdot Z + D_p f(\mathbf{x}(t), \mathbf{p}) \tag{40}$$

with $Z(0) = 0$. Solving (39) and (40) simultaneously with the system ODEs (29) we can compute $D_x\phi^\tau(\mathbf{x})$, $D_x\phi^{2\tau}(\mathbf{x})$, etc. and use these matrices to obtain the Jacobian matrix DG of the delay coordinates map G (34). For mixed or backward delay coordinates the required components can be computed by integrating the system ODE and the linearized ODEs backward in time.

1. The Rössler system

To demonstrate the observability analysis for continuous systems, we follow Aguirre and Letellier[25] and consider the Rössler system

$$\begin{aligned} \dot{x}_1 &= -x_2 - x_3, \\ \dot{x}_2 &= x_1 + ax_2, \\ \dot{x}_3 &= b + x_3(x_1 - c), \end{aligned} \tag{41}$$

with $a = 0.1$, $b = 0.1$, and $c = 14$.

Time series of different observables x_1, or x_2, or x_3 are considered, all of them consisting of $N = 10000$ values sampled with $\Delta t = 0.1$. Figure 11 shows the Rössler attractor, where color indicates the uncertainty of estimating the variable x_1 (first column), or x_2 (second column), or x_3 (third column) using forward delay coordinates. The results in the first row are obtained when observing x_1, while the diagrams in the second and third rows show results for x_2 or x_3 time series, respectively. The reconstruction dimension equals $D = 7$ and the delay time is $\tau = 0.5$. The bright yellow bullet indicates the state with the lowest uncertainty. This state and the $D - 1 = 6$ following states plotted as thick red bullets indicating the time series values that are used for the delay reconstruction. They span a window in time of length $(D-1)\tau = 6 \cdot 0.5 = 3$, which is about one half of the mean period of the chaotic oscillations $T \approx 6$. The lowest uncertainties are obtained for states whose reconstruction involves trajectory segments following the vertical x_3-excursion on the attractor. In contrast, trajectory segments starting from states with poor observability (large uncertainty) are located in the flat part of the Rössler attractor. Figures 11(a) and 11(b) show that using x_1 time series low values of ν_1 occur on parts for the attractor, where ν_2 is high (and vice versa). Interestingly, this is not the case for delay reconstructions based on x_2 time series as can be seen in Figs. 11(d) and

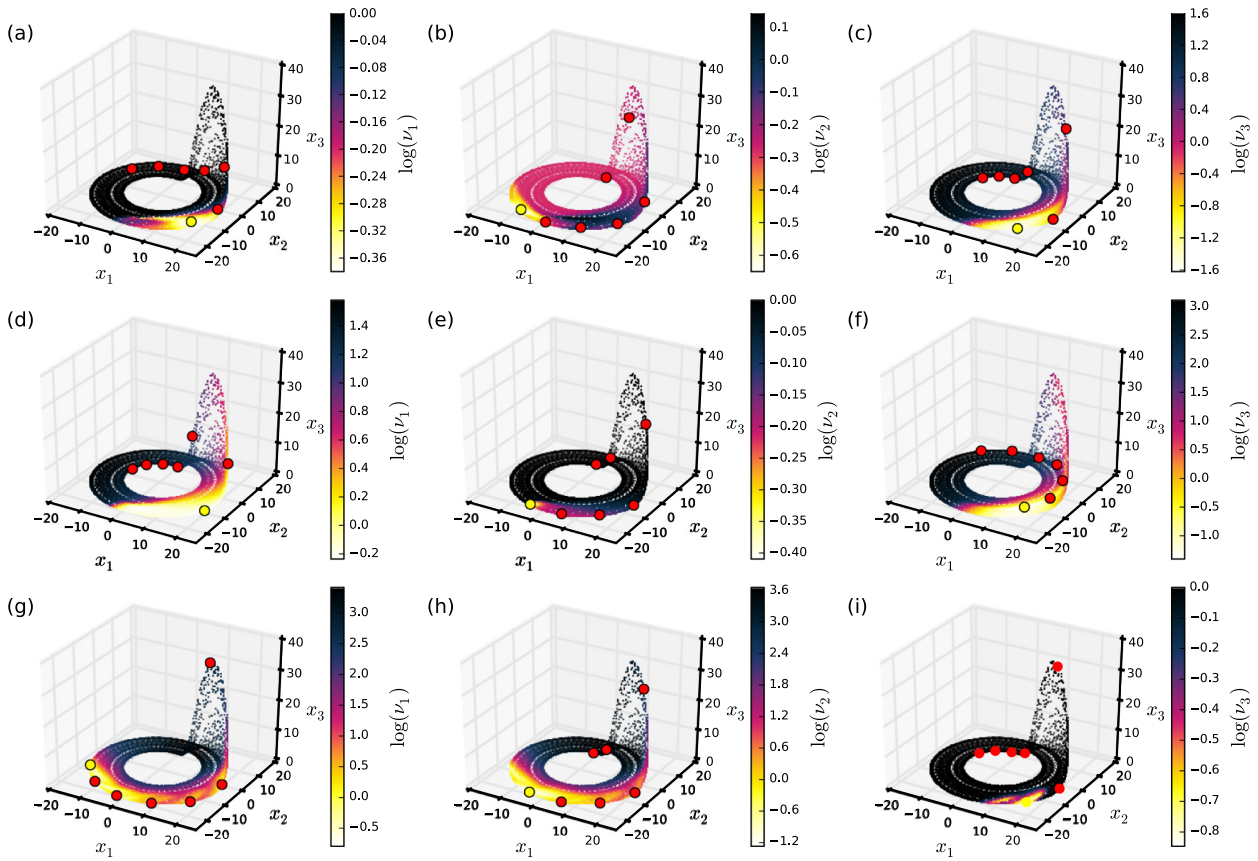

FIG. 11. Color coded Rössler attractors, where colors of points representing states are given by logarithms of uncertainty values ν_1 in the first column, ν_2 in the second column, and ν_3 in the third column. All results are computed using forward delay coordinates. The diagrams in the first row show results obtained based on a reconstruction of a x_1 time series, the second row using x_2 as an observable, and the third row uncertainties of estimates from x_3 data. The reconstruction dimension is $D = 7$ for all nine diagrams. The bright yellow bullet indicates the state with the lowest ν-value (respectively). To estimate this state time series, values at this state and at $D - 1 = 6$ subsequent states indicated by dark (red) bullets are used for delay coordinates.

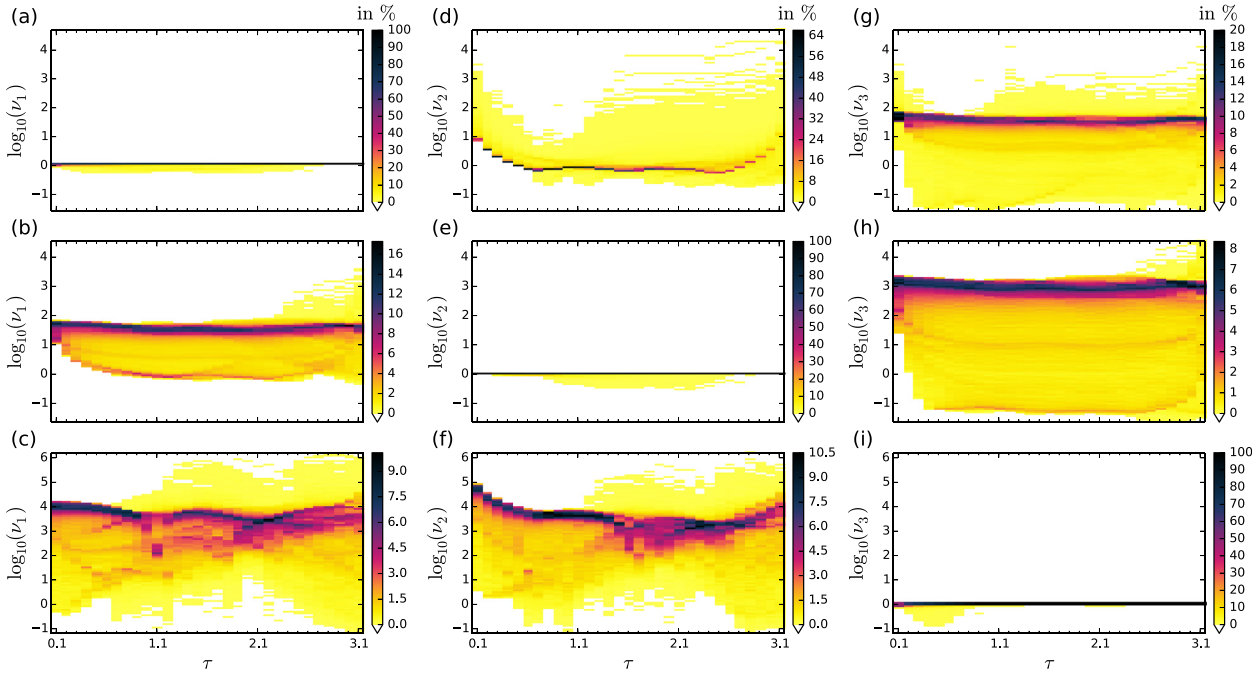

FIG. 12. Histograms of uncertainties ν_j of the Rössler system (41) vs. delay time τ. All parameters are assumed to be known ($M=3$, $P=0$) and forward delay coordinates with dimension $D=4$ are used. In the first row, a x_1 time series is given, in the second row x_2 data, and in the third row, the delay reconstruction is based on x_3. The three columns show histograms of the (logarithm of the) uncertainties ν_1, ν_2, and ν_3, respectively.

11(e), where low uncertainties of x_1 and x_2 occur in similar regions on the attractor.

In Fig. 12, distributions of uncertainty values of the Rössler system are shown that were obtained along an orbit of $N=10\,000$ states sampled with $\Delta t=0.1$. The distributions are shown as color coded histograms, estimated from the relative frequency of occurrence of the corresponding ν_j (in %). All diagrams show the dependence of the histograms on the delay time τ chosen for forward delay coordinates (horizontal axis). The reconstruction dimension is for all cases $D=4$ and all three parameters are assumed to be known (and are not part of the estimation task, i.e., $P=0$). In the first row (Figs. 12(a), 12(d), 12(g)), estimations are based on a x_1 time series from the Rössler system, and in rows two and three, x_2

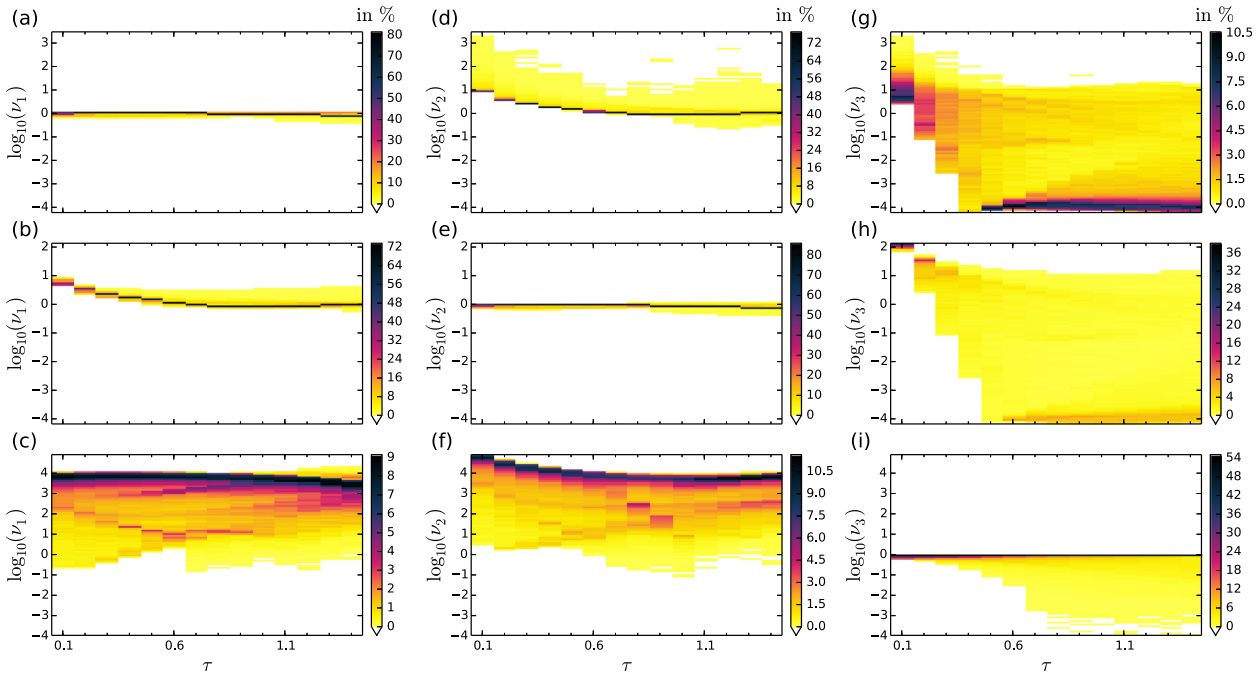

FIG. 13. Histograms of uncertainties ν_j of the Rössler system (41) vs. delay time τ. All parameters are assumed to be known ($M=3$, $P=0$) and mixed delay coordinates with dimension $D=1+D_-+D_+=4$ are used ($D_-=1$, $D_+=2$). In the first row, a x_1 time series is given, in the second row x_2 data, and in the third row, the delay coordinates are based on x_3. The three columns show histograms of the (logarithm of the) uncertainties ν_1, ν_2, and ν_3, respectively.

and x_3 time series are used, respectively. The uncertainties ν_j of the given observable x_j (Figs. 12(a), 12(e), 12(i)) mostly equal one ($\log_{10}(\nu_j) \approx 0$) or are smaller (due to the additional information provided by the delay coordinates). In general, lowest uncertainties for all variables are obtained when using x_1 time series (Figs. 12(a), 12(d), 12(g)), while x_3 data provide highest uncertainties (Figs. 12(c), 12(f), 12(i)).

Figure 13 shows the same diagrams but now computed using four dimensional mixed delay coordinates with $D_- = 1$ and $D_+ = 2$. Similar to the results obtained with the Hénon map, the uncertainties computed for mixed delay coordinates are typically smaller than those obtained with forward coordinates. Furthermore, the histograms shown in Fig. 13 suggest that for mixed delay coordinates, using x_2 as measured variable provides the best results, followed by the x_1 time series. This is in contrast to forward coordinates (Fig. 12), where x_1 data yield the smallest uncertainties for the other variables (x_2 and x_3). Similar results have been obtained with three dimensional forward or mixed coordinates.

The fact that mixed delay coordinates provide the lowest uncertainties when using x_2 time series is consistent with results for derivative coordinates obtained by Letellier *et al.*[24] who found a ranking $x_2 \rhd x_1 \rhd x_3$ (for a different set of model parameters). For better comparison with their results, we computed the (attractor) average

$$\bar{\gamma} = \frac{1}{T}\int_0^T \gamma(\mathbf{x}(t))dt \tag{42}$$

of the ratio

$$\gamma(\mathbf{x}) = \frac{\sigma^2_{min}(DG(\mathbf{x}))}{\sigma^2_{max}(DG(\mathbf{x}))} \tag{43}$$

that provides the delay reconstruction analog $\bar{\gamma}$ of the observability index (4). Figure 14 shows $\bar{\gamma}$ vs. the delay time τ for different delay coordinates (rows) and different measured time series (columns). While for forward delay coordinates, the largest values of the observability index occur if x_1 is measured (Fig. 14(c)), x_2 time series provide best observability if mixed delay coordinates are used (Fig. 14(d)). Note that, in most cases, high observability occurs for $\tau \approx 1$, which is very close to the first zero of the autocorrelation function (that is often used as preferred value for delay reconstruction).

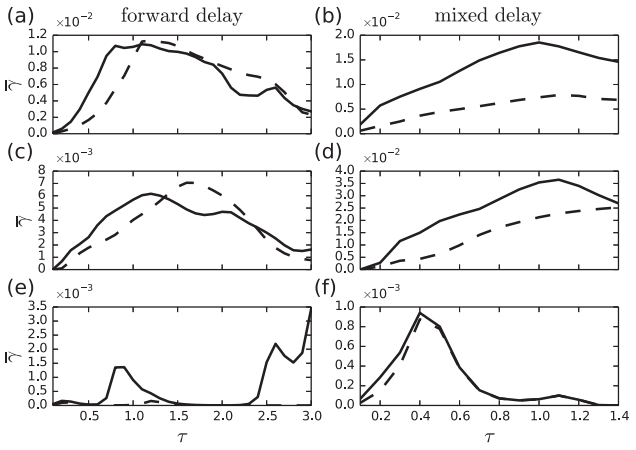

FIG. 14. Mean observability indices (42) of the Rössler system (41) vs. delay time τ based on three dimensional (dashed lines) and four dimensional (solid lines) delay coordinates. Left column ((a), (c), and (e)) forward delay coordinates. Right column ((b), (d), and (f)) mixed delay coordinates with $D_- = 1$ and $D_+ = 1$ (dashed lines) or $D_+ = 2$ (solid lines). The measured time series is in the first, second, and third rows, the variable x_1, x_2, and x_3, respectively.

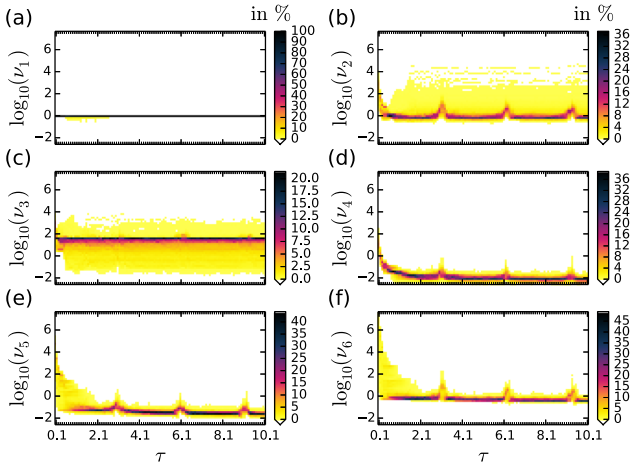

FIG. 15. Histograms of uncertainties ν_j of the Rössler system (41) vs. delay time τ. Both, all state variables ($M = 3$) and all parameters ($P = 3$) are assumed to be unknown and have to be estimated from a x_1 time series. Results are obtained using forward delay coordinates with $D = 13$. The uncertainties ν_1, ν_2, ν_3 correspond to state variables x_1, x_2, and x_3, while ν_4, ν_5, ν_6 quantify uncertainties of estimated parameters p_1, p_2, and p_3.

Fig. 15 shows similar histograms but now for the full estimation problem ($M = 3$ variables and $P = 3$ parameters). Forward delay coordinates are used and the reconstruction dimension is increased to $D = 13$ and an x_1 time series of length $N = 10\,000$ is used (with sampling time $\Delta t = 0.1$). For delay times τ that are an integer multiple of half of the mean period $T/2 \approx 3$ relatively high uncertainties occur, in particular, for ν_2, ν_4, ν_5, and ν_6. This is due to the well known fact that for these delay times, the attractor reconstruction results in points scattered near a straight (diagonal) line (an effect that also occurs when considering delay coordinates of a sinusoidal signal).

III. CONCLUSION

Starting from the question "Does some particular (measured) time series provide sufficient information for estimating a state variable or a model parameter of interest," we revisited the observability problem for nonlinear (chaotic) dynamical systems. In particular, we considered delay coordinates and the ability to recover not measured state variables and parameters from delay vectors. This requires to "invert" the delay coordinates construction process, which is at least locally possible, if the Jacobian matrix of the delay coordinates map has maximum (full) rank. Furthermore, we investigated how states near the delay vector are mapped back to the state and parameter space of the systems. In this way, it is possible to quantify the amplification of small perturbations in delay reconstruction space in different directions of the state and parameter space. This reasoning gave

rise to the concept of uncertainties of estimated variables and parameters. Both, observability and uncertainties may vary considerably in state space and on a given (chaotic) attractor. This feature was demonstrated with a discrete time system (filtered Hénon map) and a continuous system (Rössler system). Local observability and uncertainties also depend on the available measured variable (time series) and the type of delay coordinates. Best results were obtained with mixed delay coordinates, containing at least a one step backward in time.

The obtained information about (local) uncertainties in state and parameter estimation can be used in several ways for subsequent analysis. First of all, it may help to decide whether the planned estimation task is feasible at all or whether another observable has to be measured instead. For continuous time systems, relevant time scales (delay times) can be identified, where uncertainties are minimal.

The strong variations of local uncertainty values in state space (along a trajectory) occurring with the examples shown here are typical and should be taken into account by any estimation method. If the system is in a state where, for example, the uncertainty ν_1 of the first variable is high then it might be better not to try to estimate this variable in this state or close to it, because the estimate might be poor and may spoil the overall results. Instead it makes more sense to wait until the trajectory enters a region of state space, where x_1 can be estimated more reliably from the given time series.

The concrete implementation of such an adaptive approach depends on details of the estimation algorithm. For Newton-like algorithms, for example, it may consist of a simple strategy decreasing correction step sizes. Another potential application of uncertainty analysis is the identification of redundant parameters, i.e., parameter combinations that provide the same dynamical output.

ACKNOWLEDGMENTS

The research leading to these results has received funding from the European Community's Seventh Framework Program FP7/2007-2013 under Grant Agreement No. HEALTH-F2-2009-241526, EUTrigTreat. We acknowledge financial support by the German Federal Ministry of Education and Research (BMBF) Grant No. 031A147, by the Deutsche Forschungsgemeinschaft (SFB 1002: Modulatory Units in Heart Failure), and by the German Center for Cardiovascular Research (DZHK e.V.).

[1]H. U. Voss, J. Timmer, and J. Kurths, Int. J. Bifurcation Chaos **14**(6), 1905–1933 (2004).
[2]A. Raue, V. Becker, U. Klingmüller, and J. Timmer, Chaos **20**, 045105 (2010).
[3]H. Nijmeijer and I. M. Y. Mareels, IEEE Trans. Circuits Syst. I **44**, 882–890 (1997).
[4]H. J. C. Huijberts, T. Lilge, and H. Nijmeijer, Int. J. Bifurcation Chaos **11**(7), 1997–2006 (2001).
[5]U. Parlitz, L. Junge, and L. Kocarev, Phys. Rev. E **54**, 6253–6529 (1996).
[6]D. Ghosh and S. Banerjee, Phys. Rev. E **78**, 056211 (2008).
[7]H. D. I. Abarbanel, D. R. Creveling, and J. M. Jeanne, Phys. Rev. E **77**, 016208 (2008).
[8]F. Sorrentino and E. Ott, Chaos **19**, 033108 (2009).
[9]I. G. Szendro, M. A. Rodríguez, and J. M. López, J. Geophys. Res. **114**, D20109, doi:10.1029/2009JD012411 (2009).
[10]R. Konnur, Phys. Lett. A **346**, 275–280 (2005).
[11]U. S. Freitas, E. E. N. Macau, and C. Grebogi, Phys. Rev. E **71**, 047203 (2005).
[12]M. Chen and J. Kurths, Phys. Rev. E **76**, 027203 (2007).
[13]R. E. Amritkar, Phys. Rev. E **80**, 047202 (2009).
[14]P. J. van Leeuwen, Q. J. R. Meteorol. Soc. **136**, 1991–1999 (2010).
[15]H. D. I. Abarbanel, Phys. Lett. A **373**, 4044–4048 (2009).
[16]J. C. Quinn and H. D. I. Abarbanel, Q. J. R. Meteorol. Soc. **136**, 1855–1867 (2010).
[17]D. R. Creveling, P. E. Gill, and H. D. I. Abarbanel, Phys. Lett. A **372**, 2640–2644 (2008).
[18]J. Schumann-Bischoff and U. Parlitz, Phys. Rev. E **84**, 056214 (2011).
[19]J. Bröcker, Q. J. R. Meteorol. Soc. **136**, 1906–1919 (2010).
[20]E. D. Sontag, *Mathematical Control Theory: Deterministic Finite Dimensional Systems*, 2nd ed. (Springer, New York, 1998).
[21]H. Nijmeijer and A. J. van der Schaft, *Nonlinear Dynamical Control Systems* (Springer, New York, 1990).
[22]R. Hermann and A. J. Krener, IEEE Trans. Autom. Control **AC-22**(5), 728–740 (1977).
[23]H. Nijmeijer, Int. J. Control **36**(5), 867–874 (1982).
[24]C. Letellier, L. A. Aguirre, and J. Maquet, Phys. Rev. E **71**, 066213 (2005).
[25]L. A. Aguirre and C. Letellier, J. Phys. A: Math. Gen. **38**, 6311–6326 (2005).
[26]C. Letellier, L. A. Aguirre, and J. Maquet, Commun. Nonlinear Sci. Numer. Simul. **11**, 555–576 (2006).
[27]C. Letellier and L. A. Aguirre, Phys. Rev. E **79**, 066210 (2009).
[28]M. Frunzete, J.-P. Barbot, and C. Letellier, Phys. Rev. E **86**, 026205 (2012).
[29]H. Kantz and T. Schreiber, *Nonlinear Time Series Analysis*, Cambridge Nonlinear Science Series Vol. 7 (Cambridge University Press, Cambridge, 1997).
[30]H. D. I. Abarbanel, *Analysis of Observed Chaotic Data*, 2nd ed. (Springer Verlag, 1997).
[31]T. Sauer, J. A. Yorke, and M. Casdagli, J. Stat. Phys. **65**(3/4), 579–616 (1991).
[32]D. Aeyels, SIAM J. Control Optim. **19**(5), 595–603 (1981).
[33]F. Takens, Lect. Notes Math. **898**, 366–381 (1981).
[34]C. Letellier, L. A. Aguirre, and U. S. Freitas, Chaos **19**, 023103 (2009).
[35]U. Parlitz, J. Schumann-Bischoff, and S. Luther, Phys. Rev. E **89**, 050902(R) (2014).
[36]J. Schumann-Bischoff, S. Luther, and U. Parlitz, Commun. Nonlinear Sci. Numer. Simul. **18**(10), 2733–2742 (2013).
[37]H. Kawakami, IEEE Trans. Circuits Syst. **CAS-31**(3), 248–260 (1984).

7 Basin structure of optimization based state and parameter estimation

The following pages contain the article

> J. Schumann-Bischoff, U. Parlitz, H. D. I. Abarbanel, M. Kostuk, D. Rey, M. Eldridge, and S. Luther. "Basin structure of optimization based state and parameter estimation". In: *Chaos: An Interdisciplinary Journal of Nonlinear Science* 25.5 (May 2015), p. 053108. DOI: 10.1063/1.4920942.

The content of this article was for the most part of my own conceptual design. I planned, developed, performed, and analyzed all simulations. The underlying idea (described roughly from Eq. (23) to Eq. (30) on page 7) leading to results presented in Tab.II was contributed by the coauthor H.D.I. Abarbanel. I designed and created all figures and tables in this article. Furthermore, I wrote the text of Sec. I to Sec. VI which was then revised by the coauthors. The abstract was written collaboratively with the other authors.

Basin structure of optimization based state and parameter estimation

Jan Schumann-Bischoff,[1,2] Ulrich Parlitz,[1,2,a)] Henry D. I. Abarbanel,[3,4,b)] Mark Kostuk,[3] Daniel Rey,[3] Michael Eldridge,[3] and Stefan Luther[1,2,c)]
[1]*Biomedical Physics Group, Max Planck Institute for Dynamics and Self-Organization, Am Faßberg 17, 37077 Göttingen, Germany*
[2]*Institute for Nonlinear Dynamics, Georg-August-Universität Göttingen, Am Faßberg 17, 37077 Göttingen, Germany*
[3]*Department of Physics, University of California, San Diego, 9500 Gilman Drive, La Jolla, California 92093-0374, USA*
[4]*Marine Physical Laboratory (Scripps Institution of Oceanography), University of California, San Diego, La Jolla, CA 92093-0374, USA*

(Received 12 December 2014; accepted 29 April 2015; published online 14 May 2015)

Most data based state and parameter estimation methods require suitable initial values or guesses to achieve convergence to the desired solution, which typically is a global minimum of some cost function. Unfortunately, however, other stable solutions (e.g., local minima) may exist and provide suboptimal or even wrong estimates. Here, we demonstrate for a 9-dimensional Lorenz-96 model how to characterize the basin size of the global minimum when applying some particular optimization based estimation algorithm. We compare three different strategies for generating suitable initial guesses, and we investigate the dependence of the solution on the given trajectory segment (underlying the measured time series). To address the question of how many state variables have to be measured for optimal performance, different types of multivariate time series are considered consisting of 1, 2, or 3 variables. Based on these time series, the local observability of state variables and parameters of the Lorenz-96 model is investigated and confirmed using delay coordinates. This result is in good agreement with the observation that correct state and parameter estimation results are obtained if the optimization algorithm is initialized with initial guesses close to the true solution. In contrast, initialization with other exact solutions of the model equations (different from the true solution used to generate the time series) typically fails, i.e., the optimization procedure ends up in local minima different from the true solution. Initialization using random values in a box around the attractor exhibits success rates depending on the number of observables and the available time series (trajectory segment). © *2015 AIP Publishing LLC*.
[http://dx.doi.org/10.1063/1.4920942]

For many physical processes, dynamical models are available but often not all their state variables and (fixed) parameters are known or easily accessible. In meteorology, for example, sophisticated large scale models exist, which have to be continuously adapted to the true temporal changes of temperatures, wind speed, humidity, and other relevant physical quantities. In quantitative biology, mathematical models of single neural or cardiac cells or networks may contain many state variables and parameters, whose values are not easy to measure (without destroying the system). In such cases, data based estimation methods can be used to determine these unknown states and a parameters by adapting a suitable model to reproduce and predict the measured time series. This approach can be successful only if two conditions are fulfilled: (i) the available data have to provide sufficient information, i.e., the unknown state variables and parameters have to be *observable* and (ii) the estimation algorithm has to be properly initialized with initial guesses sufficiently close to the true solution. Here, we consider both problems for the Lorenz-96 model and compare different initialization methods in terms of their effective basin sizes.

I. INTRODUCTION

Estimation methods for state variables or (fixed) parameters can be implemented employing synchronization[1–5] or optimization methods,[6–9] for example. In the literature, one can find many examples with successful applications of state and parameter estimation methods even for chaotic systems.[10–14] In practice, however, attempts to fit a model (for example, a set of nonlinear ordinary differential equations (ODEs)) to given data may fail. There are many possible reasons for such a failure, including inappropriate models, poor quality of the measured time series (too noisy, too short), or external perturbations not covered by the model. But even with relatively clean data and the right model architecture, estimation may turn out to be difficult, because the available data do not contain sufficient information about the underlying process. Therefore, in this article, we address how the success of a given estimation algorithm for a given model depends on the following aspects:

[a)]Electronic mail: ulrich.parlitz@ds.mpg.de
[b)]Electronic mail: habarbanel@ucsd.edu
[c)]Electronic mail: stefan.luther@ds.mpg.de

(a) the number of available observables (in a multivariate time series),
(b) the available time series (corresponding to some particular trajectory segment), and
(c) the way the estimation algorithm is initialized (using guesses for the unknown quantities).

The focus in the presented analysis is based on models given by ODEs,

$$\frac{\mathrm{d}\mathbf{x}(t)}{\mathrm{d}t} = \mathbf{F}(\mathbf{x}(t), \mathbf{p}, t)\,, \tag{1}$$

and a measurement function

$$\mathbf{y}(t) = \mathbf{h}(\mathbf{x}(t)) \in \mathbb{R}^L\,, \tag{2}$$

representing the model output with a state vector $\mathbf{x}(t) = (x_1(t), \ldots, x_D(t))^{\mathrm{tr}} \in \mathbb{R}^D$ and model parameters $\mathbf{p} = (p_1, \ldots, p_{N_P})^{\mathrm{tr}} \in \mathbb{R}^{N_P}$. Here, and in the following, the superscript "tr" denotes the transpose. We assume that a multivariate L-dimensional (experimental) time series $\{\boldsymbol{\eta}(n)\}$ is given consisting of $N+1$ samples $\boldsymbol{\eta}(n) \hat{=} \boldsymbol{\eta}(t_n) \in \mathbb{R}^L$, analogous to the model output, and measured at times $\mathcal{T} = \{t_n = n \cdot \Delta t | n = 0, 1, \ldots, N\}$. The observation times t_n are equally spaced (with a fixed time step Δt) and start at $t_0 = 0$. Any solution of Eq. (1) at discrete times $t_n = n \cdot \Delta t$ with a fixed time step Δt is denoted by $\{\mathbf{x}(n)\}$ and consists of $N+1$ samples $\mathbf{x}(n) \hat{=} \mathbf{x}(t_n)$ at times $t_n \in \mathcal{T}$. If, from the context, Δt and the range of n are clear, this information will be dropped in the following. The same convention holds if a solution is denoted by another symbol, for example, $\mathbf{z}$ instead of $\mathbf{x}$: the solution $\{\mathbf{z}(n)\}$ consists of $N+1$ samples $\mathbf{z}(n) \hat{=} \mathbf{z}(t_n)$ measured at times $t_n \in \mathcal{T}$.

As an example, we use synthetic data from a 9-dimensional Lorenz-96 system[15] (Sec. II) and an optimization based estimation algorithm[8] (Sec. IV). We check the observability of the state variables of the Lorenz-96 model which are not "measured" (i.e., not contained in the multivariate time series) using a local analysis (Sec. III) employing the Jacobian matrix of the delay coordinates map.[16,17] This analysis indicates that even with a single observable (scalar time series) all state variables and the parameter of the Lorenz-96 system are in principle (locally) observable.

To investigate *global convergence* features (using initial guesses that are not close to the true solution), we probe the basin structure of the observability problem by considering 18 different trajectories of the Lorenz-96 system (on the same chaotic attractor, but generated with different initial conditions). From each trajectory, 15 different (multi-variate) time series are derived consisting of one, two, or three observables. Then, a particular method for generating initial guesses to initialize the optimization algorithm is chosen, and the estimation algorithm is applied to each of these 15 time series 500 times (with different random initial guesses) to obtain statistics of how often the estimation problem is solved successfully. In other words, we compute the probability that a generated initial guess is located in the basin of the true solution of the given optimization algorithm. This method of estimating the "basin size" was adopted from Menck *et al.*[18]

In Sec. II, we introduce the Lorenz-96 model, which will serve as an example for the following studies. First, local observability of the state variables and the parameter of the Lorenz-96 model is investigated and confirmed in Sec. III. Then, in Sec. IV, we present the estimation algorithm used and in Sec. V our approach for characterizing the size of the basin of the true solution is introduced. The true solution is a stable fixed point of the optimization algorithm with a basin of attraction and the desired estimation of the true solution is only possible if the optimization algorithm is initialized with guesses from this basin. To check the stability of this fixed point, the optimization procedure was initialized by initial guesses consisting of randomly perturbed true values. For all these initial guesses, the optimization results converged to the true solution. However, since, in general, the location of the true solution is not known, the size and the structure of its basin are most important for any initialization strategy. Three possible initialization methods (Sec. V B) are invested, in detail, and compared in terms of their efficacy for finding the true solution. All results are summarized in the conclusion drawn in Sec. VI.

II. EXAMPLE: THE LORENZ-96 MODEL

As an example for demonstrating the proposed analysis we consider in the following a $D = 9$ dimensional Lorenz-96 model:

$$\frac{\mathrm{d}x_i(t)}{\mathrm{d}t} = x_{i-1}(t) \cdot (x_{i+1}(t) - x_{i-2}(t)) - x_i(t) + p \tag{3}$$

with $p = 8.17$ and a cyclic index i ($x_{D+1}(t) = x_1(t)$, $x_0(t) = x_D(t)$, and $x_{-1}(t) = x_{D-1}(t)$). For the parameter value $p = 8.17$, the model generates a chaotic attractor.

The Lorenz-96 model is chosen here as an example because previous investigations showed that it is very difficult to estimate its state variables and the parameter p using only a few observables.[19] Recently, however, Rey *et al.*[5] demonstrated successful state and parameter estimation based on univariate time series consisting of a single Lorenz-96 state variable and a synchronization scheme employing delay coordinates. Law *et al.*[20] applied the extended Kalman filter and the 3D-VAR data assimilation technique to the chaotic Lorenz-96 model and also encountered difficulties in the estimation of model state variables if only few model state variables are observed.

Technically, the Lorenz-96 model (3) is used here in a twin experiment for both (i) generating the "measured" time series and (ii) as a model to be adapted to a (multivariate) time series using the optimization based estimation method described in Sec. IV.

To address the question how many observables have to be known for successful state and parameter estimation, we consider multivariate time series $\{\boldsymbol{\eta}(n)\}$ with one, two, or three state variables. More precisely, for the 9 dimensional Lorenz-96 model, we consider *all* possible combinations of one to three state variables as being "measured." For example, let us assume we can measure the state variables

(x_1, x_2, x_5). Due to the symmetry in Eq. (3), sampling (x_1, x_2, x_5) is equal to measuring (x_3, x_4, x_7) or (x_7, x_8, x_2). Hence, checking the observability of all state variables and the parameter p with the given multivariate time series (x_1, x_2, x_5) is equivalent to checking the observability with the time series (x_7, x_8, x_2). Removing all mathematically equivalent combinations results in the following 15 distinct combinations of state variables: x_1, (x_1, x_2), (x_1, x_3), (x_1, x_4), (x_1, x_5), (x_1, x_2, x_3), (x_1, x_2, x_4), (x_1, x_2, x_5), (x_1, x_2, x_6), (x_1, x_2, x_7), (x_1, x_2, x_8), (x_1, x_3, x_5), (x_1, x_3, x_6), (x_1, x_3, x_7), and (x_1, x_4, x_7).

III. LOCAL OBSERVABILITY OF MODEL STATE VARIABLES AND FIXED PARAMETERS

We consider models given by a set of D coupled ODEs, Eq. (1), with a measurement function, Eq. (2), representing the relation between model states $\mathbf{x}(n)$ and the model output $\mathbf{y}(n)$ corresponding to the observations $\{\boldsymbol{\eta}(n)\}$. The state vector(s) $\mathbf{x}(t)$ and the model parameters $\mathbf{p}$ are unknown and have to be estimated from a (multivariate) time series. The technique used in this article to adapt a model given by ODEs (1) to a (multivariate) time series given by $\{\boldsymbol{\eta}(n)\}$ with a measurement function (2) will be described in Sec. IV. Similar to other methods for state and parameter estimation, this algorithm will provide estimates for the model state variables and the (fixed) model parameters (except if, for example, numerical problems arise). The fact, however, that an algorithm produces some output does not mean that this output is correct or useful. Therefore, a method is needed, which indicates whether it is (in principle) possible to estimate $\mathbf{p}$ and $\mathbf{x}(t)$ correctly from $\{\boldsymbol{\eta}(n)\}$. This question addresses the general problem of observability, which is well known from control theory.[21–25] In Sec. III A, we shall employ *the time delay coordinates map* of the observed time series to investigate local observability following an approach presented in Refs. 16 and 17.

A. The delay coordinates map

Let the dynamical system (1) generate a flow

$$\phi^\tau : \mathbb{R}^D \otimes \mathbb{R}^{N_P} \to \mathbb{R}^D (\mathbf{x}(t), \mathbf{p}) \mapsto \mathbf{x}(t+\tau) \tag{4}$$

mapping a state $\mathbf{x}(t)$ at time $t \in \mathbb{R}$ to a (future) state $\mathbf{x}(t+\tau)$. Furthermore, delay coordinates are given via the L dimensional measurement function Eq. (2)

$$\mathbf{y}(t+\tau) = \mathbf{h}(\mathbf{x}(t+\tau)) = \mathbf{h}(\phi^\tau(\mathbf{x}(t), \mathbf{p})) \tag{5}$$

from a trajectory starting at $\mathbf{x}(t)$ with delay time τ. If the delay time is $\tau = 0$, then we obtain $\phi^0(\mathbf{x}(t), \mathbf{p}) = \mathbf{x}(t)$ and recover $\mathbf{y}(t) = \mathbf{h}(\mathbf{x}(t))$. Taking into account K time steps, we can define a $D_M = K \cdot L$-dimensional *delay coordinates map*

$$\mathbf{s} = \mathbf{S}(\mathbf{x}(t), \mathbf{p}) = (\mathbf{y}^{\mathrm{tr}}(t), \mathbf{y}^{\mathrm{tr}}(t+\tau), \ldots, \mathbf{y}^{\mathrm{tr}}(t+(K-1)\tau)). \tag{6}$$

Here, the delay coordinates map $\mathbf{S}$ is considered as a function of: (i) the state $\mathbf{x}(t)$ and the parameters $\mathbf{p}$ of the underlying system and (ii) of the delay time τ (not listed as an argument of $\mathbf{S}$ here, because τ is fixed and not part of the estimation problem). All $\mathbf{y}^{\mathrm{tr}}(t + i \cdot \tau)$, $i = 0, \ldots, K-1$ are row vectors. Hence, the right hand side of Eq. (6) is a (row) vector containing $K \cdot L$ elements.

If the delay coordinates map Eq. (6), $\mathbf{S} : \mathbb{R}^D \otimes \mathbb{R}^{N_P} \to \mathbb{R}^{D_M}$, is locally invertible, then the full state $\mathbf{x}(t)$ and the parameter vector $\mathbf{p}$ can be uniquely determined from the signal $\mathbf{h}(\mathbf{x}(t))$, which, in a real world experiment, corresponds to the measured time series $\{\boldsymbol{\eta}(t_n)\}$ Eq. (2). Mathematically, the delay coordinates map Eq. (6) has to be an immersion,[26] i.e., the Jacobian matrix $\mathrm{D}_{\mathbf{x},\mathbf{p}}\mathbf{S} = \mathrm{D}_{\mathbf{x},\mathbf{p}}\mathbf{S}(\mathbf{x}(t), \mathbf{p})$ of the delay coordinates map $\mathbf{S}$ has to have maximal (full) rank (see the Appendix).

The accuracy and robustness of estimated state variables or fixed parameters can be quantified by the *uncertainty*

$$\nu_j = \sqrt{[\mathrm{D}_{\mathbf{x},\mathbf{p}}\mathbf{S}^{\mathrm{tr}} \cdot \mathrm{D}_{\mathbf{x},\mathbf{p}}\mathbf{S}]^{-1}_{jj}} \tag{7}$$

of state variables $(j = 1, \ldots, D)$ and parameters $(j = D+1, \ldots, D+N_P)$, which was introduced in Refs. 16 and 17. Perturbations of the measured time series are amplified by ν_j, i.e., the larger ν_j the less precise is the estimation of the corresponding state variable or fixed parameter. Note that the uncertainty ν_j depends (via $\mathrm{D}_{\mathbf{x},\mathbf{p}}\mathbf{S}(\mathbf{x}(t), \mathbf{p})$) on the location in state and parameter space.

B. Local observability of the Lorenz-96 model

To assess the local observability of the states $\mathbf{x}(t)$ and the (single) model parameter p of the $D = 9$ dimensional Lorenz-96 model (3) their uncertainty is checked at 10^4 arbitrary reference points on the attractor. To obtain the reference points, the Lorenz-96 model was integrated 10^7 steps with a step size of 0.01 using a Runge-Kutta-45 integration scheme. Then, every 1000th point was picked as a reference point $\mathbf{x}(t)$ for the observability analysis described in the following.

As mentioned in Sec. II for the 9-dimensional Lorenz-96 model, there are 15 different combinations of one to three state variables constituting a multivariate time series. We select the following two cases as representative examples:

(a) measurement function $h(\mathbf{x}(t)) = x_1(t)$ (i.e., $L = 1$) with $K = 12$ and a resulting delay reconstruction dimension of $D_M = 12$ and
(b) measurement function $\mathbf{h}(\mathbf{x}(t)) = (x_1(t), x_3(t), x_6(t))$ (i.e., $L = 3$) with $K = 4$ and hence a delay reconstruction dimension of $D_M = 12$ (see Eq. (6)).

The reconstruction dimension $D_M = L \cdot K$ is the same in both cases. Histograms of the uncertainties ν_j, for $j = 1, \ldots, 10$, Eq. (7), are computed for the 10^4 reference points on the attractor. Figure 1 shows the histograms for ν_1, ν_5, and ν_{10} which are plotted vertically using color coding (relative frequencies of the corresponding uncertainties are given in percent, see color bar). All distributions shown here are unimodal. The left column shows the results for $h(\mathbf{x}(t)) = x_1(t)$ and the right column for $\mathbf{h}(\mathbf{x}(t)) = (x_1(t), x_3(t), x_6(t))$. In both cases, the uncertainty ν_1 corresponds to the "measured" state variable x_1, ν_5 corresponds to the "hidden" state variable x_5 (not measured directly), and ν_{10}

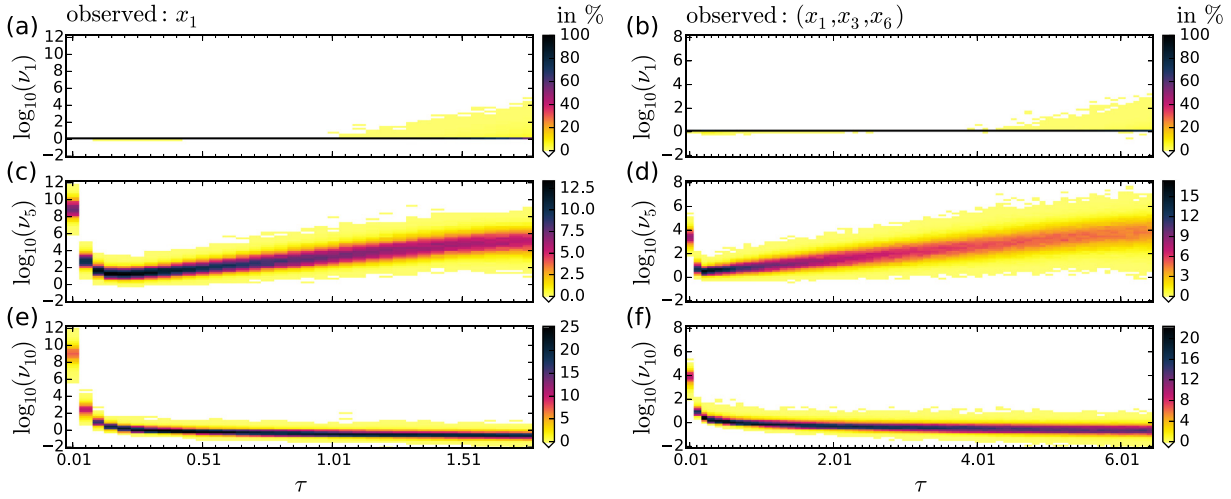

FIG. 1. Probability distributions (color coded frequency in %, vertically plotted) of uncertainties ν_1, ν_5, and ν_{10} vs. delay time τ for the Lorenz-96 model. The uncertainties ν_1 and ν_5 correspond to state variables x_1 and x_5, respectively, and ν_{10} corresponds to the parameter p. In the left column ((a), (c), and (e)), a scalar ($L = 1$ dimensional) measurement function $h(\mathbf{x}(t)) = x_1(t)$ is used for generating delay coordinates with $K = 12$. The right column ((b), (d), and (f)) shows results for the $L = 3$ dimensional measurement function $\mathbf{h}(\mathbf{x}(t)) = (x_1(t), x_3(t), x_6(t))$ and a delay reconstruction (Eq. (6)) with $K = 4$. Hence, $D_M = 12$ dimensional delay coordinates (Eq. (6)) are constructed in both cases. The histograms for ν_1 are very similar to histograms obtained for other measured state variables (x_3, x_6 in the right column), not shown here. Similarly, the histograms of ν_5 are representative for histograms of the remaining unmeasured state variables (not shown here).

corresponds to the model parameter p. Histograms for the other ν_i are not shown, because they look very similar to the histograms for ν_1 (if the corresponding state variable is measured) and ν_5 (if the corresponding model state variable is unmeasured). The reason for these similarities is the symmetry in the Lorenz-96 model equations (3).

For both measurement functions, one can see that the uncertainty values of the maxima of the histograms exhibit a U-shaped dependence on the delay time τ. The smallest uncertainties occur between $\tau = 0.11$ and $\tau = 0.21$ for the *unmeasured* state variables (Figs. 1(c) and 1(d)). In both cases, the distribution of the uncertainty ν_1 of the *measured* state variable (and similar for ν_3 and ν_6 if $R = 3$, not shown) possess a sharp peak around $\log_{10}\nu_i = 0$. In this case, the state variable x_1 is an observed quantity, and therefore, the delay reconstruction does not provide much further information about its values. For relatively large delay times ($\tau > 1$ in (a) and $\tau > 4$ in (b)), the delay reconstruction becomes rather "poor." The measurement noise is amplified resulting in a tail of the histogram with uncertainty values larger than one (the yellow areas above the horizontal line at $\log(\nu_1) = 0$). This result is not surprising, because in nonlinear time series analysis, it is well known that the delay time has to be chosen carefully and must not be too large for chaotic attractors, since otherwise, the reconstructed attractor will be heavily distorted. In contrast, the ν-values of the centers of the distributions of the uncertainty ν_{10} of the parameter p decrease with increasing τ until the maximum of the distribution is below one (see Figs. 1(e) and 1(f)) (without exhibiting a clear minimum).

As mentioned before, these two examples are representative for all multivariate time series from the Lorenz-96 model consisting of combinations of one to three state variables. The other 13 combinations show similar histograms. If a certain state variable in one of the other combinations is measured, then the corresponding histogram of the corresponding uncertainty looks similar to the histograms of ν_1 in Fig. 1(a). The same holds for state variables that are not contained in the multivariate time series (and where the corresponding ν histograms look similar to the histograms of ν_5 in Fig. 1) and the model parameter p (the corresponding ν_{10} histograms look similar to the histograms of ν_{10} in Fig. 1). With an increasing number of measured state variables (from one to three), the maxima of the distributions at the minimum of the histograms of ν for unmeasured state variables move only slightly in the direction of smaller ν (see, for example, Figs. 1(c) and 1(d)). This trend also holds for all combinations of four measured state variables (not shown here). The fact that the histograms for one to three observed state variables look almost the same means that the *local* observability of the model parameter and the unmeasured state variables is maintained, even if only a *single* model state variable is measured instead of three (or more). In the following, we shall investigate whether this local result holds for states that are not close to the true solution. Specifically, we want to know if we can uniquely recover the true solution using a univariate time series (from a single observable), even if the initial guesses are far from the true solution. Since the true solution is a stable fixed point of any optimization based estimation algorithm, we are thus interested in the "size" and the structure of the basin of attraction of this fixed point. To address this question, we shall introduce in Sec. IV a particular estimation algorithm which is used here as a prototypical example for investigating the solution basin.

IV. STATE AND PARAMETER ESTIMATION ALGORITHM

The method used in this study to adapt a model to a time series is based on minimizing a cost function and in the context of this paper it represents only one out of many different

state and parameter estimation methods,[6,7] where the same type of basin size analysis could be applied. The method was introduced in Ref. 8 and will be summarized in the following.

The goal of the estimation process is to find a set of values for the model state variables $\mathbf{x}(t)$ at each time step of its discretization and the model parameters $\mathbf{p}$ such that the model equations, given by a set of ODEs (see Eq. (1)), provide via the measurement function (2) a model times series $\{\mathbf{y}(n)\}$ consisting of $N+1$ samples $\mathbf{y}(n)\hat{=}\mathbf{y}(t_n) \in \mathbb{R}^L$ with $t_n \in \mathcal{T}\ \forall\, n$ that matches the experimental time series $\{\boldsymbol{\eta}(n)\}$. In other words, the average difference between $\boldsymbol{\eta}(n)$ and $\mathbf{y}(n)$ should be small.

Furthermore, the model equations should be fulfilled as well as possible. This means that modeling errors $\mathbf{u}(t)$ are allowed, but should be small. Therefore, model (1) is extended to include modeling errors $\mathbf{u}(t)$

$$\frac{\mathrm{d}\mathbf{x}(t)}{\mathrm{d}t} = \mathbf{F}(\mathbf{x}(t), \mathbf{p}, t) + \mathbf{u}(t) \tag{8}$$

so that when $\mathbf{u}(t)$ is small the model trajectory $\mathbf{x}(t)$ closely matches the model equations. To incorporate model error into the optimization, we discretize $\mathbf{u}(t)$ and $\mathbf{x}(t)$ at times $t_n \in \mathcal{T}$ so that the state variables $\{\mathbf{x}(n)\}$, $\mathbf{x}(n)\hat{=}\mathbf{x}(t_n)$, at each time n must be estimated in addition to $\mathbf{p}$. For simplicity, we choose $\mathbf{x}(t)$ and $\mathbf{y}(t)$ to be sampled at the same time that the data are observed. Similarly, $\mathbf{u}(t)$ is discretized to $\{\mathbf{u}(n)\}$ with $\mathbf{u}(n)\hat{=}\mathbf{u}(t_n)$ and $t_n \in \mathcal{T}$. The discretization of (8) is given by

$$\mathbf{u}(n) \approx \left.\frac{\Delta\mathbf{x}}{\Delta t}\right|_{t_n} - \mathbf{F}(\mathbf{x}(n), \mathbf{p}, t_n), \tag{9}$$

where the symbol $\left.\frac{\Delta\mathbf{x}}{\Delta t}\right|_{t_n}$ stands for the finite difference approximation of $\frac{\mathrm{d}\mathbf{x}(t)}{\mathrm{d}t}$ at time t_n.

The goal of the adaption process is to minimize (on average) the norm of $\mathbf{u}(n)$ *and* the norm of the difference $\boldsymbol{\eta}(n) - \mathbf{y}(n)$ for all $n \in \mathcal{T}$. Technically, this optimization problem can be implemented in different ways[11] and in the following we use unconstrained optimization[8] employing automatic differentiation.[9] The cost function used in this study can be derived from a general probabilistic description of the estimation problem assuming Gaussian distributions (also called weakly constrained 4D-VAR in geosciences)[12,27–29] and consists of four terms

$$C(\{\mathbf{x}(n)\}, \mathbf{p}) = C_1 + C_2 + C_3 + C_4 \tag{10}$$

with

$$C_1 = \frac{\alpha}{N+1} \cdot \sum_{n=0}^{N} (\boldsymbol{\eta}(n) - \mathbf{y}(n))^{\mathrm{tr}} \mathbf{A} (\boldsymbol{\eta}(n) - \mathbf{y}(n)), \tag{11}$$

$$C_2 = \frac{1-\alpha}{N+1} \cdot \sum_{n=0}^{N} \mathbf{u}(n)^{\mathrm{tr}} \mathbf{B} \mathbf{u}(n), \tag{12}$$

$$C_3 = \frac{1-\alpha}{N+1} \cdot \sum_{n=3}^{N-2} \left(\mathbf{x}_{\mathrm{apr}}(n) - \mathbf{x}(n)\right)^{\mathrm{tr}} \mathbf{E} \left(\mathbf{x}_{\mathrm{apr}}(n) - \mathbf{x}(n)\right), \tag{13}$$

$$C_4 = \beta \cdot \mathbf{q}(\mathbf{w}, \mathbf{w}_{\mathrm{l}}, \mathbf{w}_{\mathrm{u}})^{\mathrm{tr}} \cdot \mathbf{q}(\mathbf{w}, \mathbf{w}_{\mathrm{l}}, \mathbf{w}_{\mathrm{u}}). \tag{14}$$

The term C_1 penalizes the difference between $\boldsymbol{\eta}(n)$ and $\mathbf{y}(n)$ whereas C_2 penalizes large magnitudes of $\mathbf{u}(n)$. In the term C_3, a Hermite interpolation is performed to determine $\mathbf{x}_{\mathrm{apr}}(n)$ from neighboring points and the time derivatives which are, according to (8), given by $\mathbf{F}(\mathbf{x}(t), \mathbf{p}, t) + \mathbf{u}(t)$ and provide the approximate solutions

$$\begin{aligned}\mathbf{x}_{\mathrm{apr}}(n) = {} & \frac{11}{54}\left[\mathbf{x}(n-2) + \mathbf{x}(n+2)\right] + \frac{8}{27}\left[\mathbf{x}(n-1)\right. \\ & \left. + \mathbf{x}(n+1)\right] + \frac{\Delta t}{18}\left[\mathbf{F}\left(\mathbf{x}(n-2), \mathbf{p}, t_{n-2}\right)\right. \\ & \left. + \mathbf{u}(t_{n-2}) - \mathbf{F}\left(\mathbf{x}(n+2), \mathbf{p}, t_{n+2}\right) - \mathbf{u}(t_{n+2})\right] \\ & + \frac{4\Delta t}{9}\left[\mathbf{F}\left(\mathbf{x}(n-1), \mathbf{p}, t_{n-1}\right) + \mathbf{u}(t_{n-1})\right. \\ & \left. - \mathbf{F}\left(\mathbf{x}(n+1), \mathbf{p}, t_{n+1}\right) - \mathbf{u}(t_{n+1})\right].\end{aligned} \tag{15}$$

Smoothness of $\{\mathbf{x}(n)\}$ is enforced by small differences $\mathbf{x}_{\mathrm{apr}}(n) - \mathbf{x}(n)$. The term C_3 suppresses non-smooth (oscillating) solutions, which may occur without this term in the cost function. In this paper, the weight matrices $\mathbf{A}$, $\mathbf{B}$, and $\mathbf{E}$ are diagonal matrices. The diagonal elements can be used for an individual weighting.

The solution $(\{\hat{\mathbf{x}}(n)\}, \hat{\mathbf{p}})$ obtained through the optimization of the cost function (10) is taken to be the maximum likelihood estimate.

Let

$$\mathbf{w} = (\{\mathbf{x}(n)\}, \mathbf{p}) \tag{16}$$

be a vector containing all quantities to be estimated. To force $\mathbf{w}$ to stay between the lower and upper bounds $\mathbf{w}_{\mathrm{l}}$ and $\mathbf{w}_{\mathrm{u}}$, respectively, the vector valued function $\mathbf{q}(\mathbf{w}, \mathbf{w}_{\mathrm{l}}, \mathbf{w}_{\mathrm{u}}) = (q_1, \ldots, q_L)^{\mathrm{tr}}$ is defined as

$$q_i(w_i, w_{\mathrm{l},i}, w_{\mathrm{u},i}) = \begin{cases} w_{\mathrm{u},i} - w_{\mathrm{i}} & \text{for } w_i \geq w_{\mathrm{u},i} \\ 0 & \text{for } w_{\mathrm{l},i} < w_{\mathrm{i}} < w_{\mathrm{u},i} \\ w_{\mathrm{l},i} - w_{\mathrm{i}} & \text{for } w_i \leq w_{\mathrm{l},i}. \end{cases} \tag{17}$$

q_i is zero if the value of w_i lies within its bounds. To enforce this, the positive parameter β is set to a large number, e.g., 10^5.

The homotopy parameter α can be used to control whether the solution should be close to data ($\alpha \approx 1$) or has a smaller error in fulfilling the model equations. In Ref. 30, a technique is described to find an optimal α. Furthermore, one might use continuation (see Ref. 7), where α is stepwise decreased. Starting with $\alpha \approx 1$ results in a solution close to the data. Then, α is slightly decreased and the previously obtained solution is used as an initial guess to optimize the cost function again. This procedure is repeated until the value $\alpha = 0.5$ is reached.

Note that the cost function can be written in the form

$$C(\mathbf{w}) = \sum_{j=1}^{J} H_j(\mathbf{w})^2 = ||\mathbf{H}(\mathbf{w})||_2^2, \tag{18}$$

where $\mathbf{H}(\mathbf{w})$ is a high dimensional vector valued function of the high dimensional vector $\mathbf{w}$. To optimize (18), we use an implementation of the Levenberg-Marquardt algorithm[31,32] called sparseLM.[33] Although $C(\mathbf{w})$ will be optimized,

sparseLM requires $\mathbf{H}(\mathbf{w})$ and the sparse Jacobian of $\mathbf{H}(\mathbf{w})$ as input which is computed using the automatic differentiation tool ADOL-C,[34,35] and described in more detail in Ref. 9.

V. DETERMINING THE BASIN SIZE OF THE TRUE SOLUTION

In Sec. IV, we described a state and parameter estimation algorithm that has to be initialized with guesses for all model state variables $\mathbf{x}(t_n)$ at each time step t_n and all fixed model parameters $\mathbf{p}$. This set of values forms an *initial guess*, which must be supplied to the optimization algorithm. In this section, three different methods for generating the initial guesses are presented and simulations consisting of twin experiments are performed to determine which of these methods gives the best estimates for the model state variables and fixed parameters. These estimates are then compared with the *true solution*, which is known exactly in this case since this is a twin experiment. Due to the fact that the methods for generating the initial guesses, in a certain way, depend on random numbers and the outcome of an estimation process is either successful (estimated states and parameters are close to the ones used to generate the data time series) or not successful (estimated states and parameters are *not* close to the ones used to generate the data time series) the simulations can be considered as *Bernoulli experiments* and the basin size of initial guesses leading to the true solution can be determined, as suggested by Menck *et al.*[18] in another context.

A. The simulation

First, we generate 18 "true" trajectories $\{{}^i\mathbf{z}(n)\}$ with $i = 1,\ldots,18$ by integrating the 9-dimensional Lorenz-96 model (3) with 18 different initial conditions $\mathbf{z}(0)$ on the attractor with $\Delta t = 0.01$ and $N = 1500$ using the model parameter $p = 8.17$. Then, $N_{\text{iguess}} = 500$ initial guesses $(\{{}^i_h\mathbf{x}(n)\},{}_hp)$ $(h = 1,\ldots,N_{\text{iguess}})$ of the model state variables and the (fixed) parameter p are generated which are used for initializing the estimation procedure (the estimation algorithm was described in Sec. IV). Three different methods for generating the initial guesses will be presented in Sec. V B. The following steps in the simulation do not depend on the specific choice of the method for creating the initial guesses.

From each of the 18 true trajectories $\{{}^i\mathbf{z}(n)\}$ with $i = 1,\ldots,18$, according to Sec. II, 15 multivariate time series were extracted corresponding to the 15 different combinations of state variables assumed to be measured. This gives 270 different multivariate time series with one, two, or three state variables

$$\begin{aligned}
&\{{}^i z_1(n)\},\{{}^i(z_1(n),z_2(n))\},\{{}^i(z_1(n),z_3(n))\},\\
&\{{}^i(z_1(n),z_4(n))\},\{{}^i(z_1(n),z_5(n))\},\\
&\{{}^i(z_1(n),z_2(n),z_3(n))\},\{{}^i(z_1(n),z_2(n),z_4(n))\},\\
&\{{}^i(z_1(n),z_2(n),z_5(n))\},\{{}^i(z_1(n),z_2(n),z_6(n))\},\\
&\{{}^i(z_1(n),z_2(n),z_7(n))\},\{{}^i(z_1(n),z_2(n),z_8(n))\},\\
&\{{}^i(z_1(n),z_3(n),z_5(n))\},\{{}^i(z_1(n),z_3(n),z_6(n))\},\\
&\{{}^i(z_1(n),z_3(n),z_7(n))\},\{{}^i(z_1(n),z_4(n),z_7(n))\},
\end{aligned} \tag{19}$$

with $i = 1,\ldots,18$, $\Delta t = 0.01$, $n = 0,1,\ldots,N$, and $N = 1500$.

To make the simulation more realistic, white noise (normally distributed random numbers) is added to these 270 clean, multivariate times series. This results in 270 noisy multivariate time series $\{{}^i\boldsymbol{\eta}^c(n)\}$ with $\Delta t = 0.01$, $n = 0,1,\ldots,N$, and $N = 1500$.

Each noisy time series is computed by

$${}^i\boldsymbol{\eta}^c(n) = \mathbf{h}^c({}^i\mathbf{z}(n)) + \sigma_{\text{ts}}\,{}^i\boldsymbol{\xi}^c(n)\,, \tag{20}$$

where $\sigma_{\text{ts}} = 0.2$ and ${}^i\boldsymbol{\xi}^c(n) = ({}^i\xi^c_1(n),\ldots,{}^i\xi^c_L(n)) \in \mathbb{R}^L$ are independent, normally distributed random variables with zero mean and a variance of one, ${}^i\xi^c_l(n) \sim \mathcal{N}(0,1)$.

The index $i = 1,\ldots,18$ describes the true trajectory $\{{}^i\mathbf{z}(n)\}$ from which the data time series was extracted. Index c indicates which state variables were measured. For example, $c = (1\text{–}2\text{–}6)$ means that the state variables z_1, z_2, and z_6 are the measured state variables. The label $h = 1,\ldots,N_{\text{iguess}}$ describes with which initial guess the estimation algorithm was initialized. The measurement function $\mathbf{h}^c(\mathbf{x}(t))$ is always chosen according to the measured state variables defined by c. If, for example, the state variables z_1, z_2, and z_7 are measured (and therefore $c = 1-2-7$), then the measurement function is given by $\mathbf{h}^c(\mathbf{x}(t)) = (x_1(t),x_2(t),x_7(t))$.

To each of the 270 multivariate time series $\{{}^i\boldsymbol{\eta}^c(n)\}$, the Lorenz-96 model is adapted $N_{\text{iguess}} = 500$ times, whereas each of the N_{iguess} estimation processes is initialized with one of the previously generated N_{iguess} different (random) initial guesses using the estimation algorithms described in Sec. IV. This means that $N_{\text{iguess}} \cdot 270 = 500 \cdot 270 = 135000$ estimation problems are solved.

For each solution of the estimation processes, the difference between the true and the estimated solution is given by the *estimation error*

$${}^i_hE^c = \frac{1}{(N+1)\cdot D}\sum_{n=0}^{N} ||{}^i\mathbf{z}(n) - {}^i_h\hat{\mathbf{x}}^c(n)||_2^2\,. \tag{21}$$

The indices of ${}^i_hE^c$, ${}^i\mathbf{z}^c(n)$ and ${}^i_h\hat{\mathbf{x}}^c(n)$ have the same meaning as for $\{{}^i_h\hat{\mathbf{x}}^c(n)\}$. The smaller the error measure ${}^i_hE^c$, the closer the estimated solution for the model state variables is to the true solution and hence the more accurately the estimation problem was solved. The estimation of state variables is considered as successful if ${}^i_hE^c < 10^{-2}$, else the estimation is considered as *not* successful. The value for the estimated fixed model parameter ${}^i_h\hat{p}^c$ is considered as successful, if ${}^i_h\hat{p}^c \in [8.16, 8.18]$ (remember, the true trajectories $\{{}^i\hat{\mathbf{z}}(n)\}$ were generated with $p = 8.17$ in Eq. (3)).

We are interested in a quantity (in percentage) which tells us how many estimations with a specific true trajectory, i, and a specific combination of observed state variables, c, of the model state variables are successful. In other words: For how many of the $N_{\text{iguess}} = 500$ estimations using N_{iguess} different initial guesses with a specific true trajectory, i, and a specific combination of observed state variables, c, is the estimation of the model state variables successful, i.e., ${}^i_hE^c < 10^{-2}$? This quantity, which of course depends on the true trajectory and the combination of measured state variables, is defined here as the *success rate of the estimation* of the model state variables (in percentage)

$$\langle {}^{i}E^{c}\rangle = \frac{100\%}{N_{\text{iguess}}}\sum_{h=1}^{N_{\text{iguess}}} e_h, \quad \text{with} \quad e_h = \begin{cases} 0, & \text{if } {}^{i}_{h}E^{c} > 10^{-2} \\ 1, & \text{if } {}^{i}_{h}E^{c} \le 10^{-2}. \end{cases} \tag{22}$$

One can also define an error which depends on the estimated solution and the data, only, as

$${}^{i}_{h}E^{c}_{\text{obs}} = \frac{1}{(N+1)\cdot L}\sum_{n=0}^{N} ||{}^{i}\boldsymbol{\eta}^{c}(n) - \mathbf{h}^{c}\left({}^{i}_{h}\hat{\mathbf{x}}^{c}(n)\right)||_2^2 . \tag{23}$$

Assume one estimates the best possible solution. That is, if the estimated solution is equal to the trajectory (without noise) used to generate the data, ${}^{i}_{h}\hat{\mathbf{x}}^{c}(n) = {}^{i}\mathbf{z}(n)$. In this case, Eq. (23) is (using Eq. (20))

$$\begin{aligned} {}^{i}_{h}E^{c}_{\text{obs,opt}} &= \frac{1}{(N+1)L}\sum_{n=0}^{N}||{}^{i}\boldsymbol{\eta}^{c}(n) - \mathbf{h}^{c}\left({}^{i}\mathbf{z}^{c}(n)\right)||_2^2 \\ &= \frac{\sigma_{\text{ts}}^2}{(N+1)L}\,{}^{i}Q^{c}, \end{aligned} \tag{24}$$

where

$${}^{i}Q^{c} = \sum_{n=0}^{N}\sum_{l=1}^{L}\left[{}^{i}\xi^{c}_{l}(n)\right]^2 . \tag{25}$$

Because ${}^{i}\xi^{c}_{l}(n)$ are independent, standard normal random variables, ${}^{i}Q^{c}$ is chi-squared distributed, ${}^{i}Q^{c} \sim \chi^2_{(N+1)L}$, with $(N+1)L$ degrees of freedom.[36] The expectation value is then given by $E[{}^{i}Q^{c}] = (N+1)L$, leading to an expectation value for ${}^{i}_{h}E^{c}_{\text{obs,opt}}$ of

$$E\left[{}^{i}_{h}E^{c}_{\text{obs,opt}}\right] = \sigma_{\text{ts}}^2 . \tag{26}$$

The variance of the chi-square distribution is $\text{Var}[{}^{i}Q^{c}] = 2(N+1)L$. The variance of ${}^{i}_{h}E^{c}_{\text{obs,opt}}$ is then

$$\begin{aligned} \text{Var}\left[{}^{i}_{h}E^{c}_{\text{obs,opt}}\right] &= \text{Var}\left[\frac{\sigma_{\text{ts}}^2}{(N+1)L}\,{}^{i}Q^{c}\right] \\ &= \frac{\sigma_{\text{ts}}^4}{[(N+1)L]^2}\text{Var}\left[{}^{i}Q^{c}\right] = \frac{2\sigma_{\text{ts}}^4}{(N+1)L} \end{aligned} \tag{27}$$

giving the standard deviation

$$\text{Std}\left[{}^{i}_{h}E^{c}_{\text{obs,opt}}\right] = \sqrt{\text{Var}\left[{}^{i}_{h}E^{c}_{\text{obs,opt}}\right]} = \sigma_{\text{ts}}^2\sqrt{\frac{2}{(N+1)L}}. \tag{28}$$

As described in Sec. V A, we use $\sigma_{\text{ts}} = 0.2$ and $N = 1500$. For one observed state variable, $L = 1$, and a perfect solution of the estimation problem, we get the lower boundary for ${}^{i}_{h}E^{c}_{\text{obs}}$, Eq. (23), of

$$\sigma_{\text{ts}}^2\left[1 \pm \sqrt{\frac{2}{(N+1)L)}}\right] \approx 0.04 \pm 0.00146 . \tag{29}$$

Note that only the standard deviation depends on the number of measurements (and is largest for $L = 1$), but not the expectation value. This means that with a smooth estimate for the model state variables one cannot go below this boundary. If one goes below this threshold, the measurement noise is modelled and one has not estimated a smooth solution for the model variables. In this case, one should choose a smaller α in the cost function Eq. (10). Note that the modelling of the measurement noise is still possible if one does not fall below this boundary. Because of the perfect model scenario in our twin experiments, we can expect a value for ${}^{i}_{h}E^{c}_{\text{obs}}$ which is only slightly larger (due to small numerical errors) than the lower boundary of $0.04 \pm 1.46 \cdot 10^{-3}$. To cover these cases, we introduce an empirical margin of 0.005 which is added to the lower bound of 0.04 and we consider an estimation as successful if ${}^{i}_{h}E^{c}_{\text{obs}} \le 0.045$. Applying this bound to the error given by Eq. (23), we can define a success rate (in percentage)

$$\langle {}^{i}E^{c}_{\text{obs}}\rangle = \frac{100\%}{N_{\text{iguess}}}\sum_{h=1}^{N_{\text{iguess}}} e_h, \quad \text{with} \quad e_h = \begin{cases} 0, & \text{if } {}^{i}_{h}E^{c}_{\text{obs}} > 0.045 \\ 1, & \text{if } {}^{i}_{h}E^{c}_{\text{obs}} \le 0.045. \end{cases} \tag{30}$$

In a similar way, the *success rate of the estimation of the model parameter* (in percentage) ${}^{i}_{h}\hat{p}^{c}$ is defined as

$$\langle {}^{i}\hat{p}^{c}\rangle = \frac{100\%}{N_{\text{iguess}}}\sum_{h=1}^{N_{\text{iguess}}} p_h, \quad \text{with} \quad p_h = \begin{cases} 0, & \text{if } {}^{i}_{h}\hat{p}^{c} \notin [8.16, 8.18] \\ 1, & \text{if } {}^{i}_{h}\hat{p}^{c} \in [8.16, 8.18]. \end{cases} \tag{31}$$

Note that in a real world experiment ${}^{i}_{h}E^{c}$, and hence $\langle {}^{i}E^{c}\rangle$, typically *cannot* be computed due to the unknown true trajectory $\{{}^{i}\mathbf{z}(n)\}$. Another possibility to compute the accuracy of the estimated model state variables and the fixed model parameters is to compare predictions of the model via the measurement function $\mathbf{h}(\mathbf{x}(t))$, Eq. (2), with available (noisy) data after the estimation window. To compute the prediction, the model Eq. (1) must be integrated starting at the end of the estimation window at t_N using the estimated value ${}^{i}_{h}\hat{p}^{c}$ as model parameter and ${}^{i}_{h}\hat{\mathbf{x}}^{c}(N)$ as initial guesses. Next, the prediction $\{{}^{i}_{h}\mathbf{x}^{c}(n)\}$, $n \ge N$ can be compared with observed data $\{{}^{i}\boldsymbol{\eta}^{c}(n)\}$, $n \ge N$, by computing the *prediction error*

$${}^{i}_{h}\text{PE}^{c} = \frac{1}{(N_{\text{pred}}+1)\cdot L}\sum_{n=N}^{N+N_{\text{pred}}} ||{}^{i}\boldsymbol{\eta}^{c}(n) - \mathbf{h}^{c}\left({}^{i}_{h}\mathbf{x}^{c}(n)\right)||_2^2 \tag{32}$$

for N_{pred} time steps using the same step size Δt as for computing the true trajectories. Due to noise in the data, the prediction error cannot vanish and we consider a prediction as successful, if ${}^{i}_{h}\text{PE}^{c} < 0.5$. Analogous to Eq. (22), we define the *success rate of the prediction* (in percentage)

$$\langle {}^{i}\text{PE}^{c}\rangle = \frac{100\%}{N_{\text{iguess}}}\sum_{h=1}^{N_{\text{iguess}}} \text{pe}_h, \quad \text{with} \quad \text{pe}_h = \begin{cases} 0, & \text{if } {}^{i}_{h}\text{PE}^{c} > 0.5 \\ 1, & \text{if } {}^{i}_{h}\text{PE}^{c} \le 0.5 \end{cases} \tag{33}$$

describing for how many of the different initial guesses with the same true trajectory and the same combination of measured state variables the prediction was successful. In contrast to ${}^{i}_{h}E^{c}$, the prediction error ${}^{i}_{h}\text{PE}^{c}$ can be computed using measured data only.

B. Different methods for generating initial guesses

For the optimization process, initial guesses for the model state variables and the fixed model parameter p have to be chosen. In our simulation, we considered three methods for preparing initial guesses according to rules specified below. For each case, $N_{\text{iguess}} = 500$ different guesses $(\{{}^{i}_{h}\mathbf{x}(n)\},{}_{h}p)$ with $h = 1, \ldots, N_{\text{iguess}}$ are generated. In all three cases, the model parameter ${}_{h}p$ is picked equally distributed from the interval $[4, 20]$. In those cases, where the initial guess $\{{}^{i}_{h}\mathbf{x}(n)\}$ for the model state variables does *not* depend on the true trajectory $\{{}^{i}\mathbf{z}(n)\}$ of the estimation problem, the index i will be neglected (i.e., ${}^{i}_{h}\mathbf{x}(n) = {}_{h}\mathbf{x}(n)$). In the following, three different methods of choosing the initial guesses will be used and evaluated:

(1) **Uniformly distributed samples in a box:** For each initial guess, each model state variable ${}_{h}x_d(n)$, $d = 1, \ldots, D$ at each time step t_n is an equally distributed random number in the interval $[-9, 14]$. This interval has been chosen because it is the range of typical oscillations of all state variables of the Lorenz-96 model. Together with the model parameter the initial guesses consist of $D \cdot N + 1 = D_{\text{iguess}} = 13501$ numerical values. In other words, the initial guesses are uniformly distributed points in a box in a D_{iguess} dimensional space $\mathbb{R}^{D_{\text{iguess}}}$.
(2) **Exact solutions of the model:** Each initial guess $(\{{}_{h}\mathbf{x}(n)\},{}_{h}p)$ is an exact solution of the Lorenz-96 model Eq. (3). The initial values ${}_{h}\mathbf{x}(0)$ of these trajectories are arbitrary points on the attractor generated with $p = 8.17$ (not coinciding with the initial conditions of the true trajectories).
(3) **Samples close to the true solution:** These initial guesses depend, in contrast to methods 1 and 2, on the "true trajectories" $\{{}^{i}\mathbf{z}(n)\}$ with $i = 1, \ldots, 18$ (see Sec. V A). The estimation processes will be initialized with a "noisy" version of $\{{}^{i}\mathbf{z}(n)\}$. More precisely, for each time step t_n uniformly distributed random numbers from the interval $[-15, 15]$ are added to the values of the true state $\{{}^{i}\mathbf{z}(n)\}$ to generate the initial guesses $\{{}^{i}_{h}\mathbf{x}(n)\}$, Compared to initial guess strategy 1 and 2, this strategy does depend on the true trajectories. In a real world application, where the true trajectories are not known, this strategy cannot be used in contrast to methods 1 and 2.

C. Interpretation of the simulation as Bernoulli experiment and error estimation

As described in Sec. V A for each of the 18 true trajectories and each of the 15 combinations of measured state variables, the Lorenz-96 model was adapted $N_{\text{iguess}} = 500$ times to the corresponding (multivariate) time series using a specific method for choosing the initial guesses. If ${}^{i}_{h}E^{c} < 10^{-2}$ (Eq. (21)), then the estimation of the model state variables is considered as successful. This simulation can be interpreted as a Bernoulli experiment, because each of the independent N_{iguess} estimations of the model state variables and the fixed parameter is a Bernoulli trial with the outcome *successful* or *not successful*. The standard error of the Bernoulli process is given by

$$ {}^{i}e^{c} := \frac{\sqrt{{}^{i}p^{c}(100\% - {}^{i}p^{c})}}{\sqrt{N_{\text{iguess}}}}, \tag{34} $$

whereas ${}^{i}p^{c} \in [0\%, 100\%]$ is the expectation value of the percentage of successful cases (index i describes the used true trajectory and index c describes the combination of measured state variables). Unfortunately, we do not know ${}^{i}p^{c}$. However, we can determine the maximum of the standard error ${}^{i}e^{c}$ which occurs for ${}^{i}p^{c} = 50\%$. With $N_{\text{iguess}} = 500$ trials, the maximal standard error equals ${}^{i}e^{c}_{\max} \approx 2.24\%$ and hence is sufficiently small.

D. Results

1. Estimation error

The simulation described in Sec. V A was performed with all three methods for choosing initial guesses for the model state variables and the fixed model parameters $(\{{}^{i}_{h}\mathbf{x}(n)\},{}_{h}p)$, as described in Sec. V B. For each method of choosing the initial guesses, the percentage of successful estimations, $\langle {}^{i}E^{c}\rangle$, Eq. (22), was computed, where an estimation of the model state variables is considered as successful if ${}^{i}_{h}E^{c} < 10^{-2}$, Eq. (21) (see Sec. V A). The estimation of the model parameter is considered as successful if ${}^{i}_{h}\hat{p}^{c} \in [8.16, 8.18]$. The success rate for the fixed model parameter, $\langle {}^{i}\hat{p}^{c}\rangle$, is defined in Eq. (31). The statistic (percentage of successful estimations) was created for each of the 18 true trajectories $\{{}^{i}\mathbf{z}(n)\}$ (indexed by i), each of the 15 combinations of observed state variables, c, and all $N_{\text{iguess}} = 500$ initial guesses (indexed by h).

Table I shows the results for method 1 (uniformly distributed samples in a box). This table shows $\langle {}^{i}E^{c}\rangle$ and $\langle {}^{i}\hat{p}^{c}\rangle$ for each combination of a true trajectory $\{{}^{i}\mathbf{z}(n)\}$ and a particular choice of measured state variables. If three variables are measured, the rate of successful estimations of the model variables and the fixed parameter is (on average) higher for all combinations of measured state variables compared to the success rate for multivariate time series with only two variables. Nevertheless, certain combinations with two observed variables (x_1, x_2), (x_1, x_3), or (x_1, x_4) also give success rates that are only slightly lower than combinations of three observed state variables. They just appear less often compared to time series with three observed state variables. When (x_1, x_5) are observed, the estimation of the model state variables and the fixed parameter does not seem to work very well. None of the 18 trajectories considered here exhibit high success rate. If only x_1 is observed, the estimation of variables and the parameter fails for all 18 trajectories. As one might expect, one can see a high correlation between the success rate for the state variable estimation (Table I) and the success rate for the parameter estimation (Table I). The success rates depend not only on the combination of observed variables only but also on the trajectory $\{{}^{i}\mathbf{z}(n)\}$ used to generate the time series (i.e., the starting points on the attractor).

In Table II, the success rate of the error defined by Eq. (30) is shown. Compared to Eq. (22) this success rate can be computed from the data and the estimated model state

TABLE I. These tables show the results of the simulation explained in Sec. V A with initial guess method in Sec. V B method 1. For the 9-dimensional Lorenz-96 model Eq. (3), there exist 15 mathematically different combinations of one to three state variables constituting a multivariate time series (Sec. V A, the first rows of the tables show all these combinations). Example: 1-2-4 means that the variables z_1, z_2, and z_4 are measured. The 18 noise-free time series $\{^i\mathbf{z}(n)\}$, $i = 1, \ldots, 18$ are generated by integrating the model equations with different initial conditions. For each i, from $\{^i\mathbf{z}(n)\}$, we extract 15 different time series with different combinations of state variables. According to Eq. (20), some artificial noise is added (Sec. V A). This results in $15 \cdot 18 = 270$ different noisy multivariate time series (cf. Eq. (20)). To each of the 270 noisy time series the Lorenz-96 model is adapted $N_{\text{iguess}} = 500$ times using the state and parameter estimation algorithm described in Sec. IV with 500 different initial guesses for the model state variables and the fixed model parameter chosen according to initial guess method 1 (uniformly distributed samples in a box) (Sec. V B). For each of the 500 solutions, ${}^i_hE^c$ (Eq. (21)) is computed ($h = 1, \ldots, 500$). If ${}^i_hE^c < 10^{-2}$, then the variables estimation is considered as successful. The values in the tables show the percentages of successful estimations of state variables, $\langle {}^iE^c \rangle$ Eq. (22), and parameters, $\langle {}^i\hat{p}^c \rangle$ Eq. (31).

	Observed state variables c														
True trajectory	1	1-2	1-3	1-4	1-5	1-2-3	1-2-4	1-2-5	1-2-6	1-2-7	1-2-8	1-3-5	1-3-6	1-3-7	1-4-7
Observability of model state variables (success rate $\langle {}^iE^c \rangle$)															
$\{^1\mathbf{z}(n)\}$	0	49.8	33	42.6	0	95.6	98.8	86.8	95.8	83.6	8.6	50.2	85.4	90.2	89.8
$\{^2\mathbf{z}(n)\}$	0	3.6	0	1.6	0	2.6	89.8	90.2	18.4	65	17.4	8.6	5.2	15.6	64.8
$\{^3\mathbf{z}(n)\}$	0	1.8	5.4	0	0.2	66.2	82.2	35	2	39.6	3.4	17.6	76.4	87.8	83.4
$\{^4\mathbf{z}(n)\}$	0	1	0.4	0.2	0	77.8	94.2	90.2	2	87.8	34.6	34.8	31	28.8	18.2
$\{^5\mathbf{z}(n)\}$	0	8.4	60.6	0.6	5.2	74.8	95	90	83.2	93	41	86.6	84.6	88.2	89.8
$\{^6\mathbf{z}(n)\}$	0	37.4	0.2	0	0.2	58.2	77.6	80.8	94.6	56.2	78.8	7.8	27.8	14.4	25.4
$\{^7\mathbf{z}(n)\}$	0	2.8	2.2	6.4	0	96.4	93.6	76.4	91.4	30	30.2	37.8	55.2	36.4	82.2
$\{^8\mathbf{z}(n)\}$	0	95.2	5.2	0.8	1	97.2	98.2	92.4	85.6	86.6	94.4	83.2	65.2	59.8	89.2
$\{^9\mathbf{z}(n)\}$	0.2	87.8	80.2	76	0.2	96.8	99.4	87.4	89	87.8	12.4	89.4	83.4	77.8	89.2
$\{^{10}\mathbf{z}(n)\}$	0	92.4	28.4	1.2	2.8	98.2	98.4	94.8	85.4	50.4	81.8	81	68.4	6.2	4.2
$\{^{11}\mathbf{z}(n)\}$	0	0	0.4	0.6	5.2	4	63.8	89.2	1.6	60.8	61.8	58.8	49.4	81	87.2
$\{^{12}\mathbf{z}(n)\}$	0	24.8	1.2	1.6	0	88.6	95.4	89	1.6	3.6	12.2	20.8	2.6	0.6	86.4
$\{^{13}\mathbf{z}(n)\}$	0	4.8	27.2	0.2	3.6	82.8	95.6	81	7.2	92.6	86	67.2	67.8	66.4	86
$\{^{14}\mathbf{z}(n)\}$	0	30.6	7.8	1.4	0	90.6	95.8	78	83.8	6.6	79	56.2	68	42.6	88.6
$\{^{15}\mathbf{z}(n)\}$	0	47.2	1	0.2	0	85	96.4	89.4	44.6	85.8	87.4	66.8	36.4	58.2	82.2
$\{^{16}\mathbf{z}(n)\}$	0	14.4	14.2	0	0	95.4	96	94	59.4	76.6	96.6	27.6	9	15.6	7.2
$\{^{17}\mathbf{z}(n)\}$	0	78.4	1.4	0.4	0.2	83.6	92.4	95	92.4	5.4	28.4	16.6	3.4	1.2	87.8
$\{^{18}\mathbf{z}(n)\}$	0	37.6	2.2	1.6	0	87.6	96.6	86	86.2	71	32.8	16.4	22.8	71.8	86.2
Observability of the model parameter (success rate $\langle {}^i\hat{p}^c \rangle$)															
$\{^1\mathbf{z}(n)\}$	0	54.2	33	46.2	0	95.8	99	87	95.8	83.6	33.8	51.2	85.4	90.2	89.8
$\{^2\mathbf{z}(n)\}$	0	4.2	0	6	0.6	32.2	89.8	90.2	18.4	65	17.6	8.8	5.2	16	65.4
$\{^3\mathbf{z}(n)\}$	0.2	3.6	6	1.4	3.4	66.6	93.6	89.6	2	39.6	7.6	20.6	81.4	87.8	90
$\{^4\mathbf{z}(n)\}$	0.2	1.4	0.6	0.4	0.8	77.8	94.2	90.2	2	88.4	46.4	35.2	31	30.6	18.4
$\{^5\mathbf{z}(n)\}$	0.6	67.2	61.8	10.4	5.6	90.2	95.2	90	83.2	93	41.4	86.6	85.2	92.4	89.8
$\{^6\mathbf{z}(n)\}$	0.2	37.4	0.4	0.2	0.2	58.2	77.6	80.8	94.6	56.2	78.8	7.8	28.2	15	25.4
$\{^7\mathbf{z}(n)\}$	0.2	2.8	26	6.6	3.8	96.4	93.8	77	92	32.8	56	40	55.2	36.8	82.6
$\{^8\mathbf{z}(n)\}$	0.4	95.2	6.2	1.2	1.8	97.6	98.4	92.4	85.6	86.8	95	83.8	69.2	61.6	94.4
$\{^9\mathbf{z}(n)\}$	0.8	91	81.2	79.8	0.2	97	99.4	88.2	93.8	88	55.2	89.8	83.8	90.4	89.4
$\{^{10}\mathbf{z}(n)\}$	0	92.4	59	4.2	18.6	98.2	98.4	94.8	87	50.4	81.8	84.6	68.4	53	92.6
$\{^{11}\mathbf{z}(n)\}$	0.6	1.2	1.8	0.6	14.6	4.2	63.8	90.4	23	61.2	63.4	59.2	57.8	82	87.6
$\{^{12}\mathbf{z}(n)\}$	0	53.8	1.4	5.8	1.2	88.8	95.4	89	2.4	4.2	14.8	45.8	3.8	0.8	88
$\{^{13}\mathbf{z}(n)\}$	0.2	6.6	27.8	0.4	23.2	82.8	96.4	84	60.8	93	86	67.2	75.4	66.8	86.2
$\{^{14}\mathbf{z}(n)\}$	1.4	31.4	11.6	2.8	0.8	93.8	97	83.4	83.8	6.8	83	57.6	68.2	42.8	89.4
$\{^{15}\mathbf{z}(n)\}$	0.4	59	7	1.2	1.2	98.8	97	89.8	44.6	86.2	89	67	36.8	58.2	82.6
$\{^{16}\mathbf{z}(n)\}$	0.8	15	14.4	10.4	0.8	95.6	96.6	94	59.4	83.2	97.4	36	9.8	85.6	9.8
$\{^{17}\mathbf{z}(n)\}$	0.4	87.8	2	0.6	0.4	84.4	92.4	95	92.4	44	30	16.8	3.4	43.8	87.8
$\{^{18}\mathbf{z}(n)\}$	0	39.6	2.4	2	1.6	88.4	96.6	86	86.2	92.4	32.8	16.6	23.2	72	86.8

variables only. One can see a high correlation between Tables I and II indicating that ${}^i_hE^c_{\text{obs}}$ is a good approximation of ${}^i_hE^c$ (at least in the absence of errors in the model equations, as in these simulations). There are, however, some discrepancies. For example, if $\{^5\mathbf{z}(n)\}$ is the true trajectory and $c = 1 - 2$ is measured, Table I shows a much smaller success rate, given by Eq. (22) (only the error of all model variables is considered), compared to the success rate, given by Eq. (30), in Table II (the error of measured state variables is considered only). This shows that a good estimation of measured variables does not necessarily mean that unmeasured variables are also estimated correctly.

With initial guess method 1, the initial guess for each of the 9 model variable at 1500 locations along the (initial) trajectory is a random number (equally distributed) from the interval $[-9, 14]$ (see Sec. V B). With the guess for the unknown parameter, the full initial guess is a point in a $D_{\text{iguess}} = 13501$ dimensional box. Scanning this entire

TABLE II. Similar to Table I, except that the values in the tables show the success rate Eq. (30) which only depends on the estimated model state variables and the data.

	Observed state variables c														
True trajectory	1	1-2	1-3	1-4	1-5	1-2-3	1-2-4	1-2-5	1-2-6	1-2-7	1-2-8	1-3-5	1-3-6	1-3-7	1-4-7
$\{^1\mathbf{z}(n)\}$	0	49.8	33	42.6	0	95.6	98.8	86.8	95.8	83.6	33	50.2	85.4	90.2	89.8
$\{^2\mathbf{z}(n)\}$	0	3.6	0	1.6	0	2.6	89.8	90.2	18.4	65	17.4	8.6	5.2	15.6	64.8
$\{^3\mathbf{z}(n)\}$	0	1.8	5.4	0	0.2	66.2	82.2	35	2	39.6	3.4	17.6	76.4	87.8	83.4
$\{^4\mathbf{z}(n)\}$	0	1	0.4	0.2	0	77.8	94.2	90.2	2	87.8	34.6	34.8	31	28.8	18.2
$\{^5\mathbf{z}(n)\}$	0	67	60.6	0.6	5.2	74.8	95	90	83.2	93	41	86.6	84.6	88.2	89.8
$\{^6\mathbf{z}(n)\}$	0	37.4	0.2	0	0.2	58.2	77.6	80.8	94.6	56.2	78.8	7.8	27.8	14.4	25.4
$\{^7\mathbf{z}(n)\}$	0	2.8	2.2	6.4	0	96.4	93.6	76.4	91.4	30	30.2	37.8	55.2	36.4	82.2
$\{^8\mathbf{z}(n)\}$	0	95.2	5.2	0.8	1	97.2	98.2	92.4	85.6	86.6	94.4	83.2	65.2	59.8	89.2
$\{^9\mathbf{z}(n)\}$	0.2	87.8	80.2	76	0.2	96.8	99.4	87.4	89	87.8	12.4	89.4	83.4	77.8	89.2
$\{^{10}\mathbf{z}(n)\}$	0	92.4	28.4	1.2	2.8	98.2	98.4	94.8	85.4	50.4	81.8	84.4	68.4	6.2	4.2
$\{^{11}\mathbf{z}(n)\}$	0	0	0.4	0.6	5.2	4	63.8	89.2	1.6	60.8	61.8	58.8	49.4	81	87.2
$\{^{12}\mathbf{z}(n)\}$	0	24.8	1.2	1.6	0	88.6	95.4	89	1.6	3.6	12.2	20.8	2.6	0.6	86.4
$\{^{13}\mathbf{z}(n)\}$	0	4.8	27.2	0.2	3.6	82.8	95.6	81	7.2	92.6	86	67.2	67.8	66.4	86
$\{^{14}\mathbf{z}(n)\}$	0	30.6	7.8	1.4	0	90.6	95.8	78	83.8	6.6	79	56.2	68	42.6	88.6
$\{^{15}\mathbf{z}(n)\}$	0	47.2	1	0.2	0	85	96.4	89.4	44.6	85.8	87.4	66.8	36.4	58.2	82.2
$\{^{16}\mathbf{z}(n)\}$	0	14.4	14.2	0	0	95.4	96	94	59.4	76.6	96.6	27.6	9	15.6	7.2
$\{^{17}\mathbf{z}(n)\}$	0	78.4	1.4	0.4	0.2	83.6	92.4	95	92.4	5.4	28.4	16.6	3.4	1.2	87.8
$\{^{18}\mathbf{z}(n)\}$	0	37.6	2.2	1.6	0	87.6	96.6	86	86.2	92.4	32.8	16.4	22.8	71.8	86.2

$D_{\text{iguess}} = 13501$ dimensional rectangular box containing the initial is not an appropriate method to learn something about the basin shape of the optimal solution. Nevertheless, one can interpret the success rate $\langle {}^iE^c \rangle$ as the ratio of the size of the basin of successful estimates and the volume of the box in the $\mathbb{R}^{D_{\text{iguess}}}$ space[18] in percentage. Using the initial guess method 2 (exact solutions of the model) in Sec. V B, one can create a similar statistic (not shown here). We found that the success rate for the state variables and parameter estimation is almost zero in many if not most cases for all combinations of observed state variables and all true trajectories, i.e., method 2 gives worse success rates compared to method 1 (uniformly distributed samples in a box).

As discussed in Sec. V B using initial guess method 3 (samples close to the true solution) is usually not applicable in a real world estimation process, because the true trajectories are usually not given. We use it here to estimate the basin size around the true trajectories and it turns out that initial guesses uniformly sampled in a "tube" around the true trajectories with a radius of 15 (which is larger than the amplitude of the oscillations) provide correct estimates with a very high success rate. This means that the optimal solution is not only locally observable but also possesses a basin of considerable size. However, this basin is bent/curved in a very high dimensional space.

2. Prediction error

In contrast to considering $\langle {}^iE^c \rangle$ and $\langle {}^i\hat{p}^c \rangle$ only, we also consider the success rate of the prediction, $\langle {}^i\text{PE}^c \rangle$, Eq. (33). For initial guess method 1, the prediction success rate $\langle {}^i\text{PE}^c \rangle$ is shown in Table III. Remember that ${}^i_h\text{PE}^c$ can be computed using the solution from the estimation process and the measured data $\{{}^i\boldsymbol{\eta}^c(n)\}$ only, provided data for $N \leq n \leq N + N_{\text{pred}}$ are available. The prediction was computed for $N_{\text{pred}} = 300$ time steps. Here, due to noise in the data, an estimate of the model state variables is considered as successful if ${}^i_h\text{PE}^c < 0.5$. Note that "successful"' here does not necessarily mean that the prediction of unobserved state variables is accurate nor that in the estimation window $n \in [0, \ldots, N]$ the observed and unobserved model variables and the model parameter are estimated correctly (in the sense that ${}^i_hE^c$ is small and ${}^i_h\hat{p}^c \in [8.16, 8.18]$). One can see that even for two measured variables there are many combinations of $\{{}^i\mathbf{z}(n)\}$ and the measured variables with a large $\langle {}^i\text{PE}^c \rangle$ showing successful predictions of observed variables. Furthermore, when only a single variable is measured, the predictions fail for almost all true trajectories, as shown by $\langle {}^i\text{PE}^{(1)} \rangle \approx 0\%$. These results are consistent with the results obtained from Table I, although on average the percentages have smaller numerical values. Nevertheless, there are cases where $\langle {}^i\text{PE}^c \rangle$ is large and $\langle {}^iE^c \rangle$ is small (example: $c = (1\text{–}2)$, $i = 3$) and vice versa (example: $c = (1\text{–}3)$, $i = 1$). For both cases, estimation and prediction examples are shown in Fig. 2 left column (${}^3_{385}E^{(1-2)} > {}^3_{385}\text{PE}^{(1-2)}$) and Fig. 2 right column (${}^1_{140}E^{(1-3)} < {}^1_{140}\text{PE}^{(1-3)}$). This means that the correlation between $\langle {}^iE^c \rangle$ and $\langle {}^i\text{PE}^c \rangle$ is strong but not perfect. A good prediction does not necessarily mean a good estimation during the estimation window. It rather *indicates* that if the prediction error is small then the estimation of unobserved state variables and parameters is good.

Using the initial guess method 2 (exact solutions of the model), we found that the success rate $\langle {}^i\text{PE}^c \rangle$ is almost zero in many if not most cases for all combinations of observed variables and all true trajectories, i.e., method 2 gives worse success rates compared to method 1 (uniformly distributed samples in a box). The same was observed when considering

TABLE III. This table shows the statistic of the prediction error for initial guess method 1. The table has to be interpreted in the same way as Table I. In contrast to Table I, the numbers show $\langle {}^{i}\mathrm{PE}^{c}\rangle$, Eq. (33), which is the percentage of successful predictions by considering the prediction error ${}^{i}_{h}\mathrm{PE}^{c}$, Eq. (32). An estimation is considered as successful if ${}^{i}_{h}\mathrm{PE}^{c} < 0.5$. The length of the prediction window is $N_{\mathrm{pred}} = 300$ and time steps of length $\Delta t =$ are used.

	Observed state variables c														
True trajectory	1	1-2	1-3	1-4	1-5	1-2-3	1-2-4	1-2-5	1-2-6	1-2-7	1-2-8	1-3-5	1-3-6	1-3-7	1-4-7
$\{{}^{1}\mathbf{z}(n)\}$	0	0	0.2	50.4	0	0.2	0	90	1.2	84.2	0	52.8	88.8	91.6	90.4
$\{{}^{2}\mathbf{z}(n)\}$	0	10.4	1.2	23.4	3	3.6	91.6	0.4	19	74.8	66.8	86	59	19.6	71.2
$\{{}^{3}\mathbf{z}(n)\}$	0.2	37.6	22.4	4.6	28	66.6	95	89.8	71.6	98.8	31.2	21	87.2	95.4	95.6
$\{{}^{4}\mathbf{z}(n)\}$	0	1.8	0.6	8.4	11.6	78.2	95.2	93.8	27.8	96.4	85	66	79.4	31.2	94.8
$\{{}^{5}\mathbf{z}(n)\}$	0	67.2	63.4	0.8	5.4	92.2	96.6	90	84.2	93.4	0.6	92.4	90	92	92.8
$\{{}^{6}\mathbf{z}(n)\}$	0	37.4	0.6	1.2	4.8	60.2	78	82.2	98.6	57.8	86	16.8	29.8	38.6	26.4
$\{{}^{7}\mathbf{z}(n)\}$	0	0	2.2	7.4	0.6	1	94.2	4.2	1	37.6	30.4	41.2	57	36.6	82.6
$\{{}^{8}\mathbf{z}(n)\}$	0	0	0	2.2	3	0.6	0.6	1.4	0	86.8	0	86.4	0	61.8	96.2
$\{{}^{9}\mathbf{z}(n)\}$	0.2	94	83.4	82	1.6	0	99.4	87.4	91.4	98	88.4	91.4	88.8	93.8	96.4
$\{{}^{10}\mathbf{z}(n)\}$	0	0	58.8	1.2	0	98.2	98.4	0	1.2	0	0	0	0.8	52.4	92.4
$\{{}^{11}\mathbf{z}(n)\}$	0	3.6	2	2.2	18.8	5.4	67.2	91.2	23.2	61.6	64	85.6	51.8	86.2	91.6
$\{{}^{12}\mathbf{z}(n)\}$	0	55.4	36	7.2	0.4	90.4	96.4	92.4	20.8	5.4	25.8	61	80.6	15.8	94.4
$\{{}^{13}\mathbf{z}(n)\}$	0	0.2	38.2	3	28.6	83	1	1.2	0.8	0	0	68.6	77.8	78.4	2.8
$\{{}^{14}\mathbf{z}(n)\}$	0	31.4	1.4	4.4	0.2	0	97.4	1.8	83.8	7.4	84.4	5.6	68.2	94.8	93.4
$\{{}^{15}\mathbf{z}(n)\}$	0.2	70.6	29.2	11.4	4.4	99.8	99.2	98.8	97.8	99.8	96.4	72.6	57.6	92.2	94
$\{{}^{16}\mathbf{z}(n)\}$	0	0.2	0	0	0	95.4	0	0	0.2	0	0	2	15.6	0	0.6
$\{{}^{17}\mathbf{z}(n)\}$	0	78.4	2	10	0.4	0	0	0.2	1.4	0	0	50.2	3.4	43.8	2.8
$\{{}^{18}\mathbf{z}(n)\}$	0	43.2	17.4	46.4	11.2	91	97.2	97.8	94	98.4	92.2	58.6	83.6	92.8	92

$\langle {}^{i}E^{c}\rangle$. A possible explanation for this observation is the fact that, for exact solutions, the term C_1 (Eq. (11)) in the cost function C is the only term significantly different from zero, such that the initial values result in a relatively small value of the total cost function and this may increase the probability to be close to (and kept in) a local minimum.

When initial guess method 3 (samples close to the true solution) was used, we observed that most success rates of the prediction are close to $\langle {}^{i}\mathrm{PE}^{c}\rangle \approx 100\%$. Nevertheless, there are also combinations of a true trajectory and measured state variables with a success rate close to zero (especially for one and two measured variables) although corresponding success rates $\langle {}^{i}E^{c}\rangle$ are high. The most likely reason is the chaotic dynamics of the model and therefore the fast divergence from the data when computing the predictions.

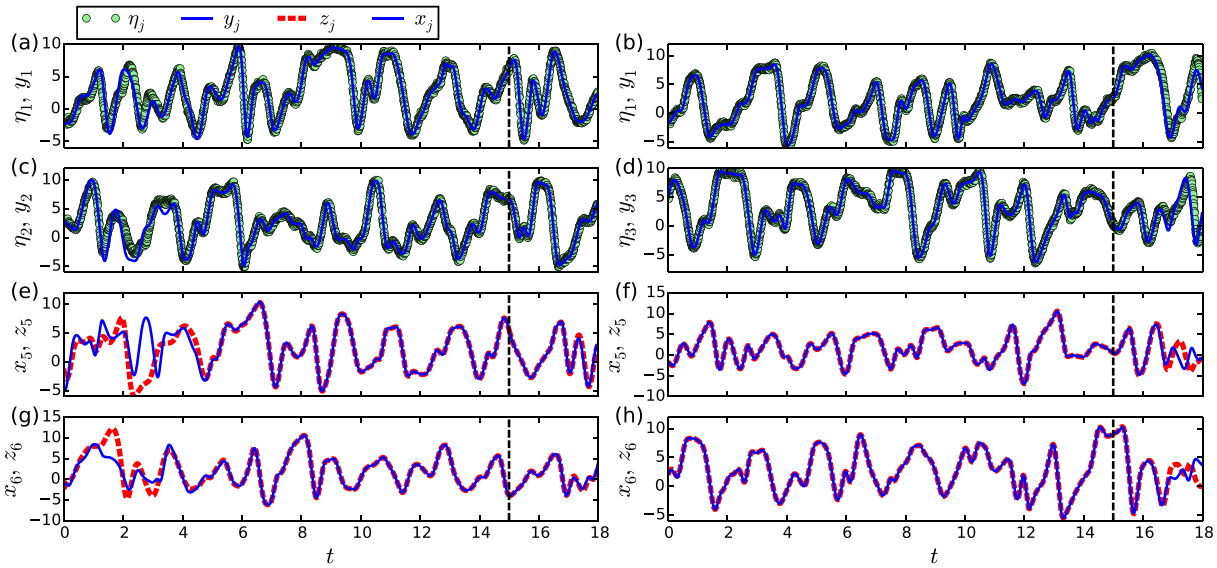

FIG. 2. This figure shows two examples, where the Lorenz-96 model Eq. (3) was adapted to a (multivariate) time series η_j. The (unmeasured) model state variables x_j and the fixed model parameter were estimated using the estimation method 1 described in Sec. IV. The output of the measurement function is y_j and the true trajectory is z_j (unknown to the estimation algorithm). The estimation was performed for $0 < t < 15$ and the prediction of the model variables for $15 \leq t < 18$ (right of the vertical black dashed line at $t = 15$). Left column, (a), (c), (e), and (g): x_1 and x_2 are measured ($c = (1-2)$) and $i = 3$, $h = 385$. The estimation error of model variables is larger than the prediction error, ${}^{3}_{385}E^{(1-2)} = 1.73 > {}^{3}_{385}\mathrm{PE}^{(1-2)} = 0.054$. Right column, (b), (d), (f), and (h): x_1 and x_3 are measured ($c = (1-3)$) and $i = 1$, $h = 140$. The estimation error of model variables is smaller than the prediction error, ${}^{1}_{140}E^{(1-3)} = 6.1 \cdot 10^{-4} < {}^{1}_{140}\mathrm{PE}^{(1-3)} = 1.98$.

VI. DISCUSSIONS AND CONCLUSIONS

Using a chaotic 9-dimensional Lorenz-96 model as a prototypical example, we studied observability of all its 9 state variables x_i and the fixed model parameter p using different multivariate time series consisting of one to three observables. Local observability was characterized by a recently introduced measure of uncertainty ν_i given in Eq. (7). This analysis indicates that all state variables and the parameter can be reconstructed, even in cases where only a univariate time system is available. It turned out that on average the values of ν_i for unmeasured state variables are minimal for a delay time τ between $\tau = 0.11$ and $\tau = 0.21$ (see Fig. 1). This is in agreement with results reported in Ref. 5, where $\tau \approx 0.1$ was found to be an appropriate delay time to synchronize a Lorenz-96 model to an observed time series using a delay coordinates based coupling scheme. Histograms of the uncertainties ν_i of the fixed model parameter and the measured and unmeasured state variables look similar, independent of the number of measured variables. This means that the successful reconstruction of the state $\mathbf{x}(t)$ and the parameter p should not depend on the number of measured state variables in a (multivariate) time series, provided one initializes the estimation algorithm close enough to the true solution (note that the observability analysis presented in Sec. III is only locally valid).

In Ref. 5, we showed that for the Lorenz-96 model synchronization to the data is indeed possible with only a single measured state variable, only, using a synchronization scheme based on delay vectors of the data time series. Hence, this result is in coincidence with the fact that the uncertainty values ν_i are relatively small already for univariate time series from the Lorenz-96 system.

Furthermore, we addressed the question whether the estimation of the model states is also possible if an estimation algorithm is initialized further away from the true trajectory of the dynamical system underlying the data. To probe this global convergence, a statistical test was performed, where an optimization based state and parameter estimation algorithm[8] was initialized with different initial guesses for the entire trajectory and the model parameter. Three different methods for generating the initial guesses were used (see Sec. V B) and compared.

With method 1, initial guesses were chosen uniformly distributed in a box. With this preparation of initial guesses of the optimization algorithm state and parameter estimation in the 9-dimensional Lorenz-96 model was possible with a very high success rate if multivariate times series with (at least) three observables are available, while for two measured state variables, only a fraction of estimation runs was successful (see success rates summarized in Table I). Note that the initial guesses generated by method 1 are typically far off the trajectory underlying the data. As a consequence state and parameter estimation based on univariate time series failed in most cases. Therefore, for practical application local observability is a necessary but not a sufficient feature of the given estimation problem.

Furthermore, it was shown that an error definition based on the difference between the estimated solution of the model variables and the noise free true trajectory (of all variables), Eq. (21), gives comparable success rates as an error definition based on the difference between the measurement function and the data, Eq. (23). For the latter, a lower bound was derived, which is valid for a smooth solution. Note that in all simulations the model equations have no errors. The question of whether both error definitions would give comparable results if errors in the model equations are present was not addressed.

Using exact trajectories (not coinciding with the true trajectory underlying the data) as initial conditions (method 2) turned out to result in very poor estimation results. Hence, initializing the estimation algorithm with an arbitrary solution of the model equations is a disadvantage compared to random initial guesses.

High success rates (close to 100%) were obtained using initial guess method 3, where the estimation algorithm is initialized with samples close to true solutions. These results are consistent with the low uncertainty observed in the local observability analysis. Note, however, that usually this initialization method cannot be applied with real world data, because the true trajectories used to generated the initial guess are typically unknown.

In addition to considering the success rate of the estimation, Eq. (22), which can only be computed if the clean trajectories of *all* state variables are known (often only one variable can be measured), the success rate of prediction, Eq. (33), was considered. This prediction error is more suitable for real world applications, because it can be computed based on measured data and the estimated model state variables and does not require further information about the dynamics. In the example considered here, a correlation between the prediction error and the success rate of the estimation was observed indicating that the prediction error is a good measure for the success of the estimation procedure. Nevertheless, it was also shown that a small estimation error does not necessarily mean a small prediction error and vice versa.

Our results indicate that successful state and parameter estimation crucially depends on the selection of available observables (univariate vs. multivariate), on the trajectory segment underlying the time series (i.e., the region of the state space the trajectory visits during measurements), and last but not least, the initialization of the estimation algorithm. The first two aspects are typically determined by and during the measurement (or experiment) and cannot be changed afterwards. Only the choice of the estimation method and of its initialization is (typically) in the hand of the person who is analyzing the data. Using a representative algorithm from the class of optimization based methods (similar to 4D-VAR), we demonstrated that the success may crucially depend on a proper choice of initial guesses. Finding suitable criteria and initialization strategies is thus an important open task for future research on state and parameter estimation algorithms.

ACKNOWLEDGMENTS

The research leading to the results has received funding from the European Community's Seventh Framework Programme FP7/2007-2013 under Grant Agreement 17 No. HEALTH-F2-2009-241526, EUTrigTreat. S.L. and U.P. acknowledge support from the BMBF (FKZ031A147,

GO-Bio), the DFG (SFB 1002), and the German Center for Cardiovascular Research (DZHK e.V.). Partial support from the Department of Energy CSGF program (DE-FG02-97ER25308) for D. Rey is appreciated. Partial support has come from the ONR MURI Program (N00014-13-1-0205).

APPENDIX: JACOBIAN MATRIX OF THE DELAY COORDINATES MAP

The Jacobian of the delay reconstruction map Eq. (6) with respect to $\mathbf{x}(t)$ and $\mathbf{p}$ is given by

$$\mathrm{D}_{\mathbf{x},\mathbf{p}}\mathbf{S}(\mathbf{x}(t),\mathbf{p}) = \begin{pmatrix} \mathrm{D}_{\mathbf{x}}\mathbf{h}(\mathbf{x}(t)) & 0 \\ \mathrm{D}_{\mathbf{x}}\mathbf{h}(\phi^{\tau}(\mathbf{x}(t),\mathbf{p}))\cdot\mathrm{D}_{\mathbf{x}}\phi^{\tau}(\mathbf{x}(t),\mathbf{p}) & \mathrm{D}_{\mathbf{x}}\mathbf{h}(\phi^{\tau}(\mathbf{x}(t),\mathbf{p})))\cdot\mathrm{D}_{\mathbf{p}}\phi^{\tau}(\mathbf{x}(t),\mathbf{p}) \\ \mathrm{D}_{\mathbf{x}}\mathbf{h}(\phi^{2\tau}(\mathbf{x}(t),\mathbf{p}))\cdot\mathrm{D}_{\mathbf{x}}\phi^{2\tau}(\mathbf{x}(t),\mathbf{p}) & \mathrm{D}_{\mathbf{x}}\mathbf{h}(\phi^{2\tau}(\mathbf{x}(t),\mathbf{p}))\cdot\mathrm{D}_{\mathbf{p}}\phi^{2\tau}(\mathbf{x}(t),\mathbf{p}) \\ \vdots & \vdots \\ \mathrm{D}_{\mathbf{x}}\mathbf{h}(\phi^{(K-1)\tau}(\mathbf{x}(t),\mathbf{p}))\cdot\mathrm{D}_{\mathbf{x}}\phi^{(K-1)\tau}(\mathbf{x}(t),\mathbf{p}) & \mathrm{D}_{\mathbf{x}}\mathbf{h}(\phi^{(K-1)\tau}(\mathbf{x}(t),\mathbf{p}))\cdot\mathrm{D}_{\mathbf{p}}\phi^{(K-1)\tau}(\mathbf{x}(t),\mathbf{p}) \end{pmatrix}, \tag{A1}$$

where

$$\mathrm{D}_{\mathbf{x}}\mathbf{h}\left(\phi^{\tau'}(\mathbf{x}(t),\mathbf{p})\right) = \left.\begin{pmatrix} \frac{\partial h_1}{\partial x_1} & \cdots & \frac{\partial h_1}{\partial x_M} \\ \vdots & & \vdots \\ \frac{\partial \dot{h}_R}{\partial x_1} & \cdots & \frac{\partial \dot{h}_R}{\partial x_M} \end{pmatrix}\right|_{\mathbf{x}(t),\mathbf{p}},$$

$$\mathrm{D}_{\mathbf{x}}\phi^{\tau'}(\mathbf{x}(t),\mathbf{p}) = \left.\begin{pmatrix} \frac{\partial \phi_1^{\tau'}}{\partial x_1} & \cdots & \frac{\partial \phi_1^{\tau'}}{\partial x_M} \\ \vdots & & \vdots \\ \frac{\partial \phi_D^{\tau'}}{\partial x_1} & \cdots & \frac{\partial \phi_D^{\tau'}}{\partial x_M} \end{pmatrix}\right|_{\mathbf{x}(t),\mathbf{p}},$$

$$\mathrm{D}_{\mathbf{p}}\phi^{\tau'}(\mathbf{x}(t),\mathbf{p}) = \left.\begin{pmatrix} \frac{\partial \phi_1^{\tau'}}{\partial p_1} & \cdots & \frac{\partial \phi_1^{\tau'}}{\partial p_P} \\ \vdots & & \vdots \\ \frac{\partial \phi_D^{\tau'}}{\partial p_1} & \cdots & \frac{\partial \phi_D^{\tau'}}{\partial p_P} \end{pmatrix}\right|_{\mathbf{x}(t),\mathbf{p}}, \tag{A2}$$

with $\tau' = 0, \tau, 2\tau, \ldots, (K-1)\tau$. To compute the Jacobian matrix $\mathrm{D}\mathbf{S}_{\mathbf{x},\mathbf{p}}(\mathbf{x}(t),\mathbf{p})$ (A1) of the delay coordinates map $\mathbf{S}(\mathbf{x}(t),\mathbf{p})$, we have to compute the Jacobians (A2) where $\mathrm{D}_x\phi^{\tau'}(\mathbf{x}(t),\mathbf{p})$ and $\mathrm{D}_p\phi^{\tau'}(\mathbf{x}(t),\mathbf{p})$ contain derivatives of the flow $\phi^{\tau'}$ generated by the dynamical system (1) with respect to state variables x_j and parameters p_j, respectively. The $D\times D$-matrix $\mathrm{D}_{\mathbf{x}}\phi^{\tau'}(\mathbf{x}(t),\mathbf{p})$ can be computed by solving the linearized dynamical equations in terms of a matrix ODE

$$\frac{\mathrm{d}}{\mathrm{d}\tau}\mathbf{Y}(\tau) = \mathrm{D}_{\mathbf{x}}\mathbf{F}(\phi^{\tau}(\mathbf{x}(t),\mathbf{p}),\mathbf{p})\cdot\mathbf{Y}(\tau), \tag{A3}$$

where $\phi^{\tau}(\mathbf{x}(t),\mathbf{p})$ is a solution of Eq. (1) with initial value $\mathbf{x}(t)$ and $\mathbf{Y}(\tau)$ is an $D\times D$ matrix that is initialized as $\mathbf{Y}(\tau=0) = \mathbb{1}_D$, where $\mathbb{1}_D$ denotes the $D\times D$ identity matrix. Similarly, the $D\times P$-matrix $\mathrm{D}_{\mathbf{p}}\phi^{\tau}(\mathbf{x}(t),\mathbf{p})$ is obtained as a solution of the matrix ODE[37]

$$\frac{\mathrm{d}}{\mathrm{d}\tau}\mathbf{Z}(\tau) = \mathrm{D}_{\mathbf{x}}\mathbf{F}(\phi^{\tau}(\mathbf{x}(t),\mathbf{p}),\mathbf{p})\cdot\mathbf{Z}(\tau) + \mathrm{D}_{\mathbf{p}}\mathbf{F}(\phi^{\tau}(\mathbf{x}(t),\mathbf{p}),\mathbf{p}) \tag{A4}$$

with $\mathbf{Z}(\tau=0) = 0$. $\mathrm{D}_{\mathbf{x}}\mathbf{F}(\ldots)$ and $\mathrm{D}_{\mathbf{p}}\mathbf{F}(\ldots)$ denote the Jacobians containing derivatives $\partial F_i(\ldots)/\partial x_j$ and $\partial F_i(\ldots)/\partial p_j$, respectively. Solving (A3) and (A4) simultaneously with the system ODEs (1), we can compute

$$\mathrm{D}_{\mathbf{x}}\phi^{\tau}(\mathbf{x}(t),\mathbf{p}) = \mathbf{Y}(\tau), \tag{A5}$$

$$\mathrm{D}_{\mathbf{x}}\phi^{2\tau}(\mathbf{x}(t),\mathbf{p}) = \mathbf{Y}(2\tau) \tag{A6}$$

$$\vdots$$

$$\mathrm{D}_{\mathbf{p}}\phi^{\tau}(\mathbf{x}(t),\mathbf{p}) = \mathbf{Z}(\tau), \tag{A7}$$

$$\mathrm{D}_{\mathbf{p}}\phi^{2\tau}(\mathbf{x}(t),\mathbf{p}) = \mathbf{Z}(2\tau) \tag{A8}$$

$$\vdots$$

and use these matrices to obtain the Jacobian matrix $\mathrm{D}_{\mathbf{x},\mathbf{p}}\mathbf{S}(\mathbf{x}(t),\mathbf{p})$ Eq. (A1) of the delay coordinates map $\mathbf{S}$ Eq. (6).

[1]U. Parlitz, L. Junge, and L. Kocarev, Phys. Rev. E **54**, 6253 (1996).
[2]N. Parekh, V. Ravi Kumar, and B. D. Kulkarni, Chaos **8**, 300 (1998).
[3]L. Junge and U. Parlitz, Phys. Rev. E **61**, 3736 (2000).
[4]I. G. Szendro, M. A. Rodrguez, and J. M. Lpez, J. Geophys. Res. **114**, D20109, doi:10.1029/2009JD012411 (2009).
[5]D. Rey, M. Eldridge, M. M. Kostuk, H. D. I. Abarbanel, J. Schumann-Bischoff, and U. Parlitz, Phys. Lett. A **378**, 869 (2014).
[6]D. R. Creveling, P. E. Gill, and H. D. I. Abarbanel, Phys. Lett. A **372**, 2640 (2008).
[7]J. Bröcker, Q. J. R. Meteorolog. Soc. **136**, 1906–1919 (2010).
[8]J. Schumann-Bischoff and U. Parlitz, Phys. Rev. E **84**, 056214 (2011).
[9]J. Schumann-Bischoff, S. Luther, and U. Parlitz, Commun. Nonlinear Sci. Numer. Simul. **18**, 2733 (2013).
[10]H. U. Voss, J. Timmer, and J. Kurths, Int. J. Bifurcation Chaos **14**, 1905 (2004).
[11]H. D. I. Abarbanel, D. R. Creveling, R. Farsian, and M. Kostuk, SIAM J. Appl. Dyn. Syst. **8**, 1341 (2009).
[12]J. C. Quinn and H. D. Abarbanel, Q. J. R. Meteorolog. Soc. **136**, 1855–1867 (2010).
[13]H. Abarbanel, *Predicting the Future: Completing Models of Observed Complex Systems* (Springer Publishing Company, Incorporated, 2013).
[14]J. Ye, N. Kadakia, P. Rozdeba, H. Abarbanel, and J. Quinn, Nonlinear Processes Geophys. **22**, 205 (2015).
[15]E. N. Lorenz, in *Proceedings of the Seminar on Predictability* (1996), Vol. 1.
[16]U. Parlitz, J. Schumann-Bischoff, and S. Luther, Phys. Rev. E **89**, 050902 (2014).
[17]U. Parlitz, J. Schumann-Bischoff, and S. Luther, Chaos **24**, 024411 (2014).

[18]P. J. Menck, J. Heitzig, N. Marwan, and J. Kurths, Nat. Phys. **9**, 89 (2013).
[19]M. Kostuk, "Synchronization and statistical methods for the data assimilation of HVc neuron models," Ph.D. dissertation (University of California, San Diego, 2012).
[20]K. J. H. Law, D. Sanz-Alonso, A. Shukla, and A. M. Stuart, e-print arXiv:1411.3113 [math].
[21]E. B. Lee and L. Markus, *Foundations of Optimal Control Theory* (John Wiley & Sons, 1967).
[22]R. Hermann and A. J. Krener, IEEE Trans. Autom. Control **22**, 728 (1977).
[23]H. Nijmeijer and A. v. d. Schaft, *Nonlinear Dynamical Control Systems* (Springer Science & Business Media, New York, 1990).
[24]E. D. Sontag, *Mathematical Control Theory: Deterministic Finite Dimensional Systems*, 2nd ed. (Springer, New York, 1998).
[25]C. Letellier, L. A. Aguirre, and J. Maquet, Phys. Rev. E **71**, 066213 (2005).
[26]T. Sauer, J. A. Yorke, and M. Casdagli, J. Stat. Phys. **65**(3/4), 579 (1991).
[27]G. Evensen, Mon. Weather Rev. **125**, 1342 (1997).
[28]P. J. van Leeuwen and G. Evensen, Mon. Weather Rev. **124**, 2898 (1996).
[29]G. Evensen, *Data Assimilation: The Ensemble Kalman Filter*, 2nd ed. (Springer, Dordrecht, New York, 2009).
[30]J. Bröcker and I. G. Szendro, Q. J. R. Meteorolog. Soc. **138**, 785–801 (2012).
[31]K. Levenberg, Q. Appl. Math. **2**, 164 (1944).
[32]D. W. Marquardt, J. Soc. Ind. Appl. Math. **11**, 431 (1963).
[33]M. I. A. Lourakis, in *Computer Vision ECCV* (2010), Vol. 2, pp. 43–56.
[34]A. Walther and A. Griewank, in *Combinatorial Scientific Computing*, edited by U. Naumann and O. Schenk (Chapman & Hall/CRC Computational Science Series, 2012).
[35]A. Griewank, D. Juedes, and J. Utke, ACM Trans. Math. Software **22**, 131–167 (1996).
[36]W. H. Press, S. A. Teukolsky, W. T. Vetterling, and B. P. Flannery, *Numerical Recipes: The Art of Scientific Computing*, 3rd ed. (Cambridge University Press, Cambridge, United Kingdom, 2007).
[37]H. Kawakami, IEEE Trans. Circuits Syst. **31**, 248 (1984).

8 Dependency analysis of model parameters based on delay coordinates

The following pages contain the preprint of

> J. Schumann-Bischoff, S. Luther, and U. Parlitz. "Dependency analysis of model parameters based on delay coordinates". submitted to *Phys. Rev. E* on February 29, 2016

which was submitted to Physical Review E on February 29, 2016.

The content of this manuscript was of my own conceptual design. I had the ideas to design and use the proposed methods. I planned, developed, performed, and analyzed all simulations for this manuscript. I designed and created all figures, tables, and the listings in this article. Furthermore, I wrote the text of Sec. I to Sec. IV which was then revised by the other authors. The abstract and Sec. V ('Conclusion') was written collaboratively with the other authors.

A revised version of this preprint was finally published in Ref. [57] on 28 September 2016.

Dependency analysis of model parameters based on delay coordinates

J. Schumann-Bischoff,* S. Luther,† and U. Parlitz‡
Biomedical Physics Group, Max Planck Institute for Dynamics and Self-Organization, Am Faßberg 17, 37077 Göttingen, Germany and
Institute for Nonlinear Dynamics, Georg-August-Universität Göttingen, Am Faßberg 17, 37077 Göttingen, Germany
(Dated: February 29, 2016)

In data driven system identification values of parameters and not observed variables of a given model of a dynamical system are estimated from measured time series. We address the question of observability, that is, whether unique results can be expected for the estimates or whether, for example, different combinations of parameter values would provide the same measured output. This question is answered by analysing the null space of the linearized delay coordinates map. Examples with zero dimensional, one dimensional, and two dimensional null spaces are presented employing the Hindmarsh-Rose model, the Colpitts oscillator, and the Rössler system.

I. INTRODUCTION

Computer simulations based on mathematical models are an important method for analyzing and applying dynamical systems in Physics and many other scientific fields. In many cases, models are given by a set of ordinary or partial differential equations (ODEs or PDEs) including parameters which have to be specified by suitable measurements or using estimation methods based on time series measured from the process the model aims at describing.

The latter data driven state and parameter estimation methods include synchronization and observer based methods [1–4], different types of Kalman filters [5–7], or particle filters [8, 9]. With optimization based methods [10, 11], the unknown states and parameters are estimated by minimizing a cost function (for example, by using numerical optimization or by solving the Euler-Lagrange equations [7, 12]). Its bayesian probabilistic background is described, for example, in Refs. [7, 13, 14]. In the geosciences these data assimilation methods are known as 4D-Var [15, 16],

All the above mentioned methods provide estimates for the model variables and parameters. However, it is also important to know how accurate and unique these estimates are. If there are different solutions for certain model variables and parameters which describe the measured data with a comparable accuracy, then this is a hint that the data do not contain enough information for achieving (almost) unique estimates. In many cases, it is therefore desirable to identify those quantities which cannot uniquely be estimated from the available time series, in other words, to quantify their observability [17–26]. While this task is completely solved for linear systems, it remains a challenge for nonlinear models. Therefore, in the following we shall focus on models given by nonlinear ODEs

$$\dot{\mathbf{x}}(t) = \mathbf{F}[\mathbf{x}(t), \mathbf{p}] \tag{1}$$

with the model state $\mathbf{x} = (x_1, x_2, \ldots, x_D)^{\mathrm{tr}}$ and the parameter vector $\mathbf{p} = (p_1, p_2, \ldots, p_{N_\mathrm{p}})^{\mathrm{tr}}$. Furthermore, a scalar measurement function is defined by

$$y(t) = h[\mathbf{x}(t)] \tag{2}$$

whose output signal $y(t)$ represents measured data. One way to investigate the observability is to consider derivative coordinates of $y(t)$ [21, 22] and the invertibility of the derivative coordinate map. In this article, however, we make use of time delay coordinates [27–31] of $y(t)$ and consider the K-dimensional forward delay coordinates map G,

$$\mathbf{G} : \mathbb{R}^D \times \mathbb{R}^{N_\mathrm{p}} \to \mathbb{R}^K, \quad (\mathbf{x}(t), \mathbf{p}) \mapsto \mathbf{G}[\mathbf{x}(t), \mathbf{p}] \tag{3}$$

with

$$\begin{aligned} \mathbf{g} &= \mathbf{G}[\mathbf{x}(t), \mathbf{p}] \\ &= \big[y(t),\ y(t+\tau),\ \ldots,\ y(t+(K-1)\tau)\big] \end{aligned} \tag{4}$$

where τ is the delay time. If the map $\mathbf{G}$ is locally invertible at given $\mathbf{x}$ and $\mathbf{p}$, then $\mathbf{x}$ and $\mathbf{p}$ can be uniquely reconstructed given $y(t)$ at present and delayed times. That is, $\mathbf{x}$ and $\mathbf{p}$ are *locally observable*. This is the case if the $K \times (D + N_\mathrm{p})$ Jacobian matrix $\mathrm{D}\mathbf{G} = \mathrm{D}\mathbf{G}(\mathbf{x}(t), \mathbf{p})$, computed with respect to $\mathbf{x}$ and $\mathbf{p}$, is locally invertible at $\mathbf{x}, \mathbf{p}$, i.e. has full rank.

Instead of considering the observability of the full system, here we focus on identifying the (local) observability of individual variables and parameters. If some of these unknown quantities (parameters and variables) are not locally observable, we investigate their relationships and address the question which parameters may be fixed to obtain local observability for all (remaining) quantities. The approach discussed in detail in Sec. II A is based on investigating the null space of the Jacobian matrix $\mathrm{D}\mathbf{G}$ of the map $\mathbf{G}$. Not observable quantities and their relationships are identified by a suitable choice of the basis of the null space using methods adopted from Ref. [32].

* Jan.Schumann-Bischoff@ds.mpg.de
† Stefan.Luther@ds.mpg.de
‡ Ulrich.Parlitz@ds.mpg.de

In Refs. [33, 34] it is investigated how small perturbations of the delay reconstruction vector $\mathbf{g}$ are mapped to small perturbations in the state and parameter space. This approach is extended in Sec. II B to find out how the unknown quantities are locally correlated.

In Sec. III the optimization based (weak-4D-Var type) state and parameter estimation algorithm from Refs. [35, 36] is revisited. This estimation method is then used in the subsequent examples to evaluate the results obtained by the application of the previously suggested analyses. In particular, we make use of the concept of a profile likelihood [37, 38], where one model parameter is manually tuned and all others are estimated (beside the model variables) by minimizing a cost function.

Three examples, the Colpitts oscillator [39], the Rössler model [40–42], and the Hindmarsh-Rose neuron model [43], are discussed in Sec. IV. In Refs. [41, 42], based on derivative coordinates, an algebraic method was presented which can be used to find functional relationships between model parameters of polynomial models (right hand side of Eq. (1) is a polynomial vector field) so that the measured variable (and its higher order time derivatives) remains unchanged. We demonstrate for the Rössler model that our (more general) approach for identifying not observable variables and parameters and their relations provides the same results as the method presented in Refs. [41, 42].

II. THEORY

We investigate the local observability of model variables and parameters of a model, Eq. (1), with a scalar measurement function, Eq. (2), by means of a delay reconstruction map, Eq. (4).

Following the approach presented in Refs. [33, 34] we consider how small perturbations of the reconstructed state $\mathbf{g}$ are related to variations of the state vector $\mathbf{x}$ and the parameters $\mathbf{p}$. In principle the approach can be easily extended to multivariate measurement functions [44]. To simplify the discussion we introduce a vector of all $N_\mathrm{w} = D + N_\mathrm{p}$ unknowns $\mathbf{w} = (w_1, w_2, \ldots, w_{N_\mathrm{w}})^{tr} = (\mathbf{x}, \mathbf{p})^\mathrm{tr} \in \mathbb{R}^{N_\mathrm{w}}$. If perturbations $\Delta\mathbf{g} = \tilde{\mathbf{g}} - \mathbf{g}$ are (infinitesimally) small, then the unknowns $\mathbf{w} = \mathbf{G}^{-1}(\mathbf{g})$ and the perturbed unknowns $\tilde{\mathbf{w}} = \mathbf{G}^{-1}(\tilde{\mathbf{g}})$ can be used in the linearization

$$\mathbf{G}^{-1}(\tilde{\mathbf{g}}) = \mathbf{G}^{-1}(\mathbf{g}) + \mathrm{D}\mathbf{G}^{-1}(\tilde{\mathbf{g}} - \mathbf{g}) \tag{5}$$

$$\Rightarrow \tilde{\mathbf{w}} - \mathbf{w} = \mathrm{D}\mathbf{G}^{-1}(\tilde{\mathbf{g}} - \mathbf{g}) \tag{6}$$

to compute the (resulting) perturbation of unknown quantities

$$\Delta\mathbf{w} = \tilde{\mathbf{w}} - \mathbf{w} = \mathrm{D}\mathbf{G}^{-1}\Delta\mathbf{g} \tag{7}$$

with $\Delta\mathbf{w} = (\Delta w_1, \Delta w_2, \ldots, \Delta w_{N_\mathrm{w}})$. The Jacobian $\mathrm{D}\mathbf{G}^{-1}$ is the (pseudo) inverse of $\mathrm{D}\mathbf{G}(\mathbf{w}) = \mathrm{D}\mathbf{G}(\mathbf{x}, \mathbf{p})$. $\mathrm{D}\mathbf{G}^{-1}$ can be computed by inversion of its singular value decomposition[32, 45] (SVD)

$$\mathrm{D}\mathbf{G} = \mathbf{U}\mathbf{S}\mathbf{V}^\mathrm{tr} \tag{8}$$

where the $K \times N_\mathrm{w}$ matrix $\mathbf{U}$ and the $N_\mathrm{w} \times N_\mathrm{w}$ matrix $\mathbf{V}$ are column orthogonal, i.e. $\mathbf{U}^\mathrm{tr} = \mathbf{U}^{-1}$ and $\mathbf{V}^\mathrm{tr} = \mathbf{V}^{-1}$. The elements of the $N_\mathrm{w} \times N_\mathrm{w}$ diagonal matrix

$$\mathbf{S} = \mathrm{diag}(\sigma_1, \sigma_2, \ldots, \sigma_{N_\mathrm{w}}) \tag{9}$$

are the singular values $\sigma_1 \geq \sigma_2 \geq \cdots \geq \sigma_{N_\mathrm{w}} \geq 0$ and the pseudo inverse of $\mathrm{D}\mathbf{G}$ is given by

$$\mathrm{D}\mathbf{G}^{-1} = \mathbf{V}\mathbf{S}^{-1}\mathbf{U}^\mathrm{tr} \ . \tag{10}$$

A. Dependency analysis of variables and parameters

The Jacobian matrix $\mathrm{D}\mathbf{G}$ contains information about the local observability of variables and parameters. To obtain these information we rewrite Eq. (7) as

$$\mathrm{D}\mathbf{G}\Delta\mathbf{w} = \Delta\mathbf{g} \ . \tag{11}$$

If there exists a $\Delta\mathbf{w} \neq 0$ for which it is $\Delta\mathbf{g} = 0$, then we know that there exist perturbations of $\mathbf{w}$ which do not lead to perturbations of $\mathbf{g}$, that is they do not affect the output signal $y(t)$. Since they have no impact on the measured signal, the values of all quantities w_i which are involved in such perturbations cannot be uniquely estimated from a y time series. To identify non observable quantities we therefore want to find out whether any $\Delta\mathbf{w} \neq 0$ exists which fulfills

$$\mathrm{D}\mathbf{G}\Delta\mathbf{w} = 0 \ , \tag{12}$$

that is, we want to compute the null space (or kernel) null($\mathrm{D}\mathbf{G}$) of the matrix $\mathrm{D}\mathbf{G}$. If the dimension of null($\mathrm{D}\mathbf{G}$), the nullity, is $D_\mathrm{N} = 0$ then the null space only contains the null vector and we know that any small variation of $\mathbf{w}$ leads to a perturbation of $\mathbf{g}$ and, hence, all quantities in $\mathbf{w}$ are locally observable. If $D_\mathrm{N} > 0$, then certain elements w_i of $\mathbf{w}$ can be varied by $\Delta w_i \neq 0$ *without* a perturbation of $\mathbf{g}$ (i.e., with $\Delta\mathbf{g} = 0$). Therefore, these quantities w_i are not locally observable and in the following they are also called *locally redundant*. Its associated columns $\mathrm{D}\mathbf{G}^{(i)}$ of $\mathrm{D}\mathbf{G}$ are linear dependent, as one can see when expanding Eq. (12) to

$$\mathrm{D}\mathbf{G}^{(1)}\Delta w_1 + \cdots + \mathrm{D}\mathbf{G}^{(N_\mathrm{w})}\Delta w_{N_\mathrm{w}} = 0 \ . \tag{13}$$

To investigate the null space we exploit the SVD [32, 45] of $\mathrm{D}\mathbf{G}$, Eq. (8). The nullity is given by the number of vanishing singular values ($\sigma_i = 0$). In cases where $D_\mathrm{N} > 0$ the null space of $\mathrm{D}\mathbf{G}$ can be spanned by D_N basis vectors. For ordered singular values $\sigma_1 \geq \sigma_2 \geq \cdots \geq \sigma_{N_\mathrm{w}-D_\mathrm{N}+1} = \cdots = \sigma_{N_\mathrm{w}} = 0$ a set of D_N orthogonal basis vectors $\mathbf{v}_\mathrm{B}^{(i)}$, $i = 1, \ldots, D_\mathrm{N}$, of null($\mathrm{D}\mathbf{G}$) is given by the last D_N columns of $\mathbf{V}$. Therefore, we introduce

a $N_\mathrm{w} \times D_\mathrm{N}$ basis matrix $\mathbf{V}_\mathrm{B} = \left[\mathbf{v}_\mathrm{B}^{(1)}, \ldots, \mathbf{v}_\mathrm{B}^{(D_\mathrm{N})}\right]$ whose columns are the last D_N columns of $\mathbf{V}$. If the ith components of all D_N basis vectors are zero, that is the ith row of $\mathbf{V}_\mathrm{B}$ contains zeros only, then the ith component w_i of $\mathbf{w}$ can be uniquely reconstructed given $\mathbf{g}$ and hence the corresponding variable or parameter is considered as locally observable.

1. *Making the system locally observable*

In the case when locally not observable variables and parameters were identified, the question arises which of them may be removed from the analysis or the estimation problem so that, as a result, all remaining quantities are locally observable. We address this issue by considering the situation for a one and a multi-dimensional null space separately.

If the null space of $\mathrm{D}\mathbf{G}$ is $D_\mathrm{N} = 1$ dimensional only and, hence, can be spanned by the basis vector $\mathbf{v}_\mathrm{B}$ (last column of $\mathbf{V}$), then it contains any variation

$$\Delta\mathbf{w} = a \cdot \mathbf{v}_\mathrm{B} \ , \tag{14}$$

where $a \in \mathbb{R}$. Let us consider the *patterns of zero and non-zero elements* of $\mathbf{v}_\mathrm{B}$ and assume that the ith component of $\mathbf{v}_\mathrm{B}$ is, among possibly other components, non zero. In other words, w_i is locally not observable. Fixing w_i by prohibiting its variation via $\Delta w_i = 0$, for example by setting w_i to a fixed value instead of estimating it in an estimation problem, immediately sets $a = 0$. Therefore, variations of all other quantities are also prohibited because of $\Delta\mathbf{w} = 0$. Setting w_i to a fixed value makes all other quantities locally observable.

Next, we consider the situation where the null space of $\mathrm{D}\mathbf{G}$ is $D_\mathrm{N} > 1$ dimensional. That means, at least D_N quantities have to be fixed by prohibiting their variation to make all quantities locally observable. The variation within the null space can be expressed by means of the basis vectors $\mathbf{v}_\mathrm{B}^{(i)}$ constituting the basis matrix $\mathbf{V}_\mathrm{B}$ (obtained via SVD, see Sec. II A), and the real coefficients $\mathbf{a} = (a_1, \ldots, a_{D+N_\mathrm{p}})^{tr}$ by

$$\begin{aligned} \Delta\mathbf{w} &= a_1\mathbf{v}_\mathrm{B}^{(1)} + \cdots + a_{D_\mathrm{N}}\mathbf{v}_\mathrm{B}^{(D_\mathrm{N})} && (15)\\ &= \mathbf{V}_\mathrm{B}\mathbf{a} \ . && (16) \end{aligned}$$

The question is now which quantities are to fix so that as a result $a_i = 0$ for all i, and with that $\Delta\mathbf{w} = 0$ and all remaining quantities are made locally observable.

The approach to identify a set of suitable quantities to be fixed is based on the patterns of zero and non-zero elements of basis vectors. This has the advantage that in practice these patterns can be easily read off from distributions of components of basis vectors computed based on SVDs of Jacobian matrices at different state vectors. In numerical simulations we observed that usually all basis vectors obtained via SVD have the same patterns of zero and non-zero elements. Based on these patterns, however, we can not easily read off which quantities to fix for obtaining local observability for all quantities. For that reason, based on the basis provided by the SVD,we want to find a new basis of the null space where all basis vectors have different patterns of zero and non-zero elements. We follow the approach from Ref. [32] of finding linear dependent columns of a matrix. Based on $\mathbf{V}_\mathrm{B}$ we have

$$\mathrm{D}\mathbf{G} \cdot \mathbf{V}_\mathrm{B} = 0 \ . \tag{17}$$

First, we choose D_N quantities and define the quadratic $D_\mathrm{N} \times D_\mathrm{N}$ matrix $\mathbf{V}_{\mathrm{B},1}$ to contain the D_N rows of $\mathbf{V}_\mathrm{B}$ which are associated with these quantities, with the restriction that $\mathbf{V}_{\mathrm{B},1}$ is nonsingular. From this it follows that the nullity of $\mathbf{V}_{\mathrm{B},1}$ is zero. Prohibiting the variations of the chosen quantities w_i via $\Delta w_i = 0$ immediately sets all coefficients $a_j = 0$ which makes every quantity locally observable and, therefore, is already an answers to the question which quantities to fix. Nevertheless, the new basis to construct also allows to read off which other quantities may be fixed instead to obtain local observability.

One possible strategy to choose D_N quantities is to try different sets of chosen quantities, compute the singular values of $\mathbf{V}_{\mathrm{B},1}$, and chose the combination with the largest ratio $\sigma_\mathrm{min}/\sigma_\mathrm{max}$. $\mathbf{V}_{\mathrm{B},2}$ contains all rows of $\mathbf{V}_\mathrm{B}$ not contained in $\mathbf{V}_{\mathrm{B},1}$. Similarly, we define $\mathrm{D}\mathbf{G}_1$ which contains the D_N columns of $\mathrm{D}\mathbf{G}$ which are associated with the chosen quantities. $\mathrm{D}\mathbf{G}_2$ contains all remaining columns of $\mathrm{D}\mathbf{G}$. Next, as suggested in Ref. [32], we rewrite Eq. (17) to

$$\begin{aligned} \begin{bmatrix}\mathrm{D}\mathbf{G}_1 & \mathrm{D}\mathbf{G}_2\end{bmatrix} \begin{bmatrix}\mathbf{V}_{\mathrm{B},1}\\ \mathbf{V}_{\mathrm{B},2}\end{bmatrix} &= \mathrm{D}\mathbf{G}_1 \cdot \mathbf{V}_{\mathrm{B},1} + \mathrm{D}\mathbf{G}_2 \cdot \mathbf{V}_{\mathrm{B},2}\\ &= 0 \ , \end{aligned} \tag{18}$$

multiply with $\mathbf{V}_{\mathrm{B},1}^{-1}$ from the right, and obtain

$$\begin{aligned} &\mathrm{D}\mathbf{G}_1 \cdot \mathbb{1}(D_\mathrm{N}) + \mathrm{D}\mathbf{G}_2 \cdot \mathbf{V}_{\mathrm{B},2}\mathbf{V}_{\mathrm{B},1}^{-1}\\ &= \begin{bmatrix}\mathrm{D}\mathbf{G}_1 & \mathrm{D}\mathbf{G}_2\end{bmatrix} \underbrace{\begin{bmatrix}\mathbb{1}(D_\mathrm{N})\\ \mathbf{V}_{\mathrm{B},2}\mathbf{V}_{\mathrm{B},1}^{-1}\end{bmatrix}}_{\widetilde{\mathbf{V}}'_\mathrm{B}} = 0 \ , \end{aligned} \tag{19}$$

where $\mathbb{1}(D_\mathrm{N})$ is the $D_\mathrm{N} \times D_\mathrm{N}$ identity matrix. Now, we reorder the columns of $\begin{bmatrix}\mathrm{D}\mathbf{G}_1 & \mathrm{D}\mathbf{G}_2\end{bmatrix}$ to obtain $\mathrm{D}\mathbf{G}$ again. If we apply the same reordering to the rows of $\widetilde{\mathbf{V}}'_\mathrm{B}$, then we obtain the $N_\mathrm{w} \times D_\mathrm{N}$ matrix $\widetilde{\mathbf{V}}_\mathrm{B}$ and therefore the newly ordered version of Eq. (19) is

$$\mathrm{D}\mathbf{G} \cdot \widetilde{\mathbf{V}}_\mathrm{B} = 0 \ . \tag{20}$$

Due to the identity matrix in $\widetilde{\mathbf{V}}'_\mathrm{B}$ the columns of $\widetilde{\mathbf{V}}'_\mathrm{B}$, and hence the columns of $\widetilde{\mathbf{V}}_\mathrm{B}$, are linearly independent. Since the number of columns of $\widetilde{\mathbf{V}}_\mathrm{B}$, D_N, is equal to the dimension of the null space of $\mathrm{D}\mathbf{G}$, the columns of

$\widetilde{\mathbf{V}}_\mathrm{B} = \left[\widetilde{\mathbf{v}}_\mathrm{B}^{(1)}, \ldots, \widetilde{\mathbf{v}}_\mathrm{B}^{(D_\mathrm{N})}\right]$ form another basis (beside the orthogonal basis $\mathbf{V}_\mathrm{B}$) of the null space of D$\mathbf{G}$. Furthermore, all basis vectors have a mutually different pattern of non-zero elements. Every variation of $\mathbf{w}$ within the null space of D$\mathbf{G}$ can then be expressed in terms of the new basis vectors with the real coefficients $\widetilde{a}_i$,

$$\Delta\mathbf{w} = \widetilde{a}_1\widetilde{\mathbf{v}}_\mathrm{B}^{(1)} + \cdots + \widetilde{a}_{D_\mathrm{N}}\widetilde{\mathbf{v}}_\mathrm{B}^{(D_\mathrm{N})} \ . \tag{21}$$

2. *Local relationships*

To reveal some local relationships between quantities we consider variations along each basis vector $\widetilde{\mathbf{v}}_\mathrm{B}^{(i)} = \left[\widetilde{v}_{\mathrm{B},1}^{(i)}, \ldots, \widetilde{v}_{\mathrm{B},D_\mathrm{N}}^{(i)}\right]^\mathrm{tr}$. In the case of a one dimensional null space it is $\widetilde{\mathbf{v}}_\mathrm{B}^{(i)} = \mathbf{v}_\mathrm{B}$, see Eq. (14). For that we assume that $\widetilde{a}_j = 0$, $i \neq j$, in Eq. (21) and obtain for variations along $\widetilde{\mathbf{v}}_\mathrm{B}^{(i)}$ and within the null space of D$\mathbf{G}$

$$\Delta\mathbf{w}^{(i)} = \widetilde{a}_i\widetilde{\mathbf{v}}_\mathrm{B}^{(i)} \ . \tag{22}$$

This illustrates that simultaneous variations of all quantities w_k, where the corresponding components $v_{\mathrm{B},k}^{(i)}$ are non-zero, are possible without affecting the output of the system at present and delayed times, $\Delta\mathbf{g} = 0$. All other quantities are kept unchanged. That indicates a local dependency between these quantities. A *set of locally dependent quantities* exists for every basis vector and contains all quantities where the corresponding component of the basis vector is non-zero. Note, that such a set is not unique because the patterns of non-zero elements of $\widetilde{\mathbf{v}}_\mathrm{B}^{(i)}$ depend of the choice of quantities to construct $\mathbf{V}_{\mathrm{B},1}$.

Furthermore, to investigate how quantities w_j and w_k locally depend on each other (still assuming variations along $\widetilde{\mathbf{v}}_\mathrm{B}^{(i)}$ only), dividing the jth row of Eq. (22) by the kth row, we consider

$$\Delta w_j^{(i)} = \frac{\widetilde{v}_{\mathrm{B},j}^{(i)}}{\widetilde{v}_{\mathrm{B},k}^{(i)}}\Delta w_k^{(i)} \ . \tag{23}$$

Whether an increase of w_k leads to an increase or a decrease of w_j depends on the signs of the components of the basis vectors. It should be noted, that computing Eq. (23) based on another basis vector than $\widetilde{\mathbf{v}}_\mathrm{B}^{(i)}$ may lead to a different dependency, but that would not be a contradiction.

B. Correlation analysis

In Sec. II A we described a way to detect locally dependent quantities (variables and parameters) by investigating the null space of D$\mathbf{G}$ for cases where the null space is one- or higher dimensional. There, no assumptions were made about the distribution of perturbations $\Delta\mathbf{g}$ in Eq. (11). Here, we follow Refs. [33, 34] and make the assumption that the perturbations $\Delta\mathbf{g}$ are normally distributed with a covariance matrix $\mathbf{\Sigma}_\mathrm{g}$ and a mean of zero,

$$\Delta\mathbf{g} \sim \mathcal{N}(0, \mathbf{\Sigma}_\mathrm{g}) \ . \tag{24}$$

Since $\Delta\mathbf{g}$ is locally mapped to $\Delta\mathbf{w}$ via the linear function Eq. (7), $\Delta\mathbf{w}$ is also normally distributed [13, theorem 2.11] with a mean of zero and a covariance matrix $\mathbf{\Sigma}_\mathrm{w}$,

$$\Delta\mathbf{w} \sim \mathcal{N}(0, \mathbf{\Sigma}_\mathrm{w}) \ . \tag{25}$$

where the covariance matrix is given by [13, theorem 2.11]

$$\mathbf{\Sigma}_\mathrm{w} = \mathrm{D}\mathbf{G}^{-1}\mathbf{\Sigma}_\mathrm{g}\left[\mathrm{D}\mathbf{G}^{-1}\right]^\mathrm{tr} \ . \tag{26}$$

Furthermore, the perturbed state $\tilde{\mathbf{w}}$, see Eq. (7), is also normally distributed [13, theorem 2.11],

$$\tilde{\mathbf{w}} \sim \mathcal{N}(\mathbf{w}, \mathbf{\Sigma}_\mathrm{w}) \ , \tag{27}$$

and has the same covariance matrix.

In Refs. [33, 34] it was assumed that the perturbations of the delay reconstruction vector $\mathbf{g}$ are uncorrelated and have the same strength ζ^2 (a typical assumption for measurement noise). That is, its covariance matrix is diagonal, $\mathbf{\Sigma}_\mathrm{g} = \zeta^2 \cdot \mathbb{1}$, where $\mathbb{1}$ denotes the unity matrix. The standard deviation of single parameters or variables is given by the diagonal elements of

$$\sqrt{\mathbf{\Sigma}_\mathrm{w}} = \zeta\sqrt{\mathrm{D}\mathbf{G}^{-1}\left[\mathrm{D}\mathbf{G}^{-1}\right]^\mathrm{tr}} \tag{28}$$

$$= \zeta\sqrt{\left[\mathbf{V}\mathbf{S}^{-2}\mathbf{V}^\mathrm{tr}\right]} \ , \tag{29}$$

where the square roots are meant to be computed component-wise. Since ζ is a factor only, we set $\zeta = 1$ and have defined the *measure of uncertainty* [33, 34] for w_k

$$\nu_k = \nu(w_k) = \sqrt{\left[\mathbf{V}\mathbf{S}^{-2}\mathbf{V}^\mathrm{tr}\right]_{kk}} \ . \tag{30}$$

The larger ν_k is, the larger is the uncertainty when estimating w_k and the worse w_k can be estimated.

In contrast to Refs. [33, 34], we now consider the non-diagonal elements to investigate the correlation between two different quantities. This is done by considering the $N_\mathrm{w} \times N_\mathrm{w}$ *linear Pearson's correlation matrix* $\boldsymbol{\rho}$ consisting of the correlation coefficients

$$\rho_{ij} = \rho(w_i, w_j) = \frac{\Sigma_{\mathrm{w},ij}}{\sqrt{\mathrm{var}(w_i)}\sqrt{\mathrm{var}(w_j)}} \in [-1, 1] \tag{31}$$

and containing the variances $\mathrm{var}(w_k) = \Sigma_{\mathrm{w},kk}$. Since $\mathbf{\Sigma}_\mathrm{w}$ is the covariance matrix of both, $\Delta\mathbf{w}$ and $\tilde{\mathbf{w}}$, their correlation matrix $\boldsymbol{\rho}$ is also equal. For the diagonal elements holds $\rho_{kk} = 1$. Now, let us consider the following cases:

$\rho_{ij} = \pm 1$**:** There is a perfect positive ($\Delta w_i > 0 \Rightarrow \Delta w_j > 0$) or negative ($\Delta w_i > 0 \Rightarrow \Delta w_j < 0$) correlation between both perturbations. In this case there is a locally linear relationship between both quantities.

$\rho_{ij} = 0$**:** Since $\Delta\mathbf{w}$ and $\tilde{\mathbf{w}}$ are normally distributed, this implies that Δw_i and Δw_j as well as $\tilde{w}_i$ and $\tilde{w}_j$ are statistically independent.

$0 < |\rho_{ij}| < 1$**:** The larger $|\rho_{ij}|$ is, the stronger is the correlation between Δw_i and Δw_j

To analyze the correlations between quantities, one can compute $\boldsymbol{\rho}$ for different states and generate histograms showing the distributions of the correlation coefficients ρ_{ij}. If, for example, $\rho_{ij} \approx -1$ for most of the analyzed states, then this is a hint that it is difficult to estimate quantity w_i and w_j simultaneously when performing state and parameter estimation. One can expect, if quantity w_i is estimated to a too large value, that the estimated value of quantity w_j is too small.

It is known, see Ref. [32], that a large correlation coefficient $|\rho_{ij}| \approx 1$ implies an (almost) linear relationship between Δw_i and Δw_j, but a linear dependency between more than two perturbations does not necessarily lead to a correlation coefficient $|\rho_{ij}| \approx 1$. Therefore, we suggest to apply the dependency analysis from Sec. II A 2 first to detect locally dependent quantities and quantities which are in principle locally observable. If D$\mathbf{G}$ is non singular ($D_{\mathrm{N}} = 0$), or if one fixes quantities in the analysis until every variation $\Delta\mathbf{w} \neq 0$ leads to $\Delta\mathbf{g} \neq 0$, then we suggest to apply the correlation analysis.

However, even in the case of a non-singular D$\mathbf{G}$ a weak dependency might not be revealed by the correlation analysis [32]. Another way to quantify weak dependencies is the collinearity diagnostics suggested in Ref. [32].

III. STATE AND PARAMETER ESTIMATION ALGORITHM

The task of state and parameter estimation is to find a trajectory for the model variables $\{\mathbf{x}(n)\}$, $\mathbf{x}(n) = \mathbf{x}(t_n) \in \mathbb{R}^D$ with $t_n = n \cdot \Delta t$ and $n = 0, \ldots, N-1$ and a vector of model parameters in such a way that the trajectory fits an (here: univariate) experimental data time series $\{\eta(n)\}$, $\eta(n) = \eta(t_n) \in \mathbb{R}$ with $t_n = n \cdot \Delta t$ and $n = 0, \ldots, N-1$, (via a measurement function Eq. (2)) on the one hand, and fulfills the model equations on the other hand. The approach chosen here [35, 36] is similar to weak constraint 4D-VAR [7, 10, 13, 46, 47] and is based on minimizing a cost function. Here, models in form of ODE Eq. (1) are used. Approximating the time derivative by a finite difference $\Delta\mathbf{x}(n)/\Delta t$ and introducing an error term $\mathbf{u}(n) = \mathbf{u}(t_n)$ in the model, the discretized equations read

$$\frac{\Delta\mathbf{x}(n)}{\Delta t} = F[\mathbf{x}(n), \mathbf{p}] + \mathbf{u}(n) \ . \tag{32}$$

To estimate a trajectory $\{\mathbf{x}(n)\}$ and model parameters $\mathbf{p}$ the cost function

$$\begin{aligned} C\left(\{\mathbf{x}(n)\}, \mathbf{p}\right) = \sum_{n=0}^{N} \Big\{ & \frac{\alpha}{N}[\eta(n) - h(\mathbf{x}(n))]^2 \\ & + \frac{\alpha - 1}{ND}\mathbf{u}(n)^{\mathrm{tr}}\mathbf{B}\mathbf{u}(n) \Big\} + C_3 + C_4 \end{aligned} \tag{33}$$

has to be minimized with respect to the entire trajectory $\{\mathbf{x}(n)\}$ and the parameters $\mathbf{p}$. The trajectory and parameters which minimize $C(\{\mathbf{x}(n)\}, \mathbf{p})$ are then considered as the solution of the estimation problem. To estimate a smooth trajectory, a Hermite interpolation is performed by the additional sum C_3 and to force variables and parameters to stay in predefined boundaries the sum C_4 is required. Both term are described more detailed in Ref. [35, 36]. Furthermore, a homotopy parameter $\alpha \in (0, 1)$ is used to cope with local minima in the cost function[12]. If $\alpha \approx 1$, the estimated trajectory is very close to the data (large modeling errors $\mathbf{u}(n)$ are allowed), and if $\alpha \approx 0$, the estimated trajectory fulfills the model equations very well, but might not match the data. Additionally, a matrix $\mathbf{B}$ is introduced for an individual weighting of the error $\mathbf{u}(n)$. In the weak constraint 4D-Var formulation $\mathbf{B}$ is the inverse covariance matrix of the modeling error $\mathbf{u}(n)$. For optimization the Levenberg-Marquard [48–50] algorithm is used, where derivatives and sparsity structures are computed by means of the automatic differentiation software ADOL-C [51–53].

IV. EXAMPLES

The aim of the examples is to demonstrate how the dependency and correlation analysis of model states and parameters discussed in Secs. II A and II B can be applied.

In case of the Colpitts oscillator (Sec. IV A) the null space of D$\mathbf{G}$, Eq. (11), is one dimensional and both, the dependency and correlation analysis is applied. The results are then compared to results obtained by applying the state and parameter estimation algorithm from Sec. III.

In Sec. IV B the dependency analysis from Sec. II A is applied to the Rössler model. A two dimensional null space of D$\mathbf{G}$ was found. Furthermore, it is demonstrated how sets of dependent variables and parameters can be found. These results are then compared to results presented in Ref. [42] where relationships between model parameters were identified in polynomial vector fields.

In the third example the Hindmarsh-Rose model is studied. It was found that the null space of D$\mathbf{G}$ is zero dimensional. In theory, this means that all variables and parameters should be observable. Applying the correlation analysis from Sec. II B, however, shows that there is still a strong correlation between certain model parameters. This correlation was also observed when the

state and parameter estimation algorithm from Sec. III is applied.

A. Colpitts oscillator

In this section we use the model of the chaotic Colpitts oscillator[39] to investigate local dependencies of model parameters and variables. The system is given by the model equations

$$\begin{aligned} \dot{x}_1 &= p_1 x_2 \\ \dot{x}_2 &= -p_2(x_1 + x_3) - p_3 x_2 \\ \dot{x}_3 &= p_4 \left(x_2 + 1 - e^{-x_1}\right) \end{aligned} \tag{34}$$

with the parameters $\mathbf{p} = (5, 0.08, 0.7, 6.3)$ (equations and parameter values are taken from Ref. [54]) and the measurement function

$$h(\mathbf{x}) = x_1 \ . \tag{35}$$

To generate states for the analysis the model Eq. (34) is integrated 10^6 steps with a step size of 0.1 (no transient included) using the parameters $\mathbf{p} = (5, 0.08, 0.7, 6.3)$. Then, every 100th point from the trajectory is used for the analysis resulting in 10^4 points. The dimension of the delay coordinate vector, Eq. (4), is set to $K = 10$.

First, we compute histograms for the singular values σ_i, $i = 1, \ldots, 7$ of D$\mathbf{G}$, Eq. (9), including all four model parameters in the analysis, see Fig. 1. The histograms are computed in the following way: (i) The delay time τ is set to the smallest considered value $\tau = 0.1$. (ii) Then, all normalized singular values σ_i/σ_1 ($i = 1, \ldots, 7$) are computed for each of the 10^4 different states on the attractor using the fixed τ. (iii) A histogram for each σ_i/σ_1 is computed and plotted vertically (color coded) in the corresponding subplot. (iv) This process is repeated with a slightly increased τ. We can see that for all investigated states and independent on τ only the smallest normalized singular values σ_7/σ_1 are very close to zero. This indicates a one dimensional null space ($D_\mathrm{N} = 1$) of D$\mathbf{G}$ and means that there exist $\Delta\mathbf{w} \neq 0$ with $\Delta\mathbf{g} = 0$, see Eq. (11) and Eq. (12). Therefore, some of the model variables or parameters are locally not observable because its variation does lead to a perturbation $\Delta\mathbf{g} \neq 0$ of the measured signal $y(t)$ at present time t and delayed times.

Since $D_\mathrm{N} = 1$, the last column of $\mathbf{V}$ (see Eq. (8)), $\mathbf{v}_\mathrm{B} = \mathbf{v}^{(7)}$, is a basis vector of the null space of D$\mathbf{G}$ (see Sec. II A). To simplify the association of the components of $\mathbf{v}_\mathrm{B}$, the associated variable or parameter is mentioned in brackets. Since both $\mathbf{v}_\mathrm{B}$ and $-\mathbf{v}_\mathrm{B}$ are valid basis vectors (and both variants may be obtained by the SVD of D$\mathbf{G}$), $\mathbf{v}_\mathrm{B}$ is normalized by the sign of the component $v_\mathrm{B}(p_4)$, $\mathbf{v}_\mathrm{B} \to \mathrm{sign}(v_\mathrm{B}(p_4)) \cdot \mathbf{v}_\mathrm{B}$.

To check whether some variables or parameters are locally observable, we consider histograms of the components of $\mathbf{v}_\mathrm{B}$, $v_\mathrm{B}(w_i)$, for the same 10^4 states and delay times τ used previously, see Fig. 2. Only $|v_\mathrm{B}(x_1)| < 10^{-10}$ and $|v_\mathrm{B}(p_3)| < 10^{-10}$ are close to zero for all 10^4 states and all considered τ. This means that it is (almost) impossible to vary x_1 and p_3 without changing $\mathbf{g}$. Hence, x_1 and p_3 are as locally observable. All other quantities are locally redundant.

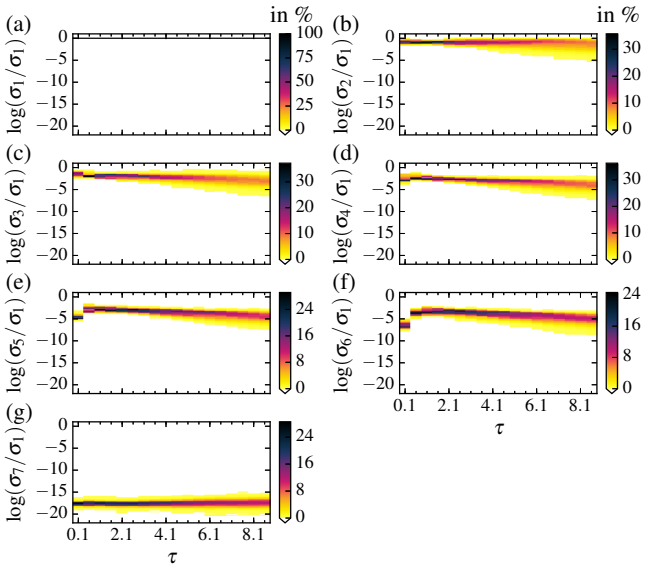

Figure 1. Histograms (color coded) of the normalized singular values σ_i/σ_1, Eq. (9), (computed with delay reconstruction dimension $K = 10$) of D$\mathbf{G}$ computed with respect to all variables ($D = 3$) and parameters ($N_\mathrm{p} = 4$) of the Colpitts oscillator, Eq. (34), where x_1 is assumed to be measured, Eq. (35). For each τ the singular values σ_i are computed for 10^4 points on the attractor using $\mathbf{p} = (5, 0.08, 0.7, 6.3)$. The smallest normalized singular values σ_7/σ_1 is of magnitude smaller than 10^{-15} for (almost) all states and τ and, hence, is numerically very close to zero indicating a one dimensional null space of D$\mathbf{G}$, Eq. (11).

Local variations of the redundant quantities keeping $\mathbf{g}$ unchanged are only simultaneously possible, see Eq. (14). To find out how these quantities pairwise depend on each other, see Eq. (23), we consider the ratio of the signs of $v_\mathrm{B}(w_i)$ read off from Fig. 2. The histograms associated with the model parameters show that there the signs of $v_\mathrm{B}(w_i)$ are independent on the state and the delay time τ. According to Eq. (23) we see that, (i) a positive variation of p_4, $\Delta p_4 > 0$, leads to a negative variation of p_1 and p_2, $\Delta p_1, \Delta p_2 < 0$, because of $v_\mathrm{B}(p_4)/v_\mathrm{B}(p_1) < 0$ and $v_\mathrm{B}(p_4)/v_\mathrm{B}(p_2) < 0$ and vice versa. (ii) A variation $\Delta p_4 \neq 0$ leads to no change of p_3.

To confirm that only x_1 and p_3 are locally observable, the measure of uncertainty $\nu(w_i)$, Eq. (30), was computed for the same 10^4 points from the attractor and delay times τ as previously with $K = 10$. First, $\nu(w_i)$ was computed including all four model parameters in the analysis. Histograms for all $\nu(w_i)$ are shown in Fig. 3.

One can see that on average $\nu(w_i)$ is very large (magnitude 10^{10} to 10^{15}) for all i, except $\nu(x_1)$ and $\nu(p_3)$. This indicates a high uncertainty for x_2, x_3, p_1, p_2, and p_4.

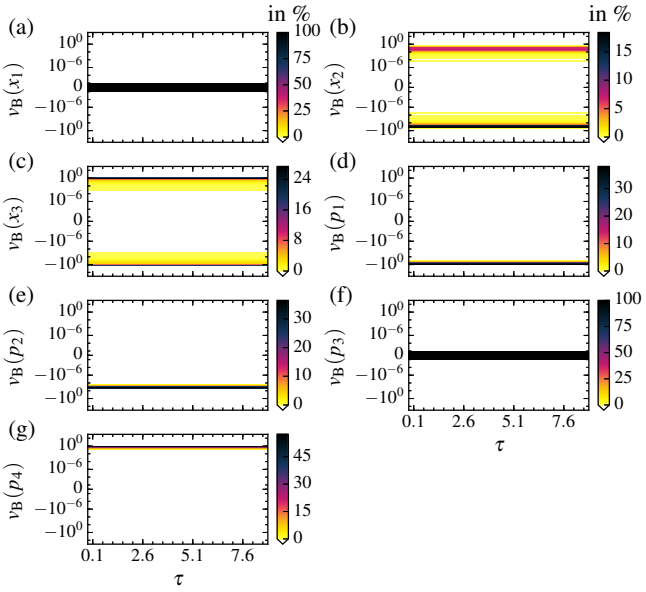

Figure 2. Histograms (color coded) of the components $v_{\mathrm{B}}(w_i)$ of a basis vector spanning the one dimensional (see Fig. 1) null space of D$\mathbf{G}$ (computed with delay reconstruction dimension $K = 10$) computed with respect to all variables ($D = 3$) and parameters ($N_{\mathrm{p}} = 4$) of the Colpitts oscillator, Eq. (34), where x_1 is assumed to be measured, Eq. (35). For each τ the components $v_{\mathrm{B}}(w_i)$ are computed for 10^4 points from the attractor using $\mathbf{p} = (5, 0.08, 0.7, 6.3)$. Only $v_{\mathrm{B}}(x_1)$ and $v_{\mathrm{B}}(p_3)$ are within the interval $[-10^{-10}, 10^{-10}]$ for (almost) all states and delay times τ and numerically very close to zero indicating that only x_1 and p_3 are locally observable.

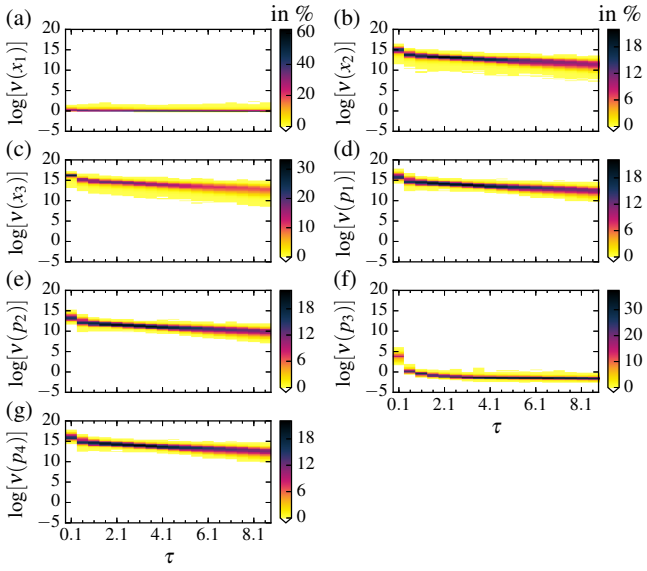

Figure 3. Histograms (color coded) of the measure of uncertainty $\nu(w_i)$, Eq. (30), (computed with delay reconstruction dimension $K = 10$) of all variables ($D = 3$) and parameters $N_{\mathrm{p}} = 4$ of the Colpitts oscillator where x_1 is assumed to be measured, Eq. (35). For each delay time τ the measure of uncertainty $\nu(w_i)$ (see Eq.(30)) is computed for 10^4 points on the attractor using $\mathbf{p} = (5, 0.08, 0.7, 6.3)$. On average $\nu(w_i)$ is quite large for x_2, x_3, p_1, p_2, and p_4, and much smaller for x_1 and p_3 indicating a good local observability only for x_1 and p_3.

However, estimating x_1 and p_3 should give more accurate results due to much smaller $\nu(w_i)$ (on average). This coincides with the results from investigating the null space of D$\mathbf{G}$ which also indicated a good local observability of x_1 and p_3 since variations of these quantities lead to variations of $\mathbf{g}$.

To check this result a twin experiment is performed where all model parameters are estimated beside the model variables from a x_1 time series using the estimation method from Sec. III. To obtain the data time series the model Eq. (34) was integrated and the true solution $\mathbf{z}(t)$ is used to generate the time series $\{\eta(t_n)\}$ ($t_n = n \cdot 0.01$, $n = 0, \ldots, 6000$) with

$$\eta(t_n) = z_1(t_n) \ . \tag{36}$$

The corresponding measurement function Eq. (35) is then used for the estimation of all model variables and all parameters. Figure 4 shows the estimated solution. In (a) one can see that the output of $h(\mathbf{x})$ (blue line) perfectly matches the data (light green line). In (b), (d), and (e) one can see that the estimated solution of the corresponding model variable x_i (blue line) matches the true solution z_i (red dashed line) only for the first variable x_1. Furthermore, one can see in (c), a zoomed version of (b), that the magnitude of the estimated solution of x_2 is much smaller than the true

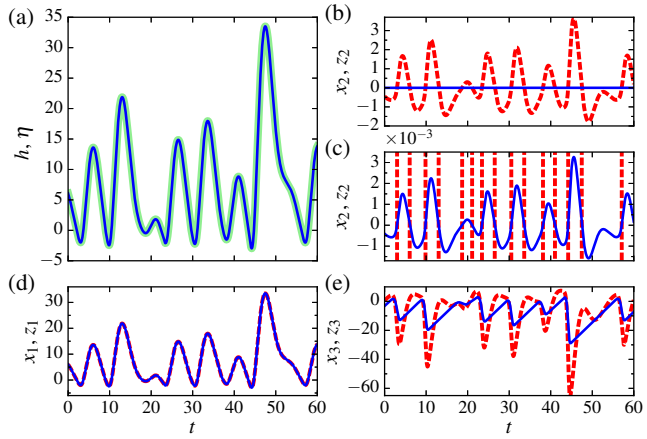

Figure 4. State and parameter estimation of the Colpitts oscillator Eq. (34) via measurement function $h(\mathbf{x}(t))$, Eq. (35), from the data time series $\{\eta(t_n)\}$, Eq. (36). (a): Output of $h(\mathbf{x}(t))$ (blue line) matches the data $\{\eta(t_n)\}$ (light green line). (b), (d), (e): Estimated model variables x_i (blue line) and the true solutions z_i, $i = 1, 2, 3$, (red dashed line) used to generate $\{\eta(t_n)\}$. (c): Zoomed version of (b). Only x_1 matches its true solution z_1. Parameters are estimated to $\mathbf{p} = (5573.7, 1.62 \cdot 10^{-4}, 0.700, 2.79)$. That is, only p_3 was estimated to the value used to generate the data.

solution z_i. The model parameters are estimated to $\mathbf{p} = (5573.7, 1.62 \cdot 10^{-4}, 0.700, 2.79)$. Only p_3 was estimated to the correct value used to generate the data. These results were correctly predicted by the previously computed measure of uncertainty ($\nu(p_3)$ is much smaller compared to the uncertainties of the other parameters), Fig. 3, and the components $v_\mathrm{B}(w_i)$ of a basis vector of the null space of D$\mathbf{G}$, Fig. 2. The component $v_\mathrm{B}(p_3)$ is very close to zero indicating that a variation of p_3 is (almost) impossible without a change of $\mathbf{g}$.

There exists one set of locally dependent quantities (since $D_\mathrm{N} = 1$) consisting of x_2, x_3, p_1, p_2, and p_4. Prohibiting variations of one of these quantities via $\Delta w_i = 0$ in Eq. (14), for example by setting w_i to a fixed value instead of estimating it in an estimation problem, sets $a = 0$. As a result, variations of all other quantities are not possible within the null space of D$\mathbf{G}$, which means that all other quantities became locally observable. For example, fixing p_3 does not set a to zero in Eq. (14) because, according to Fig. 2, $v_\mathrm{B}(p_3)$ is (very close to) zero. Therefore, fixing p_3 would not make all other quantities locally observable.

We decided to remove p_4 from the analysis. One can verify that the null space of D$\mathbf{G}$, with the column associated with p_4 removed, is zero dimensional by considering the singular values of D$\mathbf{G}$ (not shown here). Then, we consider the correlation coefficients $\rho(w_i, w_j)$, Eq. (31), which describes local correlations between quantities. The correlation analysis from Sec. II B was performed for all model variables x_1, x_2, and x_3, and the model parameters p_1, p_2, and p_3. The computation of the correlation coefficients is based on the same 10^4 states from the Colpitts attractor and the measurement function Eq. (35), as previously. Figure 5 shows the histograms of all correlation coefficients (without the diagonal elements of $\boldsymbol{\rho}$, because they are 1 anyway) for different τ and a reconstruction dimension of $K = 10$. The plots (a) to (o) show histograms of $\rho(w_i, w_j)$ for different quantities w_i and w_j using different delay times τ. In all plots the correlation coefficients are, independent of τ, distributed over the whole interval $[-1, 1]$. One can see that no perfect correlations occur because there is no histogram with $\rho(w_i, w_j) \approx \pm 1$ for all investigated states and delay times τ. Therefore, state and parameter estimation should give accurate results.

In a twin experiment in Ref. [35] the parameters p_1, p_2, and p_3 of the Colpitts oscillator were estimated from a noisy time series of the first model variable x_1. All estimated parameter values coincide with the values used to generate the data and are hence estimated correctly. This also coincides with results obtained when computing the measure of uncertainty only with the first three, instead of all four, model parameters. To obtain this result the previous computation of $\nu(w_i)$ was repeated including only x_1, x_2, x_3, p_1, p_2, and p_3 in the analysis. Histograms of $\nu(w_i)$ are shown in Fig. 6. We can see that the uncertainties are of magnitude 1 (for larger τ) and, hence, much smaller than in Fig. 3 (where all four parameter are included in the analysis).

To confirm that the set of locally dependent quantities is correctly predicted by the dependency analysis, the twin experiment from the beginning of this section is repeated. There, the model of the Colpitts oscillator, Eq. (34), was adapted to a x_1 time series (no measurement noise) and all four parameters were estimated. Instead of estimating all four parameters simultaneously, we adapt the concept of a profile likelihood [37, 38]. Only the first three parameters are estimated and p_4 is set to different values. The dependency of the estimated values of p_1, p_2, and p_3 on the parameter p_4 is shown in Fig. 7. In more detail, the simulation was performed in the following steps: (i) p_4 is fixed to $p_4 = 4.0$. (ii) Beside the model variables, the parameters p_1, p_2, and p_3 are estimated, as shown (blue dots) in plot (a), (b), and (c). The corresponding value of the cost function C, Eq. (33), for the estimated solution is shown in (d). (iii) p_4 is slightly increased and the estimation is repeated. The red dashed lines in (a) - (c) show the value of the corresponding parameter used to generate the data. In plot (a) - (d) the vertical black line at $p_4 = 6.3$ shows the value of p_4 used to generate the data.

First of all, one can see that for all values of p_4 the cost at the estimated solution is very small (order of magnitude of 10^{-8}) so that it is likely that the estimated solutions are in a global minimum of the cost function. A possible reason, why C is not exactly constant for different p_4, might be truncation errors. Further, for $p_4 = 6.3$ the estimated values of all other parameters coincide with the values used to generate the data. If p_4 is fixed to a value slightly smaller than 6.3 (for example $p_4 = 5.5$), then the estimated values for p_1 and p_2 are larger than the values used to generate the data (therefore $\Delta p_1, \Delta p_2 > 0$), as shown in Fig. 7(a), and Fig. 7(b), respectively. If now p_4 is fixed to a slightly larger value than 6.3 (for example $p_4 = 7.0$), then p_1 and p_2 are estimated to too small values. In Fig. 7(b) one can see, that the dependencies are only locally correct (around $p_4 = 6.3$) because for $p_4 < 5$ the parameter p_2 is estimated to too small values. Furthermore, p_3 is independent of p_4.

This results coincide with the local dependencies found in the dependency analysis when considering the ration of the components of the basis vectors (see Fig. 2).

B. Rössler model

In this section we use the Rössler model [40] in a form presented in Ref. [41, 42]. The model equations read

$$\begin{aligned} \dot{x}_1 &= p_1 x_2 + p_2 x_3 \\ \dot{x}_2 &= p_3 x_1 + p_4 x_2 \\ \dot{x}_3 &= p_5 + p_6 x_3 + p_7 x_1 x_3 \end{aligned} \tag{37}$$

where in the following the parameter values $\mathbf{p} = (-1, -1, 1, 0.1, 0.1, -14, 1)$ are used. To compare

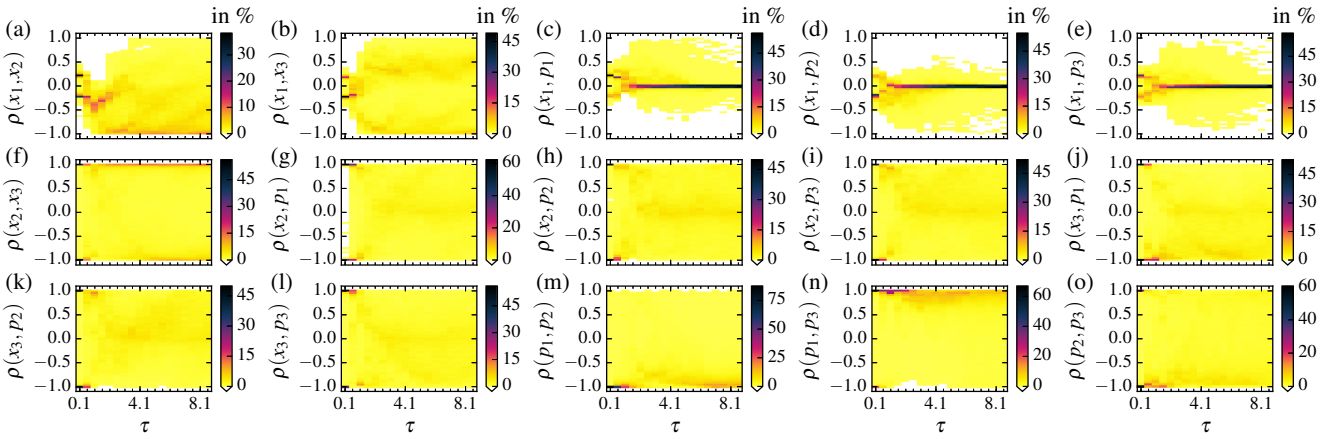

Figure 5. Histograms (color coded) of the correlation coefficients $\rho(w_i, w_j)$, Eq. (31), (computed with reconstruction dimension of $K = 10$) of all variables and the parameters p_1, p_2, and p_3 of the Colpitts oscillator, Eq. (34), where x_1 is assumed to be measured, Eq. (35). For each delay time τ the coefficients $\rho(w_i, w_j)$ are computed for 10^4 points on the attractor. In all plot it is $-1 < \rho(w_i, w_j) < 1$ for many states and τ indicating not very strong local dependencies between the quantities.

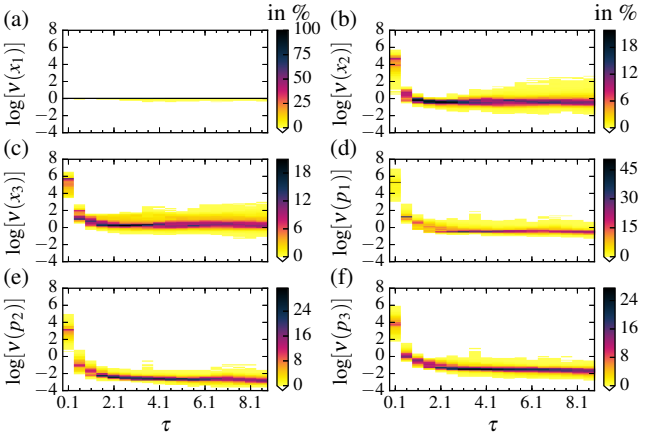

Figure 6. Similar to Fig. 3, but the measure of uncertainty, $\nu(w_i)$, was only computed for x_1, x_2, x_3, p_1, p_2, and p_3 (without p_4). For all quantities $\nu(w_i)$ is very small (on average) indicating that states and parameters can be estimated correctly.

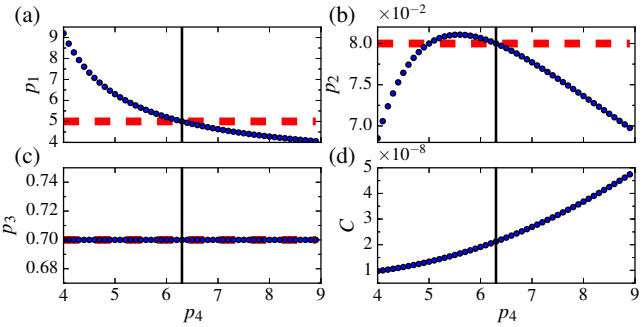

Figure 7. State and parameter estimation (using the algorithm from Sec. III) of the Colpitts oscillator, Eq. (34), from a clean x_1 time series, Eq. (35). (a) - (c): To generate the data the parameter values p_1, p_2, p_3 indicated by the red dashed lines and $p_4 = 6.3$ (black vertical line in (a) - (d)) were used. For each fixed p_4 the other parameters (blue dots) and the model variables were estimated (concept of profile likelihood [37, 38]). (a), (b): The local dependency of p_1 and p_2 on p_4 around $p_4 = 6.3$ is consistent with the dependency analysis, see Fig. 2, since $\Delta p_4 > 0 \Rightarrow \Delta p_1, \Delta p_2 < 0$ and vice versa. (c): p_3 is estimated correctly independent of p_4 (consistent with the dependency analysis). (d): Cost function C, Eq. (33), is very small at the estimated solutions indicating a relatively flat valley in the minimum.

our results with Ref. [42] we also assume that x_2 is measured,

$$h(\mathbf{x}) = x_2 \ . \tag{38}$$

To investigate the observability we first integrate the Rössler model, Eq. (37), for 10^4 time steps with a step size of 0.1. Then, every 10th state (1000 different states in total) is used for the following analysis. For each state and for different delay times τ the Jacobian D$\mathbf{G}$, Eq. (8), and its SVD of the $K = 50$ dimensional delay reconstruction map Eq. (4) were computed with respect to all three model states and all 7 model parameters. Therefore, D$\mathbf{G}$ is a 50×10 matrix.

Histograms of the normalized singular values σ_i/σ_1, $i = 1, \ldots, 10$, Eq. (9), of D$\mathbf{G}$ are shown in Fig. 8. We can see that the smallest normalized singular values, σ_9/σ_1 and σ_{10}/σ_1 are, for almost all states and τ, smaller than 10^{-15} and, hence, are very close to zero. This means, that the null space of D$\mathbf{G}$ is $D_\mathrm{N} = 2$ dimensional for all investigated states and all τ, and it can be spanned by the two basis vectors $\mathbf{v}_\mathrm{B}^{(1)} = \mathbf{v}^{(9)}$ and $\mathbf{v}_\mathrm{B}^{(2)} = \mathbf{v}^{(10)}$ (two last columns of $\mathbf{V}$), see Sec. II A. Both vectors are orthogonal and constitute the 10×2 basis matrix $\mathbf{V}_\mathrm{B} = [\mathbf{v}_\mathrm{B}^{(1)}, \mathbf{v}_\mathrm{B}^{(2)}]$, see Eq. (17). If now the ith row of $\mathbf{V}_\mathrm{B}$ contains zeros only, then the quantity w_i is locally observable because

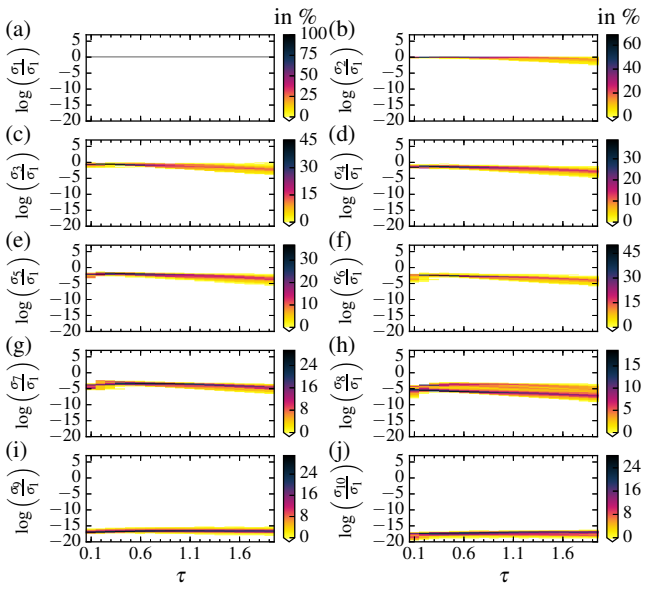

Figure 8. Histograms (color coded) of the normalized singular values σ_i/σ_1, Eq. (9), (computed with delay reconstruction dimension $K = 50$) using all variables ($D = 3$) and parameters ($N_\mathrm{p} = 7$) of the Rössler-model, Eq. (37), where x_2 is assumed to be measured, Eq. (38). For each delay time τ the normalized singular values σ_i/σ_1 of D$\mathbf{G}$ are computed for 1000 states from the attractor. The two smallest normalized singular values σ_9/σ_1 and σ_{10}/σ_1 are of magnitude smaller than 10^{-15} for (almost) all states and τ and, hence, are numerically very close to zero. This indicates a two dimensional null space of D$\mathbf{G}$ and, therefore, the existence of redundant variables or parameters.

a perturbation of this quantity is not possible inside the null space of D$\mathbf{G}$ and, therefore, would lead to a perturbation $\Delta\mathbf{g} \neq 0$, see Eq. (11).

In this example, all quantities are ordered by $\mathbf{w} = [x_1, x_2, x_3, p_1, p_2, p_3, p_4, p_5, p_6, p_7]$. Hence, the quantity w_i is associated with the components $v^{(1)}_{\mathrm{B},i}$ and $v^{(2)}_{\mathrm{B},i}$ of the basis vectors. For example, $v^{(1)}_{\mathrm{B},5}$ and $v^{(2)}_{\mathrm{B},5}$ are associated with p_2. To simplify the notation in the following discussion, the associated quantities will be provided in brackets, e.g. $v^{(1)}_{\mathrm{B},5} = v^{(1)}_\mathrm{B}(p_2)$ and $v^{(2)}_{\mathrm{B},5} = v^{(2)}_\mathrm{B}(p_2)$. Then, the basis matrix is

$$\mathbf{V}_\mathrm{B} = \begin{pmatrix} v^{(1)}_\mathrm{B}(x_1) & v^{(2)}_\mathrm{B}(x_1) \\ v^{(1)}_\mathrm{B}(x_2) & v^{(2)}_\mathrm{B}(x_2) \\ v^{(1)}_\mathrm{B}(x_3) & v^{(2)}_\mathrm{B}(x_3) \\ v^{(1)}_\mathrm{B}(p_1) & v^{(2)}_\mathrm{B}(p_1) \\ v^{(1)}_\mathrm{B}(p_2) & v^{(2)}_\mathrm{B}(p_2) \\ v^{(1)}_\mathrm{B}(p_3) & v^{(2)}_\mathrm{B}(p_3) \\ v^{(1)}_\mathrm{B}(p_4) & v^{(2)}_\mathrm{B}(p_4) \\ v^{(1)}_\mathrm{B}(p_5) & v^{(2)}_\mathrm{B}(p_5) \\ v^{(1)}_\mathrm{B}(p_6) & v^{(2)}_\mathrm{B}(p_6) \\ v^{(1)}_\mathrm{B}(p_7) & v^{(2)}_\mathrm{B}(p_7) \end{pmatrix} . \tag{39}$$

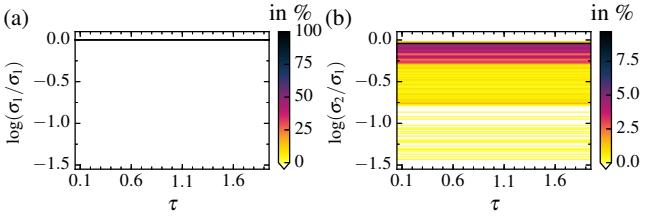

Figure 9. Histograms (color coded) of the normalized singular values σ_i/σ_1 of the square matrix $\mathbf{V}_{\mathrm{B},1}$, Eq. (40), using all variables ($D = 3$) and parameters ($N_\mathrm{p} = 7$) of the Rössler model, Eq. (37), (based on the same states, delay times τ, etc. as in Fig. 8). Since for all states and τ the smallest normalized singular values σ_1/σ_2 are relatively large, $\mathbf{V}_{\mathrm{B},1}$ is not singular and has, therefore, a unique inverse.

To identify quantities where prohibiting its variation, for example fixing them in an estimation problem, makes all quantities locally observable, we apply the dependency analysis suggested in Sec. II A. As already mentioned, we observed in numerical simulations that usually the patterns of zero and non-zero elements of all basis vectors obtained via SVD are equal. Therefore, we construct a new basis of the null space of D$\mathbf{G}$ where all basis vectors will have mutually different patterns of non-zero elements. In the first step we chose the two quantities p_5 and p_7 and split $\mathbf{V}_\mathrm{B}$ into

$$\mathbf{V}_{\mathrm{B},1} = \begin{pmatrix} v^{(1)}_\mathrm{B}(p_5) & v^{(2)}_\mathrm{B}(p_5) \\ v^{(1)}_\mathrm{B}(p_7) & v^{(2)}_\mathrm{B}(p_7) \end{pmatrix} \tag{40}$$

and

$$\mathbf{V}_{\mathrm{B},2} = \begin{pmatrix} v^{(1)}_\mathrm{B}(x_1) & v^{(2)}_\mathrm{B}(x_1) \\ v^{(1)}_\mathrm{B}(x_2) & v^{(2)}_\mathrm{B}(x_2) \\ v^{(1)}_\mathrm{B}(x_3) & v^{(2)}_\mathrm{B}(x_3) \\ v^{(1)}_\mathrm{B}(p_1) & v^{(2)}_\mathrm{B}(p_1) \\ v^{(1)}_\mathrm{B}(p_2) & v^{(2)}_\mathrm{B}(p_2) \\ v^{(1)}_\mathrm{B}(p_3) & v^{(2)}_\mathrm{B}(p_3) \\ v^{(1)}_\mathrm{B}(p_4) & v^{(2)}_\mathrm{B}(p_4) \\ v^{(1)}_\mathrm{B}(p_6) & v^{(2)}_\mathrm{B}(p_6) \end{pmatrix} . \tag{41}$$

Next, we split D$\mathbf{G}$ into the 50×2 matrix D$\mathbf{G}_1 = [\mathrm{D}\mathbf{G}^{(8)}, \mathrm{D}\mathbf{G}^{(10)}]$ containing the 8th and the 10th column of D$\mathbf{G}$ (the first column is associated with p_5 and the second column is associated with p_7) and the 50×8 matrix D$\mathbf{G}_2$ containing the remaining columns of D$\mathbf{G}$.

Histograms of both normalized singular values σ_i/σ_1 of $\mathbf{V}_{\mathrm{B},1}$, computed based on the same states and delay times τ as previously, are shown in Fig. 9. Since the smallest singular value is relatively large (larger than 10^{-2}) for all states and τ, $\mathbf{V}^{-1}_{\mathrm{b},1}$ exists and is unique.

Therefore, we can compute $\widetilde{\mathbf{V}}'_\mathrm{B}$ in Eq. (19) for each considered state and τ. In the next step we reorder the columns of $[\mathrm{D}\mathbf{G}_1, \mathrm{D}\mathbf{G}_2]$ in a way such that we obtain D$\mathbf{G}$ again. Performing the same reordering on the rows of $\widetilde{\mathbf{V}}'_\mathrm{B}$

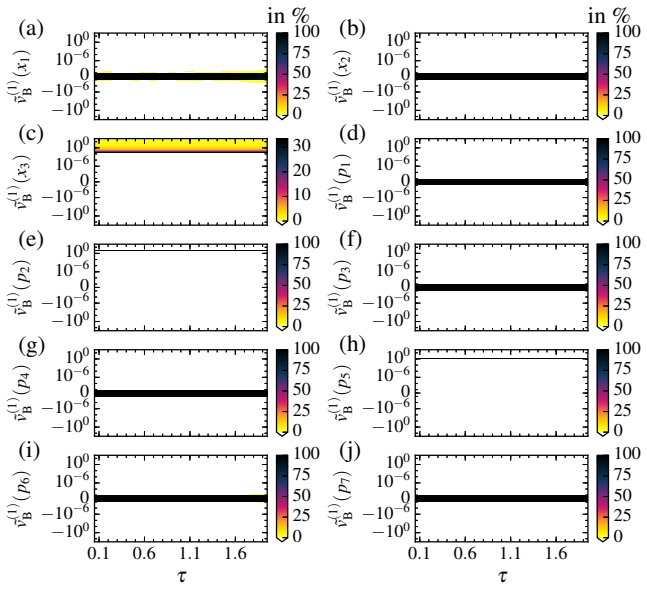

Figure 10. Histograms (color coded) of the components of the first basis vector $\widetilde{\mathbf{v}}_{\mathrm{B}}^{(1)}$, Eq. (42), of the two dimensional null space of D$\mathbf{G}$ using all variables ($D = 3$) and parameters ($N_{\mathrm{p}} = 7$) of the Rössler model, Eq. (37), (based on the same states, delay times τ, etc. as in Fig. 8). (c),(e),(h): Only the components associated with x_3, p_2, and p_5 are non-zero for all states and τ. (a),(b),(d),(f),(g),(i),(j): All other components are within the interval $[-10^{-10}, 10^{-10}]$ for (almost) all states and delay times τ and, hence, numerically very close to zero.

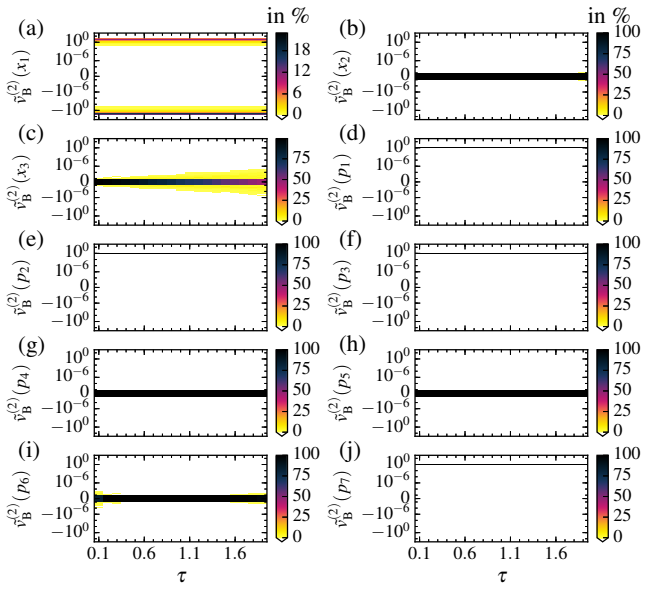

Figure 11. As Fig 10, but histograms of the components of $\widetilde{\mathbf{v}}_{\mathrm{B}}^{(2)}$, Eq. (42), are shown. (a),(c),(d),(e),(f),(j): Only the components associated with x_1, x_3, p_1, p_2, p_3, and p_7 are non-zero for all states and τ. (b),(c),(g),(h),(i): All other components are within the interval $[-10^{-10}, 10^{-10}]$ and, hence, numerically very close to zero for (almost) all states and delay times τ.

yields

$$\widetilde{\mathbf{V}}_{\mathrm{B}} = \begin{pmatrix} \tilde{v}_{\mathrm{B}}^{(1)}(x_1) & \tilde{v}_{\mathrm{B}}^{(2)}(x_1) \\ \tilde{v}_{\mathrm{B}}^{(1)}(x_2) & \tilde{v}_{\mathrm{B}}^{(2)}(x_2) \\ \tilde{v}_{\mathrm{B}}^{(1)}(x_3) & \tilde{v}_{\mathrm{B}}^{(2)}(x_3) \\ \tilde{v}_{\mathrm{B}}^{(1)}(p_1) & \tilde{v}_{\mathrm{B}}^{(2)}(p_1) \\ \tilde{v}_{\mathrm{B}}^{(1)}(p_2) & \tilde{v}_{\mathrm{B}}^{(2)}(p_2) \\ \tilde{v}_{\mathrm{B}}^{(1)}(p_3) & \tilde{v}_{\mathrm{B}}^{(2)}(p_3) \\ \tilde{v}_{\mathrm{B}}^{(1)}(p_4) & \tilde{v}_{\mathrm{B}}^{(2)}(p_4) \\ 1 & 0 \\ \tilde{v}_{\mathrm{B}}^{(1)}(p_6) & \tilde{v}_{\mathrm{B}}^{(2)}(p_6) \\ 0 & 1 \end{pmatrix} = \begin{bmatrix} \widetilde{\mathbf{v}}_{\mathrm{B}}^{(1)} & \widetilde{\mathbf{v}}_{\mathrm{B}}^{(2)} \end{bmatrix} \tag{42}$$

and fulfills Eq. (20). The vectors $\widetilde{\mathbf{v}}_{\mathrm{B}}^{(1)}$ and $\widetilde{\mathbf{v}}_{\mathrm{B}}^{(2)}$ contain the components of the first and the second column of $\widetilde{\mathbf{V}}_{\mathrm{B}}$, respectively. Due to the ones and zeros in $\widetilde{\mathbf{V}}_{\mathrm{B}}$ both vectors are linear independent and, since the null space of D$\mathbf{G}$ is $D_{\mathrm{N}} = 2$, form a basis of D$\mathbf{G}$ with different patterns of non-zero elements. In this basis it is $\tilde{v}_{\mathrm{B}}^{(1)}(p_5) = \tilde{v}_{\mathrm{B}}^{(2)}(p_7) = 1$ and $\tilde{v}_{\mathrm{B}}^{(2)}(p_5) = \tilde{v}_{\mathrm{B}}^{(1)}(p_7) = 0$.

To further investigate the structure of the null space of D$\mathbf{G}$ we consider histograms of all components of $\widetilde{\mathbf{v}}_{\mathrm{B}}^{(1)}$ (Fig. 10) and $\widetilde{\mathbf{v}}_{\mathrm{B}}^{(2)}$ (Fig. 11) computed using the same states and delay times τ as previously. Every variation $\Delta\mathbf{w}$ within the null space of D$\mathbf{G}$ can be expressed as

$$\Delta\mathbf{w} = \tilde{a}_1 \widetilde{\mathbf{v}}_{\mathrm{B}}^{(1)} + \tilde{a}_2 \widetilde{\mathbf{v}}_{\mathrm{B}}^{(2)} \ , \tag{43}$$

see Eq. (21). $\Delta\mathbf{w}$ is thus controlled by two scalars $\tilde{a}_1$ and $\tilde{a}_2$. By reading off the patterns of zero and non-zero elements of $\widetilde{\mathbf{v}}_{\mathrm{B}}^{(1)}$ and $\widetilde{\mathbf{v}}_{\mathrm{B}}^{(2)}$ from Fig. 10 and Fig. 11, the structure of Eq. (43) is

$$\Delta\mathbf{w} = \begin{pmatrix} \Delta x_1 \\ \Delta x_2 \\ \Delta x_3 \\ \Delta p_1 \\ \Delta p_2 \\ \Delta p_3 \\ \Delta p_4 \\ \Delta p_5 \\ \Delta p_6 \\ \Delta p_7 \end{pmatrix} = \tilde{a}_1 \begin{pmatrix} 0 \\ 0 \\ * \\ 0 \\ * \\ 0 \\ 0 \\ * \\ 0 \\ 0 \end{pmatrix} + \tilde{a}_2 \begin{pmatrix} * \\ 0 \\ 0 \\ * \\ * \\ * \\ 0 \\ 0 \\ 0 \\ * \end{pmatrix} . \tag{44}$$

A '0' means that this component is zero and '$*$' means that this component is non-zero for (almost) all investigated states and τ.

One can read off from Eq. (44) that variations $\Delta x_2, \Delta p_4, \Delta p_6 \neq 0$ are not possible without leaving the null space of D$\mathbf{G}$. Therefore, variations of x_2, p_4, and p_6 lead to a perturbation $\Delta\mathbf{g} \neq 0$ and, thereby, to a perturbation of $\mathbf{g}$ in Eq. (4), that is, of the output of the system at present and delayed times. This means that these quantities are locally observable.

One can also read off from Eq. (44) how all other unknown quantities can be made locally observable by prohibiting the variation of only two quantities. In a state and parameter estimation problem these two quantities would then be set to fixed values and not be estimated. The goal is to prohibit variations of quantities until $\widetilde{a}_1 = \widetilde{a}_2 = 0$. To accomplish that, in this example there exist several ways. For examples, fixing p_1 and p_5 by $\Delta p_1 = \Delta p_5 = 0$ implies $\widetilde{a}_1 = \widetilde{a}_2 = 0$ because $\widetilde{v}_{\mathrm{B}}^{(1)}(p_5)$ and $\widetilde{v}_{\mathrm{B}}^{(2)}(p_1)$ are non-zero. Or by setting $\Delta p_3 = 0$, which sets $\widetilde{a}_2 = 0$, and $\Delta p_2 = 0$, which then sets $\widetilde{a}_1 = 0$.

This shows the advantage of considering the basis vectors $\widetilde{\mathbf{v}}_{\mathrm{B}}^{(1)}$ and $\widetilde{\mathbf{v}}_{\mathrm{B}}^{(1)}$ instead of $\mathbf{v}_{\mathrm{B}}^{(1)}$ and $\mathbf{v}_{\mathrm{B}}^{(2)}$ (directly obtained via SVD). Since, according to our observations in numerical simulations, the patterns of non-zero elements of the latter two basis vectors is usually equal, this way of making all quantities locally observable would not work.

In Refs. [41, 42] the authors also assumed that x_2 is measured and they used an analytical calculation based on derivative coordinates to show that Eq. (37) can be rewritten as

$$\begin{aligned} \dot{x}_1 &= \frac{1}{b} p_1 x_2 + \frac{1}{ab} p_2 x_3 \\ \dot{x}_2 &= b p_3 x_1 + p_4 x_2 \\ \dot{x}_3 &= a p_5 + p_6 x_3 + b p_7 x_1 x_3 \end{aligned} \tag{45}$$

with the (introduced) scaling parameters $a, b \in \mathbb{R}$. This model can produce the same dynamics of the second model variable for arbitrary a and b. Therefore, a and b have a comparable role as $\widetilde{a}_1$ and $\widetilde{a}_2$ in Eq. (43) and Eq. (44). It should only be possible to uniquely recover the parameters p_4 and p_6 from a x_2 time series (only these parameters have no scaling factors). This coincides with our results from the dependency analysis that the only locally observable parameters are p_4 and p_6.

With the scaling parameter a in Eq. (45) the same model parameters can be varied as with $\widetilde{a}_1$ in Eq. (44). The same holds for b in Eq. (45) and $\widetilde{a}_2$ in Eq. (44).

Furthermore, the way of how parameters pairwise locally depend on each other is predicted correctly by the dependency analysis when using the same parameter values also used in the model Eq. (37) for the previous analysis, $\mathbf{p} = (-1,\ -1,\ 1,\ 0.1,\ 0.1,\ -14,\ 1)$. Let us start with $a = b = 1$ and slightly change $a \mapsto a > 1$. This leads to the following variations: $p_5 \mapsto a p_5 > p_5$ because $p_5 > 0$, and $p_2 \mapsto p_2/a > p_2$ because $p_2 < 0$. Hence, an increase of p_5 goes along with an increase of p_2. Since, according to Fig. 10, the ratio of the associated components of the basis vector $\widetilde{\mathbf{v}}_{\mathrm{B}}^{(1)}$ is $\widetilde{v}_{\mathrm{B}}^{(1)}(p_2)/\widetilde{v}_{\mathrm{B}}^{(1)}(p_5) > 0$ for all states and delay times τ, a small variation $\Delta p_5 >$ leads to a variation $\Delta p_2 > 0$, see Eq. (23). In the same way one can verify, by considering a small variation of b and the components of $\widetilde{\mathbf{v}}_{\mathrm{B}}^{(2)}$ in Fig. 11, that the pairwise local dependency between the other model parameters is equally predicted by Eq. (45) and by the dependency analysis.

It should be noted that choosing p_5 and p_7 is not the only possible combination to construct $\mathbf{V}_{\mathrm{B},1}$, Eq. (40), and with that a different $\widetilde{\mathbf{V}}_{\mathrm{B}}$. We repeated the dependency analysis by choosing p_2 and p_7, checking that $\mathbf{V}_{\mathrm{B},1}$ is non-singular for the investigated states and delay times τ, and were able to verify that the results of the analysis are consistent with a transformation of the model Eq. (45). For that, we introduced new scaling parameters e and f, where setting $a = e/f$ and $b = f$ in Eq. (45) yields

$$\begin{aligned} \dot{x}_1 &= \frac{1}{f} p_1 x_2 + \frac{1}{e} p_2 x_3 \\ \dot{x}_2 &= f p_3 x_1 + p_4 x_2 \\ \dot{x}_3 &= \frac{e}{f} p_5 + p_6 x_3 + f p_7 x_1 x_3 \ . \end{aligned} \tag{46}$$

Equation (46) was then used for the verification.

C. Hindmarsh-Rose model

In this example we use the Hindmarsh-Rose (HR) neuron model [43], which generates typical neuronal activity such as spiking and bursting governed by dynamics on separated time scales. The system consists of the model equations

$$\begin{aligned} \dot{x}_1 &= -x_1^3 + p_1 x_1^2 + x_2 - x_3 \\ \dot{x}_2 &= 1 - p_2 x_1^2 - x_2 \\ \dot{x}_3 &= p_3 [x_1 + p_5 (p_4 - x_3)] \end{aligned} \tag{47}$$

and a measurement function

$$h(\mathbf{x}) = x_1 \ , \tag{48}$$

where x_1 denotes the membrane potential. x_2 and x_3 describe slow and fast ion current rates, respectively, and the values of the model parameters are $\mathbf{p} = (3, 5, 0.004, 3.19, 0.25)$.

To obtain representative states of the system we first integrate the model Eq. (47) for 10^6 steps with a step size of 0.1. Then, every 100th state was used for the analysis resulting in 10^4 states from the attractor. For each state the Jacobian matrix $\mathrm{D}\mathbf{G}$ of the delay reconstruction map Eq. (4) was computed with respect to all $D = 3$ model variables and all $N_{\mathrm{p}} = 5$ model parameters for different delay times τ using a reconstruction dimension of $K = 10$.

Histograms of the normalized singular values σ_i/σ_1 of $\mathrm{D}\mathbf{G}$, Eq. (9), computed based on all states and for different τ are shown in Fig. 12. We can see that even the smallest singular value σ_8/σ_1 is of magnitude $\sigma_8/\sigma_1 \approx 10^{-7} > 0$ for increasing τ. Because the example using the Colpitts oscillator shows that in this context singular values can numerically also be much closer to zero (σ_7/σ_1 in Fig. 1 converges to values of magnitude 10^{-16}) we interpret this result that for the smallest singular value is non-zero. Therefore, the dimension of the null

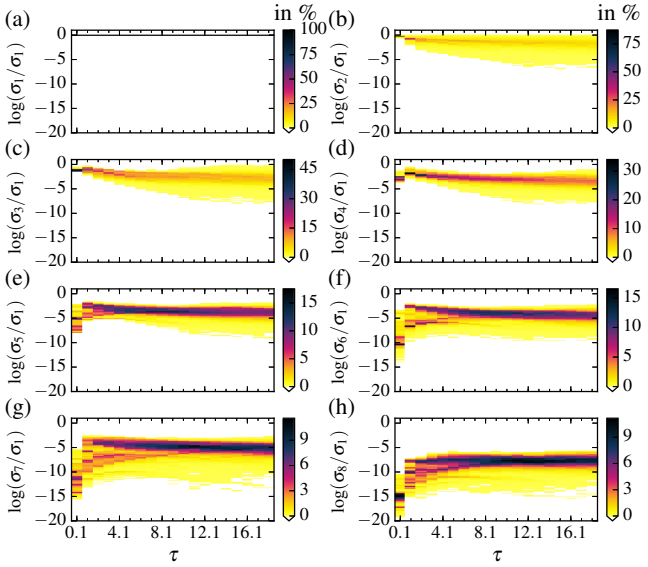

Figure 12. Histograms (color coded) of the normalized singular values σ_i/σ_1, Eq. (9), (computed with delay reconstruction dimension $K = 10$) using all variables ($D = 3$) and parameters $N_\mathrm{p} = 5$ of the HR-model, Eq. (47), where x_1 is assumed to be measured, Eq. (48). For each τ the singular values σ_i are computed for 10^4 points on the attractor using $\mathbf{p} = (3, 5, 0.004, 3.19, 0.25)$. The smallest normalized singular value σ_8/σ_1 is of magnitude $\sigma_8/\sigma_1 \approx 10^{-7}$ and, hence, numerically greater than zero.

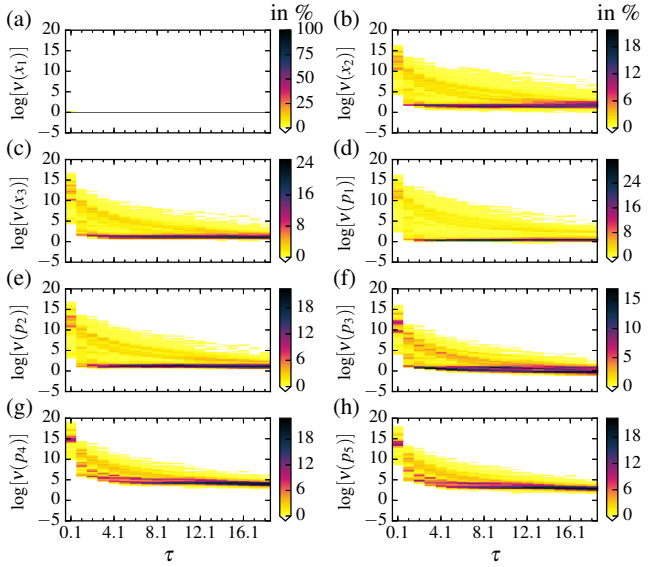

Figure 13. Histograms (color coded) of the measure of uncertainty $\nu(w_i)$, Eq.(30), (computed with delay reconstruction dimension $K = 10$) of all $D = 3$ variables and all $N_\mathrm{p} = 5$ parameters for the HR-model, Eq. (47), where x_1 is assumed to be measured, Eq. (48). For each delay time τ, $\nu(w_i)$ are computed for 10^4 points on the attractor using $\mathbf{p} = (3, 5, 0.004, 3.19, 0.25)$. (a)-(f): Uncertainties of x_1, x_2, x_3, p_1, p_2, and p_3 converge (on average) to comparatively small values for larger τ. (g),(h): Uncertainties of p_4 and p_5 converge (on average) to comparatively larger values indicating a worse local observability compared to the other quantities.

space of D$\mathbf{G}$, see Eq. (11) and Eq. (12), is $D_\mathrm{N} = 0$. This means, that for all investigated states and delay times τ there exist no variation of model parameters or variables $\Delta\mathbf{w} \neq 0$ such that the output of the system at present and delayed times is kept unchanged, $\Delta\mathbf{g} = 0$. Therefore, in principle all quantities are locally observable.

Next, we consider histograms of the uncertainties Eq. (30) for all 3 model variables and all 5 parameters based on the same 10^4 states, K, measurement function Eq. (48) and τ as previously, see Fig. 13. For large τ on average $\nu(p_4)$ and $\nu(p_5)$ are relatively large. This is a hint that the estimation of p_4 and p_5 from a x_1 time series is difficult. In Ref.[33] comparable histograms of $\nu(w_i)$ were considered for a fixed delay time and different reconstruction dimensions K (up to $K \approx 2000$) giving the same result that $\nu(p_4)$ and $\nu(p_5)$ converge to large values.

In the following we consider histograms of the correlation coefficients $\rho(w_i, w_j)$, Eq. (31), computed for all $D = 3$ model variables and all $N_\mathrm{p} = 5$ model parameters based on the same 10^4 states, K, measurement function Eq. (48), and τ as previously, see Fig. 14. In Fig. 14(a)-(g) the distributions of correlation coefficients between all quantities and x_1 are shown. One can see that for most states and delay times τ the correlation coefficients are numerically close to zero indicating only a weak correlation between x_1 and the other quantities. Taking into account that the uncertainty of x_1 is comparably small, see Fig. 13, it should be relatively easy to estimate x_1 from a x_1 time series.

In Fig. 14(h) to Fig. 14(a1) the distributions of the correlation coefficients are spread over the whole interval $\rho(w_i, w_j) \in [-1, 1]$, almost independent of τ. Since for many states and τ it is $1 < \rho(w_i, w_j) < 1$, correlations between the quantities exist, but are not all too strong (on average).

Special attention should be payed to the distributions of $\rho(p_4, p_5)$ shown in Fig. 14(b1). $\rho(p_4, p_5)$ is (close to) -1 for almost all of the analyzed states and τ indicating a relatively strong negative correlation between p_4 and p_5. This is a hint of an almost linear relation between both quantities. It is very likely that an increase of p_4 leads to a decrease of p_5 by keeping the delay reconstruction vector $\mathbf{g}$ in Eq. (4), that is the output of the system at present and delayed times, almost unchanged. However, there are still analyzed states where $\rho(p_4, p_5)$ is not (close to) -1 (especially for smaller τ) indicating that the negative correlation is not perfect. Hence, in principle it should be possible to estimate p_4 and p_5 from a x_1 time series, but one can expect that the estimation will be difficult.

Hence, one can expects that the simultaneous estimation of all variables and all parameters should give good results, but it is likely that the estimated values of p_4 and

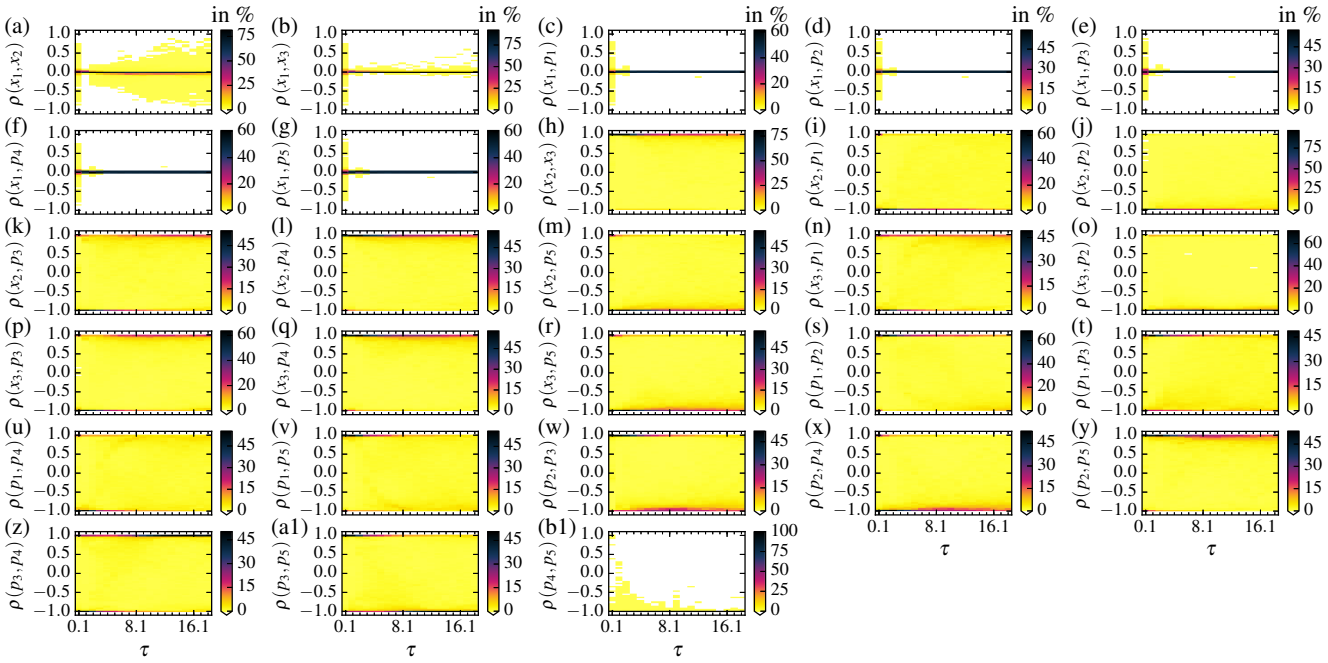

Figure 14. Histograms (color coded) of the correlation coefficients ρ_{ij} (computed with $K = 10$) of all variables and parameters of the HR-model, Eq. (47), where x_1 is assumed to be measured, Eq. (48). For each τ the correlation matrix $\boldsymbol{\rho}$, Eq.(31) is computed for 10^4 points on the attractor using $\mathbf{p} = (3, 5, 0.004, 3.19, 0.25)$. (a)-(a1): The quantities are not very correlated indicating that they should be estimable from a x_1 time series. (b1): There is a strong, but not perfect, negative correlation between p_4 and p_5.

p_5 are sensitive with respect to small numerical (truncation) errors or small variations in the data (for example the length of the time series, its underlying dynamics, or a slightly different noise level).

To illustrate this effect, a twin experiment is performed where all variables and parameters of the HR model Eq. (47) are estimated from noisy artificial data of the first model variable x_1 using the estimation method described in Sec. III. To generate the data, the model was integrated using the parameters $\mathbf{p} = (3, 5, 0.004, 3.19, 0.25)$. The solution $\mathbf{z}(t)$ (denoted as the 'true solution') is then used to create the noisy data time series $\{\eta(t_n)\}$, $t_n = 0, 0.5, \ldots 1500$, with

$$\eta(t_n) = z_1(t_n) + \xi(t_n) \ , \quad \xi(t_n) \sim \mathcal{N}(0, 0.004) \qquad (49)$$

(SNR = 18.3db). All model variables have to be estimated at the times $t_m = 0, 0.05, \ldots, 1500$ using the measurement function Eq. (48) together with all five model parameters. Hence, data are only available at every tenth time step. Figure 15(b),(c),(d) show that estimated solutions of x_i (blue lines) for the model variables and the corresponding true solution z_i (red dashed lines) match quite well. In Fig. 15(a) one can see that the output of the measurement function $h(\mathbf{x}(t))$ (blue line) coincides with the noisy data $\{\eta(t_n)\}$ (green circles). As predicted by the correlation analysis, the estimated values of the first three parameters ($p_1 = 3.00$, $p_2 = 4.99$, and $p_3 = 0.00402$) are very close to the values used to generate the data. However, p_4 and p_5 are estimated to $p_4 = 4.19$ and $p_5 = 0.191$ which is a much larger deviation to the values used to generate the data. This is in coincidence with that the uncertainties of p_4 and p_5 are larger compared to uncertainties of the other parameters (on average), see Fig. 13.

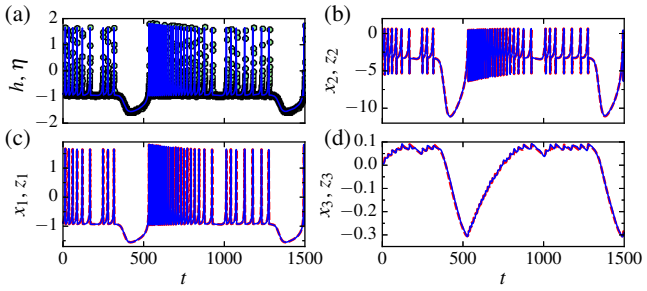

Figure 15. State and parameter estimation (using the method from Sec. III) of all $D = 3$ variables and all $N_\mathrm{p} = 5$ parameters of the HR-model Eq. (47), from a noisy x_1 time series $\{\eta(t_n)\}$, Eq. (49), using the measurement function $h(\mathbf{x})$, Eq. (48). (a): Output $h(\mathbf{x})$ (blue line) matches the data $\{\eta(t_n)\}$ (green circles). (b), (c), (d): Estimated model variables x_i (blue lines) match the true solutions z_i (red dashed lines; used to generate $\{\eta(t_n)\}$). Parameters are estimated to $\mathbf{p} = (3.00, 4.99, 0.00402, 4.19, 0.191)$. That is, p_1, p_2, and p_3 are estimated to values similar to those used to generate the data. p_4 and p_5 are estimated to much less accurate values.

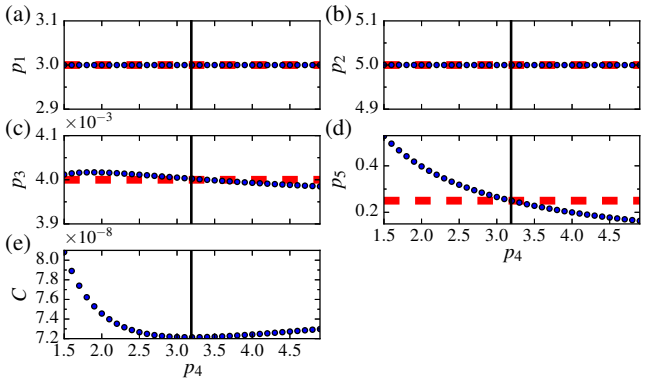

Figure 16. State and parameter estimation (using algorithm in Sec. III) of the HR model, Eq. (47), from a clean x_1 time series. (a) - (d): The parameter values shown by the red dashed lines were used, beside $p_4 = 3.19$ (black vertical line in (a) - (e)), to generate the data. For each fixed p_4 all other parameters were estimated (blue dots) beside the model variables (profile likelihood approach [37, 38]). That p_5 is estimated to a too small value, if p_4 is too large, is consistent with the negative correlation between both parameters, see Fig. 14(b1). Nevertheless, p_1, p_2, and p_3 are estimated (almost) correctly to values used to generate the data, (almost) independent of the value of p_4. (e): Although Cost function C, Eq. (33), is very small for all p_4, C exhibits a minimum around $p_4 \approx 3.19$ (used to generate the data).

The parameter p_4 is estimated to a too large and p_5 to a too small value. This relation coincides with the negative correlation found in the correlation analysis, see Fig. (14).

Although p_4 and p_5 are not estimated close to the correct values, its estimates are not completely wrong. Another twin experiment showed that it is possible to estimate all five parameters close to the values used to generate the data, if one removes the measurement noise in Eq. (49) and provides data at every time step the variables will be estimated. This confirms the hypothesis that the simultaneous estimation of p_4 and p_5 should in principle be possible, but it will not be very robust.

To confirm the predicted negative correlation of p_4 and p_5 the twin experiment is repeated without measurement noise in the data. Furthermore, data are available at every time step where the model variables are estimated. p_4 is fixed to different values and p_1, p_2, p_3, and p_5 are estimated beside the model variables. The dependency of the estimated parameter values on p_4 (profile likelihood approach [37, 38]) is shown in Fig. 16.

The horizontal red dashed lines in Fig. 16(a) to Fig. 16(d) show the parameter values p_1, p_2, p_3, and p_5, respectively, used to generate the data. The value of p_4 used for generating the data is shown in Fig. 16(a) to Fig. 16(e) by the vertical black line at $p_4 = 3.19$. In Fig. 16(a) to Fig. 16(c) one can see that the estimated values of p_1 and p_2 coincide with true values (red dashed lines) used to generate the data sufficiently well, independently of the value of p_4. Only a very weak dependency of p_3 on p_4 was observed. Figure 16(d) shows that an increase of $p_4 > 3.19$ goes along with estimated values of $p_5 < 0.25$ which are smaller than the value used to generate the data. This dependency between both parameters was predicted correctly by the negative correlation $\rho(p_4, p_5) \approx -1$ for most states and τ, see Fig. 14(b1).

Figure 16(e) shows that the value of the cost function Eq. (33) at the estimated solution is relatively small for all considered values of p_4. Nevertheless, the cost function exhibits a minimum around $p_4 = 3.19$. The fact, that it is not very steep, makes the estimation process not very robust. Errors in the estimation problem (measurement noise, truncation errors, ...) may easily shift the minimum to a different value of p_4 and, hence, lead to a wrong estimation of p_4 and p_5. This is likely to be the reason why the state and parameter estimation from a noisy time series with fewer data points, see Fig. 15, gives worse results for p_4 and p_5.

V. CONCLUSION

Features of the null space of the Jacobian matrix of the delay coordinates map were exploited to identify parameters and variables of dynamical model which cannot be uniquely estimated from a measured times (generated by the same model or a process the model aims at describing). This analysis not only provides those unknown quantities which are not observable (in a strict sense), but also information about their relations. Using this information one can specify the impact of setting one (or more) of the unobservable quantities to fixed values. If the dimension of the null space of the Jacobian matrix of the delay coordinates map is D_N then setting D_N not observable unknowns to fixed values makes all remaining unknowns observable. Criteria for selecting these D_N unknowns are obtained from the structure of the null space. These aspects were illustrated with (time series from) the Colpitts oscillator and the Rössler system. Even if all parameters and not measured variables are locally observable there may still be unknowns which are strongly correlated. This case can be identified by a suitable correlation analysis, as shown with the Hindmarsh-Rose model. All concepts presented and discussed can in principle be generalized to multivariate time series and spatially extended systems.

ACKNOWLEDGMENTS

S.L. and U.P. acknowledge support from the BMBF (FKZ031A147, GO-Bio), the DFG (SFB 1002), and the German Center for Cardiovascular Research (DZHK e.V.).

[1] L. M. Pecora and T. L. Carroll, Phys. Rev. Lett. **64**, 821 (1990).
[2] U. Parlitz, L. Junge, and L. Kocarev, Phys. Rev. E **54**, 6253 (1996).
[3] D. Rey, M. Eldridge, M. Kostuk, H. D. I. Abarbanel, J. Schumann-Bischoff, and U. Parlitz, Phys. Lett. A **378**, 869 (2014).
[4] D. Rey, M. Eldridge, U. Morone, H. D. I. Abarbanel, U. Parlitz, and J. Schumann-Bischoff, Phys. Rev. E **90**, 062916 (2014).
[5] R. E. Kalman, J. Basic. Eng. **82**, 35 (1960).
[6] G. Evensen, J. Geophys. Res. **99**, 10143 (1994).
[7] G. Evensen, *Data Assimilation: The Ensemble Kalman Filter*, 2nd ed. (Springer, Dordrecht ; New York, 2009).
[8] P. J. van Leeuwen, Mon. Wea. Rev. **137**, 4089 (2009).
[9] P. J. van Leeuwen, Q. J. R. Meteorol. Soc. **136**, 1991 (2010).
[10] Y. Sasaki, Mon. Wea. Rev. **98**, 875 (1970).
[11] H. D. I. Abarbanel, D. R. Creveling, R. Farsian, and M. Kostuk, SIAM J. Appl. Dyn. Syst. **8**, 1341 (2009).
[12] J. Bröcker, Q. J. R. Meteorol. Soc. **136**, 1906– (2010).
[13] A. H. Jazwinski, *Stochastic Processes and Filtering Theory* (Academic Press, New York u.a., 1970).
[14] H. Abarbanel, *Predicting the Future: Completing Models of Observed Complex Systems* (Springer Publishing Company, Incorporated, 2013).
[15] O. Talagrand and P. Courtier, Q. J. R. Meteorol. Soc. **113**, 1311 (1987).
[16] P. Courtier and O. Talagrand, Q. J. R. Meteorol. Soc. **113**, 1329 (1987).
[17] E. B. Lee and L. Markus, *Foundations of Optimal Control Theory* (John Wiley & Sons, 1967).
[18] R. Hermann and A. J. Krener, IEEE Trans. Autom. Control **22**, 728 (1977).
[19] E. D. Sontag, *Mathematical Control Theory: Deterministic Finite Dimensional Systems*, 2nd ed. (Springer, New York, 1998).
[20] H. Nijmeijer, Int. J. Control **36**, 867 (1982).
[21] C. Letellier, L. A. Aguirre, and J. Maquet, Phys. Rev. E **71**, 066213 (2005).
[22] C. Letellier, L. Aguirre, and J. Maquet, Commun. Nonlinear. Sci. Numer. Simul. **11**, 555 (2006).
[23] H. Nijmeijer and A. v. d. Schaft, *Nonlinear Dynamical Control Systems* (Springer Science & Business Media, 1990).
[24] L. Aguirre, IEEE Trans. Educ. **38**, 33 (1995).
[25] R. E. Kalman, in *Proc. First IFAC Congress*, Vol. 1 (1961) p. 481–492.
[26] R. E. Kalman, SIAM J. Control **1**, 152 (1963).
[27] D. Aeyels, SIAM J. Control Optim. **19**, 595 (1981).
[28] F. Takens, in *Dynamical Systems and Turbulence, Warwick 1980*, Lecture Notes in Mathematics No. 898, edited by D. Rand and L.-S. Young (Springer Berlin Heidelberg, 1981) pp. 366–381.
[29] T. Sauer, J. A. Yorke, and M. Casdagli, J. Stat. Phys. **65**, 579 (1991).
[30] H. Kantz and T. Schreiber, *Nonlinear time series analysis*, Cambridge Nonlinear Science Series, Vol. 7 (Cambridge University Press, 1997).
[31] H. D. I. Abarbanel, *Analysis of Observed Chaotic Data*, 2nd ed. (Springer Verlag, 1997).
[32] D. A. Belsley, *Conditioning Diagnostics: Collinearity and Weak Data in Regression*, 1st ed. (Wiley-Interscience, New York, 1991).
[33] U. Parlitz, J. Schumann-Bischoff, and S. Luther, Phys. Rev. E **89**, 050902 (2014).
[34] U. Parlitz, J. Schumann-Bischoff, and S. Luther, Chaos **24**, 024411 (2014).
[35] J. Schumann-Bischoff and U. Parlitz, Phys. Rev. E **84**, 056214 (2011).
[36] J. Schumann-Bischoff, S. Luther, and U. Parlitz, Commun. Nonlinear. Sci. Numer. Simul. **18**, 2733 (2013).
[37] A. Raue, C. Kreutz, T. Maiwald, J. Bachmann, M. Schilling, U. Klingmüller, and J. Timmer, Bioinformatics **25**, 1923 (2009).
[38] A. Raue, V. Becker, U. Klingmüller, and J. Timmer, Chaos **20**, 045105 (2010).
[39] M. Kennedy, IEEE Transactions on Circuits and Systems I: Fundamental Theory and Applications **41**, 771 (1994).
[40] O. E. Rössler, Phys. Lett. A **57**, 397 (1976).
[41] C. Lainscsek, Phys. Rev. E **84**, 046205 (2011).
[42] C. Lainscsek, J. Weyhenmeyer, T. J. Sejnowski, and C. Letellier, Chaos, Solitons & Fractals **76**, 182 (2015).
[43] J. L. Hindmarsh and R. M. Rose, Proc. R. Soc. Lond. B **221**, 87 (1984).
[44] J. Schumann-Bischoff, U. Parlitz, H. D. I. Abarbanel, M. Kostuk, D. Rey, M. Eldridge, and S. Luther, Chaos **25**, 053108 (2015).
[45] W. H. Press, S. A. Teukolsky, W. T. Vetterling, and B. P. Flannery, *Numerical Recipes: The Art of Scientific Computing*, 3rd ed. (Cambridge University Press, Cambridge, UK ; New York, 2007).
[46] P. J. van Leeuwen and G. Evensen, Mon. Wea. Rev. **124**, 2898 (1996).
[47] A. C. Lorenc, Quart. J. R. Met. Soc. **112**, 1177 (1986).
[48] K. Levenberg, Q. Appl. Math. **2**, 164 (1944).
[49] D. W. Marquardt, J. Soc. Ind. Appl. Math. **11**, 431 (1963).
[50] M. I. Lourakis, "Sparselm," (2015).
[51] A. Griewank, D. Juedes, and J. Utke, ACM Trans. Math. Softw. **22**, 131–167 (1996).
[52] S. F. Walter, "Pyadolc," (2015).
[53] A. Walther and A. Griewank, "Combinatorial scientific computing," (Chapman & Hall / CRC Computational Science Series, 2012) Chap. Getting Started with ADOL-C, pp. 181–202.
[54] D. R. Creveling, P. E. Gill, and H. D. I. Abarbanel, Phys. Lett. A **372**, 2640 (2008).

9 Shinriki oscillator

The Shinriki oscillator [30] is a nonlinear oscillating electronic circuit which can be used as an experimental setup to study nonlinear and chaotic phenomena [58, 59]. Here, the oscillator is used as an experimental system to test the dependency analysis (see Chap. 8) and the observability analysis (see Chap. 5 and Chap. 6). Finally, states and parameters of a model of the oscillator are estimated from an experimentally measured time series using the weak constraint 4D-Var like estimation method from [33] (this method is also used in Sec. 4, and Sec. 7).

First, in Sec. 9.1 the oscillator is described and model equations for the oscillator are provided. Then, the dependency, observability, and correlation analysis are applied in Sec. 9.2, and Sec. 9.3 to experimental data from the oscillator. After identifying locally redundant parameters it is demonstrated in Sec. 9.4 that the remaining parameters can be uniquely estimated from an experimentally observed univariate time series.

In large parts, the notation used in this chapter is adopted from Sec. 8.

9.1 The oscillator

Figure 9.1 (replicated from Ref. [60, 61] and modified) shows the circuit layout of the Shinriki oscillator used here. The RLC circuit, given by R_3, L, and C_2, has a resonance frequency [62, Chap. 6.1.1] of

$$f_0 = \frac{1}{2\pi}\sqrt{\frac{1}{LC_2} - \frac{R_3^2}{4L^2}} \approx 889\text{Hz} \ . \tag{9.1}$$

Two coupled Zener diodes D_1 and D_2, in parallel to the potentiometer R_2, form the nonlinearity.

In general, an omic resistor can only have a *positive* resistance. However, a *negative impedance converter* (NIC), as used in the circuit, is an active electronic circuit which acts as a resistor with a *negative* resistance [63, Chap. 12.5]. Hence, a NIC can be described by $V = -R_{\text{NIC}} \cdot I$ with $R_{\text{NIC}} > 0$, where V is the voltage at the NIC, I the current through the NIC, and $-R_{\text{NIC}}$ its resistance. According to Ref. [63, Chap. 12.5], in our case the negative resistance of the NIC is given by $-R_{\text{NIC}} = (-4.7\text{k}\Omega/4.7\text{k}\Omega) \cdot 6.8\text{k}\Omega$ and hence $R_{\text{NIC}} = 6.8\text{k}\Omega$. The operation amplifier TL071 is used here in the NIC.

The potentiometers R_1 and R_2 are the control parameters of the circuit. They can be tuned to obtain chaotic dynamics [58].

To obtain the current-voltage characteristic $I_{\text{D}}(V)$ of the two coupled Zener diodes D_1 and D_2, the test circuit Fig. 9.2a was built. For different $V \geq 0$ the current $I_{\text{D}}(V)$

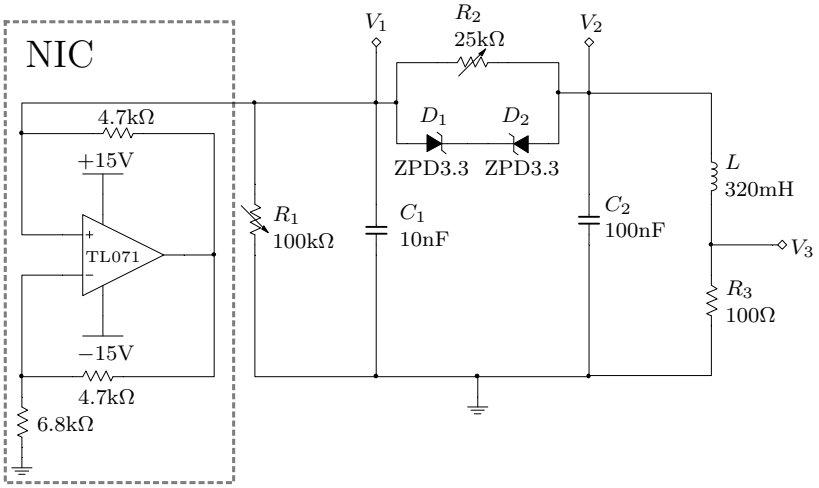

Figure 9.1: Layout of the Shinriki oscillator (replicated from Ref. [60, 61] and modified). The voltages V_1 and V_2 together with the current $I_3 = V_3/R_3$ can be described by Eq. (9.3). The potentiometers R_1 and R_2 can be used to change the dynamical behavior.

was measured (Fig. 9.2b, blue dots). Due to the symmetry in the circuit the data are mirrored at the center. The function

$$I_{\mathrm{D}}(V) = a \cdot \left(e^{bV} - e^{-bV} \right) \tag{9.2}$$

used here to describe the data depends on two parameters a and b. Both parameters were estimated simultaneously by a least square fit (Fig. 9.2b, black line) to $a = 2.295 \cdot 10^{-5}\mathrm{mA}$ and $b = 3.003\mathrm{V}^{-1}$.

The equations describing the oscillator can be derived from the circuit layout using Kirchhoff's laws [59–61]. They read

$$\begin{aligned} \dot{V}_1 &= \frac{1}{C_1}\left[V_1 \left(\frac{1}{R_{\mathrm{NIC}}} - \frac{1}{R_1} \right) - I_{\mathrm{D}}(V_1 - V_2) - \frac{V_1 - V_2}{R_2} \right] \\ \dot{V}_2 &= \frac{1}{C_2}\left[I_{\mathrm{D}}(V_1 - V_2) + \frac{V_1 - V_2}{R_2} - I_3 \right] \\ \dot{I}_3 &= \frac{1}{L}\left(-I_3 R_3 + V_2 \right) \ . \end{aligned} \tag{9.3}$$

For simplicity the $D = 3$ model variables and the $N_{\mathrm{p}} = 9$ model parameters are summarized in $\mathbf{x} = (V_1, V_2, I_3)$ and $\mathbf{p} = (a, b, C_1, C_2, R_1, R_2, R_3, R_{\mathrm{NIC}}, L)$. All model parameter values are given in Tab. 9.1.

As in Ref. [61], each of both voltages V_1 and V_2 are measured by means of a voltage buffer [64, Chap. 15.3] (see Fig. 9.3a). This minimizes the influence of the measurement device on the Shinriki oscillator. For that, V_1 and V_2 in Fig. 9.1 are connected to V_{in} of a voltage buffer. The output voltage V_{out} is given by the input-output relation [64,

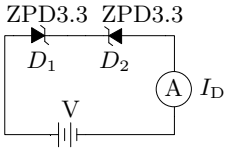

(a) Test circuit

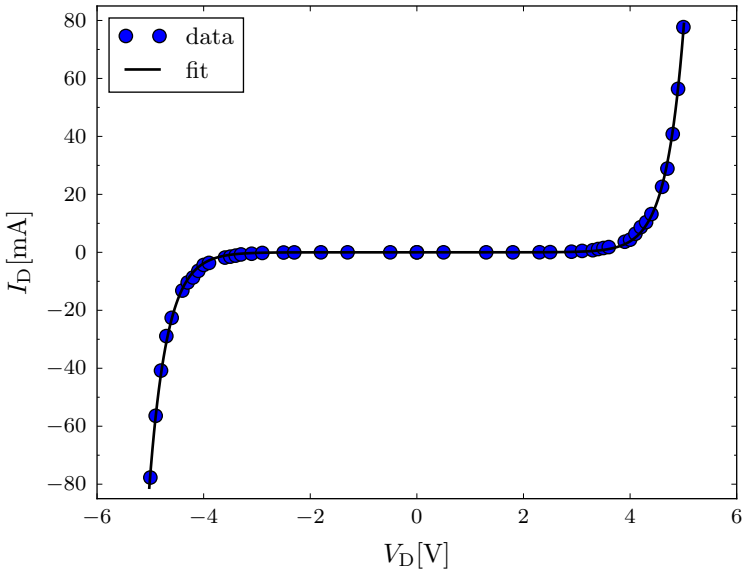

(b) Current-voltage characteristic

Figure 9.2: Test circuit (a) is used to measure the current voltage characteristic of the coupled Zener diodes (blue circles in (b)) which can be described by Eq. (9.2). Both parameters are estimated by a least-square fit (black line) to $a = 2.295 \cdot 10^{-5}$mA and $b = 3.003\text{V}^{-1}$.

Table 9.1: Model parameters of the Shinriki oscillator (values adopted from Ref. [60, 61]) and its model equations Eq. (9.3). The resistance of the potentiometers R_1 and R_2 can be set to arbitrary values within the specified range.

parameter	value	unit
a	$2.295 \cdot 10^{-5}$	[mA]
b	3.003	[V^{-1}]
C_1	0.01 ± 0.002	[µF]
C_2	0.1 ± 0.02	[µF]
R_1	0 to 100	[kΩ]
R_2	0 to 25	[kΩ]
R_3	0.1 ± 0.005	[kΩ]
R_{NIC}	6.8	[kΩ]
L	0.32	[H]

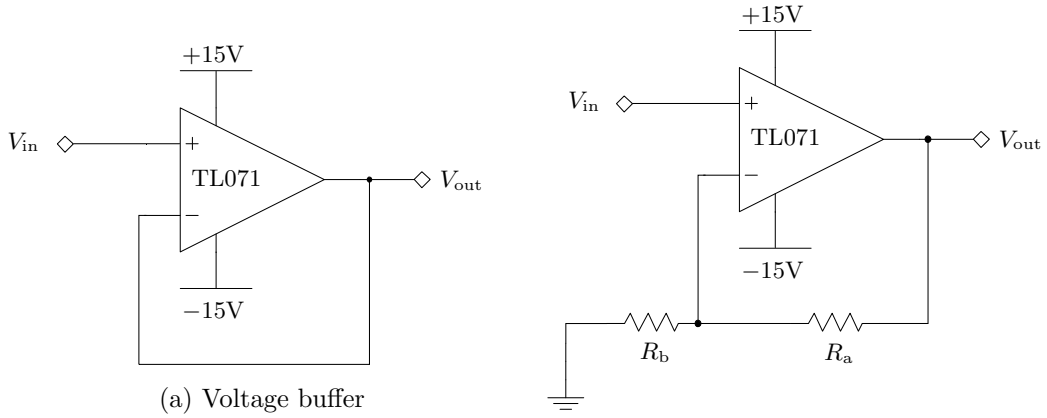

(a) Voltage buffer

(b) Noninverting amplifier

Figure 9.3: In our application in both circuits V_{in} is connected to an electrical circuit and V_{out} to an oscilloscope (or a voltmeter). (a): A voltage buffer [64, Chap. 15.3] minimizes the influence of the measurement device on the circuit and has the input-output relation Eq. (9.4). (b): The noninverting amplifier [64, Chap. 15.4] amplifies the input voltage V_{in} by the input-output relation Eq. (9.5).

Chap. 15.3]

$$V_{\text{out}} = V_{\text{in}} \ . \tag{9.4}$$

To increase the signal to noise ratio, the voltage V_3 (which has a relatively small amplitude) is amplified using a noninverting amplifier [64, Chap. 15.4] (see Fig. 9.3b). Therefore, V_3 in Fig. 9.1 is connected to V_{in}. The output signal is given by the input-output relation [64, Chap. 15.4]

$$V_{\text{out}} = \left(1 + \frac{R_a}{R_b}\right) V_{\text{in}} \ . \tag{9.5}$$

Using the resistors $R_a = 12\text{k}\Omega$ and $R_b = 1.3\text{k}\Omega$ the output signal is $V_{\text{out},3} = V_{\text{out}} \approx 10V_{\text{in}} = 10V_3$. Current I_3 can then be computed from the measured voltage $V_{\text{out},3}$ by $I_3 = V_3/R_3 = 0.01\Omega^{-1} \cdot V_3 = 0.001\Omega^{-1} \cdot V_{\text{out},3}$.

Data time series of V_1, V_2, and V_3 are measured using an oscilloscope (model: Tektronix MDO3034).

The investigations in Sec. 9.2 to Sec. 9.4 are based on experimentally measured time series of V_1, V_2, and I_3 where the potentiometers are tuned to $R_1 = 22.05\text{k}\Omega$ and $R_2 = 16.92\text{k}\Omega$. A typical measured time series and the corresponding attractor are shown in Fig. 9.4a and Fig. 9.4b.

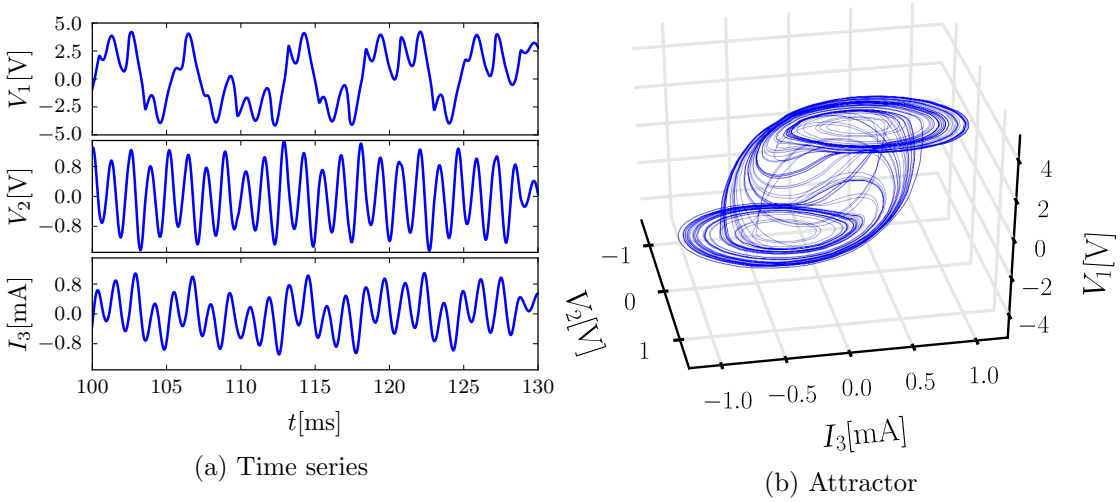

(a) Time series

(b) Attractor

Figure 9.4: Experimentally measured time series (a) and the attractor (b) of the Shinriki oscillator Fig. 9.1. The potentiometers are set to $R_1 = 22.05\text{k}\Omega$ and $R_2 = 16.92\text{k}\Omega$.

9.2 Dependency and Observability analysis for the Shinriki Oscillator

The observability of model variables and parameters and the dependencies between them is investigated on the basis of experimentally measured states $\mathbf{x}_{\text{dat}} = (V_{\text{dat},1}, V_{\text{dat},2}, I_{\text{dat},3})$ from the Shinriki oscillator, Sec. 9.1. $V_{\text{dat},1}$, $V_{\text{dat},2}$, and $I_{\text{dat},3}$ are measured at V_1, V_2, and I_3 in Fig. 9.1, respectively, by means of two voltage buffers for V_1 and V_2 (see Fig. 9.3a) and a noninverting amplifier for I_3 (see Fig. 9.3b). A description of the observability analysis is provided in Sec. 5, Sec. 6, and Sec. 8. In Sec. 8, additionally, the dependency and correlation analysis is described. The notation used in this section is mainly adopted from Sec. 8.

For the analysis it is assumed that only the first model variable V_1 of the $D = 3$ dimensional Shinriki oscillator Eq. (9.3) is observed leading to the measurement function

$$h[\mathbf{x}(t)] = V_1(t) \ , \tag{9.6}$$

where $\mathbf{x} = (V_1, V_2, I_3)$. The model parameter values from Tab. 9.1 are used here, beside $R_1 = 22.05\text{k}\Omega$ and $R_2 = 16.92\text{k}\Omega$. Since the dependency, observability, and correlation analysis are based on a delay reconstruction map $\mathbf{G}$ of the measured signal, Sec. 8, Eq. (3), we define the $K = 50$ dimensional delay reconstruction (see Sec. 8, Eq. (4))

$$\begin{aligned} \mathbf{G}(\mathbf{x}(t), \mathbf{p}) &= \big[V_1(t), \quad V_1(t+\tau), \quad \ldots, \quad V_1(t+(K-1)\tau)\big] \\ &= \mathbf{g} \ , \end{aligned} \tag{9.7}$$

where τ is the delay time. If $\mathbf{G}$ is locally invertible, then $\mathbf{x}(t)$ and $\mathbf{p}$ can be uniquely

reconstructed given the measured signal $[V_1(t), V_1(t+\tau), \ldots, V_1(t+(K-1)\tau)]$, i.e. $\mathbf{x}(t)$ and $\mathbf{p}$ are locally observable. The local invertibility can be investigated by means of the $K \times (N_\mathrm{p} + D)$ Jacobian matrix

$$\mathrm{D}\mathbf{G}(\mathbf{x}(t), \mathbf{p}) = \mathrm{D}\mathbf{G} = \begin{pmatrix} \frac{\partial V_1(t)}{\partial V_1(t)} & \frac{\partial V_1(t)}{\partial V_2(t)} & \frac{\partial V_1(t)}{\partial I_3(t)} & \frac{\partial V_1(t)}{\partial p_1} & \cdots & \frac{\partial V_1(t)}{\partial p_9} \\ \frac{\partial V_1(t+\tau)}{\partial V_1(t)} & \frac{\partial V_1(t+\tau)}{\partial V_2(t)} & \frac{\partial V_1(t+\tau)}{\partial I_3(t)} & \frac{\partial V_1(t+\tau)}{\partial p_1} & \cdots & \frac{\partial V_1(t+\tau)}{\partial p_9} \\ \vdots & \vdots & \vdots & \vdots & \ddots & \vdots \\ \frac{\partial V_1(t+i\tau)}{\partial V_1(t)} & \frac{\partial V_1(t+i\tau)}{\partial V_2(t)} & \frac{\partial V_1(t+i\tau)}{\partial I_3(t)} & \frac{\partial V_1(t+i\tau)}{\partial p_1} & \cdots & \frac{\partial V_1(t+i\tau)}{\partial p_9} \\ \vdots & \vdots & \vdots & \vdots & \ddots & \vdots \\ \frac{\partial V_1(t+(K-1)\tau)}{\partial V_1(t)} & \frac{\partial V_1(t+(K-1)\tau)}{\partial V_2(t)} & \frac{\partial V_1(t+(K-1)\tau)}{\partial I_3(t)} & \frac{\partial V_1(t+(K-1)\tau)}{\partial p_1} & \cdots & \frac{\partial V_1(t+(K-1)\tau)}{\partial p_9} \end{pmatrix}, \tag{9.8}$$

computed with respect to the model variables and parameters. $V_1(t + i\tau)$ denotes the value of the first model variable computed by integrating the model Eq. (9.3) from the time t to $t + i\tau$ using the initial values $\mathbf{x}(t)$ and the model parameters $\mathbf{p}$. The partial derivatives with respect to the model variables are extracted from the solution (i.e. the flow) of the matrix ODE Sec. 6, Eq. (39). Similarly, the partial derivatives with respect to the model parameters are extracted from the solution of Sec. 6, Eq. (40). The observability, dependency, and correlation analysis are based on $\mathrm{D}\mathbf{G}(\mathbf{x}(t), \mathbf{p})$. For simplicity (as in Sec. 8) all variables and parameters are summarized in the vector $\mathbf{w} = (V_1, V_2, I_3, a, b, C_1, C_2, R_1, R_2, R_3, R_\mathrm{NIC}, L)$ of unknowns.

To investigate which quantities (model variables and parameters) are locally observable, as suggested in Sec. 8.II, we consider how small perturbations $\Delta\mathbf{g}$ on the delay reconstruction vector $\mathbf{g}$ map to perturbations

$$\begin{aligned} \Delta\mathbf{w} = \big(&\Delta V_1, \quad \Delta V_2, \quad \Delta I_3, \quad \Delta a, \quad \Delta b, \quad \Delta C_1, \quad \Delta C_2, \quad \Delta R_1, \quad \Delta R_2, \\ &\Delta R_3, \quad \Delta R_\mathrm{NIC}, \quad \Delta L\big) \end{aligned} \tag{9.9}$$

of $\mathbf{w}$ and vice versa. After linearization of Eq. (9.7) the relation between $\Delta\mathbf{g}$ and $\Delta\mathbf{w}$ is given by Sec. 8, Eq. (11),

$$\mathrm{D}\mathbf{G} \cdot \Delta\mathbf{w} = \Delta\mathbf{g} \ . \tag{9.10}$$

The D_N dimensional null space of $\mathrm{D}\mathbf{G}$ contains all $\Delta\mathbf{w}$ which fulfill Sec. 8, Eq. (12),

$$\mathrm{D}\mathbf{G} \cdot \Delta\mathbf{w} = 0 \ . \tag{9.11}$$

If $D_\mathrm{N} \geq 1$, then there exist perturbations $\Delta\mathbf{w} \neq 0$ which do not affect the measured signal $\mathbf{g}$. In this case not all quantities are locally observable and, therefore, cannot be uniquely reconstructed given the measured signal. As described in Sec. 8.II.A the dimension D_N of the null space of $\mathrm{D}\mathbf{G}$ is computed by means of the singular value

decomposition (SVD) Sec. 8, Eq. (8),

$$\mathrm{D}\mathbf{G} = \mathbf{U}\mathbf{S}\mathbf{V}^{\mathrm{tr}} \ , \tag{9.12}$$

where $\mathbf{U}$ and $\mathbf{V}$ are orthogonal matrices and the diagonal elements of the diagonal matrix $\mathbf{S}$ are the singular values $\sigma_1 \geq \sigma_2 \ldots \geq \sigma_{D+N_\mathrm{p}}$. The dimension D_N is then given by the number of vanishing singular values, $\sigma_i = 0$ with $i = D + N_\mathrm{p} - D_\mathrm{N}, \ldots, D + N_\mathrm{p}$, of D$\mathbf{G}$. For the following simulations we used a threshold of $\sim 10^{-13}$ to distinguish between vanishing and not vanishing singular values.

In the experimental setup the values of the potentiometers of the electrical circuit of the Shinriki oscillator Fig. 9.1 are tuned to $R_1 = 22.05\mathrm{k}\Omega$ and $R_2 = 16.92\mathrm{k}\Omega$. The time series of V_1, V_2, and I_3 (see Fig. 9.1) consist of 10^6 samples each and are sampled with a step size of 0.01ms. Every 1000th measured state $\mathbf{x}_\mathrm{dat} = [V_{\mathrm{dat},1}, V_{\mathrm{dat},2}, I_{\mathrm{dat},3}]$ is then used for the analyses to cover a large part of the attractor Fig. 9.4b. In other words, every 10ms a state is extracted from the time series resulting in $N = 1000$ different states in total.

To investigate the observability we first consider histograms of the singular values (see Fig. 9.5) which are computed in the following way:

1. The delay time is fixed to $\tau = 0.01$ms.
2. D$\mathbf{G}$ is computed for the $N = 1000$ different experimental states $\mathbf{x}_\mathrm{dat}$ with $\tau = 0.01$ms using the parameter values from Tab. 9.1 and $R_1 = 22.05\mathrm{k}\Omega$ and $R_2 = 16.92\mathrm{k}\Omega$.
3. For each D$\mathbf{G}$ the $D + N_\mathrm{p} = 12$ singular values σ_i are computed.
4. A histogram of each normalized singular value σ_i/σ_1 is plotted vertically (color coded) at $\tau = 0.01$ms.
5. The procedure is repeated with a slightly increased delay time τ.

One can see that the for all investigated states and independent of τ the two smallest normalized singular values σ_{11}/σ_1 and σ_{12}/σ_1 are of magnitude 10^{-20} and are hence very close to zero. All other singular values are order of magnitude larger. This indicates a $D_\mathrm{N} = 2$ dimensional null space of D$\mathbf{G}$. Therefore, not all quantities are locally observable. The null space of D$\mathbf{G}$ can be spanned by the last $D_\mathrm{N} = 2$ (orthogonal) columns $\mathbf{v}_\mathrm{B}^{(1)}$ and $\mathbf{v}_\mathrm{B}^{(2)}$ of $\mathbf{V}$ (see Sec. 8.II.A.1). Both vectors form a basis of the null space of D$\mathbf{G}$ and are summarized in the $D + N_\mathrm{p} \times D_\mathrm{N} = 12 \times 2$ basis matrix $\mathbf{V}_\mathrm{B} = [\mathbf{v}_\mathrm{B}^{(1)}, \mathbf{v}_\mathrm{B}^{(2)}]$ (see Sec. 8, Eq. (17)). Every quantity w_i is locally observable if the ith element of both $\mathbf{v}_\mathrm{B}^{(1)}$ and $\mathbf{v}_\mathrm{B}^{(2)}$ is zero, i.e. the ith row of $\mathbf{V}_\mathrm{B}$ contains zeros only. In this case every perturbation where $\Delta w_i \neq 0$ of w_i leads to a perturbation $\Delta\mathbf{g} \neq 0$ and, therefore, one would leave the null space of D$\mathbf{G}$.

Instead of considering histograms of the components of $\mathbf{v}_\mathrm{B}^{(1)}$ and $\mathbf{v}_\mathrm{B}^{(2)}$ to identify locally observable quantities, we apply the dependency analysis described in Sec. 8.II.A which, additionally, provides insights about the local dependencies of variables and parameters.

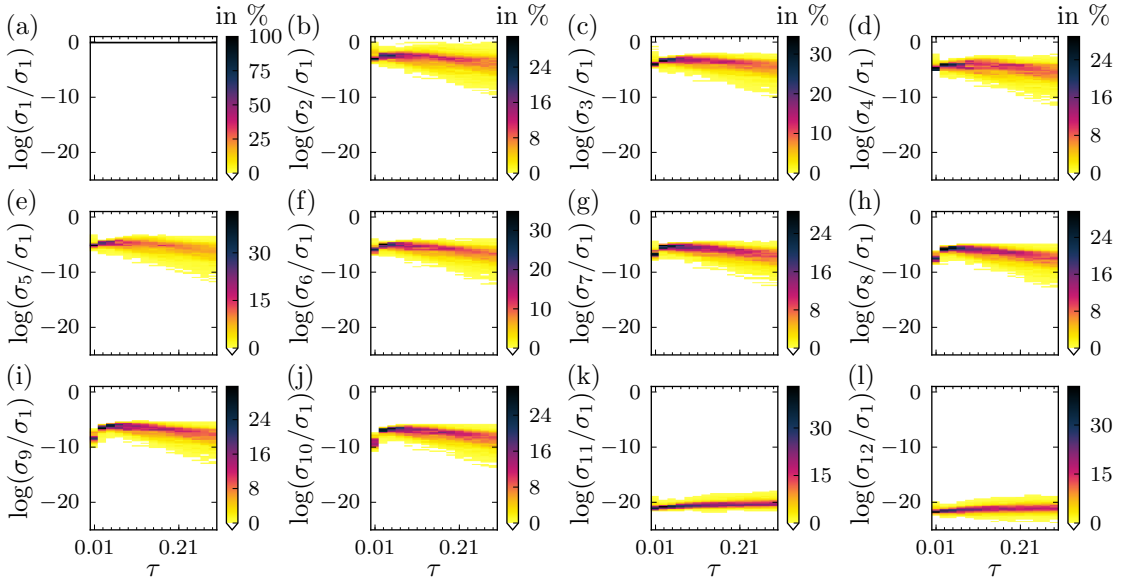

Figure 9.5: Histograms (color coded, vertically plotted) of normalized singular values σ_i/σ_1 of D$\mathbf{G}$, Eq. (9.8), computed based on all $D = 3$ model variables and all $N_\mathrm{p} = 9$ model parameters using the model of the Shinriki oscillator, Eq. (9.3), and the measurement function Eq. (9.6) for different delay times τ and a delay reconstruction dimension of $K = 50$. For each τ the histograms are computed based on $N = 1000$ different experimentally observed states $\mathbf{x}_\mathrm{dat}$ (values for the potentiometers in the circuit Fig. 9.1 and the model Eq. (9.3) are $R_1 = 22.05\mathrm{k}\Omega$ and $R_2 = 16.92\mathrm{k}\Omega$). The two smallest (normalized) singular values σ_{11} and σ_{12} are on average significantly closer to zero than the others which, therefore, indicate a $D_\mathrm{N} = 2$ dimensional null space of D$\mathbf{G}$.

As mentioned in Sec. 8.II.A, the components of the basis vectors derived from the SVD of D$\mathbf{G}$ usually do not contain the information about the local dependencies of model variables and parameters for the case $D_\mathrm{N} > 1$ because either the ith, $i = 1, \ldots, 12$, component of both basis vectors are $v^{(1)}_{\mathrm{B},i} = v^{(2)}_{\mathrm{B},i} = 0$ or $v^{(1)}_{\mathrm{B},i} \neq 0$ and $v^{(2)}_{\mathrm{B},i} \neq 0$. The idea of the dependency analysis is to find new basis vectors of the null space of D$\mathbf{G}$ where each basis vector contains a different pattern of zeros.

We start with Sec. 8, Eq. (17). First we choose both quantities R_1 and L and split D$\mathbf{G}$ into D$\mathbf{G}_1$ and D$\mathbf{G}_2$. D$\mathbf{G}_1$ consists of both columns of D$\mathbf{G}$ which are associated with R_1 and L. D$\mathbf{G}_2$ consists of all other columns. To simplify the discussion we write the quantities associated with the components of the basis vectors in brackets, e.g.

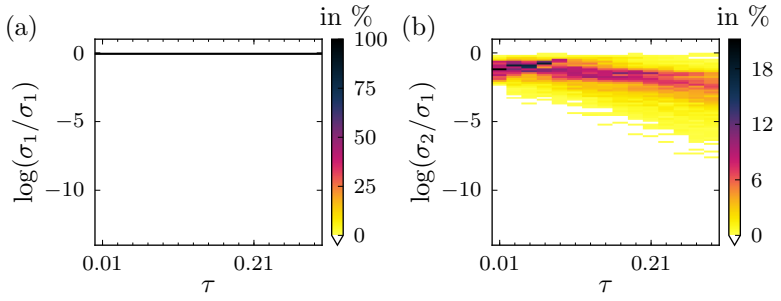

Figure 9.6: Histograms (color coded, vertically plotted) of normalized singular values σ_i/σ_1 of $\mathbf{V}_{\mathrm{B},1}$, Eq. (9.13), using the model of the Shinriki oscillator, Eq. (9.3). The setup (states, measurement function, delay reconstruction dimension, etc.) is the same as in Fig. 9.5. Since the smallest (normalized) singular value is larger than zero for all investigated states and τ, the inverse of $\mathbf{V}_{\mathrm{B},1}$ is unique and Sec. 8, Eq. (19) can be evaluated.

$v^{(2)}_{\mathrm{B},5} = v^{(2)}_{\mathrm{B}}(w_5) = v^{(2)}_{\mathrm{B}}(b)$. We also split $\mathbf{V}_{\mathrm{B}}$ into

$$\mathbf{V}_{\mathrm{B},1} = \begin{pmatrix} v^{(1)}_{\mathrm{B}}(R_1) & v^{(2)}_{\mathrm{B}}(R_1) \\ v^{(1)}_{\mathrm{B}}(L) & v^{(2)}_{\mathrm{B}}(L) \end{pmatrix} \quad \text{and} \quad \mathbf{V}_{\mathrm{B},2} = \begin{pmatrix} v^{(1)}_{\mathrm{B}}(V_1) & v^{(2)}_{\mathrm{B}}(V_1) \\ v^{(1)}_{\mathrm{B}}(V_2) & v^{(2)}_{\mathrm{B}}(V_2) \\ v^{(1)}_{\mathrm{B}}(I_3) & v^{(2)}_{\mathrm{B}}(I_3) \\ v^{(1)}_{\mathrm{B}}(a) & v^{(2)}_{\mathrm{B}}(a) \\ v^{(1)}_{\mathrm{B}}(b) & v^{(2)}_{\mathrm{B}}(b) \\ v^{(1)}_{\mathrm{B}}(C_1) & v^{(2)}_{\mathrm{B}}(C_1) \\ v^{(1)}_{\mathrm{B}}(C_2) & v^{(2)}_{\mathrm{B}}(C_2) \\ v^{(1)}_{\mathrm{B}}(R_2) & v^{(2)}_{\mathrm{B}}(R_2) \\ v^{(1)}_{\mathrm{B}}(R_3) & v^{(2)}_{\mathrm{B}}(R_3) \\ v^{(1)}_{\mathrm{B}}(R_{\mathrm{NIC}}) & v^{(2)}_{\mathrm{B}}(R_{\mathrm{NIC}}) \end{pmatrix}, \tag{9.13}$$

where $\mathbf{V}_{\mathrm{B},1}$ consists of the rows of $\mathbf{V}_{\mathrm{B}}$ associated with R_1 and L and $\mathbf{V}_{\mathrm{B},2}$ consists of all remaining rows. To evaluate Sec. 8, Eq. (19), the inverse of the square matrix $\mathbf{V}_{\mathrm{B},1}$ is required. We verify the unique invertibility of $\mathbf{V}_{\mathrm{B},1}$ by considering histograms of both (normalized) singular values of $\mathbf{V}_{\mathrm{B},1}$. The histograms shown in Fig. 9.6 are computed based on the same state vectors (and hence Jacobian matrices D$\mathbf{G}$), delay reconstruction dimension K, measurement function, and delay times τ as in Fig. 9.5. The smallest (normalized) singular value σ_2/σ_1 is of order of magnitude 1 to 10^{-5} and, hence, larger than zero. Therefore, $\mathbf{V}_{\mathrm{B},1}$ is uniquely invertible and $\widetilde{\mathbf{V}}'_{\mathrm{B}}$ in Sec. 8, Eq. (19) can be evaluated. Next, the columns of $[\mathrm{D}\mathbf{G}_1, \mathrm{D}\mathbf{G}_2]$ are reordered to obtain D$\mathbf{G}$ again.

We apply the same reordering to the rows of $\widetilde{\mathbf{V}}'_{\mathrm{B}}$ and obtain the new matrix

$$\widetilde{\mathbf{V}}_{\mathrm{B}} = \begin{pmatrix} \widetilde{v}_{\mathrm{B}}^{(1)}(V_1) & \widetilde{v}_{\mathrm{B}}^{(2)}(V_1) \\ \widetilde{v}_{\mathrm{B}}^{(1)}(V_2) & \widetilde{v}_{\mathrm{B}}^{(2)}(V_2) \\ \widetilde{v}_{\mathrm{B}}^{(1)}(I_3) & \widetilde{v}_{\mathrm{B}}^{(2)}(I_3) \\ \widetilde{v}_{\mathrm{B}}^{(1)}(a) & \widetilde{v}_{\mathrm{B}}^{(2)}(a) \\ \widetilde{v}_{\mathrm{B}}^{(1)}(b) & \widetilde{v}_{\mathrm{B}}^{(2)}(b) \\ \widetilde{v}_{\mathrm{B}}^{(1)}(C_1) & \widetilde{v}_{\mathrm{B}}^{(2)}(C_1) \\ \widetilde{v}_{\mathrm{B}}^{(1)}(C_2) & \widetilde{v}_{\mathrm{B}}^{(2)}(C_2) \\ \widetilde{v}_{\mathrm{B}}^{(1)}(R_1) & \widetilde{v}_{\mathrm{B}}^{(2)}(R_1) \\ \widetilde{v}_{\mathrm{B}}^{(1)}(R_2) & \widetilde{v}_{\mathrm{B}}^{(2)}(R_2) \\ \widetilde{v}_{\mathrm{B}}^{(1)}(R_3) & \widetilde{v}_{\mathrm{B}}^{(2)}(R_3) \\ \widetilde{v}_{\mathrm{B}}^{(1)}(R_{\mathrm{NIC}}) & \widetilde{v}_{\mathrm{B}}^{(2)}(R_{\mathrm{NIC}}) \\ \widetilde{v}_{\mathrm{B}}^{(1)}(L) & \widetilde{v}_{\mathrm{B}}^{(2)}(L) \end{pmatrix} = \begin{pmatrix} \widetilde{v}_{\mathrm{B}}^{(1)}(V_1) & \widetilde{v}_{\mathrm{B}}^{(2)}(V_1) \\ \widetilde{v}_{\mathrm{B}}^{(1)}(V_2) & \widetilde{v}_{\mathrm{B}}^{(2)}(V_2) \\ \widetilde{v}_{\mathrm{B}}^{(1)}(I_3) & \widetilde{v}_{\mathrm{B}}^{(2)}(I_3) \\ \widetilde{v}_{\mathrm{B}}^{(1)}(a) & \widetilde{v}_{\mathrm{B}}^{(2)}(a) \\ \widetilde{v}_{\mathrm{B}}^{(1)}(b) & \widetilde{v}_{\mathrm{B}}^{(2)}(b) \\ \widetilde{v}_{\mathrm{B}}^{(1)}(C_1) & \widetilde{v}_{\mathrm{B}}^{(2)}(C_1) \\ \widetilde{v}_{\mathrm{B}}^{(1)}(C_2) & \widetilde{v}_{\mathrm{B}}^{(2)}(C_2) \\ 1 & 0 \\ \widetilde{v}_{\mathrm{B}}^{(1)}(R_2) & \widetilde{v}_{\mathrm{B}}^{(2)}(R_2) \\ \widetilde{v}_{\mathrm{B}}^{(1)}(R_3) & \widetilde{v}_{\mathrm{B}}^{(2)}(R_3) \\ \widetilde{v}_{\mathrm{B}}^{(1)}(R_{\mathrm{NIC}}) & \widetilde{v}_{\mathrm{B}}^{(2)}(R_{\mathrm{NIC}}) \\ 0 & 1 \end{pmatrix} = \begin{bmatrix} \widetilde{\mathbf{v}}_{\mathrm{B}}^{(1)} & \widetilde{\mathbf{v}}_{\mathrm{B}}^{(2)} \end{bmatrix} \quad (9.14)$$

which fulfills Sec. 8, Eq. (20), and consists of the two column vectors $\widetilde{\mathbf{v}}_{\mathrm{B}}^{(1)}$ and $\widetilde{\mathbf{v}}_{\mathrm{B}}^{(2)}$. One can already see that due to the identity matrix in $\widetilde{\mathbf{V}}'_{\mathrm{B}}$ (see Sec. 8, Eq. (19)), and hence the ones and zeros in $\widetilde{\mathbf{V}}_{\mathrm{B}}$, both vectors $\widetilde{\mathbf{v}}_{\mathrm{B}}^{(1)}$ and $\widetilde{\mathbf{v}}_{\mathrm{B}}^{(2)}$ do not have the same pattern of zero and non-zero elements. Therefore, $\widetilde{\mathbf{v}}_{\mathrm{B}}^{(1)}$ and $\widetilde{\mathbf{v}}_{\mathrm{B}}^{(2)}$ are linear independent and form a new basis for the null space of D$\mathbf{G}$. Every perturbation $\Delta\mathbf{w}$ which is an element of the null space of D$\mathbf{G}$, i.e. fulfills Eq. (9.11), can be expressed as a linear combination

$$\Delta\mathbf{w} = a_1\widetilde{\mathbf{v}}_{\mathrm{B}}^{(1)} + a_2\widetilde{\mathbf{v}}_{\mathrm{B}}^{(2)} \ , \quad (9.15)$$

where $a_1, a_2 \in \mathbb{R}$. Using the basis vectors directly provided by the SVD of D$\mathbf{G}$ the same perturbation can be expressed as a linear combination

$$\Delta\mathbf{w} = b_1\mathbf{v}_{\mathrm{B}}^{(1)} + b_2\mathbf{v}_{\mathrm{B}}^{(2)} \ , \quad (9.16)$$

where $b_1, b_2 \in \mathbb{R}$. A substitution $\mathbf{w} \to \mathbf{w} + \Delta\mathbf{w}$ in the model Eq. (9.3) does not change the measured signal $\mathbf{g}$.

To reveal, which quantities are locally observable and the local dependencies between the quantities, we consider histograms of the components of $\widetilde{\mathbf{v}}_{\mathrm{B}}^{(1)}$ and $\widetilde{\mathbf{v}}_{\mathrm{B}}^{(2)}$. The histograms shown in Fig. 9.7a and Fig 9.7b are computed for the same experimentally observed states $\mathbf{x}_{\mathrm{dat}}$, delay reconstruction dimension $K = 50$, and different delay times τ as previously.

For all investigated states and τ perturbations $\Delta\mathbf{w}$ in the null space of D$\mathbf{G}$ are given

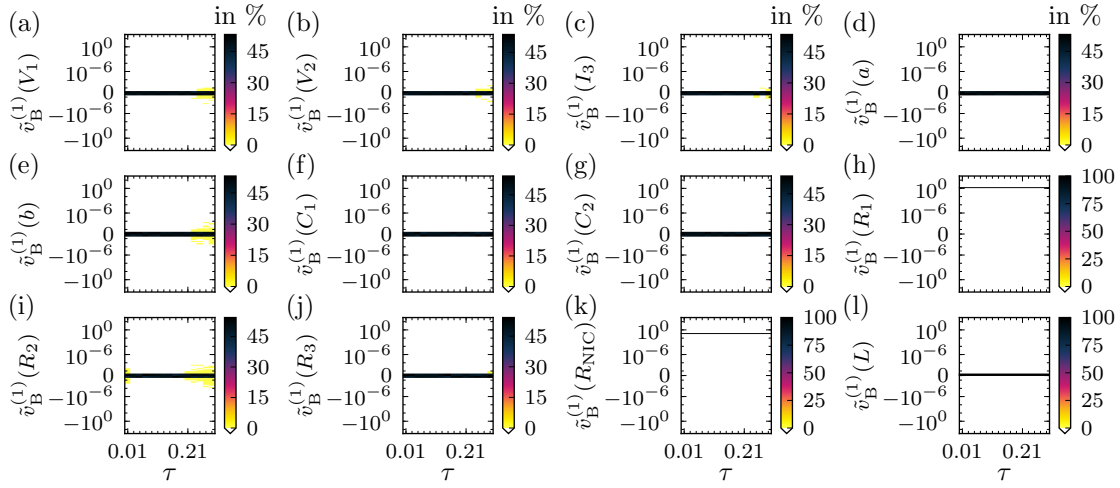

(a) Components of $\widetilde{\mathbf{v}}_{\mathrm{B}}^{(1)}$

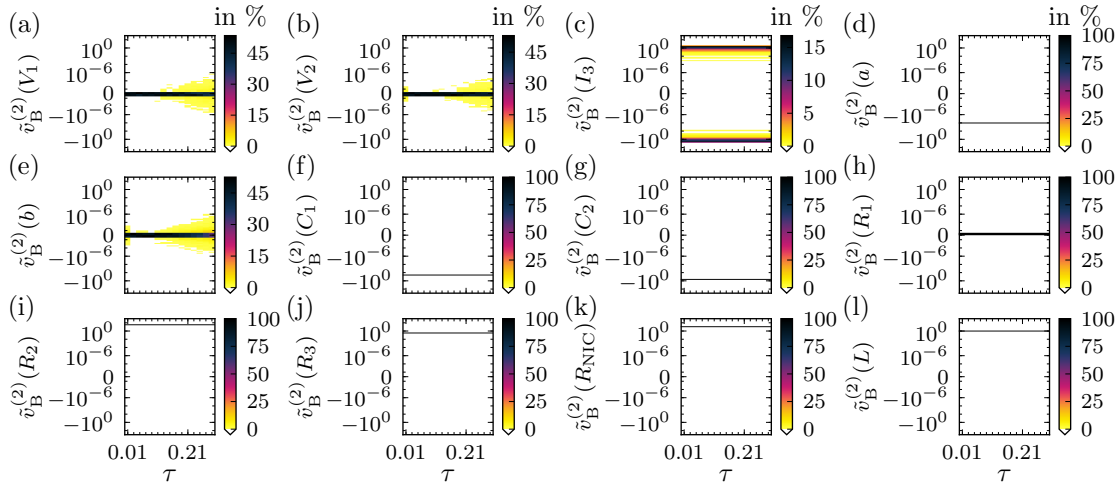

(b) Components of $\widetilde{\mathbf{v}}_{\mathrm{B}}^{(2)}$

Figure 9.7: Histograms (color coded, vertically plotted) of the components of the two new basis vectors $\widetilde{\mathbf{v}}_{\mathrm{B}}^{(1)}$ (Fig. a) and $\widetilde{\mathbf{v}}_{\mathrm{B}}^{(2)}$ (Fig. b) from Eq. (9.14) spanning the null space of D$\mathbf{G}$. The setup (states, measurement function, delay reconstruction dimension, etc.) is the same as in Fig. 9.5. Since the components of both basis vectors associated with V_1, V_2, and b are close to zero for most investigated states and τ, only these quantities are locally observable.

by Eq. (9.15) and have the structure

$$\begin{pmatrix} \Delta V_1 \\ \Delta V_2 \\ \Delta I_3 \\ \Delta a \\ \Delta b \\ \Delta C_1 \\ \Delta C_2 \\ \Delta R_1 \\ \Delta R_2 \\ \Delta R_3 \\ \Delta R_{\mathrm{NIC}} \\ \Delta L \end{pmatrix} = a_1 \begin{pmatrix} 0 \\ 0 \\ 0 \\ 0 \\ 0 \\ 0 \\ 0 \\ * \\ 0 \\ 0 \\ * \\ 0 \end{pmatrix} + a_2 \begin{pmatrix} 0 \\ 0 \\ * \\ * \\ 0 \\ * \\ * \\ 0 \\ * \\ * \\ * \\ * \end{pmatrix} . \tag{9.17}$$

A '0' means that this component is numerically zero (i.e. within the interval $[-10^{-10}, 10^{-10}]$) and '$*$' means that this component is non-zero for (almost) all investigated states and τ (see Fig. 9.7). Equation (9.17) contains useful information about the local observability and for state and parameter estimation. Since for every a_1 and a_2 it is $\Delta V_1 = \Delta V_2 = \Delta b = 0$, a variation of V_1, V_2, and b is only possible by leaving the null space of D$\mathbf{G}$ which, therefore, would lead to a perturbation of the measured signal $\mathbf{g}$ ($\Delta\mathbf{g} \neq 0$ in Eq. (9.10)). Hence, V_1, V_2, and b are locally observable. All other quantities are not locally observable, i.e. they are locally redundant. As pointed out in Sec. 8.II.A: (i) the columns of D$\mathbf{G}$ associated with non-zero elements in $\widetilde{\mathbf{v}}_{\mathrm{B}}^{(1)}$, namely R_1 and R_{NIC}, are linear dependent. (ii) the columns of D$\mathbf{G}$ associated with non-zero elements in $\widetilde{\mathbf{v}}_{\mathrm{B}}^{(2)}$, namely I_3, a, C_1, C_2, R_2, R_3, R_{NIC} and L, are collinear.

In contrast to $\widetilde{\mathbf{v}}_{\mathrm{b}}^{(1)}$ and $\widetilde{\mathbf{v}}_{\mathrm{b}}^{(2)}$ (where we know in advance that $\widetilde{v}_{\mathrm{B}}^{(1)}(R_1) = \widetilde{v}_{\mathrm{B}}^{(2)}(L) = 1$ and $\widetilde{v}_{\mathrm{B}}^{(1)}(L) = \widetilde{v}_{\mathrm{B}}^{(2)}(R_1) = 0$) the orthogonal basis vectors $\mathbf{v}_{\mathrm{b}}^{(1)}$ and $\mathbf{v}_{\mathrm{b}}^{(2)}$ have a less predetermined direction in the null space of D$\mathbf{G}$. The structure of Eq. (9.16) reads

$$\begin{pmatrix} \Delta V_1 \\ \Delta V_2 \\ \Delta I_3 \\ \Delta a \\ \Delta b \\ \Delta C_1 \\ \Delta C_2 \\ \Delta R_1 \\ \Delta R_2 \\ \Delta R_3 \\ \Delta R_{\mathrm{NIC}} \\ \Delta L \end{pmatrix} = b_1 \begin{pmatrix} 0 \\ 0 \\ * \\ * \\ 0 \\ * \\ * \\ * \\ * \\ * \\ * \\ * \end{pmatrix} + b_2 \begin{pmatrix} 0 \\ 0 \\ * \\ * \\ 0 \\ * \\ * \\ * \\ * \\ * \\ * \\ * \end{pmatrix} . \tag{9.18}$$

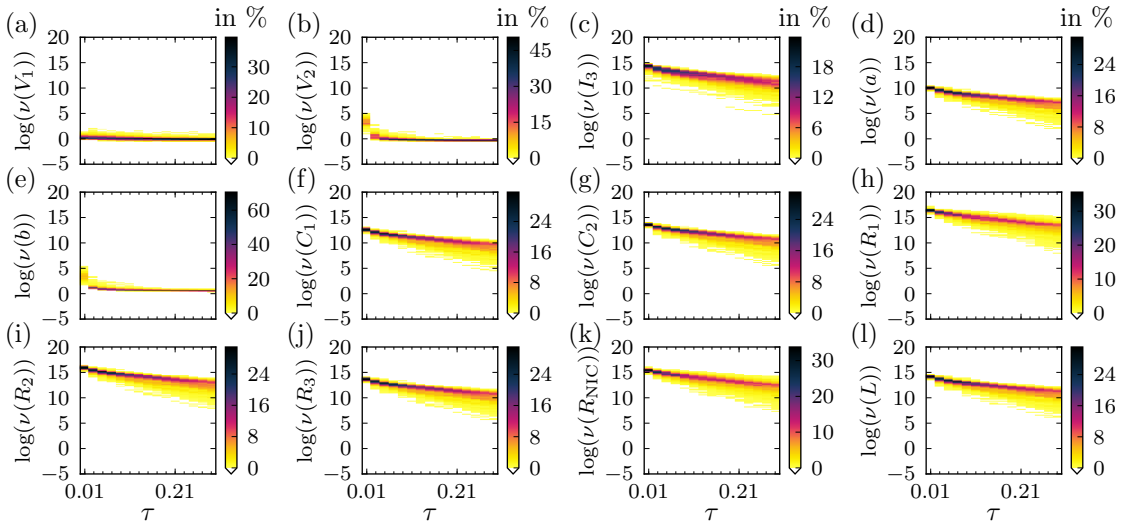

Figure 9.8: Histograms (color coded, vertically plotted) of the uncertainties $\nu(w_i)$, Sec. 8, Eq. (30), computed based on all $D = 3$ model variables and all $N_\mathrm{p} = 9$ model parameters of the Shinriki oscillator Eq. (9.3). The setup (states, measurement function, delay reconstruction dimension, etc.) is the same as in Fig. 9.5. The small uncertainties of V_1, V_2, and b indicate a much better observability of V_1, V_2, and b than of the other quantities.

and can be obtained by considering histograms of the components of $\mathbf{v}_\mathrm{b}^{(1)}$ and $\mathbf{v}_\mathrm{b}^{(2)}$ (histograms not shown here). To identify locally observable quantities it is enough to consider the components of $\mathbf{v}_\mathrm{b}^{(1)}$ and $\mathbf{v}_\mathrm{b}^{(2)}$ instead of $\widetilde{\mathbf{v}}_\mathrm{b}^{(1)}$ and $\widetilde{\mathbf{v}}_\mathrm{b}^{(2)}$ because the components of $\mathbf{v}_\mathrm{b}^{(1)}$ and $\mathbf{v}_\mathrm{b}^{(2)}$ associated with V_1, V_2, and b are also numerically zero for all states and τ.

Next, we consider the measure of uncertainty $\nu(w_i)$, defined in Sec. 8, Eq. (30) (or Sec. 5, Eq. (10), or Sec. 6, Eq. (27)), for all $D = 3$ model variables and all $N_\mathrm{p} = 9$ model parameters. The larger $\nu(w_i)$ is, the worse the quantity w_i can be reconstructed. Using the same states, delay times τ, delay reconstruction dimension $K = 50$, measurement function Eq. (9.6), etc., histograms of $\nu(w_i)$ for the Shinriki oscillator are shown in Fig. 9.8. The uncertainties of V_1, V_2, and b are of magnitudes 1 to 10 (at least for larger τ) and hence orders of magnitude smaller than the uncertainties of the other quantities (which are of magnitude 10^{10} to 10^{15}). This indicates a good observability of V_1, V_2, and b and a very bad observability of all other quantities. Therefore, this is consistent with the result obtained by considering basis vectors of the null space of $\mathrm{D}\mathbf{G}$.

If one wants to estimate model states and parameters from a V_1 time series, then it is not possible to uniquely estimate the locally redundant quantities. It is only possible to uniquely estimate V_1, V_2, and b. Hence, it is desirable to remove the redundancy of as many quantities as possible and make them locally observable. The more quantities are observable the more quantities can be uniquely estimated given the V_1 time series and the less quantities have to be determined from another source (literature, estimated

using another experimental setup, ...). If one fixes a quantity to a certain value and does not want to estimate it, then one prevents variations of this quantity. For example, if one removes a from the list of quantities to estimate, then one prevents variations of this quantity by $\Delta a = 0$. According to Eq. (9.17) this sets $a_2 = 0$ and reduces the dimension of the null space of D$\mathbf{G}$ to $D_{\mathrm{N}} = 1$. Furthermore, this sets $\Delta I_3 = \Delta C_1 = \Delta C_2 = \Delta R_2 = \Delta R_3 = \Delta L = 0$ for all states independent off τ and, therefore, makes I_3, C_1, C_2, R_2, R_3, and L locally observable because with perturbations of these quantities one would leave the null space of D$\mathbf{G}$. R_1 and R_{NIC} are still locally redundant. Removing R_{NIC} from the list of quantities to estimate, i.e. setting $\Delta R_{\mathrm{NIC}} = 0$, sets $a_1 = 0$ (and hence $\Delta R_1 = 0$) and makes R_1 locally observable. Then, the null space of D$\mathbf{G}$ contains only the null vector $\Delta\mathbf{w} = 0$ and is zero dimensional. All quantities are then locally observable, i.e. could in principle be estimated from a V_1 time series.

Since the pattern of zero and non-zero elements of $\mathbf{v}_{\mathrm{B}}^{(1)}$ and $\mathbf{v}_{\mathrm{B}}^{(2)}$ are equal (see Eq. (9.16) and Eq. (9.18)), Eq. (9.16) does not provide the information which locally not observable quantities could be removed from the estimation problem to make all remaining quantities locally observable. This illustrates one key advantage of considering the basis vectors $\widetilde{\mathbf{v}}_{\mathrm{B}}^{(1)}$ and $\widetilde{\mathbf{v}}_{\mathrm{B}}^{(2)}$ instead of $\mathbf{v}_{\mathrm{B}}^{(1)}$ and $\mathbf{v}_{\mathrm{B}}^{(1)}$.

To verify that $D_{\mathrm{N}} = 0$ for all states and τ we consider histograms of the (normalized) singular values of D$\mathbf{G}$ (based on the same states, delay time τ , etc. as previously) where the Jacobian D$\mathbf{G}$ is computed with respect to all $D = 3$ model variables and all parameters except a and R_{NIC}. Figure 9.9 shows that the smallest (normalized) singular value σ_{10}/σ_1 is of magnitude 10^{-6} to 10^{-10} and hence of magnitudes greater than the smallest (normalized) singular value shown in Fig. 9.5. Hence, D$\mathbf{G}$ is indeed non-singular and has a zero dimensional null space for all investigated states and τ.

Figure 9.10 shows histograms of the uncertainties $\nu(w_i)$ (Sec. 8, Eq. (30)) computed for the same states and τ as in Fig. 9.8, but only based on all model variables and all parameters except a and R_{NIC} ($N_{\mathrm{p}} = 7$). The uncertainties $\nu(V_1)$, $\nu(V_2)$, and $\nu(b)$ are of the same order of magnitude as in Fig. 9.8 (where all $N_{\mathrm{p}} = 9$ parameters are considered). All other uncertainties are orders of magnitude smaller than in Fig. 9.8 and of comparable order of magnitude as $\nu(V_1)$, $\nu(V_2)$, and $\nu(b)$. Accordingly, the observability of I_3, C_1, C_2, R_1, R_2, R_3, and L has improved significantly and is comparable to V_1, V_2, and b.

Of course, removing a and R_{NIC} from the list of quantities to estimate is not the only possibility to make all remaining quantities locally observable. One can remove any quantities until it is $a_1 = a_2 = 0$ in Eq. (9.17) and Eq. (9.15) (and therefore $D_{\mathrm{N}} = 0$). Since the null space of D$\mathbf{G}$ is $D_{\mathrm{N}} = 2$ dimensional, at least two quantities have to be removed. For example, removing C_1 and R_3 is not enough to make all remaining quantities locally observable because setting $\Delta C_1 = \Delta R_3 = 0$ sets $a_2 = 0$, but a_1 can still have an arbitrary value. Hence, the redundancy of R_1 and R_{NIC} would still be present.

This redundancy can be directly found in the model equations Eq. (9.3). Both, R_1 and R_{NIC} only appear in the expression $p_{\mathrm{red}} := 1/R_{\mathrm{NIC}} - 1/R_1$. It is clear that only p_{red} can be uniquely estimated, but not R_1 and R_{NIC} (in this case independent of the measurement function). Substituting the expression containing the two parameters R_1 and R_{NIC} with

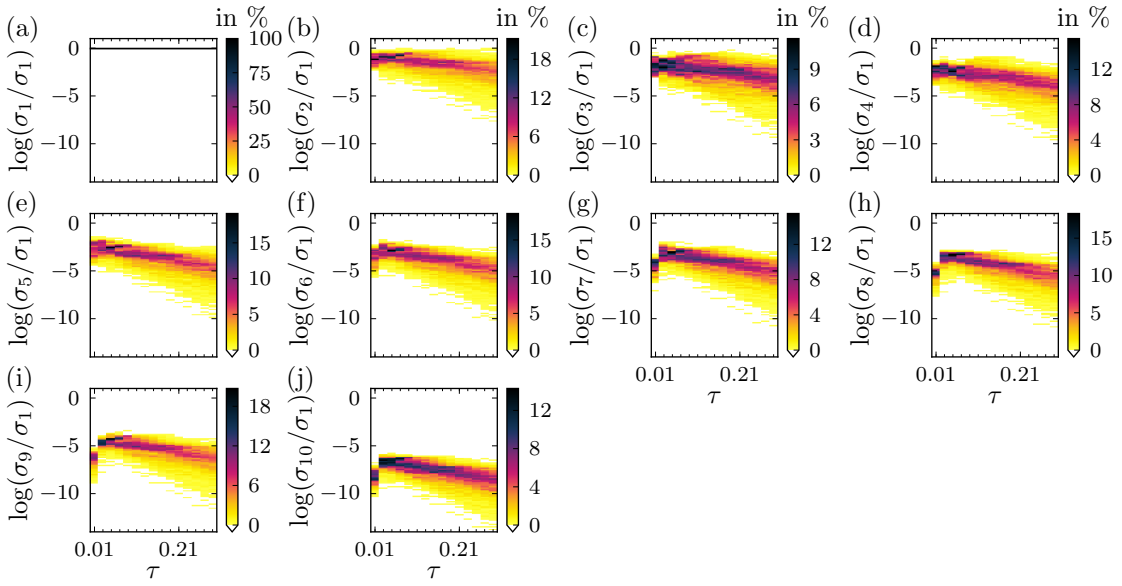

Figure 9.9: Histograms of (normalized) singular values σ_i/σ_1 of D**G** computed based on all model variables and all parameters except a and R_{NIC} of the Shinriki oscillator, Eq. (9.3). The setup (states, measurement function, delay reconstruction dimension, etc.) is the same as in Fig. 9.5. Since the smallest (normalized) singular value is larger than zero for all investigated states and τ, D**G** is non-singular and has a zero dimensional null space. Therefore, the quantities V_1, V_2, I_3, b, C_1, C_2, R_1, R_2, R_3, and L are locally observable.

p_{red} reduces the number of model parameters and, therefore, the complexity of the model.

For $a_2 = 0$ in Eq. (9.15) and Eq. (9.17) small variations of R_1 and R_{NIC} are related (by dividing the 8th by the 11th row in Eq. (9.15)) via

$$\Delta R_1 = \frac{\widetilde{v}_{\mathrm{B}}^{(1)}(R_1)}{\widetilde{v}_{\mathrm{B}}^{(1)}(R_{\mathrm{NIC}})} \Delta R_{\mathrm{NIC}} \ . \tag{9.19}$$

Since $\widetilde{v}_{\mathrm{B}}^{(1)}(R_1), \widetilde{v}_{\mathrm{B}}^{(1)}(R_{\mathrm{NIC}}) > 0$ and hence $\widetilde{v}_{\mathrm{B}}^{(1)}(R_1)/\widetilde{v}_{\mathrm{B}}^{(1)}(R_{\mathrm{NIC}}) > 0$ for all states and τ (see Fig. 9.7a), a variation $\Delta R_1 > 0$ can be compensated with a variation $\Delta R_{\mathrm{NIC}} > 0$ which keeps p_{red} constant. We summarize the quantities associated with non-zero elements of $\widetilde{\mathbf{v}}_{\mathrm{B}}^{(1)}$, namely R_1 and R_{NIC}, in the first subset of redundant quantities.

For the case $a_1 = 0$ only I_3, a, C_1, C_2, R_2, R_3, R_{NIC}, and L can be varied, where the variations are controlled only by a_2. Therefore, these quantities (associated with non-zero elements of $\widetilde{\mathbf{v}}_{\mathrm{B}}^{(2)}$) are summarized in the second subset of redundant quantities. A variation of quantities in the first subset of redundant quantities is possible keeping the quantities in the second subset unchanged (except R_{NIC} because R_{NIC} is an element of both sets) and vice versa.

To find distinct subsets of redundant quantities, the considered basis vectors spanning

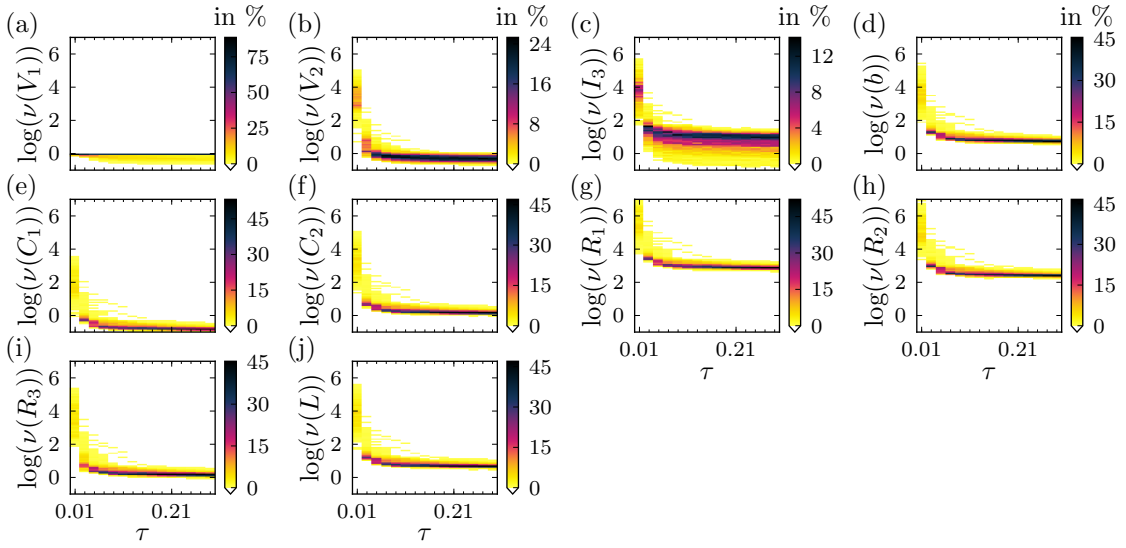

Figure 9.10: Histograms (color coded, vertically plotted) of the uncertainties $\nu(w_i)$, Sec. 8, Eq. (30), computed based on all $D = 3$ model variables and all model parameters except a and R_{NIC} of the Shinriki oscillator Eq. (9.3). The setup (states, measurement function, delay reconstruction dimension, etc.) is the same as in Fig. 9.8. Compared to Fig. 9.8, the uncertainties $\nu(w_i)$ of I_3, C_1, C_2, R_1, R_2, R_3, and L are orders of magnitude smaller indicating a much better observability beside V_1, V_2, and b.

the null space must have a different pattern of non-zero components (as $\widetilde{\mathbf{v}}_{\mathrm{B}}^{(1)}$ and $\widetilde{\mathbf{v}}_{\mathrm{B}}^{(2)}$ have, but not $\mathbf{v}_{\mathrm{B}}^{(1)}$ and $\mathbf{v}_{\mathrm{B}}^{(2)}$ have, see Eq. (9.17)). Otherwise all subsets would contain the same quantities (namely all locally not observable quantities).

9.3 Correlation analysis for the Shinriki Oscillator

In Sec. 9.2 we considered the observability of all $D = 3$ model variables and $N_{\mathrm{p}} = 9$ model parameters of the model of the Shinriki oscillator Eq. (9.3) assuming the first model variable V_1 is measured, Eq. (9.6). All considered statistics are based on $N = 1000$ different experimentally observed states and different delay times τ using the parameter values $R_1 = 22.05\mathrm{k}\Omega$ and $R_2 = 16.92\mathrm{k}\Omega$ in the circuit Fig. 9.1 and in the model. The remaining model parameters are taken from Tab. 9.1.

We observed that only V_1, V_2, and b are locally observable. All other quantities are locally not observable because (i) only variations of V_1, V_2, and b leave the $D_{\mathrm{N}} = 2$ dimensional null space of D$\mathbf{G}$, Eq. (9.11), and (ii) the uncertainties $\nu(V_1)$, $\nu(V_2)$, and $\nu(b)$ are of order of magnitude 1 to 10 (see Fig. 9.8). The uncertainties of all other quantities are of orders of magnitude 10^{10} to 10^{15} and hence considerably larger.

After removing the model parameters a and R_{NIC} from the analyses, the dimension of the null space of D$\mathbf{G}$ got $D_{\mathrm{N}} = 0$ (no vanishing singular values in Fig. 9.9) and the

uncertainties $\nu(w_i)$ of the previously not observable quantities decreased to values of order of magnitude as V_1, V_2, and b (see Fig. 9.10). The conclusion was that then all model variables and parameters, namely V_1, V_2, I_3, b, C_1, C_2, R_1, R_2, R_3, and L are locally observable.

The question to address now is how well these quantities can be reconstructed measuring only V_1, Eq. (9.6). Although the quantities are in principle locally observable, in practice there might still exist an 'almost' redundancy between (some of) them. Therefore, we perform the correlation analysis described in Sec. 8.II.B. The basis of the correlation analysis is that small perturbations $\Delta\mathbf{g}$ on the delay reconstruction vector $\mathbf{g}$, Eq. (9.7), are mapped to perturbations $\Delta\mathbf{w}$, Eq. (9.9) by the approximation (linear relation) Sec. 8, Eq. (7). Assuming that $\Delta\mathbf{g}$ is normally distributed with a zero mean and a covariance matrix Σ_g, Sec. 8, Eq. (24), then $\Delta\mathbf{w}$ is also normally distributed with a zero mean and a covariance matrix Σ_w, Sec. 8, Eq. (25), where Σ_w is given by Sec. 8, Eq. (26). Furthermore, assuming that $\Sigma_\mathrm{g} = \zeta^2 \cdot \mathbb{1}$ with $\zeta \in \mathbb{R}$, the correlation matrix $\boldsymbol{\rho}$ of Σ_w is given by Sec. 8, Eq. (31). An element $\rho_{ij} = \rho(w_i, w_j) \in [-1, 1]$ of the correlation matrix describes the correlation between Δw_i and Δw_j. If $|\rho(w_i, w_j)| = 1$, then there is a linear relation between Δw_i and Δw_j, and therefore between w_i and w_j indicating redundancy. Also the case $|\rho(w_i, w_j)| \approx 1$ might occur indicating almost redundancy.

To investigate if V_1, V_2, I_3, b, C_1, C_2, R_1, R_2, R_3, and L (a and R_NIC are excluded) are observable in practice, we consider the pairwise correlation coefficients $\rho(w_i, w_j)$ of these quantities based on the same (experimentally observed) states, measurement function Eq. (9.6), delay times τ, etc. as in Sec. 9.2. Figure 9.11 shows histograms of all $\rho(w_i, w_j)$, except if the model variables V_1, V_2, and I_3 are involved. In all plots we see that $|\rho(w_i, w_j)| \approx 1$ for many states if the delay times τ is small. For increasing τ it is $|\rho(w_i, w_j)| \approx 1$ for more and more states and for $\tau \geq 0.2$ all coefficients are $\rho(w_i, w_j) = \pm 1$ indicating a redundancy. Therefore, it is likely that state and parameter estimation is still difficult.

Accordingly, we remove two additional parameters, C_1 and R_3, from the analysis and compute the correlation coefficients again, see Fig. 9.12. Compared to Fig 9.11 most coefficients $\rho(w_i, w_j)$ are more uniformly distributed, independent of τ. The correlation between C_2 and L forms an exception because it is $\rho(C_2, L) \approx -1$ for larger τ. Nevertheless, in contrast to the plots in Fig 9.11 the correlation is somewhat less clear. Figure 9.13 shows the uncertainties $\nu(w_i)$, Sec. 8, Eq. (30), for the same quantities as analyzed in Fig. 9.12. On average the uncertainties $\nu(w_i)$ of I_3, b, C_2, R_1, R_2, and L are smaller compared to Fig. 9.10 (where C_1 and R_3 are included). V_1 and V_2 are of the same order of magnitude. Therefore, state and parameter estimation of all model variables and the parameters b, C_2, R_1, R_2, and L from a V_1 time series should provide accurate estimates.

It should be emphasized again that the correlation analysis can help to identify linear relations. A correlation coefficient of $\rho(w_i, w_j) = \pm 1$ indicates a perfect linear relation, but a value $|\rho(w_i, w_j)| < 1$ does not necessarily proof the absence of a perfect linear relation [65].

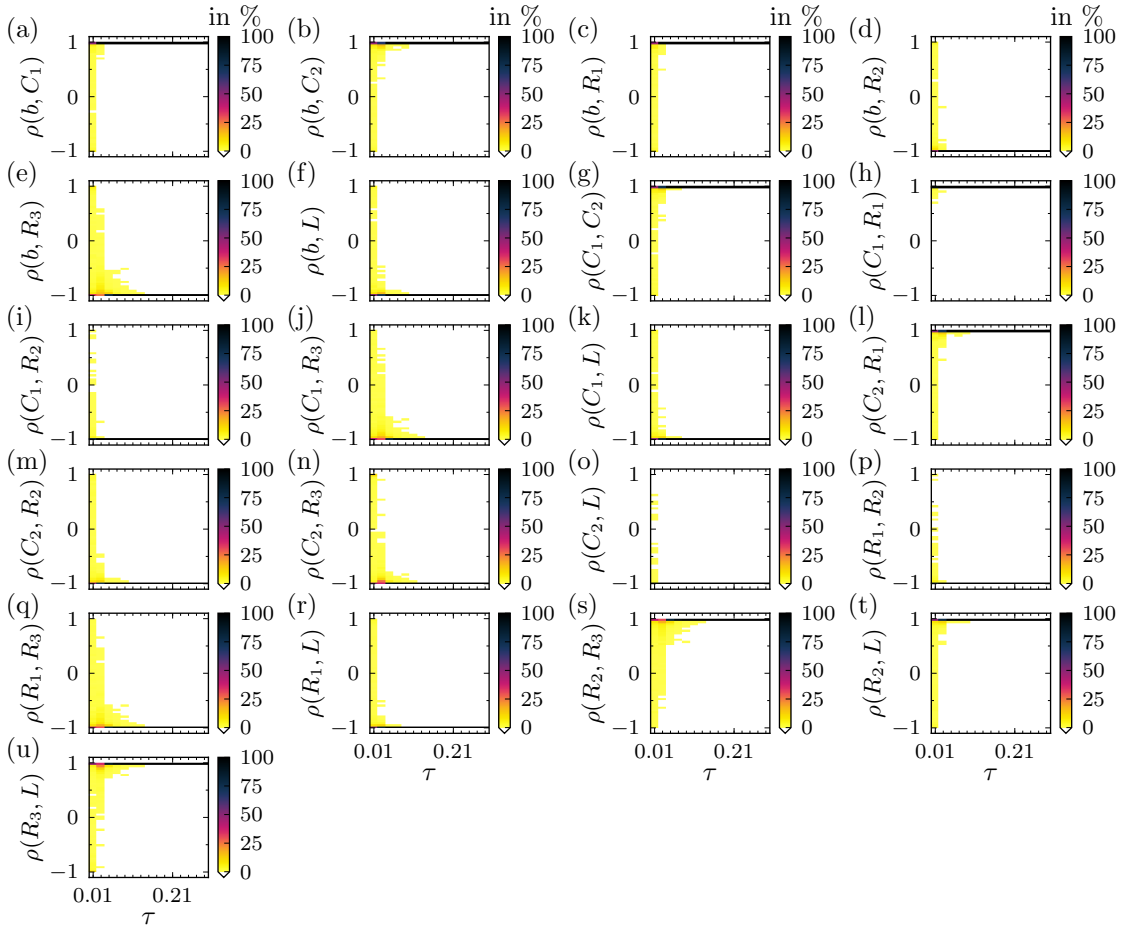

Figure 9.11: Histograms (color coded, vertically plotted) of the correlation coefficients $\rho(w_i, w_j)$, Sec. 8, Eq. (31), computed based on all $D = 3$ model variables and all model parameters except a and R_{NIC} of the Shinriki oscillator Eq. (9.3). The setup (states, measurement function, delay reconstruction dimension, etc.) is the same as in Sec. 9.2. Coefficients where the model variables V_1, V_2, and I_3 are involved are not shown here. Although all considered quantities are in principle locally observable (see Sec. 9.2), we see large correlation coefficients $|\rho(w_i, w_j)| \approx 1$ for many states for smaller delay times τ, and for most states for larger delay times τ indicating redundancy of quantities.

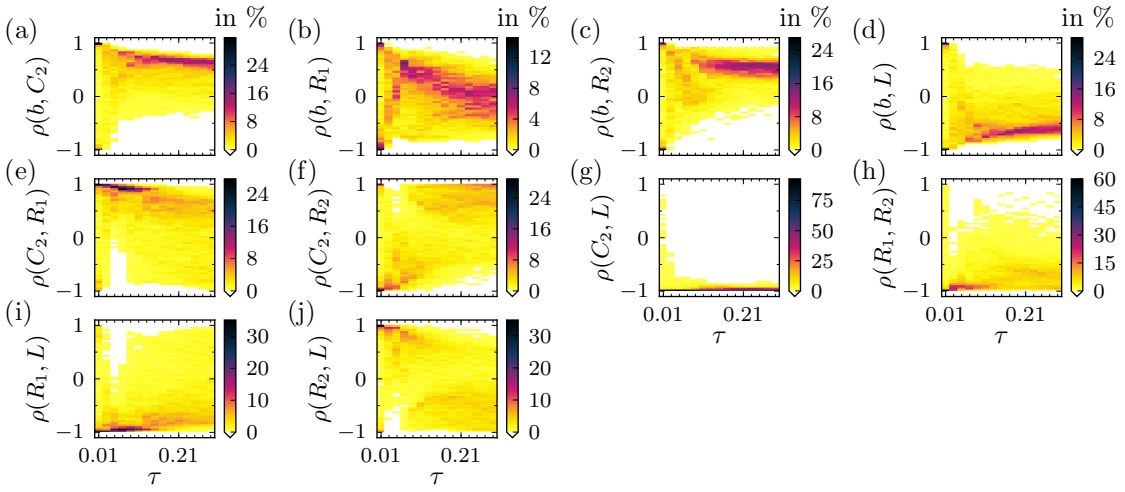

Figure 9.12: Similar to Fig 9.11, but correlation coefficients $\rho(w_i, w_j)$ are computed based on all $D = 3$ model variables and all model parameters except C_1, R_3, a and R_{NIC} of the Shinriki oscillator Eq. (9.3). In contrast to Fig 9.11 in all plots except (g) the coefficients are more equally distributed in the interval $[-1, 1]$, independent of τ. Only $\rho(C_2, L) \approx -1$ for larger τ still indicates a relatively large correlation,

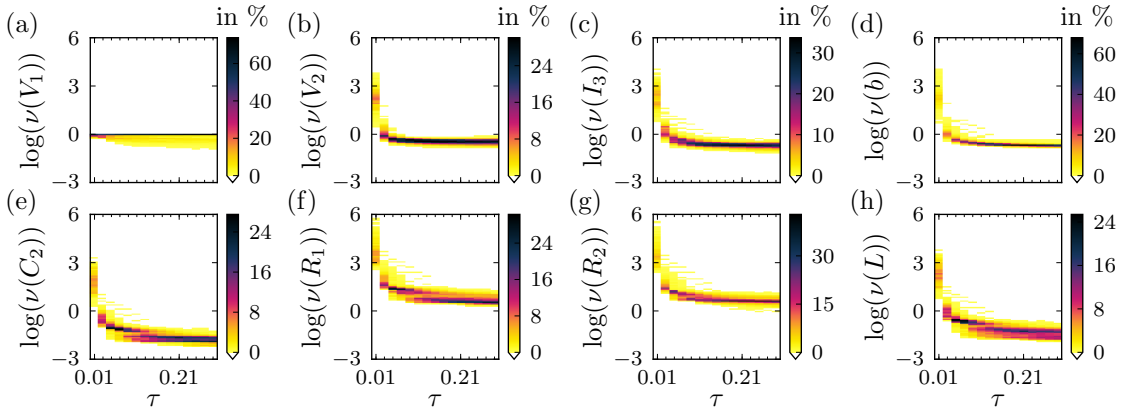

Figure 9.13: Histograms (color coded, vertically plotted) of the uncertainties $\nu(w_i)$, Sec. 8, Eq. (30), computed based on all $D = 3$ model variables and all model parameters except C_1, R_3, a and R_{NIC} of the Shinriki oscillator Eq. (9.3). The setup (states, measurement function, delay reconstruction dimension, etc.) is the same as in Fig. 9.12. Compared to Fig. 9.10, on average the uncertainties $\nu(w_i)$ of I_3, b, C_2, R_1, R_2, and L are smaller indicating a better observability.

9.4 State and parameter estimation using the Shinriki Oscillator

Based on the analyses in Sec. 9.2 it was stated that state and parameter estimation of the Shinriki oscillator, assuming V_1 is measured, (circuit: Fig. 9.1, model: Eq. (9.3)) should in principle be possible, even if all model variables and parameters (except a and R_{NIC}) are to estimate. Nevertheless, the correlation analysis from Sec. 9.3 has shown that large correlations between quantities occur making state and parameter estimation still difficult in practice. Removing the parameters C_1 and R_3 from the list of quantities to estimate decreased the correlations and, therefore, makes state and parameter estimation easier.

In this section results are presented where all model variables and the model parameters b, C_2, R_1, R_2, and L are estimated from an experimentally measured V_1 data time series

$$\{\eta(t_n)\},\ t_n = 0\mathrm{ms}, 0.1\mathrm{ms}, \ldots, 300\mathrm{ms},\ \text{with}\ \eta(t_n) = V_{\mathrm{dat},1}(t_n) \tag{9.20}$$

consisting of 3001 samples. Here, and in the following, the subscript 'dat' of a quantity means that the value of the quantity is experimentally measured. The corresponding measurement function (see Eq. (9.6)) is

$$h(\mathbf{x}) = V_1\ . \tag{9.21}$$

Trajectories $\{V_1(t_m)\}$, $\{V_2(t_m)\}$, $\{I_3(t_m)\}$, $t_m = 0, 0.02\mathrm{ms}, \ldots, 300\mathrm{ms}$, of the model variables are estimated beside the model parameters b, C_2, R_1, R_2, and L using the state an parameter estimation algorithm from Ref. [33]. This algorithm is similar to weak constraint 4D-Var (see Sec. 2.3) and is briefly revised in Sec. 4.2, Sec. 7.IV, and Sec. 8.III. To estimate the variables and parameters the cost function Sec. 8, Eq. (33), is minimized (where $\mathbf{B} = \mathbb{1}$ is the 3×3 identity matrix) with respect to the whole trajectories $\{V_1(t_m)\}$, $\{V_2(t_m)\}$, $\{I_3(t_m)\}$ and the parameters b, C_2, R_1, R_2, and L resulting in 45008 numerical values to estimate. As suggested in Ref. [33] we use the Levenberg-Marquardt [45, 46] algorithm to minimize the cost function. The sparse Jacobian is computed by means of automatic differentiation (see Sec. 4 for a discussion about this method). Furthermore, continuation [13] is used here starting with $\alpha = 0.999$ in the cost function. Then, the estimated solution for the variables and parameters is used as initial guess and the cost function is optimized again with $\alpha = 0.99$. This process is repeated with $\alpha = 0.9$ and $\alpha = 0.5$. The solution obtained with $\alpha = 0.5$ is then considered as the solution of the estimation problem.

The parameter values of the circuit Fig. 9.1 and its estimates are summarized in Tab. 9.2. Not estimated model parameters are fixed to the values of the data column. Estimated parameter values coincide with the values used in the circuit quite well.

Figure 9.14 shows the solutions for the model variables. In Fig. 9.14.a we see that the output of the measurement function h (blue line) matches the data η (light green line). To evaluate the estimated solutions of the model variable, time series $\{V_{\mathrm{dat},2}\}$

Table 9.2: Parameters of the electronic implementation of the Shinriki oscillator. *data:* Values of the circuit Fig. 9.1 used to measure the data time series $\{V_{\mathrm{dat},1}\}$, $\{V_{\mathrm{dat},2}\}$ and $\{I_{\mathrm{dat},3}\}$. *estimated:* Estimated parameter values from an experimentally measured V_1 time series Eq. (9.20). Parameters with an empty entry are not estimated but fixed in the model Eq. (9.3) to values from the 'data' column.

parameter	data	estimated	unit
a	$2.295 \cdot 10^{-5}$		[mA]
b	3.003	3.196	[V^{-1}]
C_1	0.01 ± 0.002		[µF]
C_2	0.1 ± 0.02	0.112	[µF]
R_1	22.05	25.63	[kΩ]
R_2	16.92	16.45	[kΩ]
R_3	0.1 ± 0.005		[kΩ]
R_{NIC}	6.8		[kΩ]
L	0.32	0.307	[H]

and $\{I_{\mathrm{dat},3}\}$ are also measured beside $\{V_{\mathrm{dat},1}\}$ (in the following considered as the 'true solution'), but not provided to the estimation algorithm. Figure 9.14.b to Fig. 9.14.d show the true solutions (red dashed lines) and for $t < 300$ms the estimated solutions (blue lines) for the variables. In the estimation window $t \in [0\mathrm{ms}, 300\mathrm{ms}]$ the estimated solutions of all variables match the corresponding true solutions (shown in the figure only for $t \in [260\mathrm{ms}, 300\mathrm{ms}]$).

The estimated state $[V_1(300\mathrm{ms}), V_2(300\mathrm{ms}), I_3(300\mathrm{ms})]$ at the end of the estimation window at $t = 300$ms is then used as initial state for the prediction. For that, the free running model Eq. (9.3) is integrated from $t = 300$ms to $t = 310$ms (blue lines in Fig 9.14.b to Fig. 9.14.d for $t > 300$ms) using the estimated parameter values from Tab. 9.2. Not estimated parameter values are set to the values from the data column. Roughly the first two oscillations of the prediction match the true solutions. Then, due to the chaotic nature of the oscillator, the prediction diverges from the true solution for all variables.

Usually, the true solution in both the estimation and the prediction window is not available to compare them with the estimated solution of the model variables. Then, comparing the prediction of the measured variable (here V_1) with the data (green line in Fig 9.14.a and red dashed line in Fig 9.14.b) can give a hint about the correctness of the estimated model variables and parameters. If the prediction matches the future data, then it is likely that the estimated solutions of the model variables also match the corresponding (not measured) quantity of the experiment (if redundancies of variables and parameters are identified and removed beforehand). The same holds for the estimated model parameters.

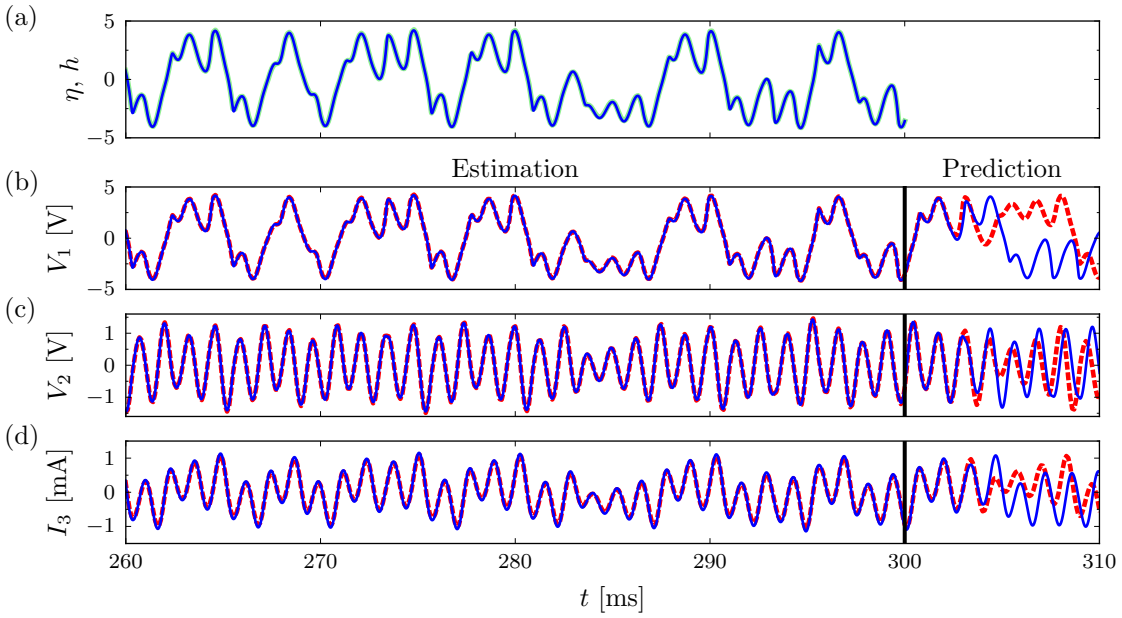

Figure 9.14: States and parameters of the Shinriki oscillator Eq. (9.3) are estimated from an experimentally measured V_1 time series for $t \in [0\text{ms}, 300\text{ms}]$ using the estimation algorithm from Ref. [33] (described e.g. in Sec. 8.III). (a): Data time series $\{\eta(t_n)\}$, Eq. (9.20), (light green line) matches the output of the measurement function h, Eq. (9.21). (b), (c), (d), $t < 300$ms: Estimated solutions of the model variables (blue lines) match the true solutions (red dashed lines). The values of the estimated model parameters b, C_2, R_1, R_2, and L are summarized in Tab. 9.2 and match quite well the values used in the circuit Fig. 9.1. (b), (c), (d), $t > 300$ms: Prediction of the model variables by integrating the free running model Eq. (9.20) (blue lines) matches the experimentally observed true solution (red dashed lines) for roughly two oscillations.

9.5 Discussion

For the analyses in this chapter an electronic circuit of the three dimensional nonlinear Shinriki oscillator was realized.

Before estimating the states and model parameters of an experimentally measured time series of the Voltage V_1 in Fig. 9.1 its observability is investigated in Sec. 9.2. For that, the dependency analysis from Chap. 8 was applied first to different states from the experimentally measured attractor and using different delay times. The analysis is based on the delay reconstruction map Eq. (9.7) mapping from the state and parameter space to the delay coordinates of the measured signal V_1. Small perturbations of states and parameters are mapped to small perturbation of the delay reconstruction vector via the linear relation Eq. (9.10). It turned out that the Jacobian matrix Eq. (9.8) of the

delay reconstruction map is singular for all investigated states and delay times and has a two dimensional null space. Therefore, there exist small perturbations of model states and parameters which do not lead to small perturbations of the delay reconstruction of V_1. Only the quantities V_1, V_2, and b are locally observable because perturbations of these quantities necessarily lead to perturbations of the delay reconstruction vector of V_1. This is in agreement with the uncertainty analysis. The uncertainties of V_1, V_2, and b are much smaller compared with the uncertainties of the other quantities (see Fig. 9.8). All remaining variables and parameters are locally redundant and can not be reconstructed from a V_1 signal.

For successful state and parameter estimation some quantities have to be removed from the estimation problem. The dependency analysis was used to identity R_{NIC} and a which are then removed from the analysis, so that the Jacobian matrix has full rank. In principle all remaining states and parameters should be locally observable. This is confirmed by considering the uncertainty of these quantities which are orders of magnitude smaller as if R_{NIC} and a are included (compare Fig. 9.10 with Fig. 9.8).

To investigate whether the remaining quantities can be uniquely estimated from a V_1 time series in practice, the correlation analysis from Sec. 8 is applied in Sec. 9.3. It was assumed that the small perturbations on the delay reconstruction vector of V_1 are normally distributed. Then, the perturbations on the state and parameters are also normally distributed. Considering the correlation coefficients between model parameters, see Fig. 9.11, we still find that many coefficients are ± 1 for most states and τ indicating an almost linear relationship between the parameters. Removing two further parameters from the analysis, namely C_1 and R_3, leads to correlation coefficients spread more regularly in the interval $[-1, 1]$ (see Fig. 9.12). This indicate weaker linear relations and, hence, a better local observability. The decreased uncertainties in Fig. 9.13 confirm this result.

In Sec. 9.4 it was demonstrated that all model variables and the remaining parameters can be estimated correctly from a V_1 time series using the weak constraint 4D-Var like estimation method from Ref. [33]. Since time series of V_2 and I_3 are also measured, the estimated trajectories can be compared with the measured trajectories. The estimated trajectories match the measured ones and the values of the five estimated model parameters match the corresponding values in the circuit, see Fig. 9.14 and Tab. 9.2.

10 Summary and Discussion

State and parameter estimation and observability with the focus on nonlinear models, mainly ordinary differential equations (ODEs) and iterated maps, are the key issues in this thesis.

Dynamical processes, such as the weather, cardiac dynamics, or electrical circuits, form a large group of systems and play an important role in various fields like systems biology, geosciences, or engineering. These processes have the property that their state can change over time, so that dynamical systems, in general nonlinear, are appropriate mathematical models to describe them. All to often there is the situation that one is interested in the internal states of the process, but its direct measurement is not feasible. Instead, based on (noisy) measured data of the process, one can estimate the state variables and the parameters of the mathematical model using a state and parameter estimation algorithm [1–13]. In the geosciences this procedure is also known as data assimilation [8].

To estimate states and parameters an optimization based estimation method from Ref. [33] is used in this thesis which is similar to a method known in the geosciences as weak-constraint 4D-Var [16, 34, 35, 37, 66, 67]. Since this method is used in Chap. 4, Chap. 7, Chap. 8 and Chap. 9, its probabilistic background based on bayesian statistics is revisited in Chap. 2. An advantage of this method is that errors in the model equations are allowed. In the cost function to minimize both, the deviation between the model output and the data on the one hand and the error in the model equations on the other hand, are penalized.

Of course the estimated model variables and parameters should have a unique solution. If for different states and parameter values the model output would match the data with a similar accuracy, then one would not know which solution is the best in the sense that it describes the underlying process most precisely. Hence, it is desirable to know if the measured signal is sufficient to uniquely reconstruct the model variables and parameters [27–29]. In other words, one is interested in the observability [18–26, 68, 69]. As an introduction to the topic, the observability for linear and nonlinear systems (ODEs and iterated maps) is revisited in Chap. 3.

10.1 Chapter 4: Nonlinear system identification employing automatic differentiation

Many optimization methods, as the Levenberg-Marquardt (LM) algorithm [45, 46] used here to minimize a cost function for estimating model states and parameters, require exact information about derivatives. The focus of Chap. 4, which contains the article

Ref. [70], is on how the derivatives can be computed efficiently.

For example, one could use numerical or symbolical differentiation. However, the former is numerically not exact. Symbolic differentiation by hand and the implementation of derivatives in a computer function, can be sophisticated and error prone. Tools might help at this point, but the function to differentiate must still be available as a single mathematical expression. Its implementation in a computer function is typically not enough.

It turned out that a technique called *automatic differentiation* (AD) [47] is a powerful alternative to compute derivatives which has many advantages. It is numerically exact and only requires a source code implementation of the (multivariate and vector-valued) function to differentiate. AD takes over the complete task of computing derivatives. This may include the detection of sparsity pattern in cases were the Jacobian matrix of a vector-valued function has a sparse structure. That is, most of its elements are always zero. Only the function to differentiate has to be implemented which, in practice, is usually a much less complex task than the implementation of derivatives. A suitable implementation of the optimization algorithm, as SparseLM [71, 72] used here, may then exploit the sparsity structure.

As an example the variables and the parameter of the nine dimensional chaotic Lorenz-96 [49] model are successfully estimated from a multivariate noisy time series in a twin experiment. This means, that the data are generated beforehand by integrating the Lorenz-96 model and adding some noise. Since, due to AD, a manual implementation of the Jacobian matrix occurring in the LM algorithm is not necessary any more, an extension of the estimation method from ordinary to delay differential equations (DDE) was possible with relatively little effort. The change of the Jacobian matrix and its sparsity pattern is automatically accomplished by AD. As an example for DDEs the Mackey-Glass [73] model is successfully fitted to noisy data in a twin experiment.

10.2 Chapter 5 and Chap. 6: Local uncertainty analysis of states and parameters in nonlinear systems

An important question in the context of state and parameter estimation is whether the measured signal is suitable to accurately reconstruct model variables and parameters from it. A large uncertainty of a specific variable or parameter is a hint that the considered signal contains only insufficient information about that quantity. Since it is desirable to know how accurately quantities can be reconstructed, in Chap. 5 and Chap. 6, which contain the articles Ref. [69] and Ref. [68], we suggest a measure to quantify these uncertainties.

The approach chosen here is based on delay coordinates. For that, the delay coordinate map, which maps the model variables and parameters via a measurement function onto the model output (which might be experimentally accessible) at present and delayed times, is considered. In principle, all model variables and parameters can be reconstructed from the delay coordinates if the map is (locally) invertible. That is, if its Jacobian matrix has full rank.

Based on the linearization of the delay coordinate map a local measure is suggested which quantifies how small perturbations on the delay coordinates are locally mapped to perturbations of individual variables and parameters. Large amplification of perturbations are an indicator that the considered quantity is difficult to reconstruct from the measured signal. This would make its estimation difficult.

As examples the local uncertainties of the 2D Ikeda [74] and Hénon [75] map and the 3D Rössler [76] and Hindmarsh-Rose [77] model are considered. Its distributions give a hint about which model variables and parameters are easy to determine and which are difficult to estimate. Furthermore, it is illustrated that the measure of uncertainty can be used to identify regions in the state space with smaller and larger uncertainties. This knowledge can help to plan and perform state and parameter estimation.

The uncertainties might also be used to search for redundant model parameters. This topic is elaborated in Chap. 8, where the suggested analysis is also based on the linearization of the delay reconstruction map.

10.3 Chapter 7: Basin structure of optimization based state and parameter estimation

In Chap. 7, which contains the article [78], the nine dimensional chaotic Lorenz-96 [49] model is used as an example system to investigate the observability of its model variables and the parameter. This includes the dependency of the observability on the number and combination of measured variables. First, the local uncertainty analysis from Chap. 5 and Chap. 6 is applied. Then, the weak constraint 4D-Var like state and parameter estimation algorithm from Ref. [33] (which is also used in Chap. 4) is used in twin experiments to compare three different strategies of initializing the algorithm. For that, different measured signals consisting of one to three model variables are considered.

For each of the measured signals histograms of the uncertainties for all model variables and the parameter are considered. It turned out that the uncertainties are sufficiently small (at least for delay times around 0.1) and the form of the histograms are independent of the number and combination of measured variables. Therefore, accurate state and parameter estimation from multivariate as well as univariate data should be possible. Indeed, a delay time of around 0.1 seems to be a good choice for state and parameter estimation based on delay coordinates [79, 80].

The comparison of initialization strategies for the state and parameter estimation algorithm are based on generated data which are extracted from a clean trajectory (referred to as the 'true solution' of the estimation problem) of the model. Since the algorithm used here has to be initialized with an initial guess consisting of a trajectory for each model variable (and not only its initial value) and a value for the model parameter, the following three different initialization strategies are compared in a statistical analysis: (i) The model parameter and each model variable at each time step is initialized with uniquely distributed random value. (ii) Randomly chosen states from the attractor are used as initial values for a model trajectory. (iii) The true solution, used to generate the data, is used for initialization, where noise is added to the trajectories of each model

variable at each time step. Of course, this strategy is usually not applicable in a typical setup because the true solution is typically unknown.

It turned out that strategy (i) clearly outperforms strategy (ii), independent of the number and combination of measured variables. That means, initial trajectories consisting of random numbers lead much more often to correct estimates compared to exact solution of the model equations. Using strategy (ii) estimated trajectories almost never match the true solution, which, using strategy (i), was only observed for univariate data.

The best results are obtained with strategy (iii). Success rates close to 100% are obtained even for univariate data. That means that in principle successful state and parameter estimation from univariate data using a 9-dimensional Lorenz-96 model is possible – at least if the initial guess is close enough to the true solution. The local observability based on a single measured variable was predicted by the uncertainty analysis and demonstrates that local observability is a necessary, but not sufficient property for successful state and parameter estimation.

The comparison of the estimated trajectories with the true solutions is only possible if the latter are available, which, as pointed out before, is usually not the case. Therefore, we also compare predictions computed with the model (initialized with the final estimated state at the end of the estimation window) with future data. This is possible without knowing the true solution. It turned out, that if the prediction is close to future data, then it is very likely that the estimates of the model variables and the parameter are close to the true solution. Therefore, comparing predictions with future data is a good indicator for correct estimates.

10.4 Chapter 8: Dependency analysis of model parameters and variables based on delay coordinates

Chapter 8, which contains a submitted manuscript, is about identifying redundant model variables and parameters. A set of quantities is considered as redundant if a change of its values does not lead to a change of the output of the model (via measurement function). Then, the measured signal does not contain enough information to uniquely estimate these quantities. A strategy is suggested to identify redundant quantities and, additionally, to find a (maybe minimal) subset of them so that its removal from the analysis or estimation task would make all remaining quantities in principle (locally) observable. Nevertheless, in practice its estimation may still be difficult, so that a subsequent correlation analysis is suggested which may be used to identify further 'almost' redundancies.

As in Chap. 5 and Chap. 6, the approach used here is based on time delay coordinates of the measured signal. If there exist small perturbations in the state and parameter space which locally do *not* lead to perturbations in the delay coordinate space, then the perturbed quantities are locally redundant. To identify redundancies, we consider the Jacobian matrix of the delay coordinate map, or, to be more precise, its null space.

In the case of a one dimensional null space, redundant quantities are identified by considering the pattern of non-zeros of an basis vector. Removing an arbitrary redundant quantity from the analysis makes all remaining quantities in principle locally observable.

If the null space is $D_{\mathrm{N}} > 1$ dimensional, then the situation is more sophisticated. To identify a set of redundant quantities, so that their removal from the analysis makes all remaining quantities in principle locally observable, an approach from detecting linear dependent columns of a matrix is adapted from Ref. [65] and used to construct a special basis of the null space. The basis vectors have the useful property that their patterns of zeros are mutually different, so that the quantities can be identified.

Even if all quantities are in principle locally observable, it is still possible that some quantities are 'almost redundant' in the sense that there exist strong relationships between them. For that reason, a correlation analysis is suggested where large correlation coefficients are an indication for a strong relationships. Nevertheless, it is a property of correlation coefficients that it is not guaranteed that the analysis reveals all strong relationships.

The Colpitts oscillator [81], the Rössler model [29, 76] , and the Hindmarsh-Rose model [77] are considered as examples for a one, two, and zero dimensional null space, respectively. Quantities which are (almost) redundant are identified and the results are confirmed by (i) the uncertainty analysis from Chap. 5 and Chap. 6, (ii) a profile likelihood [27] based on the state and parameter estimation method [33], and (iii) analytical results from the literature [29].

10.5 Chapter 9: The Shinriki oscillator

In Chap. 9 results are presented where the methods from the previous chapters were applied to experimentally measured data. As an experimental system the Shinriki oscillator [30], a nonlinear electronic circuit, is used for which a suitable three dimensional model is available.

Based on an univariate measured signal, first, the dependency analysis from Chap. 8 is applied for experimentally measured states to identify locally redundant model variables and parameters. Removing some redundant quantities from the analysis makes all remaining quantities in principle locally observable. Nevertheless, applying the correlation analysis from Chap. 8 reveals some almost redundant quantities. Removing even more quantities from the analysis finally makes the remaining variables and parameters locally observable.

These results are confirmed by the uncertainty analysis from Chap. 5 and Chap. 6.

Before estimating states and parameters, time series of all variables are measured. The remaining variables and parameters are then estimated from a time series of only one variable using the estimation method from Ref. [33]. To evaluate the accuracy of the estimates, the estimated solutions of all variables are compared with the available experimentally measured time series. Similarly, the estimated values of the model parameters are compared with the corresponding values of the electronic elements in the circuit. The estimated solutions of all model variables and parameters match with the measured time series and parameters values from the circuit. Furthermore, predictions using the free running model match future data for a few oscillations.

Acknowledgment

I want to thank everyone who supported me during the research leading to this thesis.

I am especially grateful for all the inspiring discussions and advice from my supervisor and committee member Prof. Ulrich Parlitz. He spent plenty of time over the years conducting this work and showed great effort and skill in supporting me.

For the continuing support and his encouragement from the very beginning of my work I want to thank the committee member and leader of our research group, Prof. Stefan Luther. I very much appreciated his kind support. Furthermore, I want to thank Prof. Florentin Wörgötter for agreeing to be a member of the thesis committee. In addition I would like to thank Prof. Andreas Dillmann, Prof. Wolfram Kollatschny, and Prof. Marc Timme for taking the time to review my thesis.

During my research I was given the opportunity to spend one month working with the group of Prof. Henry D. I. Abarbanel at the BioCircuits Institute - University of California, San Diego, which was very motivating and stimulating. I am grateful for that.

For the pleasant and comfortable daily collaboration I want to thank my colleagues in the Biomedical Physics Group.

In the end I want to thank my wife Andrea and my family for their ongoing encouragement during the whole time.

Bibliography

[1] P. J. van Leeuwen. "Particle Filtering in Geophysical Systems". In: *Mon. Wea. Rev.* 137.12 (2009), pp. 4089–4114. DOI: 10.1175/2009MWR2835.1.

[2] P. J. van Leeuwen. "Nonlinear data assimilation in geosciences: an extremely efficient particle filter". In: *Q. J. R. Meteorol. Soc.* 136.653 (2010), pp. 1991–1999. DOI: 10.1002/qj.699.

[3] P. J. v. Leeuwen, Y. Cheng, and S. Reich. *Nonlinear Data Assimilation*. Frontiers in Applied Dynamical Systems: Reviews and Tutorials 2. Springer International Publishing, 2015. DOI: 10.1007/978-3-319-18347-3.

[4] R. E. Kalman. "A New Approach to Linear Filtering and Prediction Problems". In: *J. Basic. Eng.* 82.1 (1960), pp. 35–45. DOI: 10.1115/1.3662552.

[5] G. Evensen. "Sequential data assimilation with a nonlinear quasi-geostrophic model using Monte Carlo methods to forecast error statistics". In: *J. Geophys. Res.* 99.C5 (1994), pp. 10143–10162. DOI: 10.1029/94jc00572.

[6] S. J. Julier and J. K. Uhlmann. "New extension of the Kalman filter to nonlinear systems". In: vol. 3068. 1997, pp. 182–193. DOI: 10.1117/12.280797.

[7] S. Julier and J. Uhlmann. "Unscented filtering and nonlinear estimation". In: *Proc. IEEE* 92.3 (2004), pp. 401–422. DOI: 10.1109/JPROC.2003.823141.

[8] G. Evensen. *Data Assimilation: The Ensemble Kalman Filter*. 2nd ed. Springer-Verlag Berlin Heidelberg, 2009. DOI: 10.1007/978-3-642-03711-5.

[9] E. Baake, M. Baake, H. G. Bock, and K. M. Briggs. "Fitting ordinary differential equations to chaotic data". In: *Phys. Rev. A* 45.8 (1992), pp. 5524–5529. DOI: 10.1103/PhysRevA.45.5524.

[10] U. Parlitz, L. Junge, and L. Kocarev. "Synchronization-based parameter estimation from time series". In: *Phys. Rev. E* 54.6 (1996), pp. 6253–6259. DOI: 10.1103/PhysRevE.54.6253.

[11] L. M. Pecora and T. L. Carroll. "Synchronization in chaotic systems". In: *Phys. Rev. Lett.* 64.8 (1990), pp. 821–824. DOI: 10.1103/PhysRevLett.64.821.

[12] H. D. I. Abarbanel, D. R. Creveling, R. Farsian, and M. Kostuk. "Dynamical State and Parameter Estimation". In: *SIAM J. Appl. Dyn. Syst.* 8.4 (2009), pp. 1341–1381. DOI: 10.1137/090749761.

[13] J. Bröcker. "On variational data assimilation in continuous time". In: *Q. J. R. Meteorol. Soc.* 136.652 (2010), pp. 1906–1919. DOI: 10.1002/qj.695.

[14] J. C. Quinn and H. D. Abarbanel. "State and parameter estimation using Monte Carlo evaluation of path integrals". In: *Q. J. R. Meteorol. Soc.* 136.652 (2010), pp. 1855–1867. DOI: 10.1002/qj.690.

[15] R. Daley. *Atmospheric Data Analysis*. Cambridge University Press, 1993. DOI: 10.4267/2042/51948.

[16] E. Kalnay. *Atmospheric Modeling, Data Assimilation and Predictability*. Cambridge University Press, 2003. DOI: 10.1017/cbo9780511802270.

[17] S. Dokos and N. H. Lovell. "Parameter estimation in cardiac ionic models". In: *Progress in Biophysics and Molecular Biology*. Modelling Cellular and Tissue Function 85.2 (2004), pp. 407–431. DOI: 10.1016/j.pbiomolbio.2004.02.002.

[18] R. E. Kalman. "On the general theory of control systems". In: *Proc. First IFAC Congress*. Vol. 1. 1961, pp. 481–492.

[19] R. E. Kalman. "Mathematical Description of Linear Dynamical Systems". In: *SIAM J. Control* 1.2 (1963), pp. 152–192. DOI: 10.1137/0301010.

[20] T. Kailath. *Linear Systems*. Prentice-Hall, 1980. 712 pp.

[21] E. B. Lee and L. Markus. *Foundations of Optimal Control Theory*. John Wiley & Sons, 1967.

[22] R. Hermann and A. J. Krener. "Nonlinear controllability and observability". In: *IEEE Trans. Autom. Control* 22.5 (1977), pp. 728–740. DOI: 10.1109/TAC.1977.1101601.

[23] E. D. Sontag. *Mathematical Control Theory: Deterministic Finite Dimensional Systems*. 2nd ed. Springer New York, 1998. DOI: 10.1007/978-1-4612-0577-7.

[24] H. Nijmeijer. "Observability of autonomous discrete time non-linear systems: a geometric approach". In: *Int. J. Control* 36.5 (1982), pp. 867–874. DOI: 10.1080/00207178208932936.

[25] C. Letellier, L. A. Aguirre, and J. Maquet. "Relation between observability and differential embeddings for nonlinear dynamics". In: *Phys. Rev. E* 71.6 (2005), p. 066213. DOI: 10.1103/PhysRevE.71.066213.

[26] C. Letellier, L. Aguirre, and J. Maquet. "How the choice of the observable may influence the analysis of nonlinear dynamical systems". In: *Commun. Nonlinear. Sci. Numer. Simul.* Dynamical systems—theory and applications 11.5 (2006), pp. 555–576. DOI: 10.1016/j.cnsns.2005.01.003.

[27] A. Raue, C. Kreutz, T. Maiwald, J. Bachmann, M. Schilling, U. Klingmüller, and J. Timmer. "Structural and practical identifiability analysis of partially observed dynamical models by exploiting the profile likelihood". In: *Bioinformatics* 25.15 (2009), pp. 1923–1929. DOI: 10.1093/bioinformatics/btp358.

[28] A. Raue, V. Becker, U. Klingmüller, and J. Timmer. "Identifiability and observability analysis for experimental design in nonlinear dynamical models". In: *Chaos* 20.4 (2010), p. 045105. DOI: 10.1063/1.3528102.

[29] C. Lainscsek, J. Weyhenmeyer, T. J. Sejnowski, and C. Letellier. "Discovering independent parameters in complex dynamical systems". In: *Chaos, Solitons & Fractals* 76 (2015), pp. 182–189. DOI: 10.1016/j.chaos.2015.04.001.

[30] M. Shinriki, M. Yamamoto, and S. Mori. "Multimode oscillations in a modified Van Der Pol oscillator containing a positive nonlinear conductance". In: *Proc. IEEE* 69.3 (1981), pp. 394–395. DOI: 10.1109/PROC.1981.11973.

[31] A. H. Jazwinski. *Stochastic processes and filtering theory*. New York u.a.: Academic Press, 1970.

[32] G. Xu. *GPS - Theory, Algorithms and Applications*. Springer Berlin Heidelberg, 2007. DOI: 10.1007/978-3-540-72715-6.

[33] J. Schumann-Bischoff and U. Parlitz. "State and parameter estimation using unconstrained optimization". In: *Phys. Rev. E* 84.5 (2011), p. 056214. DOI: 10.1103/PhysRevE.84.056214.

[34] D. Zupanski. "A General Weak Constraint Applicable to Operational 4DVAR Data Assimilation Systems". In: *Mon. Wea. Rev.* 125.9 (1997), pp. 2274–2292. DOI: 10.1175/1520-0493(1997)125<2274:AGWCAT>2.0.CO;2.

[35] Y. Tr'emolet. "Accounting for an imperfect model in 4D-Var". In: *Q.J.R. Meteorol. Soc.* 132.621 (2006), pp. 2483–2504. DOI: 10.1256/qj.05.224.

[36] Y. Trémolet. "Model-error estimation in 4D-Var". In: *Q.J.R. Meteorol. Soc.* 133.626 (2007), pp. 1267–1280. DOI: 10.1002/qj.94.

[37] A. Apte, C. K. R. T. Jones, A. M. Stuart, and J. Voss. "Data assimilation: Mathematical and statistical perspectives". In: *Int. J. Numer. Meth. Fluids* 56.8 (2008), pp. 1033–1046. DOI: 10.1002/fld.1698.

[38] R. N. Miller, M. Ghil, and F. Gauthiez. "Advanced Data Assimilation in Strongly Nonlinear Dynamical Systems". In: *J. Atmos. Sci.* 51.8 (1994), pp. 1037–1056. DOI: 10.1175/1520-0469(1994)051<1037:ADAISN>2.0.CO;2.

[39] E. N. Lorenz. "Deterministic Nonperiodic Flow". In: *J. Atmos. Sci.* 20.2 (1963), pp. 130–141. DOI: 10.1175/1520-0469(1963)020<0130:DNF>2.0.CO;2.

[40] H. Abarbanel. *Predicting the Future: Completing Models of Observed Complex Systems*. Springer New York, 2013. DOI: 10.1007/978-1-4614-7218-6.

[41] J. C. Quinn and H. D. I. Abarbanel. "Data assimilation using a GPU accelerated path integral Monte Carlo approach". In: *Journal of Computational Physics* 230.22 (2011), pp. 8168–8178. DOI: 10.1016/j.jcp.2011.07.015.

[42] M. Kostuk, B. A. Toth, C. D. Meliza, D. Margoliash, and H. D. I. Abarbanel. "Dynamical estimation of neuron and network properties II: path integral Monte Carlo methods". In: *Biol Cybern* 106.3 (2012), pp. 155–167. DOI: 10.1007/s00422-012-0487-5.

[43] O. Talagrand and P. Courtier. "Variational Assimilation of Meteorological Observations With the Adjoint Vorticity Equation. I: Theory". In: *Q.J.R. Meteorol. Soc.* 113.478 (1987), pp. 1311–1328. DOI: 10.1002/qj.49711347812.

[44] P. Courtier and O. Talagrand. "Variational Assimilation of Meteorological Observations With the Adjoint Vorticity Equation. II: Numerical Results". In: *Q.J.R. Meteorol. Soc.* 113.478 (1987), pp. 1329–1347. DOI: 10.1002/qj.49711347813.

[45] K. Levenberg. "A method for the solution of certain problems in least squares". In: *Q. Appl. Math.* 2 (1944), pp. 164–168.

[46] D. W. Marquardt. "An Algorithm for Least-Squares Estimation of Nonlinear Parameters". In: *J. Soc. Ind. Appl. Math.* 11.2 (1963), pp. 431–441. DOI: 10.1137/0111030.

[47] A. Griewank, D. Juedes, and J. Utke. "Algorithm 755: ADOL-C: A Package for the Automatic Differentiation of Algorithms Written in C/C++". In: *ACM Trans. Math. Softw.* 22.2 (1996), pp. 131–167. DOI: 10.1145/229473.229474.

[48] A. Walther and A. Griewank. "Getting Started with ADOL-C". In: *Combinatorial Scientific Computing*. Ed. by U. Naumann and O. Schenk. Chapman & Hall / CRC Computational Science Series, 2012, pp. 181–202.

[49] E. N. Lorenz. "Predictability: A problem partly solved". In: *Proc. Seminar on predictability*. Vol. 1. 1. 1996.

[50] D. Aeyels. "Generic Observability of Differentiable Systems". In: *SIAM J. Control Optim.* 19.5 (1981), pp. 595–603. DOI: 10.1137/0319037.

[51] T. Sauer, J. A. Yorke, and M. Casdagli. "Embedology". In: *J. Stat. Phys.* 65.3-4 (1991), pp. 579–616. DOI: 10.1007/BF01053745.

[52] F. Takens. "Detecting strange attractors in turbulence". In: *Dynamical Systems and Turbulence, Warwick 1980*. Ed. by D. Rand and L.-S. Young. Lecture Notes in Mathematics 898. Springer Berlin Heidelberg, 1981, pp. 366–381. DOI: 10.1007/bfb0091924.

[53] H. Kantz and T. Schreiber. *Nonlinear Time Series Analysis*. Vol. 7. Cambridge University Press, 2003. DOI: 10.1017/cbo9780511755798.

[54] L. A. Aguirre and C. Letellier. "Observability of multivariate differential embeddings". In: *J. Phys. A: Math. Gen.* 38.28 (2005), pp. 6311–6326. DOI: 10.1088/0305-4470/38/28/004.

[55] W. H. Press, S. A. Teukolsky, W. T. Vetterling, and B. P. Flannery. *Numerical Recipes: The Art of Scientific Computing*. 3rd ed. Cambridge, UK ; New York: Cambridge University Press, 2007.

[56] C. Letellier, L. A. Aguirre, and U. S. Freitas. "Frequently asked questions about global modeling". In: *Chaos* 19.2 (2009), p. 023103. DOI: 10.1063/1.3125705.

[57] J. Schumann-Bischoff, S. Luther, and U. Parlitz. "Estimability and dependency analysis of model parameters based on delay coordinates". In: *Phys. Rev. E* 94.3 (2016), p. 032221. DOI: 10.1103/PhysRevE.94.032221.

[58] E. Freire, L. Franquelo, and J. Aracil. "Periodicity and chaos in an autonomous electronic system". In: *IEEE Trans. Circuits Syst.* 31.3 (1984), pp. 237–247. DOI: 10.1109/TCS.1984.1085496.

[59] M. A. van Wyk and W.-H. Steeb. *Chaos in Electronics*. Ed. by R. Lowen. Vol. 2. Mathematical Modelling: Theory and Applications. Springer Netherlands, 1997. DOI: 10.1007/978-94-015-8921-5.

[60] M. Siefert, A. Kittel, R. Friedrich, and J. Peinke. "On a quantitative method to analyze dynamical and measurement noise". In: *Europhys. Lett.* 61.4 (2003), p. 466. DOI: 10.1209/epl/i2003-00152-9.

[61] *Bauanleitung Shinriki-Oszillator*. 2015. URL: http://www.physik.uni-wuerzburg.de/~slueck/PhyAmSa09/Home_files/Shinriki_Anleitung.pdf.

[62] W. Demtröder. *Experimentalphysik 2 - Elektrizität und Optik*. 4. Aufl. Springer-Lehrbuch. Springer Berlin Heidelberg, 2006. DOI: 10.1007/978-3-540-33795-9.

[63] U. Tietze and C. Schenk. *Halbleiter-Schaltungstechnik*. 11. Aufl. Springer, 2002.

[64] R. L. Boylestad and L. Nashelsky. *Electronic Devices and Circuit Theory*. 7th ed. Prentice Hall, 1999.

[65] D. A. Belsley. *Conditioning Diagnostics: Collinearity and Weak Data in Regression*. 1st ed. Wiley & Sons, 1991.

[66] A. F. Bennett. *Inverse Methods in Physical Oceanography*. Cambridge University Press, 1992. DOI: 10.1017/cbo9780511600807.

[67] G. Evensen. "Advanced Data Assimilation for Strongly Nonlinear Dynamics". In: *Mon. Wea. Rev.* 125.6 (1997), pp. 1342–1354. DOI: 10.1175/1520-0493(1997)125<1342:ADAFSN>2.0.CO;2.

[68] U. Parlitz, J. Schumann-Bischoff, and S. Luther. "Local observability of state variables and parameters in nonlinear modeling quantified by delay reconstruction". In: *Chaos* 24.2 (2014), p. 024411. DOI: 10.1063/1.4884344.

[69] U. Parlitz, J. Schumann-Bischoff, and S. Luther. "Quantifying uncertainty in state and parameter estimation". In: *Phys. Rev. E* 89.5 (2014), p. 050902. DOI: 10.1103/PhysRevE.89.050902.

[70] J. Schumann-Bischoff, S. Luther, and U. Parlitz. "Nonlinear system identification employing automatic differentiation". In: *Commun. Nonlinear. Sci. Numer. Simul.* 18.10 (2013), pp. 2733–2742. DOI: 10.1016/j.cnsns.2013.02.017.

[71] M. I. Lourakis. "Sparse Non-linear Least Squares Optimization for Geometric Vision". In: *Computer Vision – ECCV*. Vol. 2. 2010, pp. 43–56. DOI: 10.1007/978-3-642-15552-9_4.

[72] M. I. Lourakis. *SparseLM*. 2016. URL: http://users.ics.forth.gr/~lourakis/sparseLM/.

[73] M. C. Mackey and L. Glass. "Oscillation and chaos in physiological control systems". In: *Science* 197.4300 (1977), pp. 287–289. DOI: 10.1126/science.267326.

[74] K. Ikeda. "Multiple-valued stationary state and its instability of the transmitted light by a ring cavity system". In: *Opt. Commun.* 30.2 (1979), pp. 257–261. DOI: 10.1016/0030-4018(79)90090-7.

[75] M. Hénon. “A two-dimensional mapping with a strange attractor”. In: *Commun. Math. Phys.* 50.1 (1976), pp. 69–77. DOI: 10.1007/BF01608556.

[76] O. E. Rössler. “An equation for continuous chaos”. In: *Phys. Lett. A* 57.5 (1976), pp. 397–398. DOI: 10.1016/0375-9601(76)90101-8.

[77] J. L. Hindmarsh and R. M. Rose. “A Model of Neuronal Bursting Using Three Coupled First Order Differential Equations”. In: *Proc. R. Soc. Lond. B* 221.1222 (1984), pp. 87–102. DOI: 10.1098/rspb.1984.0024.

[78] J. Schumann-Bischoff, U. Parlitz, H. D. I. Abarbanel, M. Kostuk, D. Rey, M. Eldridge, and S. Luther. “Basin structure of optimization based state and parameter estimation”. In: *Chaos: An Interdisciplinary Journal of Nonlinear Science* 25.5 (2015), p. 053108. DOI: 10.1063/1.4920942.

[79] D. Rey, M. Eldridge, M. Kostuk, H. D. I. Abarbanel, J. Schumann-Bischoff, and U. Parlitz. “Accurate state and parameter estimation in nonlinear systems with sparse observations”. In: *Phys. Lett. A* 378.11–12 (2014), pp. 869–873. DOI: 10.1016/j.physleta.2014.01.027.

[80] D. Rey, M. Eldridge, U. Morone, H. D. I. Abarbanel, U. Parlitz, and J. Schumann-Bischoff. “Using waveform information in nonlinear data assimilation”. In: *Phys. Rev. E* 90.6 (2014), p. 062916. DOI: 10.1103/PhysRevE.90.062916.

[81] M. Kennedy. “Chaos in the Colpitts oscillator”. In: *IEEE Transactions on Circuits and Systems I: Fundamental Theory and Applications* 41.11 (1994), pp. 771–774. DOI: 10.1109/81.331536.